2019

ECOPHYSIOLOGICAL RESPONSES OF TROPICAL WOODY SPECIES TO AMBIENT AND ELEVATED TEMPERATURES

Kelsey R. Carter
Michigan Technological University, kcarter@mtu.edu

ECOPHYSIOLOGICAL RESPONSES OF TROPICAL WOODY SPECIES TO AMBIENT AND ELEVATED TEMPERATURES

By

Kelsey R. Carter

A DISSERTATION

Submitted in partial fulfillment of the requirements for the degree of

DOCTOR OF PHILOSOPHY

In Forest Science

MICHIGAN TECHNOLOGICAL UNIVERSITY

2019

This dissertation has been approved in partial fulfillment of the requirements for the Degree of DOCTOR OF PHILOSOPHY in Forest Science.

School of Forest Resources and Environmental Science

Dissertation Advisor: *Molly Cavaleri*

Committee Member: *Robert Froese*

Committee Member: *Andrew Burton*

Committee Member: *Sarah Green*

School Dean: *Andrew Storer*

Table of Contents

Preface

Chapter 2 is a collaborative effort facilitated by the US Geological Survey John Wesley Powell Center Working Center of Analysis and Synthesis. The manuscript is being prepared for submission to a peer reviewed journal article, with co-authors and contributions listed below. Molly A. Cavaleri, Sasha C. Reed, and Tana E. Wood acquired funding for the working group. Molly A. Cavaleri, Alistair Rogers, Shawn P. Serbin, Kim S. Ely, Richard J. Norby, Anthony P. Walker, Peter B. Reich conceived the project and provided ideas for experimental design. Kelsey R. Carter conducted the data analysis and wrote the manuscript. Molly A. Cavaleri provided feedback to the data analysis and gave feedback and contributed to the manuscript text. Molly A. Cavaleri, Kelsey R. Carter, Alistair Rogers, Shawn P. Serbin, Kim S, Elsa C. Schwartz, Owen K. Atkin, Nur H. A. Bahar, Keith J. Bloomfield, Alex W. Cheesman, Kristine Y. Crous, Chris E. Doughty, Mirindi E. Dusenge, John R. Evans, Jéssica Fonseca da Silva, Jeff W. G. Kelly, Alida C. Mau, Belinda E. Medlyn, Patrick Meir, Jennifer Read, , Martijn Slot, Johan Uddling, Angelica Vårhammar, Klaus Winter, and Jin Wu provided data for the meta-analysis. All authors have provided feedback on data analysis and synthesis.

Chapter 3 was submitted for peer review in the journal New Phytologist and was rejected with encouragement to resubmit. The manuscript will be resubmitted to New Phytologist shortly after completion of the dissertation. Coauthors on this manuscript are Molly A. Cavaleri, Tana E. Wood, Sasha C. Reed, Elsa C. Schwartz , Madeline B. Reinsel, and Xi Yang. Molly A. Cavaleri, Tana E. Wood, and Sasha C. Reed designed the TRACE

experiment and acquired financial support for the overall study. Kelsey R. Carter and Molly A. Cavaleri designed the physiological study. Kelsey R. Carter collected the photosynthesis, respiration, and leaf trait data. Elsa C. Schwartz collected the stomatal size and density data. Madeline B. Reinsel collected the chlorophyll fluorescence data. Kelsey R. Carter carried out all of the statistical analysis and wrote the first draft of the manuscript. Molly A. Cavaleri provided additional advice and contributed to revisions of the text. All authors provided input and revisions to the final draft.

Chapter 4 is being prepared for submission to a peer reviewed journal with coauthors: Molly A. Cavaleri, Tana E. Wood, Sasha C. Reed, and Kaylie M. Butts. Molly A. Cavaleri, Tana E. Wood, and Sasha C. Reed designed the study. Kelsey R. Carter and Molly A. Cavaleri were responsible for physiological study design. Kelsey R. Carter collected all data presented in Chapter 4. Kaylie M. Butts collected dark-adapted chlorophyll fluorescence data that will be incorporated into the manuscript for publication but not included in the dissertation. Kelsey R. Carter conducted all of the statistical analysis and prepared the first draft of the manuscript. Molly A. Cavaleri provided feedback on manuscript.

Acknowledgements

I am incredibly grateful to my advisor, Molly Cavaleri for her endless encouragement, guidance, and mentorship throughout my PhD research. Thank you for the opportunity to pursue my PhD working on such an exciting project, with a great group of scientists. My committee members Andrew Burton, Robert Froese, and Sarah Green provided constructive criticism and thought-provoking discussions throughout pursuing my degree. I am also very thankful to TRACE project co-PIs, Tana Wood and Sasha Reed, for their wonderful support and advice.

A very special thanks to the amazing Cavaleri lab and TRACE project technicians, without whom, I would not have been able to complete this work: Michael Schmid, Jack Zwart, Heidi Harmala, GraceAnna Schilz, Brian Peacock, Talia Anderson, and Jamarys Torres-Díaz. I am especially thankful to technicians Elsa Schwartz, Kaylie Butts, and Benjamin Miller who worked with me throughout my entire graduate career. I am forever grateful for your excellent work and for the wonderful memories made. I would not have been able to complete this work without the invaluable logistical assistance from the TRACE project managers Aura Alonzo-Rodríguez and Megan Berberich. Mark Sloat in Michigan Technological University's Electrical and Computer Engineering designed the canopy warming device that was used in Chapter 4.

I am very grateful my graduate cohort and friends, who challenged and encouraged me along the way. Your friendship and support made it all worthwhile. Thank you to all of the wonderful people that I met in Puerto; you truly make Luquillo feel like home. I am fortunate to have a wonderful family who have always supported and encouraged me to

pursue my education. Thank you for always reminding me that anything is possible with hard work and dedication. Lastly, thank you to my amazing husband, Carl Carter. This would not have been possible without your patience, love, and support.

Funding for this dissertation was provided by U.S. Department of Energy award numbers DE-SC-0011806, 89243018S-SC-000014, and DE-SC-0018942. Additional support was provided by USDA Forest Service International Institute of Tropical Forestry, University of Puerto Rico-Río Piedras, National Institute of Food and Agriculture U.S. Department of Agriculture McIntire-Stennis Cooperative Forestry Research Program Grant #1001534. Additional funding was provided by US Biological Survey John Wesley Powell Center Working Center for Analysis and Synthesis., Michigan Technological University Ecosystem Science Center, the DeVlieg Fellowship, and a Finishing Fellowship at Michigan Technological University.

Abstract

Tropical forests cycle one third of Earth's carbon, yet we are still unsure how tropical vegetation will respond to climate warming. Tropical biomes experience a smaller temperature margin compared to other systems, possibly making them less capable of thermal adjustments. In addition, thermal responses of vegetation have been identified as one of the areas of greatest uncertainty for global carbon models. This dissertation works to quantify tropical forest photosynthetic responses to temperature as well as assessing physiological thermal acclimation of four tropical species. In Chapter, 2 we conducted a meta-analysis to investigate global tropical photosynthetic responses to temperature. We presented algorithms that quantify how instantaneous temperature responses vary for different climate regimes within the tropics. We found that mean annual temperature was the single variable that best predicted most temperature response variables. Stepwise regression showed that including light in net photosynthetic models improved predictive power but, overall, we need better representations of tropical responses to different growth types and conditions. We implemented two *in situ* warming experiments in a Puerto Rican rainforest to assess physiological thermal acclimation. One experiment was implemented in the understory (Chapter 3) and one in the canopy (Chapter 4). Our understory warming experiment found evidence for net photosynthetic acclimation; however, acclimation did not systematically occur across both warming studies. Some species showed evidence of acclimation of the optimum temperature for photosynthesis (T_{opt}) or both T_{opt} and the photosynthetic rate; while, neither of our canopy species photosynthetically acclimated. Contrary to common hypotheses surrounding plant

respiration, only one of the four species showed evidence of respiratory acclimation. Our understory vegetation temperature responses were more strongly controlled by soil moisture than temperature itself. Specifically, the photosynthetic rate declined as soils dried, a response that coincided with stomatal conductance. Surprisingly, T_{opt} decreased with increasing height for our canopy species, and this response was likely, in part, due to higher thermal sensitivity of stomatal conductance in the mid and upper canopies. Additionally, our canopy species were found to be operating right at or above their T_{opt}. The results of this dissertation better quantify tropical physiological responses to temperature, as well as assesses the potential of tropical plants to physiologically acclimate.

1 Introduction

Mean global temperatures have already risen 0.87 °C since preindustrial times and, with continued increases of greenhouse gas inputs into the atmosphere, global averages are expected to rise as high as 4.8 °C by the year 2100 (Collins *et al.*, 2013). Additionally, most land regions on Earth have experienced average temperatures more than 1.5 °C above average for one or more seasons, and these rises in temperatures have had substantial impacts on Earth's systems (Allen *et al.*, 2018). Worldwide, forests play a critical role in controlling climate feedbacks, as forest store large amounts of carbon and are responsible for 75% of terrestrial gross primary production (Beer *et al.*, 2010). Tropical forests are an important component of the global primary production because they cycle more carbon than any other biome (Pan *et al.*, 2013). Although warming is expected to occur to a lesser degree in the tropics (Ciais *et al.*, 2013), tropical forests are expected to reach temperatures beyond historical climate margins earlier than other regions (Wright *et al.*, 2009; Anderson, 2011; Diffenbaugh & Scherer, 2011; Mora *et al.*, 2013). Even with the important role that tropical forests play in the global carbon cycle, there is a considerable lack of data in tropical forests, allowing for particularly high uncertainty regarding how these forests will respond to future conditions (Booth *et al.*, 2012; Cavaleri *et al.*, 2015; Mercado *et al.*, 2018). Improving our ability to predict how these systems will respond to climate warming is critical for our ability to accurately represent the future global climate.

Ecosystem carbon balance is determined by the balance between CO_2 uptake, through the process of photosynthesis, and CO_2 release, through ecosystem respiration.

Within vegetative processes alone, more than 50% of CO_2 assimilated through photosynthesis can be lost through autotrophic respiration (Amthor & Baldocchi, 2001; Chambers *et al.*, 2004). Photosynthesis has a peaked response to temperature, where the rate of photosynthesis declines after the temperature optimum (T_{opt}; Berry and Bjorkman 1980; Way and Yamori 2014). Respiration increases nonlinearly with temperature (Atkin *et al.*, 2005; Heskel *et al.*, 2016), and will eventually decline at temperatures higher than the photosynthetic T_{opt} (Atkin & Tjoelker, 2003; Heskel *et al.*, 2016; O'Sullivan *et al.*, 2017). If rates of respiration continue to rise with warming temperatures, and photosynthesis is not effectively upregulated, ecosystems could shift their carbon balance toward higher CO_2 release (White *et al.*, 2000; Cramer *et al.*, 2001). A disruption of ecosystem carbon balance can be prevented if the processes of photosynthesis and respiration can acclimate to warmer temperature regimes.

Photosynthetic acclimation can come in the form of an upregulation of the rate of net photosynthesis at the optimum temperature (A_{opt}), an increase in the optimum temperature of net photosynthesis (T_{opt}), or a through widening of the net photosynthetic response curve (Ω) (Berry & Bjorkman, 1980; Way & Yamori, 2014). Acclimation occurs due to alterations in the underlying processes controlling net photosynthesis: the rate of stomatal conductance (g_s), the rate of Rubisco carboxylation (V_{cmax}), and the rate of electron transport (J_{max}). Both V_{cmax} and J_{max} often have peaked responses to temperature (Medlyn *et al.*, 2002a), with the peak occurring at higher temperatures than net photosynthesis (e.g. Kumarathunge *et al.* 2019). Stomatal conductance, on the other hand, can respond to rising temperature through an increase (Mott & Peak, 2010; Mendes

& Marenco, 2017), decrease (Slot *et al.*, 2019), peak in a similar manor to net photosynthesis (Zhou *et al.*, 2015; Slot *et al.*, 2016), or peak and then decouple from photosynthesis by increasing again at particularly high temperatures (Slot *et al.*, 2016; Urban *et al.*, 2017; Drake *et al.*, 2018). Studies often measure these underlying processes, alongside the rate of net photosynthesis to investigate drivers of both photosynthetic thermal declines and acclimation. Additionally, the biochemical components of photosynthesis (J_{max} and V_{cmax}) are often used in global carbon models instead of the net photosynthetic response to temperature (e.g. Clark *et al.* 2011); therefore, studying how these component processes of photosynthesis respond to temperature is critical to accurately representing tropical vegetation within the global carbon budget.

Respiration acclimation to warmer temperature occurs by down regulating, often described as a lowered basal rate of respiration or a decline in the exponential response to rising temperature (Atkin and Tjoelker 2003; Atkin *et al.* 2005; but see Heskel *et al.* 2016). Respiratory acclimation to warmer temperatures often occurs through substrate limitation (Dewar *et al.*, 1999; Aspinwall *et al.*, 2016), or through limitations of adenosine diphosphate supply (Atkin & Tjoelker, 2003; Jarvi & Burton, 2018). Respiratory thermal acclimation can also occur due to changes in enzymatic capacities through alterations in the size and density of mitochondria (Atkin & Tjoelker, 2003; Armstrong *et al.*, 2006); although, enzymatic capacity is more likely to play a limiting role for respiration in cold temperature (Atkin & Tjoelker, 2003).

Warming experiments (Gunderson *et al.*, 2000, 2010; Sendall *et al.*, 2015; Aspinwall *et al.*, 2016; Reich *et al.*, 2016; Smith & Dukes, 2017), seasonal variation

studies (Atkin *et al.*, 2000; Medlyn *et al.*, 2002b; Wright *et al.*, 2006), and analyses investigating global temperature gradients (Atkin *et al.*, 2015; Vanderwel *et al.*, 2015) have shown that both photosynthesis and respiration can acclimate to warmer temperatures. In addition, acclimation has been shown to occur in timescales of less than a week (Berry & Bjorkman, 1980; Bolstad *et al.*, 1999; Lee *et al.*, 2005; Slot *et al.*, 2014; Smith & Dukes, 2017). Even though physiological acclimation can occur across many species, global vegetation models often do not specifically incorporate acclimation within their model predictions (Arneth *et al.*, 2012; Smith & Dukes, 2013; Smith *et al.*, 2016); possibly overestimating elevated temperature induced loss of CO_2 to the atmosphere (Smith *et al.*, 2016; Mercado *et al.*, 2018).

Tropical forests experience lower annual temperature variation compared with other biomes, and this has been hypothesized to limit tropical forests' ability for thermal acclimation (Janzen 1967; Cunningham and Read 2002, 2003; Drake *et al.* 2015; but see (Lloyd & Farquhar, 2008). Recent studies investigating tropical saplings and seedlings have found evidence of both photosynthetic and respiratory acclimation (Scafaro *et al.*, 2017; Slot & Winter, 2017, 2018; Smith & Dukes, 2017); however, photosynthetic acclimation was more limited (Slot & Winter, 2017, 2018). Although these studies suggest that tropical species can acclimate to warmer temperatures, acclimation occurs more readily in immature tissues (Campbell *et al.*, 2007); therefore, more investigations of acclimation on mature tropical plants are needed to more fully understand how tropical forest will respond to climate warming. In addition, there is a growing body of evidence that tropical forests will exceed their thermal safety margins as temperatures continue to

warm (Doughty & Goulden, 2008; Vårhammar *et al.*, 2015; Mau *et al.*, 2018; Pau *et al.*, 2018; Huang *et al.*, 2019); making it critical to gain a better understanding of tropical forest acclimation capabilities.

The aim of this dissertation is to close the gap in our understanding of how tropical forests respond to temperature. Chapter two of this dissertation uses a meta-analytic approach to quantify tropical woody plant photosynthetic-temperature responses to various climate factors across 16 studies on 4 continents. We additionally compared how tropical temperature responses varied across different growth types and conditions. Chapter three investigates plant physiological responses to *in situ* field scale +4 °C experimental warming in two Puerto Rican tropical shrub species after 3 and 8 months of experimental warming. Chapter four implements *in situ* leaf-level warming throughout the canopy of a Puerto Rican tropical forest. We investigated physiological acclimation of two canopy tree species after approximately one month of experimental +3 °C warming. This dissertation provides results of plant physiological responses to both the first-ever field scale warming experiment in a tropical forest and the first leaf-level canopy warming study investigating both photosynthetic and respiratory acclimation.

1.1 References

Allen MR, Dube OP, Solecki W, Aragón-Durand F, Cramer W, Humphreys S, Kainuma M, Kala J, Mahowald N, Mulugetta Y, *et al.* 2018. *Framing and Context* (V Masson-Delmotte, P Zhai, H-O Pörtner, D Roberts, J Skea, PR Shukla, A Pirani, W Moufouma-Okia, C Péan, R Pidcock, *et al.*, Eds.). In Press.

Amthor JS, Baldocchi DD. **2001**. *Terrestrial Higher Plant Respiration and Net Primary Production* (H Roy, HA Mooney, and Saugier B, Eds.). San Diego, CA, USA: Academic Press.

Anderson BT. **2011**. Near-term increase in frequency of seasonal temperature extremes prior to the 2°C global warming target. *Climatic Change* **108**: 581–589.

Armstrong AF, Logan DC, Tobin AK, O'Toole P, Atkin OK. **2006**. Heterogeneity of plant mitochondrial responses underpinning respiratory acclimation to the cold in Arabidopsis thaliana leaves. *Plant, Cell and Environment* **29**: 940–949.

Arneth A, Mercado L, Kattge J, Booth BBB. **2012**. Future challenges of representing land-processes in studies on land-atmosphere interactions. *Biogeosciences* **9**: 3587–3599.

Aspinwall MJ, Drake JE, Campany C, Vårhammar A, Ghannoum O, Tissue DT, Reich PB, Tjoelker MG. **2016**. Convergent acclimation of leaf photosynthesis and respiration to prevailing ambient temperatures under current and warmer climates in Eucalyptus tereticornis. *New Phytologist* **212**: 354–367.

Atkin OK, Bloomfield KJ, Reich PB, Tjoelker MG, Asner GP, Bonal D, Bönisch G, Bradford MG, Cernusak LA, Cosio EG, *et al.* 2015. Global variability in leaf respiration in relation to climate, plant functional types and leaf traits. *New Phytologist* **206**: 614–636.

Atkin OK, Bruhn D, Hurry VM, Tjoelker MG. **2005**. The hot and the cold : unravelling the variable response of plant respiration to temperature. *Functional Plant Biology* **32**: 87–105.

Atkin OK, Holly C, Ball MC. **2000**. Acclimation of snow gum (Eucalyptus pauciflora) leaf respiration to seasonal and diurnal variations in temperature: The importance of changes in the capacity and temperature sensitivity of respiration. *Plant, Cell and Environment* **23**: 15–26.

Atkin OK, Tjoelker MG. **2003**. Thermal acclimation and the dynamic response of plant respiration to temperature. *Trends in Plant Science* **8**: 343–351.

Beer C, Reichstein M, Tomelleri E, Ciais P, Jung M, Carvalhais N, Rodenbeck C, Arain MA, Baldocchi D, Bonan GB, *et al.* 2010. Terrestrial gross carbon dioxide uptake: global distribution and covariation with climate. *Science* **329**: 834–839.

Berry J, Bjorkman O. **1980**. Photosynthetic response and adaptation to temperature in higher plants. *Annual Review of Plant Physiology* **31**: 491–543.

Bolstad P, Mitchell K, Vose J. **1999**. Foliar temperature-respiration response functions for broad-leaved tree species in the southern Appalachians. *Tree physiology* **19**: 871–878.

Booth BBB, Jones CD, Collins M, Totterdell IJ, Cox PM, Sitch S, Huntingford C, Betts R a, Harris GR, Lloyd J. **2012**. High sensitivity of future global warming to land carbon cycle processes. *Environmental Research Letters* **7**: 024002.

Campbell C, Atkinson L, Zaragoza-Castells J, Lundmark M, Atkin O, Hurry V. **2007**. Acclimation of photosynthesis and respiration is asynchronous in response to changes in temperature regardless of plant functional group. *New Phytologist* **176**: 375–389.

Cavaleri MA, Reed SC, Smith WK, Wood TE. **2015**. Urgent need for warming

experiments in tropical forests. *Global Change Biology* **21**: 2111–2121.

Chambers JQ, Tribuzy ES, Toledo LC, Crispim BF, Santos J, Araújo AC, Kruijt B, Nobre AD, Trumbore SE. **2004**. Respiration from a Tropical Forest Ecosystem : Partitioning of Sources and Low Carbon Use Efficiency. *Ecological Applications* **14**: 72–88.

Ciais P, Sabine C, Bala G, Bopp L, Brovkin V, Canadell J, Chhabra A, DeFries R, Galloway J, Heimann M, *et al.* 2013. *Carbon and other biogeochemical cycles* (TF Stocker, D Qin, G-K Plattner, M Tignor, SK Allen, J Boschung, A Nauels, Y Xia, VB And, and PM Midgley, Eds.). Campbridge, United Kingdom and New York, NY, USA: Cambridge University Press.

Clark DB, Mercado LM, Sitch S, Jones CD, Gedney N, Best MJ, Pryor M, Rooney GG, Essery RLH, Blyth E, *et al.* 2011. The Joint UK Land Environment Simulator (JULES), model description – Part 2: Carbon fluxes and vegetation dynamics. *Geoscientific Model Development* **4**: 701–722.

Collins M, Knutti R, Arblaster J, Dufresne J-L, Fichefet T, Friedlingstein P, Gao X, Gutowski WJ, Johns T, Krinner G, *et al.* 2013. *Long-term climate change: Projections, commitments and irreversibility* (TF Stocker, D Qin, G-K Plattner, M Tignor, SK Allen, J Boschung, A Nauels, Y Xia, VB And, and PM Midgley, Eds.). Campbridge, United Kingdom and New York, NY, USA: Cambridge University Press.

Cramer W, Bondeau A, Woodward FI, Prentice IC, Betts RA, Brovkin V, Cox PM, Fisher V, Foley J, Friend AD, *et al.* 2001. Global response of terrestrial ecosystem structure and function to CO2 and climate change: results from six dynamic global vegetation models. *Global Change Biology* **7**: 357–373.

Cunningham S, Read J. **2002**. Comparison of temperate and tropical rainforest tree species: photosynthetic responses to growth temperature. *Oecologia* **133**: 112–119.

Cunningham SC, Read J. **2003**. Do temperate rainforest trees have a greater ability to acclimate to changing temperatures than tropical rainforest trees? *New Phytologist* **157**: 55–64.

Dewar RC, Medlyn BE, Mcmurtrie RE. **1999**. Acclimation of the respiration/photosynthesis ratio to temperature: insights from a model. *Global Change Biology* **5**: 615–622.

Diffenbaugh NS, Scherer M. **2011**. Observational and model evidence of global emergence of permanent, unprecedented heat in the 20th and 21st centuries. *Climatic Change* **107**: 615–624.

Doughty CE, Goulden ML. **2008**. Are tropical forests near a high temperature threshold? *Journal of Geophysical Research: Biogeosciences* **114**: 1–12.

Drake JE, Aspinwall MJ, Pfautsch S, Rymer PD, Reich PB, Smith R a., Crous KY, Tissue DT, Ghannoum O, Tjoelker MG. **2015**. The capacity to cope with climate warming declines from temperate to tropical latitudes in two widely distributed Eucalyptus species. *Global Change Biology* **21**: 459–472.

Drake JE, Tjoelker MG, Vårhammar A, Medlyn BE, Reich PB, Leigh A, Pfautsch S, Blackman CJ, López R, Aspinwall MJ, *et al.* 2018. Trees tolerate an extreme heatwave via sustained transpirational cooling and increased leaf thermal tolerance. *Global Change Biology* **24**: 2390–2402.

Gunderson CA, Norby RJ, Wullschleger SD. **2000**. Acclimation of photosynthesis and respiration to simulated climatic warming in northern and southern populations of Acer saccharum: laboratory and field evidence. *Tree physiology* **20**: 87–96.

Gunderson CA, O'Hara KH, Campion CM, Walker A V., Edwards NT. **2010**. Thermal plasticity of photosynthesis: the role of acclimation in forest responses to a warming climate. *Global Change Biology* **16**: 2272–2286.

Heskel MA, O'Sullivan OS, Reich PB, Tjoelker MG, Weerasinghe LK, Penillard A, Egerton JJG, Creek D, Bloomfield KJ, Xiang J, *et al.* 2016. Convergence in the temperature response of leaf respiration across biomes and plant functional types. *Proceedings of the National Academy of Sciences of the United States of America* **113**: 3832–3837.

Huang M, Piao S, Ciais P, Peñuelas J, Wang X, Keenan TF, Peng S, Berry JA, Wang K, Mao J, *et al.* 2019. Air temperature optima of vegetation productivity across global biomes. *Nature Ecology and Evolution* **3**: 772–779.

Janzen DH. **1967**. Why Mountain Passes are Higher in the Tropics. *The American Naturalist* **101**: 233–249.

Jarvi MP, Burton AJ. **2018**. Adenylate control contributes to thermal acclimation of sugar maple fine-root respiration in experimentally warmed soil. *Plant Cell and Environment* **41**: 504–516.

Kumarathunge DP, Medlyn BE, Drake JE, Tjoelker MG, Aspinwall MJ, Battaglia M, Cano FJ, Carter KR, Cavaleri MA, Cernusak LA, *et al.* 2019. Acclimation and adaptation

components of the temperature dependence of plant photosynthesis at the global scale. *New Phytologist* **222**: 768–784.

Lee TD, Reich PB, Bolstad P V. 2005. Acclimation of leaf respiration to temperature is rapid and related to specific leaf area, soluble sugars and leaf nitrogen across three temperate deciduous tree species. *Functional Ecology* **19**: 640–647.

Lloyd J, Farquhar GD. **2008**. Effects of rising temperatures and [CO2] on the physiology of tropical forest trees. *Philosophical transactions of the Royal Society of London. Series B, Biological sciences* **363**: 1811–7.

Mau A, Reed S, Wood T, Cavaleri M. **2018**. Temperate and tropical forest canopies are already functioning beyond their thermal thresholds for photosynthesis. *Forests* **9**: 47.

Medlyn BE, Dreyer E, Ellsworth D, Forstreuter M, Harley PC, Kirschbaum MUF, Le Roux X, Montpied P, Strassemeyer J, Walcroft A., *et al.* 2002a. Temperature response of parameters of a biochemically based model of photosynthesis. II. A review of experimental data. *Plant, Cell and Environment* **25**: 1167–1179.

Medlyn BE, Loustau D, Delzon S. **2002b**. Temperature response of parameters of a biochemically based model of photosynthesis. I. Seasonal changes in mature maritime pine (Pinus pinaster Ait.). *Plant, Cell and Environment* **25**: 1155–1165.

Mendes KR, Marenco RA. **2017**. Stomatal opening in response to the simultaneous increase in vapor pressure deficit and temperature over a 24-h period under constant light in a tropical rainforest of the central Amazon. *Theoretical and Experimental Plant Physiology* **29**: 187–194.

Mercado LM, Medlyn BE, Huntingford C, Oliver RJ, Clark DB, Sitch S, Zelazowski P, Kattge J, Harper AB, Cox PM. **2018**. Large sensitivity in land carbon storage due to geographical and temporal variation in the thermal response of photosynthetic capacity. *New Phytologist* **218**: 1462–1477.

Mora C, Frazier AG, Longman RJ, Dacks RS, Walton MM, Tong EJ, Sanchez JJ, Kaiser LR, Stender YO, Anderson JM, *et al.* 2013. The projected timing of climate departure from recent variability. *Nature* **502**: 183–7.

Mott KA, Peak D. **2010**. Stomatal responses to humidity and temperature in darkness. *Plant, Cell and Environment* **33**: 1084–1090.

O'Sullivan OS, Heskel MA, Reich PB, Tjoelker MG, Weerasinghe LK, Penillard A, Zhu L, Egerton JJG, Bloomfield KJ, Creek D, *et al.* 2017. Thermal limits of leaf metabolism across biomes. *Global Change Biology* **23**: 209–223.

Pan Y, Birdsey RA, Phillips OL, Jackson RB. **2013**. The Structure, Distribution, and Biomass of the World's Forests. *Annual Review of Ecology, Evolution, and Systematics* **44**: 593–622.

Pau S, Detto M, Kim Y, Still CJ. **2018**. Tropical forest temperature thresholds for gross primary productivity. *Ecosphere* **9**: 1–12.

Reich PB, Sendall KM, Stefanski A, Wei X, Rich RL, Montgomery RA. **2016**. Boreal and temperate trees show strong acclimation of respiration to warming. *Nature* **531**: 633–636.

Scafaro AP, Xiang S, Long BM, Bahar NHA, Weerasinghe LK, Creek D, Evans JR, Reich

PB, Atkin OK. **2017**. Strong thermal acclimation of photosynthesis in tropical and temperate wet-forest tree species: The importance of altered Rubisco content. *Global Change Biology* **23**: 2783–2800.

Sendall KM, Reich PB, Zhao C, Jihua H, Wei X, Stefanski A, Rice K, Rich RL, Montgomery RA. **2015**. Acclimation of photosynthetic temperature optima of temperate and boreal tree species in response to experimental forest warming. *Global Change Biology* **21**: 1342–1357.

Slot M, Garcia MA, Winter K. **2016**. Temperature response of CO 2 exchange in three tropical tree species. *Functional Plant Biology* **43**: 468–478.

Slot M, Krause GH, Krause B, Hernández GG, Winter K. **2019**. Photosynthetic heat tolerance of shade and sun leaves of three tropical tree species. *Photosynthesis Research* **141**: 119–130.

Slot M, Rey-Sánchez C, Gerber S, Lichstein JW, Winter K, Kitajima K. **2014**. Thermal acclimation of leaf respiration of tropical trees and lianas: Response to experimental canopy warming, and consequences for tropical forest carbon balance. *Global Change Biology* **20**: 2915–2926.

Slot M, Winter K. **2017**. Photosynthetic acclimation to warming in tropical forest tree seedlings. *Journal of Experimental Botany* **68**: 2275–2284.

Slot M, Winter K. **2018**. High tolerance of tropical sapling growth and gas exchange to moderate warming. *Functional Ecology* **32**: 599–611.

Smith NG, Dukes JS. **2013**. Plant respiration and photosynthesis in global-scale models:

Incorporating acclimation to temperature and CO2. *Global Change Biology* **19**: 45–63.

Smith NG, Dukes JS. **2017**. Short-term acclimation to warmer temperatures accelerates leaf carbon exchange processes across plant types. *Global Change Biology*: 4840–4853.

Smith NG, Malyshev SL, Shevliakova E, Kattge J, Dukes JS. **2016**. Foliar temperature acclimation reduces simulated carbon sensitivity to climate. *Nature Climate Change* **6**: 407–411.

Urban J, Ingwers MW, McGuire MA, Teskey RO. **2017**. High temperature opens stomata and decouples net photosynthesis from stomatal conductance in Pinus taeda and Populus deltoides x nigra. *Journal of Experimental Botany* **68**: 1757–1767.

Vanderwel MC, Slot M, Lichstein JW, Reich PB, Kattge J, Atkin OK, Bloomfield KJ, Tjoelker MG, Kitajima K. **2015**. Global convergence in leaf respiration from estimates of thermal acclimation across time and space. *The New phytologist*.

Vårhammar A, Wallin G, Mclean CM, Dusenge ME, Medlyn BE, Hasper TB, Nsabimana D, Uddling J. **2015**. Photosynthetic temperature responses of tree species in Rwanda: Evidence of pronounced negative effects of high temperature in montane rainforest climax species. *New Phytologist* **206**: 1000–1012.

Way DA, Yamori W. **2014**. Thermal acclimation of photosynthesis: On the importance of adjusting our definitions and accounting for thermal acclimation of respiration. *Photosynthesis Research* **119**: 89–100.

White A, Cannell MGR, Friend AD. **2000**. CO2 stabilization, climate change and the terrestrial carbon sink. *Global Change Biology* **6**: 817–833.

Wright SJ, Muller-Landau HC, Schipper J. **2009**. The future of tropical species on a warmer planet. *Conservation Biology* **23**: 1418–1426.

Wright IJ, Reich PB, Atkin OK, Lusk CH, Tjoelker MG, Westoby M. **2006**. Irradiance, temperature and rainfall influence leaf dark respiration in woody plants: Evidence from comparisons across 20 sites. *New Phytologist* **169**: 309–319.

Zhou H, Xu M, Pan H, Yu X. **2015**. Leaf-age effects on temperature responses of photosynthesis and respiration of an alpine oak, Quercus aquifolioides, in southwestern China. *Tree physiology*: tpv101-.

2 Photosynthetic responses to temperature across the tropics: a meta-analytic approach

2.1 Abstract

Tropical forests exchange more carbon dioxide with the atmosphere than any other terrestrial biome on Earth. Yet, uncertainty in the projected global carbon balance over the next century is ~3 times greater for the tropics than for any other latitude. Our poor knowledge of tropical plant physiological responses to climate change – particularly photosynthetic responses – has been identified as one of the greatest sources of uncertainty in multiple efforts to estimate and forecast the global terrestrial carbon sink. Furthermore, tropical regions are expected to experience temperatures beyond their historical climate ranges within the next two decades, and evidence suggests that tropical forest canopies are already operating beyond thermal thresholds for photosynthesis. We used a meta-analytic approach to help reduce the gap in our understanding of tropical tree photosynthetic temperature sensitivity. We gathered 16 published and unpublished photosynthetic temperature response datasets from tropical biomes spanning different temperature, rainfall, and elevation gradients, representing 60 (net photosynthesis) and 33 (biochemical rates of photosynthesis) species. We investigated how photosynthetic parameters, including both net photosynthetic (A_{net}) and biochemical components of photosynthesis, maximum electron transport (J_{max}) and maximum Rubisco carboxylation (V_{cmax}), responded to a suite of environmental drivers, including mean yearly temperature, yearly temperature range, and precipitation. Optimum temperatures for A_{net} increased with mean annual temperature (MAT), and the intercept and slope of this response was similar to global trends. Optimum temperature of V_{cmax} and J_{max} also

increased with MAT; however, slopes and intercepts were lower than trends found globally. This suggests that separate algorithms should be used when including J_{max} and V_{cmax} in tropical vegetation responses to temperature in global carbon models. Light played an important role in predicting A_{net} responses to temperature; however, we need more studies that include information on plant growth environment and strategy to more accurately model tropical photosynthetic responses to climate. In addition, we found that J_{max} might play a more prominent role in limiting A_{net} than V_{cmax} in tropical forests, a trend that is divergent to global findings. This research will improve modeling efforts to quantify tropical ecosystem carbon cycling and provide more accurate representations of how these key ecosystems will respond to altered temperature and rainfall patterns under climate warming.

2.2 Introduction

Tropical forests have been characterized as one of the regions with the most uncertainty regarding the accuracy in which large scale models can estimate carbon fluxes (Booth *et al.* 2012; Cavaleri *et al.* 2015; Lombardozzi *et al.* 2015; Mercado *et al.* 2018). Addressing this information gap is critical because tropical forests have high biomass and store large amounts of carbon (Dixon *et al.* 1994; Pan *et al.* 2013), and alterations in tropical forest carbon uptake could significantly impact global carbon cycling (Anderegg *et al.* 2015). Historically, these forests have been thought to have little capacity to acclimate to changes in growth temperature because they have evolved under reduced thermal ranges compared to other biomes (Janzen 1967; Read 1990; Battaglia *et al.* 1996; Cunningham and Read 2002). In addition, these forests are expected to surpass their historical climate margin within the next quarter century (Williams *et al.* 2007), a trend expected to occur earlier for the tropics than other global regions (Diffenbaugh & Scherer, 2011; Mora *et al.*, 2013). Tropical forests are already thought to be operating near or outside of their photosynthetic thermal thresholds (Doughty and Goulden 2008; Vårhammar *et al.* 2015; Mau *et al.* 2018), making them particularly vulnerable to the impacts of climate warming.

Due to high uncertainties within tropical biomes, better representation of vegetation processes is needed to more accurately inform Earth system and dynamic vegetation models (Friedlingstein *et al.* 2006; Matthews *et al.* 2007; Booth *et al.* 2012; Rogers 2016). In particular, quantifying photosynthetic temperature responses will help to minimize model uncertainty (Matthews *et al.* 2007; Booth *et al.* 2012). Photosynthesis

has a peaked response to temperature, where the rate of photosynthesis increases and then declines after the optimum temperature (T_{opt}; Table 2.1) is reached. We can investigate the drivers of temperature dependent photosynthetic declines by investigating the biochemical processes that control photosynthesis. These biochemical processes include the maximum rate of CO_2 fixation by Rubisco (V_{cmax}) and the maximum rate of photosynthetic electron transport (J_{max}), which are derived from well-established kinetic models (Farquhar *et al.* 1980; von Caemmerer and Farquhar 1981). Global vegetation models rely on temperature responses of these underlying mechanisms controlling photosynthesis to accurately predict carbon uptake at larger scales (Lin *et al.* 2012; Smith and Dukes 2013; Mercado *et al.* 2018).

There have been important and robust efforts to quantify these photosynthetic response parameters at the global scale (Medlyn *et al.* 2002; Kattge and Knorr 2007; Kumarathunge *et al.* 2019); however, quantifying these processes within biomes can also be important to help us understand how temperature responds both at global and regional scales (Mercado *et al*. 2018). These studies have shown that species can acclimate to their growth environment, and algorithms developed in Kattge and Knorr (2007) have been implemented in some Earth system and vegetation models to more accurately represent photosynthetic acclimation (e.g. Arneth *et al.* 2012; Lombardozzi *et al.* 2015; Smith *et al.* 2016; Mercado *et al.* 2018). However, Kattge and Knorr (2007) were unable to represent tropical species in their meta-analysis; therefore, carbon models often incorporate temperature responses into models without including the tropical biome. More recently, Kumarathunge *et al.* (2019) published updated algorithms that included six datasets from

tropical forests that will undoubtedly improve global carbon models. Even so, because tropical forests cycle a disproportionate amount of carbon, a specific quantification of tropical photosynthetic responses to temperature alone will help minimize uncertainty (Booth *et al.* 2012).

There is strong evidence suggesting that, globally, T_{opt} is determined by its growth temperature (Berry and Bjorkman 1980; Kattge and Knorr 2007; Kumarathunge *et al.* 2019); however, it is still unclear if this holds true within tropical ecosystems. Genetic variation, along with growth temperature, plays an important role in determining species ability to acclimate and adjust to their growth temperature (Berry and Bjorkman 1980; Yamori *et al.* 2014), and common garden datasets on tropical species suggest that species from warm climates have a lesser ability to acclimate to a warmer growth temperature than those from colder climates (Cunningham and Read 2003; Vårhammar *et al.* 2015). Studies that have investigated the T_{opt} in tropical forests have found evidence that T_{opt} is either closely associated with mean (Vargas and Cordero 2013, Kositsup *et al.* 2009, Tan *et al.* 2017) or maximum temperature (Read 1990; Slot and Winter 2017a; Mau *et al.* 2018); however, it is still unknown if tropical forest, overall, follow similar trends as more global analyses (e.g. Kattge and Knorr 2007; Kumarathunge *et al.* 2019). The few examples of tropical J_{max} optimum temperature (T_{optJ}) and V_{cmax} optimum temperature (T_{optV}) within tropical forests suggests that both variables are closely associated with their growth temperatures (Vårhammar *et al.* 2015; Slot and Winter 2017c). Additionally, a common garden study by Vårhammar *et al.* (2015) found that tropical species that operate under a lower diurnal temperature range have a lower optimum temperature for

J_{max} than species that are native to environments with larger ranges in diurnal temperature; although, species with higher diurnal ranges also had higher maximum temperatures in their home climate. This variation in 'controls' of photosynthetic responses suggest that, in order to more accurately model global carbon fluxes, we need a better understanding of the drivers of temperature response. More, we have little understanding of how strong of a role other climate factors, such as precipitation, might play in determining tropical photosynthetic temperature responses.

Factors other than the growth climate, such as plant functional type, growth strategy (i.e. functional or successional type) and conditions, can also impact plant photosynthetic responses to temperature. Growth strategies are often characterized by their 'economy', with some strategies, such as early successional species and lianas, incorporating a fast growth strategy, while others, such as late successional and evergreen species employing a slower growth strategy (Bloom *et al.* 1985, Box *et al.* 1996; Wright *et al.* 2004; Michaletz *et al.* 2016). Trees of contrasting growth forms differ in their overall photosynthetic rates (Koike *et al.* 2001; Santiago and Wright 2007) and biochemical capacities (Medlyn *et al.* 2002). Studies have also shown that optimum temperature across different functional types in different biomes can vary (Medlyn *et al.* 2002, Yamori *et al.* 2014). Recent studies of canopy species in Panama found that early successional seedlings had a higher T_{opt} than late successional seedlings (Slot *et al.* 2016, Slot & Winter, 2018), although, the difference in T_{opt} may diminish with ontogeny changes, especially when species are existing under similar growth temperatures (Slot and Winter 2017a). Early successional forests have more variable surface temperature

fluxes than late successional (Cao and Sanchez-Azofeifa 2017); therefore, they may have adapted a greater ability to adjust T_{opt} to their growth environment. While our understanding of T_{opt} and growth form is still limited in tropical ecosystems, early evidence suggests that T_{opt} will be higher in the dynamic environment of early successional forests.

In addition to successional strategy, different plant functional types, or growth forms, may employ different temperature responses. Shorter lived leaves have a greater variability in leaf phenotypes, making them more responsive to seasonal changes (Kitajima *et al.* 1997). Compared to longer-lived evergreen leaves, shorter-lived deciduous leaves tend to have a lesser ability to thermally regulate their leaves (Michaletz *et al.* 2016); instead they have wider widths of their photosynthetic temperature response curve, or thermal niches (Michaletz *et al.* 2016). Evergreen species have been found to be less able to acclimate their growth rates to warmer temperatures than deciduous species (Way and Oren 2010). This, in addition to longer-lived leaves having more narrow thermal niches and lower rates of photosynthesis (Michaletz *et al.* 2016), suggests that evergreen and deciduous species may have different capabilities to respond to their growth environment.

Growth conditions, such as light conditions, may also play a role in controlling plant photosynthetic responses to temperature. Models of canopy photosynthesis and global primary productivity often separate leaves into ‘sun’ leaves and ‘shade’ leaves as they have different responses to irradiance (Sinclair *et al.* 1976; De Pury and Farquhar 1997; Wang and Leuning 1998; Ryu *et al.* 2011). Because leaf temperature is strongly

controlled by irradiance (Rey-Sánchez *et al.* 2016; Fauset *et al.* 2018), it follows that sun leaves that have developed under higher irradiance are acclimated to operate at higher temperatures. Even so, comparisons of leaves growing in different light environments in tropical forests have found large differences in photosynthetic capacity but little to no differences in photosynthetic temperature responses between sun and shade leaves (Pearcy 1987; Slot *et al.* 2019). The limited evidence that we have comparing tropical temperature responses of sun and shade leaves suggest that light may play a large role in controlling the overall rate of photosynthesis but less so for leaves' photosynthetic temperature responses.

In order to better understand tropical net photosynthetic and biochemical responses to temperature, we used a meta-analytic approach to quantify how common temperature response parameters respond to different climate and growth environment factors. We hypothesized that T_{opt} will be more closely correlated with mean annual temperatures (MAT) than other primary climate variables (mean annual precipitation, MAP; yearly temperature range, T_{range}). We then aimed to develop a model including four, easy to quantify, environmental drivers to best predict the temperature parameters of both net photosynthesis and the biochemical reactions driving photosynthesis. We further hypothesized that incorporating the plant's growth light environment (either sun or shade) would improve explanatory power of the 'best' prediction model that quantify the rates of photosynthesis but not for models that quantify the T_{opt} or the photosynthetic thermal niche (Ω). Lastly, we compared temperature response variables of leaves grown in different environments (light environment and *in*/*ex situ*), plant functional types

(evergreen or semi-deciduous), and growth strategy (early, mid, late successional). We hypothesized that sun leaves would have higher photosynthetic capacities than shaded leaves; however, T_{opt} would not differ between light environments. Additionally, we hypothesized that early successional species would have a higher T_{opt} than late successional species and evergreen leaves would have more narrow thermal niches but lower T_{opt} than semi-deciduous species.

2.3 Methods

2.3.1 Meta-analysis data collection and selection

For this meta-analysis, we gathered datasets where photosynthetic measurements were collected at different leaf temperatures on woody species within a tropical forest. These data come in the form of net photosynthesis (A_{net}) vs leaf temperature (T_{leaf}) response curves, biochemical responses (V_{cmax} and J_{max}) vs T_{leaf} response curves (estimated from net assimilation response to different leaf internal CO_2 concentrations, AC_i curves, measured at different temperatures), A_{max} vs T_{leaf} response curves (estimated from light response curves, or A_{net} response to different irradiances, at different temperatures), and measurements of A_{net} and AC_i curves at multiple ambient temperatures through time. Data were gathered from any ecosystem within the tropical latitudes, including tropical montane systems. Climate data were collected from the WorldClim database (Fick & Hijmans, 2017) using provided latitude and longitudinal data. Data were extracted from the WorldClim database using the 'getData' function in the 'raster' package in R version 3.5.0 (R Core Team 2018). Successional stage and growth form (deciduous or evergreen) were either provided by the contributing data author or found

within the literature. Species that were classified as “pioneer” and “shade-intolerant” were designated as a “early successional” species. If the species was classified as “shade-tolerant” the species was considered “late successional”, and some of the A_{net} dataset species were classified as “mid successional”. We gathered data in two ways 1) contribution of raw photosynthesis response to temperature data and 2) extraction from published articles. Data were digitized from published articles using Digitize It 2016 version 4.2.0 software (Alcasa). Raw data was provided from both published and unpublished sources. Some of the datasets that were shared with us also included a ‘treatment’ warming effect. For these data, we only used leaves grown in the ‘control’ environment.

2.3.2 Net photosynthesis parameter extraction

In most cases, parameter means of different species and canopy class (shaded or sun) from the same study were treated as separate, independent samples (Curtis and Wang 1998). In some studies, there was a wide range of species measured across a range of temperatures, and species had to be combined to fit the temperature response curve (see Table 2.2 for details on data summary).

The net photosynthetic temperature optimum of each sample was extracted from a peaked curve (June *et al.* 2004):

$$A_{net} = A_{opt} \times e^{-\left(\frac{T_{leaf} - T_{opt}}{\Omega}\right)} \qquad \text{Equation 1}$$

Where A_{net} (μmol m^{-2} s^{-1}) is the rate of net assimilation at the leaf temperature (T_{leaf}) in °C, T_{opt} (°C) is the optimum temperature for photosynthesis, and A_{opt} (μmol m^{-2} s^{-1}) is the rate of photosynthesis at T_{opt}. Ω, or net photosynthetic thermal niche, is the temperature where photosynthesis declines to 37% of A_{opt}. Ω (°C) describes the width of the response curve, where wide curves have a higher Ω and narrower curves have a lower Ω. Prior to fitting Equation 1, A_{net} outliers greater than two standard deviations from the mean for each sample were removed from the dataset. In addition, datapoints with $Ci < 0$ were removed as they were determined to be bad measurements. In total, we removed 256 data points, less than 2% of our data.

To compare the rates of net photosynthesis across studies, we extracted the rate of photosynthesis at 25 °C (A_{25}) by allowing T_{leaf} to equal 25 in Equation 1 for each set of extracted temperature parameters. Using similar methods as Kumarathunge *et al.* (2019), we further increased the size of our dataset by extracting A_{net} values from AC_i curves. For these data, we extracted the first data point from each AC_i curve where the data point was taken at ambient CO_2 concentrations. A_{net} values were only kept if the CO_2 concentrations were between 300 and 410 ppm. 40 additional curves were added to the A_{net} dataset using this method. One dataset measured light response curves at different temperatures. The light saturated rate of photosynthesis (A_{max}) was estimated by extracting the light saturated photosynthetic rate from light response curves using a non-rectangular curve (Marshall and Biscoe 1980), and fitting A_{max} to Equation 1. Temperature response curves were removed if T_{opt} or A_{opt} were over or under estimated by Equation 1. A total of 74

A_{net} temperature response curve samples were successfully extracted using Equation 1. Ω was negative for one of the curves; therefore, Ω sample size was 73.

2.3.3 Biochemical parameter extraction

Biochemical rates, J_{max} and V_{cmax}, were estimated from photosynthetic response to internal CO_2 concentration (AC_i) curves. Most datasets collected AC_i curves starting at an ambient CO_2 concentration, 360-410 ppm. AC_i curves were collected by gradually decreasing the CO_2 below ambient concentrations (as low as 0 ppm). CO_2 concentrations were then brought back up to ambient concentrations and then gradually brought above ambient, saturating conditions (up to 2100 ppm). Measurements were made at each 'step' as CO_2 concentrations were controlled above and below ambient conditions. Prior to fitting the AC_i curves, datapoints with C_i less than 0 and greater than 2500 ppm were removed from the dataset as they were outside of the range of CO_2 concentration given to the leaf. We further removed datapoints where A_{net} was less than -10 and greater than 70 μmol m^{-2} m^{-1} as they were not considered reasonable A_{net} rates. In total we removed less than 0.5% of total AC_i datapoints. J_{max} and V_{cmax} were extracted using the 'fitaci' function from the 'plantecophys' package (Duursma 2015) in R version 3.5.0 (R Core Team, 2018), which extracts parameters using the Farquhar, von Caemmerer, and Berry model (FvCB model; (Farquhar *et al.* 1980, von Caemmerer and Farquhar 1981)). We looked at the fitted plots for each curve with RMSE > 5.0 and individually removed curves with poor fits, with a final overall RMSE of 2.67. We further removed curves where J_{max} and V_{cmax} values were less than 0 μmol m^{-2} s^{-1}. After the initial data removal, we removed

outliers where J_{max} or V_{cmax} were greater than two standard deviations from the mean J_{max} and V_{cmax} values, removing a total of 16.5% of our total curves.

Temperature response parameters for J_{max} and V_{cmax} were extracted using the peaked Arrhenius function (Medlyn *et al.* 2002):

$$(T_k) = (k_{opt}) \frac{H_d \exp\left(\frac{H_a(T_k - T_{opt})}{(T_k R T_{opt})}\right)}{H_d - H_a[1 - \exp\left(\frac{H_d(T_k - T_{opt})}{(T_k R T_{opt})}\right)]} \qquad \text{Equation (2)}$$

where T_k is the measured leaf temperature in Kelvin, (k_{opt}) is the value of J_{max} or V_{cmax} at the optimum temperature (μmol m^{-2} s^{-1}), H_a is the activation energy in the Arrhenius function (kJ mol^{-1}), or exponential increase in J_{max} or V_{cmax} before T_{opt}, H_d is the decrease in J_{max} or V_{cmax} after T_{opt} (kJ mol^{-1}), R is the universal gas constant (8.314 $JK^{-1}mol^{-1}$). To avoid over-parameterization of the temperature responses function, we set H_d = 200 kJ mol^{-1} and estimated T_{opt}, k_{opt}, and H_a from Equation 2. Similar to the A_{net} parameter extractions, we extracted the rate of V_{cmax} (V_{25}) and J_{max} (J_{25}) at 25 °C by setting T_k equal to 298.15 K. Curves were removed if T_{opt}, k_{opt}, or H_a values were over or underestimated, resulting in 30 V_{cmax} and 33 J_{max} good temperature response curves.

2.3.4 Meta-analytic statistical analyses

Biases for effect size were accounted for by weighting each extracted parameter with the number of observations what were used in each temperature response curve. The weighting factor was calculated as (Hedges and Olkin 1985; Gurevitch *et al.* 1992):

$$J = 1 - \left(\frac{3}{4(n-1)}\right) \qquad \text{Equation 3}$$

where J is the weighting factor and n is the number of datapoints used to fit each temperature response curve. The weighted mean was incorporated into the linear model by adding 1/J into the 'weights' component of the 'lm' function in base R version 3.5.0 (R Core Team, 2018).

Stepwise regressions of climate (mean annual temperature, MAT; mean annual precipitation, MAP, yearly mean temperature range, T_{range}; altitude) and leaf light environment (sun or shade) were used to select the best fit model to predict T_{opt}, T_{optJ}, T_{optV}, A_{25}, V_{25}, J_{25}, Ω, E_{aV}, and E_{aJ}. We used the variance inflation factors (VIF) to test for collinearity between independent variables. When VIF of a predictor in the best fit model was greater than 5, the variable was removed from the model (Zuur *et al.* 2009). Altitude often had a high VIF when added to a model with MAT and we found that altitude was highly correlated with mean annual temperature (MAT) (Fig. 2.1). We removed altitude as a continuous variable and grouped the data into four altitudinal groups (0-500m, 500-

1000m, 1000-2000m, and >2000m). Mean annual temperature (MAT), mean annual precipitation (MAP), mean annual temperature range, 'altitude group', and light environment were used in the A_{net} parameter (T_{opt}, A_{25}, Ω) stepwise model selections. Due to a limited sample size, neither light conditions nor altitude groups were included in the biochemical parameter (T_{optJ}, T_{optV}, V_{25}, J_{25}, E_{aV}, E_{aJ}) model selection. Additionally, bivariate regression analyses were used to investigate relationships between A_{net} and biochemical parameters (T_{opt}, T_{optJ}, T_{optV}, A_{25}, V_{25}, J_{25}, Ω, E_{aV}, and E_{aJ}) and each climate variable. Student's *t* tests or ANOVAs were used to compare plant functional type, successional strategy, and growth conditions. Due to available characterizations for our dataset, light environment (sun or shade) and plant functional type (deciduous or evergreen) were compared for A_{net} parameters only and growth environment (*in* or *ex situ*) were only compared for biochemical parameters. Successional strategy (early, mid, or late) was compared for both A_{net} and biochemical parameters; however, mid and late successional species had to all be combined into 'late successional' for the biochemical parameters.

2.4 Results

2.4.1 Primary climate variable influences on temperature parameters

All three climate variables were correlated with the net photosynthetic optimum temperatures (T_{opt}), temperature was the only variable that influenced the optimum temperature of maximum Rubisco carboxylation (T_{optV}), and both temperature and precipitation were correlated with the temperature optimum of the maximum rate of electron transport (T_{optJ}). T_{opt} was positively correlated with mean annual temperature

(MAT), where MAT alone explained 36% of T_{opt} variance (Fig. 2.2A; Table 2.3). T_{opt} had a polynomial response to mean annual precipitation (MAP; $r^2 = 0.10$) and decreased with increasing mean annual temperature range (T_{range}; $r^2 = 7\%$) (Figs. 2.2B-C; Table 2.3). T_{optV} increased with MAT but was not correlated with either MAP or T_{range} (Figs. 2.2D-F). T_{optJ} increased with both MAT and MAP, with each individually explaining 19 and 18%, respectively, of T_{optJ} variance (Fig. 2.2G,H; Table 2.3). T_{optJ} was not correlated with T_{range} (Fig. 2.2I).

While net photosynthesis at 25 °C (A_{25}) did not how clear relationships with climate variables, the rate of both maximum Rubisco carboxylation (V_{cmax}) and maximum electron transport (J_{max}) at 25 °C (V_{25} and J_{25}) decreased with warmer and wetter climate. A_{25} was not correlated with MAT, MAP, or T_{range} (Fig. 2.3A-C; Table 2.3). V_{25} and J_{25} at 25 °C both decreased as MAT and MAP increased; whereas, neither variable was influenced by T_{range} (Fig. 2.3D-I; Table 2.3). The ratio between J_{max} and V_{cmax} at 25 °C ($J:V$) decreased with both increasing temperature and precipitation and had a peaked response to mean annual temperature range. $J:V$ decreased as MAT and MAP increased, which explained 34% and 29% of $J:V$ variation (Fig. 2.5A,B; Table 2.3). Finally, T_{range} explained 50% of $J:V$ variation and the response had a polynomial trend (Fig. 2.5C).

Net photosynthetic thermal niche (Ω) was broader in warmer forests, while activation energy for both V_{cmax} and J_{max} showed different relationships with climate variables. Ω was positively correlated with MAT, which explained 9% of Ω variance and neither MAP nor T_{range} were correlated with Ω (Fig. 2.4A-C; Table 2.3). E_{aV}, which

describes the exponential increase in V_{cmax} before T_{optV}, did not respond to any climate variable (Fig. 2.4D-F). The activation energy of photosynthetic electron transport (E_{aJ}) was positively correlated with both MAT and MAP, which alone each described 19% and 17% of E_{aJ} variation (Figs 2.4G,H). T_{range} was not correlated with E_{aJ} (Fig. 2.4I; Table 2.3).

2.4.2 Multivariate model selection

Mean annual temperature and light were important predictors in the 'best fit' model for net photosynthetic temperature response variables (T_{opt} and Ω); while climate predictors alone were not strong predictors of the photosynthetic rate (A_{25}). There was a strong correlation between MAT and altitude for both the A_{net} ($p < 0.001$; $r^2 = 0.92$) and V_{cmax}/J_{max} datasets ($p < 0.001$; $r^2 = 0.96$; Fig. 2.1); therefore, altitude was not included as a continuous variable in our model. We added 'altitude' to the A_{net} predictive models only by grouping the data into altitudinal groups (0-500m, 500-1000m, 1000-2000m, and did group data into different altitude groups for the A_{net} model selection only. The altitude grouping variable was not selected for any best fit A_{net} models (Table 2.4). T_{opt} was best predicted by MAT, MAP, T_{range}, and the interaction between MAP and light environment (sun or shaded) and explained 49% of T_{opt} variation ($p < 0.001$; $F_{4,71} = 19.02$, Tables 2.4,2.5). Model selection for A_{25} only included the light environment and no climate variables (Table 2.4). The light environment only includes two categorical variables; therefore, this factor alone cannot be used as a predictive model for A_{25}. To build a predictive model, the "light environment" variable was removed. The full model was re-ran with MAT, MAP, T_{range}, altitude group, and interactions between climate variables

and altitude group/light. The model selected after rerunning the model only included T_{range} which, alone, was not a strong predictor of A_{25} ($p = 0.859$, $F_{1,74} = 0.032$, Tables 2.4,2.5). Ω best fit model included MAT and light environment with no interactions and the interaction between the light environment and T_{range} (Table 2.4). The model explained 31% of Ω variability ($p < 0.001$; $F_{4,68} = 9.02$; Table 2.5).

MAT was the best predictor of most biochemical component parameters of photosynthesis; although, MAP was the best predictor for V_{25} and H_{aV}. Because we were limited by the number of V_{cmax} and J_{max} samples, we only included the main effects of the three continuous categorical variables (MAT, MAP, and T_{range}) in the J_{max} and V_{cmax} temperature response parameter model selection. MAT was the only predictor included in the best model T_{optV} model and explained 12% of T_{optV} variation ($p = 0.047$; $F_{1,24} = 4.40$). MAP was the only predictor included in the other two V_{cmax} temperature response parameters (Table 2.4), where MAP explained 24% of V_{25} ($p = 0.006$; $F_{1,24} = 4.40$) and only 6% of H_{aV} variation ($p = 0.063$; $F_{1,24} = 2.67$; Table 2.5). MAT was the only predictor in the best model for all J_{max} variables (Table 2.4) and explained 19% of T_{optJ} ($p = 0.008$; $F_{1,29} = 8.19$), 42% of J_{25} ($p < 0.0001$; $F_{1,29} = 22.69$), and 19% of H_{aJ} variation ($p = 0.009$; $F_{1,29} = 7.80$; Table 2.5). Similarly, MAT was the only predictor in the best fit model for $J:V$ and explained 34% of $J:V$ variation ($p = 0.003$; $F_{1,20} = 11.86$; Table 2.4,2.5).

2.4.3 Growth environment influences on temperature response parameters

A_{25} was higher in sun compared to shade leaves but T_{opt} and Ω was not different between light environments. Sun and shade leaf T_{opt} were not different from one another

(Student's *t* test; p = 0.079; Fig. 2.6A). A_{25} was ~65% higher in sun leaves compared to shaded leaves (p = 0.004; Fig. 2.6B). Similar to T_{opt}, there was no difference in Ω between the two light environments (p = 0.386; Fig. 2.6C).

Whether the plants were grown *in situ* or *ex situ* did not affect the V_{cmax} temperature response parameters (T_{optV}, V_{25}, E_{aV}); however, temperature response parameters associated with J_{max} had lower rates (J_{25}) but higher optimum temperatures and activation energy (T_{optJ}, E_{aJ}) for species grown *in situ*. Neither T_{optV} (Student's *t* test p = 0.074), V_{25} (p = 0.065), nor E_{aV} (p = 0.104) differed between plants grown *in situ* and *ex situ* (Fig. 2.7A,C,E); although, they did follow a similar trend to J_{max} parameter results (Fig. 2.7B,D,F). T_{optJ} was ~3.5 C higher in plants grown *in situ* compared to *ex situ* grown plants (p = 0.032, Fig. 2.7B). J_{25} was ~50% lower (p = 0.017, Fig. 2.7D) and E_{aJ} was 50% higher for *in situ* compared to *ex situ* grown leaves (p = 0.024, Fig 2.7F). Lastly, *J:V* was higher by 25% when grown *ex situ* compared to *in situ* (p = 0.012, Fig. 2.7G).

2.4.4 Plant functional and successional type influences on temperature response parameters

T_{opt} was higher in semi-deciduous species compared to evergreen species but there were no differences in A_{25} and Ω between the two plant functional types. T_{opt} was ~1 °C higher in semi-deciduous compared to evergreen species (p = 0.013; Fig. 2.8A). There were no differences between evergreen and deciduous species for both A_{25} (p = 0.108; Fig. 2.8B) and Ω (p = 0.070; Fig. 2.8C).

There were limited A_{net} parameter differences between successional types; however, Ω in early successional species was higher than in late successional species. There were no differences between successional types for either T_{opt} (ANOVA p = 0.572; Fig. 2.9A) or A_{25} (p = 0.699; Fig. 2.9B); however, Ω did have a significant successional type effect (p = 0.037). *Posthoc* Tukey tests showed that late successional species Ω was almost half that of early successional species (p = 0.029); however, there were no differences between early – mid and mid-late successional species (p = 0.149 and p = 0.916 respectively; Fig. 2.9C).

Early successional species had a higher V_{25} compared to late successional species but there were no differences found for any other biochemical temperature response variables. Due to limited datasets, J_{max} and V_{cmax} parameter 'mid successional' data were labeled as 'late successional' and successional types were compared using Student's t-tests. Neither T_{optV} nor T_{optJ} showed differences between early and late successional species (p = 0.807 and p = 0.185 respectively; Fig. 2.10A,B). Early successional species mean V_{25} was almost double that of late successional species (p = 0.032; Fig. 2.10C), but there were no J_{25} differences between successional types (p = 0.090; Fig. 2.10C). In addition, there were no differences between successional types for E_{aV} (p = 0.651; Fig. 10E), E_{aJ} (p = 0.120; Fig. 2.10F), or $J:V$ (p = 0.338; Fig. 2.10G).

2.5 Discussion

2.5.1 Climate drivers of the optimum temperature of photosynthesis

Globally (Kattge and Knorr 2007; Kumarathunge *et al.* 2019) and in tropical ecosystems (Tan *et al.* 2017), studies have found that the optimum temperature increases as growth temperatures increase. In contrast, Medlyn *et al.* (2002) found little evidence for a correlation between the optimum temperature and growth temperature; however, species growing in boreal climates did have lower optimum temperatures than species in temperate regions, and tropical species were not represented (Medlyn *et al.* 2002). In support of our first hypothesis, the optimum temperatures of net photosynthesis (T_{opt}), maximum Rubisco carboxylation (T_{optV}), and photosynthetic electron transport (T_{optJ}) all increased with increasing mean annual temperature (MAT; Fig. 2.2A,D,G). In addition, the slope and intercept of our tropical species responses to MAT (14.9(2.3)β_0 + 0.6(0.1)MAT; Table 2.3), is similar to a global analysis of T_{opt} response to growth temperature (T_{growth}; 12.5(1.4)β_0 + 0.62(0.1)T_{growth}; Kumarathunge *et al.* 2019), suggesting that similar T_{opt} algorithms can be used to model both tropical and global photosynthetic temperature responses. Our results for V_{cmax} and J_{max} were not as consistent with Kumarathunge *et al.* (2019) results, where T_{optV} and T_{optJ} had a higher intercepts and lower slopes (T_{optV}: 33.17(3.17)β_0 + 0.27(0.13)MAT; T_{optJ}: 25.4(3.9)β_0 + 0.27(0.5)MAT; Table 2.3) than the global analysis (T_{optV}:24.3(3.8)β_0 + 0.71(.2)T_{growth}; T_{optJ}: 19.9(2.9)β_0 + 0.63(0.2)T_{growth}; Kumarathunge *et al.* 2019). The higher intercepts seen in the tropical species is likely the result of the higher temperature experienced in tropical regions. The lower slope is likely also, in part, influenced by the smaller

temperature ranges that these species experience compared to the global analysis. Additionally, the lower T_{optV} and T_{optJ} MAT slope response provides some support for the common hypothesis that tropical species may have a lesser capability to acclimate to warmer temperatures due to their more narrow climatic envelopes (Janzen 1967; Cunningham and Read 2003). It should be noted, however, that our J_{max} and V_{cmax} datasets cover MAT at a smaller range than our A_{net} dataset and additional datasets measuring these biochemical parameters would provide greater clarity on how temperature responses of these parameters differ from more global datasets.

As we hypothesized, precipitation alone did not play as large of a role in predicting photosynthetic temperature responses. The only net photosynthetic parameter correlated with MAP was T_{opt} which had a peaked response, where T_{opt} began declining at around 2500 mm MAP (Fig. 2.2B). The three datasets above 2500 mm MAP are from contrasting MAP (22.9 - 26.2 °C), suggesting that there may be a precipitation threshold for tropical species T_{opt}. Compared with temperature, fewer studies have investigated the responses of the optimum temperature to rainfall; however, recent, more limited, studies have found that T_{opt} increases as soils dry in a Puerto Rican tropical forest (Carter *et al.* unpublished; Ch. 3 Fig. 3.5C,D) and savanna grassland ecosystem (Ma *et al.* 2017). Although A_{25} did not respond to MAP (Fig. 2.2B), both V_{25} and J_{25} decline with increasing MAP (Fig. 2.2E,H). The wettest sites in the J_{max} and V_{cmax} datasets, however, corresponded with the warmest sites in the MAT (Table 2.2). Since J_{25} and V_{25} both decreased with increasing temperature, MAT could have been the actual driver of the J_{25} and V_{25} response to precipitation. To date, the few studies that have investigated large-

scale environmental controls on the biochemical components of photosynthesis focus solely on how temperature controls these important model parameters (Kattge and Knorr 2007; Tan *et al.* 2017; Kumarathunge *et al.* 2019). As both temperature and rainfall play important roles in modeled carbon reductions in the Amazon rainforest (Galbraith *et al.* 2010), future studies should investigate how other climate factors, such as rainfall, influence photosynthetic optimum temperatures.

2.5.2 Photosynthetic electron transport limits tropical net photosynthesis

Globally, limitations on the optimum temperature of net photosynthesis are often attributed to limitations of Rubisco carboxylation (Lin *et al.* 2012; Yamaguchi *et al.* 2016; although not always Wise *et al.* 2004; Cen and Sage 2005). Across our temperature range, we found the opposite of other global meta-analyses (Medlyn *et al.* 2002; Hikosaka *et al.* 2006; Kattge and Knorr 2007; Kumarathunge *et al.* 2019), where the activation energy term of J_{max} (E_{aJ}) increased with increasing temperature instead of E_{aV} (Fig 4 D,G). Similarly, the optimum temperature for J_{max} is often higher than for V_{cmax} (Kirschbaum and Farquhar 1984; Lin *et al.* 2012); however, this might not be the case for some tropical species (Vårhammar *et al.* 2015; Slot and Winter 2017c). Recently, Smith and Dukes (2017) found that across most plant functional types and biomes, species acclimated through upregulation of V_{cmax} at a higher growth temperature; however, tropical species acclimated through upregulation of J_{max}. This suggests that, unlike common global trends, tropical T_{opt} increases may be more strongly controlled by J_{max} than V_{cmax}. This makes sense because J_{max} tends to be the primary limiting factor to T_{opt} at the highest portions of temperature response curves (Sage and Kubien 2007), often due to

higher ion leakage in the thylakoid membrane limiting photosynthetic electron transport and RuBP regeneration capacity (Muraoka *et al.* 2000; Schrader *et al.* 2004; Wise *et al.* 2004). Additionally, due to a steeper decline in J_{25} response to temperature compared to V_{25} (Fig. 2.3D,G), the ratio between J_{max} and V_{cmax} (*J:V*) decreases with increasing temperature (Fig. 2.5A) suggesting that J_{max} becomes more limiting at higher temperatures.

2.5.3 Photosynthetic differences between growth conditions, deciduousness, and successional types

Similar to the few studies that have investigated differences in photosynthetic responses to different light levels (Pearcy 1987; Slot *et al.* 2019), we found that the rate of photosynthesis was higher in sun leaves, but there were no T_{opt} differences between sun and shade leaves (Fig. 2.6). Studies from other biomes have found opposing results, where studies investigating differences in T_{opt} between upper canopy and understory leaves have found that T_{opt} either does not differ (Carter and Cavaleri 2018) or is higher in the upper canopy leaves (Jurik *et al.* 1988). Niinemets *et al.* (1999) showed that the optimum temperature of electron transport is higher in upper canopy compared to lower canopy leaves, suggesting that the component process of photosynthesis associated with light can adjust to different light conditions. We did not have J_{max} data classified as "shaded"; therefore, we were unable to make this comparison within our dataset. More studies should investigate how temperature responses of both $A_{net,}$ and the biochemical components of photosynthesis differ between sun and shade leaves.

Even though plant functional types, such as evergreen and deciduous species, often have different temperature responses (Yamori *et al.* 2014), global vegetation models do not often implement separate temperature response functions for different functional types (Lombardozzi *et al.* 2015; Smith *et al.* 2016; Mercado *et al.* 2018). Globally, woody evergreen species have a lower optimum temperatures than woody deciduous species (Yamori *et al.* 2014). This could be advantageous to temperate and boreal species, as evergreen leaves in these systems are kept over-winter under lower temperature conditions. Tropical ecosystems experience much lower annual temperature variations; however, we found that tropical evergreen leaves had a slightly lower T_{opt} than semi-deciduous leaves (Fig. 2.8A). Although, all species labeled as 'semi-deciduous' came from the same study (Slot and Winter 2017a). This site was had the highest MAT (26.6 °C) of all the study sites included in the A_{net} dataset (Table 2.2), which could have been a larger determining factor in T_{opt} than plant functional type itself. 75% of species in the A_{net} dataset classified whether the species was evergreen or deciduous; however, only one study included semi-deciduous species. Additionally, no species in our A_{Ci} dataset were characterized as either 'deciduous' or 'semi-deciduous' (Table 2.2), preventing any analysis on differences between plant functional types between for J_{max} and V_{cmax} data. Greater efforts should be made to better characterize differences between different plant functional types within the tropics.

Generally, fast growing, early successional species have higher rates of photosynthesis (Wright *et al.* 2004). Additionally, early successional species tend to reside in higher temperature conditions due to the higher light environment in an early

successional forest (Cao and Sanchez-Azofeifa 2017), suggesting that early successional species might have higher optimum temperatures. We did not find support for this hypothesis and, instead, found no differences between successional types for either T_{opt}, T_{optV}, or T_{optJ} (Figs. 2.9A, 2.10A,B). Our results support findings from Slot and Winter (2017b) but differ from the results of Slot *et al.* (2016) and Slot and Winter (2018). We did find that the net photosynthetic thermal niche (Ω) was higher for early successional species than late successional species (Fig 2.9C). This is consistent with theory on 'fast' species with high rates of photosynthesis, as these species tend to invest in traits that allow productivity under a wide range of temperatures instead of investing in traits associated with thermoregulation (Michaletz *et al.* 2016). A wider thermal niche is likely beneficial to early successional forests that experience a wider, more dynamic range of temperatures (Holbo and Luvall 1989).

2.5.4 Predictive equations for tropical photosynthesis

Providing support for our main hypothesis, MAT played a strong role in controlling many of our temperature response variables. MAT was selected as variable in the 'best fit' model for all photosynthetic temperature response variables except A_{25}, V_{25}, and E_{aV}. Optimum temperatures of A_{net}, V_{cmax}, and J_{max} either only included MAT (T_{optV} and T_{optJ}) or included MAT (T_{opt}) as a main effect in the model, further supporting studies globally that MAT plays an important role in determining optimum temperatures (Kattge and Knorr 2007; Kumarathunge *et al.* 2019). MAT was the only predictor in the 'best' model for all J_{max} parameters (T_{optJ}, J_{25}, E_{aV}), suggesting that MAT plays a strong role in controlling the temperature response of J_{max}.

A key finding of our study is that the equations that we developed to estimate net photosynthesis across tropical ecosystems all included the light environment. Even though the final model that we selected to predict A_{25} did not include light, the initial chosen 'best predictor' was light environment alone (Table 2.4). Furthermore, the final model that we used to predict A_{25} was not a good predictor of A_{25}, suggesting that the rate of photosynthesis may be more controlled by factors other than growth climate, such as light environment or plant functional type. Many models allow robust inclusions of leaf light environment (e.g. JULES and community land model); however, models often make predictions based on 'sun' leaves (e.g. Mercado *et al.* 2018). Including information about the light environment could help improve estimations of tropical forest carbon dynamics.

Three temperature response parameters included MAP in the 'best fit' model (T_{opt}; V_{25}; E_{aV}) and two of the parameters only included MAP (V_{25} and E_{aV}; Table 2.3). While stepwise regression showed that MAP was the sole best predictor of V_{25} and E_{aV}, both models only had a slightly higher explanatory power than MAT (Table 2.4). This, combined with high V_{cmax} MAP datapoints corresponding with high MAT, suggests that a more robust dataset would provide clarity on which climate variables are the 'best predictors' of V_{25} and E_{aV}.

2.5.5 Opportunities for better parameterized functions

We present predictive equations for the temperature parameters of net photosynthetic and biochemical processes of net photosynthesis; however, both stomatal conductance and daytime respiration can also play large roles in controlling photosynthetic temperature responses (Lin *et al.* 2012). Stomatal conductance, or vapor

pressure deficit (VPD) which is the primary climate variable controlling stomatal conductance (Farquhar and Sharkey 1982), has been estimated to be the strongest predictors of photosynthetic decline with tropical climate warming (Lloyd and Farquhar 2008, Wu *et al.* 2017). This could have important implications when comparing tropical ecosystems with contrasting rainfall regimes. A recent study found that, in a seasonally dry tropical forest, photosynthetic decline after T_{opt} is primarily driven by lowered stomatal conductance compared with species in a wet forest (Slot and Winter 2017b). Ecosystem level studies have found support for strong stomatal limitations to T_{opt} as well (Tan *et al.* 2017; Wu *et al.* 2017). This relationship between temperature, moisture, and stomatal conductance should also be investigated across tropical forests and is critical to understand photosynthetic responses to temperature as tropical forests become hotter and dryer (Malhi *et al.* 2008).

Our predictive models could have also been further improved if we had included leaf functional traits. Some of our photosynthetic parameters were not well explained by any climate (E_{aV}, T_{optV}) or climate and light/altitude group (A_{25}) (Table 2.4). A recent meta-analysis by Atkin *et al.* (2015) found that including information on plant functional types (broadleaf, conifer, grass type, shrubs) was the factor that had the most explanatory power for predicting the rate of respiration globally. In addition, including other plant trait factors, such as leaf nitrogen and leaf mass per area improved their predictive models (Atkin *et al.* 2015). Including the commonly identified plant function types is not always available tropical datasets; however, including other factors, such as plant form or

growth strategy (e.g. evergreen or deciduous; successional type) could provide valuable information for tropical biome photosynthesis modeling.

2.5.6 Conclusions

This study reports new algorithms that describe photosynthetic temperature responses to different climate factors and describes across-tropic differences between plant growth conditions, plant functional types, and successional strategies. We found that the T_{opt} responses to mean temperatures tend to align with global trends; however, the optimum temperature of the biochemical components of photosynthesis (T_{optV} and T_{optJ}) do not align with results found globally. Global carbon models should consider these potential differences found within tropical biomes, as a misrepresentation of tropical photosynthesis could induce large errors in our estimations of global carbon fluxes.

2.6 Acknowledgements

Funding was provided by US Biological Survey John Wesley Powell Center Working Center for Analysis and Synthesis. Funding was also provided by U. S. Department of Energy award DE-SC-0011806. Additional funding was provided by USDA Forest Service International Institute of Tropical Forestry.

2.7 References

Anderegg WRL, Schwalm C, Biondi F, *et al.* 2015. Pervasive drought legacies in forest ecosystems and their implications for carbon cycle models. *Science* **349**: 528–532.

Arneth A, Mercado L, Kattge J, Booth BBB. **2012**. Future challenges of representing land-processes in studies on land-atmosphere interactions. *Biogeosciences* **9**: 3587–3599.

Atkin OK, Bloomfield KJ, Reich PB, *et al.* 2015. Global variability in leaf respiration in relation to climate, plant functional types and leaf traits. *New Phytologist* **206**: 614–636.

Battaglia M, Beadle C, Loughhead S. **1996**. Photosynthetic temperature responses of Eucalyptus globus and Eucalyptus nitens. *Tree Physiology* **16**: 81–89.

Berry J, Bjorkman O. **1980**. Photosynthetic response and adaptation to temperature in higher plants. *Annual Review of Plant Physiology* **31**: 491–543.

Bloom AJ, Chapin FS, Mooney HA. **1985**. Plants-an Economic Analogy. *Annual Review of Ecological Systems* **16**: 363–392.

Booth BBB, Jones CD, Collins M, *et al.* 2012. High sensitivity of future global warming to land carbon cycle processes. *Environmental Research Letters* **7**: 024002.

Box E. **1996**. Plant functional types and climate at the global scale. *Journal of Vegetation Science* **7**: 309–320.

von Caemmerer S, Farquhar GD. **1981**. Some relationships between the biochemistry of photosynthesis and the gas exchange of leaves. *Planta* **153**: 376–387.

Cao S, Sanchez-Azofeifa A. **2017**. Modeling seasonal surface temperature variations in secondary tropical dry forests. *International Journal of Applied Earth Observation and Geoinformation* **62**: 122–134.

Carter KR, Cavaleri MA. **2018**. Within-Canopy Experimental Leaf Warming Induces Photosynthetic Decline Instead of Acclimation in Two Northern Hardwood Species. *Frontiers in Forests and Global Change* **1**.

Cavaleri MA, Reed SC, Smith WK, Wood TE. **2015**. Urgent need for warming experiments in tropical forests. *Global Change Biology* **21**: 2111–2121.

Cen YP, Sage RF. **2005**. The regulation of Rubisco activity in response to variation in temperature and atmospheric CO2 partial pressure in sweet potato. *Plant Physiology* **139**: 979–990.

Cunningham S, Read J. **2002**. Comparison of temperate and tropical rainforest tree species: photosynthetic responses to growth temperature. *Oecologia* **133**: 112–119.

Cunningham SC, Read J. **2003**. Do temperate rainforest trees have a greater ability to acclimate to changing temperatures than tropical rainforest trees? *New Phytologist* **157**: 55–64.

Curtis PS, Wang X. **1998**. International Association for Ecology A Meta-Analysis of Elevated CO_2 Effects on Woody Plant Mass , Form , and Physiology. *Oecologia* **113**: 299–313.

Diffenbaugh NS, Scherer M. **2011**. Observational and model evidence of global emergence of permanent, unprecedented heat in the 20th and 21st centuries. *Climatic Change* **107**: 615–624.

Dixon RK, Brown S, Houghton RA, Solomon AM, Trexler MC, Wisniewski J. **1994**. Carbon pools and flux of global forest ecosystems. *Science* **263**: 185–190.

Doughty CE, Goulden ML. **2008**. Are tropical forests near a high temperature threshold? *Journal of Geophysical Research* **113**: G00B07.

Duursma RA. **2015**. Plantecophys - An R Package for Analysing and Modelling Leaf Gas Exchange Data. *PLoS ONE* **10**: e0143346.

Farquhar GD, Caemmerer S Von, Berry JA. 1980. A biochemical model of

photosynthesis CO2 fixation in leaves of C3 species. *Planta* **149**: 78–90.

Farquhar GD, Sharkey TD. **1982**. Stomatal conductance and photosynthesis. *Annual Review of Plant Physiology* **33**: 317–345.

Fauset S, Freitas HC, Galbraith DR, *et al.* 2018. Differences in leaf thermoregulation and water-use strategies between three co-occurring Atlantic forest tree species. *Plant, Cell & Environment* **41**: 1618–1631.

Fick SE, Hijmans RJ. **2017**. WorldClim 2: new 1-km spatial resolution climate surfaces for global land areas. *International Journal of Climatology* **37**: 4302–4312.

Friedlingstein P, Cox P, Betts R, *et al.* 2006. Climate-carbon cycle feedback analysis: Results from the C4MIP model intercomparison. *Journal of Climate* **19**: 3337–3353.

Galbraith D, Levy PE, Sitch S, *et al.* 2010. Multiple mechanisms of Amazonian forest biomass losses in three dynamic global vegetation models under climate change. *New Phytologist* **187**: 647–665.

Gurevitch J, Morrow LL, Wallace A, Walsh JS. **1992**. A Meta-Analysis of Competition in Field Experiments Author (s): Jessica Gurevitch , Laura L . Morrow , Alison Wallace , Joseph S . Walsh Published by : The University of Chicago Press for The American Society of Naturalists Stable URL : http://www.jstor. *The American Naturalist* **140**: 539–572.

Hedges L V., Olkin I. **1985**. *Statistical methods for meta-analysis*. New York, Academic.

Hikosaka K, Ishikawa K, Borjigidai A, Muller O, Onoda Y. **2006**. Temperature acclimation of photosynthesis: Mechanisms involved in the changes in temperature dependence of photosynthetic rate. *Journal of Experimental Botany* **57**: 291–302.

Holbo HR, Luvall JC. **1989**. Modeling surface temperature distributions in forest landscapes. *Remote Sensing of Environment* **27**: 11–24.

Janzen DH. **1967**. Why Mountain Passes are Higher in the Tropics. *The American Naturalist* **101**: 233–249.

June T, Evans JR, Farquhar GD. **2004**. A simple new equation for the reversible temperature dependence of photosynthetic electron transport: a study on soybean leaf. *Functional Plant Biology* **31**: 275–283.

Jurik TW, Weber JA, Gates DM. **1988**. Effects of Temperature and Light on Photosynthesis of Dominant Species of a Northern Hardwood Forest. *Botanical Review* **149**: 203–208.

Kattge J, Knorr W. **2007**. Temperature acclimation in a biochemical model of photosynthesis: A reanalysis of data from 36 species. *Plant, Cell and Environment* **30**: 1176–1190.

Kattge J, Knorr W, Raddatz T, Wirth C. **2009**. Quantifying photosynthetic capacity and its relationship to leaf nitrogen content for global-scale terrestrial biosphere models. *Global Change Biology* **15**: 976–991.

Kirschbaum UF, Farquhar GD. **1984**. Temperature Dependence of Whole-leaf Photosynthesis in Eucalyptus pauciflora Sieb. ex Spreng. *Australian Journal of Plant Physiology* **11**: 519–538.

Kitajima K, Mulkey SS, Wright SJ. **1997**. Seasonal leaf phenotypes in the canopy of a tropical dry forest: Photosynthetic characteristics and associated traits. *Oecologia* **109**: 490–498.

Koike T, Kitao M, Maruyama Y, Mori S, Lei TT. **2001**. Leaf morphology and

photosynthetic adjustments among deciduous broad-leaved trees within the vertical canopy profile. *Tree physiology* **21**: 951–8.

Kositsup B, Montpied P, Kasemsap P, Thaler P, Améglio T, Dreyer E. **2009**. Photosynthetic capacity and temperature responses of photosynthesis of rubber trees (Hevea brasiliensis Müll. Arg.) acclimate to changes in ambient temperatures. *Trees - Structure and Function* **23**: 357–365.

Kumarathunge DP, Medlyn BE, Drake JE, *et al.* 2019. Acclimation and adaptation components of the temperature dependence of plant photosynthesis at the global scale. *New Phytologist* **222**: 768–784.

Lin YS, Medlyn BE, Ellsworth DS. **2012**. Temperature responses of leaf net photosynthesis: The role of component processes. *Tree Physiology* **32**: 219–231.

Lloyd J, Farquhar GD. **2008**. Effects of rising temperatures and [CO2] on the physiology of tropical forest trees. *Philosophical transactions of the Royal Society of London. Series B, Biological sciences* **363**: 1811–7.

Lombardozzi DL, Bonan GB, Smith NG, Dukes JS, Fisher RA. **2015**. Temperature acclimation of photosynthesis and respiration: A key uncertainty in the carbon cycle-climate feedback. *Geophysical Research Letters* **42**: 8624–8631.

Ma S, Osuna JL, Verfaillie J, Baldocchi DD. **2017**. Photosynthetic responses to temperature across leaf–canopy–ecosystem scales: a 15-year study in a Californian oak-grass savanna. *Photosynthesis Research* **132**: 277–291.

Malhi Y, Roberts JT, Betts RA, Killeen TJ, Li W, Nobre C a. **2008**. Climate Change, Deforestation, and the Fate of the Amazon. *Science* **319**: 169–172.

Marshall B, Biscoe P V. 1980. A model for C3 leaves describing the dependence of net

photosynthesis on irradiance II. *Journal of Experimental Botany* **31**: 41–48.

Matthews HD, Eby M, Ewen T, Friedlingstein P, Hawkins BJ. **2007**. What determines the magnitude of carbon cycle-climate feedbacks? *Global Biogeochemical Cycles* **21**: 1–12.

Mau A, Reed S, Wood T, Cavaleri M. **2018**. Temperate and tropical forest canopies are already functioning beyond their thermal thresholds for photosynthesis. *Forests* **9**: 47.

Medlyn B. E., Dreyer E, Ellsworth D, *et al.* 2002. Temperature response of parameters of a biochemically based model of photosynthesis. II. A review of experimental data. *Plant, Cell and Environment* **25**: 1167–1179.

Medlyn B E, Dreyer E, Ellsworth D. **2002**. Temperature response of parameters of a biochemically-based model of photosynthesis. II. A review of experimental data. *Plant Cell Environ* **25**: 1167–1179.

Mercado LM, Medlyn BE, Huntingford C, *et al.* 2018. Large sensitivity in land carbon storage due to geographical and temporal variation in the thermal response of photosynthetic capacity. *New Phytologist* **218**: 1462–1477.

Michaletz ST, Weiser MD, McDowell NG, *et al.* 2016. The energetic and carbon economic origins of leaf thermoregulation. *Nature Plants* **2**: 1–8.

Mora C, Frazier AG, Longman RJ, *et al.* 2013. The projected timing of climate departure from recent variability. *Nature* **502**: 183–7.

Muraoka H, Tang Y, Terashima I, Koizumi H, Washitani I. **2000**. Contributions of diffusional limitation, photoinhibition and photorespiration to midday depression of photosynthesis in Arisaema heterophyllum in natural high light. *Plant, Cell and Environment* **23**: 235–250.

Niinemets Ü, Oja V, Kull O. **1999**. Shape of leaf photosynthetic electron transport versus temperature response curve is not constant along canopy light gradients in temperate deciduous trees. *Plant, Cell & Environment* **22**: 1497–1513.

Pan Y, Birdsey RA, Phillips OL, Jackson RB. **2013**. The Structure, Distribution, and Biomass of the World's Forests. *Annual Review of Ecology, Evolution, and Systematics* **44**: 593–622.

Pearcy R. **1987**. Photosynthetic gas exchange responses of Australian tropical forest trees in canopy, gap and understorey micro-environments. *Functional Ecology* **1**: 169–178.

De Pury DGG, Farquhar GD. **1997**. Simple scaling of photosynthesis from leaves to canopies without the errors of big-leaf models. *Plant, Cell and Environment* **20**: 537–557.

R Core Team. **2018**. *R: A language and environment for statistical computing. R Foundation for Statical Computing*.

Read J. **1990**. Some Effects of Acclimation Temperature on Net Photosynthesis in Some Tropical and Extra- Tropical Australasian Nothofagus Species. *Journal of Ecology* **78**: 100–112.

Rey-Sánchez A, Slot M, Posada J, Kitajima K. **2016**. Spatial and seasonal variation in leaf temperature within the canopy of a tropical forest. *Climate Research* **71**: 75–89.

Rogers A. **2016**. Viewpoints A roadmap for improving the representation of photosynthesis in Earth system models. *New Phytologist*: 22–42.

Ryu Y, Baldocchi DD, Kobayashi H, *et al.* 2011. Integration of MODIS land and atmosphere products with a coupled-process model to estimate gross primary productivity and evapotranspiration from 1 km to global scales. *Global Biogeochemical*

Cycles **25**: 1–24.

Sage RF, Kubien DS. **2007**. The temperature response of C3 and C4 photosynthesis. *Plant, Cell and Environment* **30**: 1086–1106.

Santiago LS, Wright SJ. **2007**. Leaf functional traits of tropical forest plants in relation to growth form. *Functional Ecology* **21**: 19–27.

Schrader SM, Wise RR, Wacholtz WF, Ort DR, Sharkey TD. **2004**. Thylakoid membrane responses to moderately high leaf temperature in Pima cotton. *Plant, Cell and Environment* **27**: 725–735.

Sinclair TR, Murphy CE, Knoerr KR. **1976**. Development and evaluation of simplified models for simulating canopy photosynthesis and transpiration. *Journal of Applied Ecology* **13**: 813–829.

Slot M, Garcia MA, Winter K. **2016**. Temperature response of CO 2 exchange in three tropical tree species. *Functional Plant Biology* **43**: 468–478.

Slot M, Krause GH, Krause B, Hernández GG, Winter K. **2019**. Photosynthetic heat tolerance of shade and sun leaves of three tropical tree species. *Photosynthesis Research* **141**: 119–130.

Slot M, Winter K. **2017a**. In situ temperature response of photosynthesis of 42 tree and liana species in the canopy of two Panamanian lowland tropical forests with contrasting rainfall regimes. *New Phytologist*.

Slot M, Winter K. **2017b**. In situ temperature relationships of biochemical and stomatal controls of photosynthesis in four lowland tropical tree species. *Plant Cell and Environment* **40**: 3055–3068.

Slot M, Winter K. **2018**. High tolerance of tropical sapling growth and gas exchange to

moderate warming. *Functional Ecology* **32**: 599–611.

Smith NG, Dukes JS. **2013**. Plant respiration and photosynthesis in global-scale models: Incorporating acclimation to temperature and CO2. *Global Change Biology* **19**: 45–63.

Smith NG, Dukes JS. **2017**. Short-term acclimation to warmer temperatures accelerates leaf carbon exchange processes across plant types. *Global Change Biology*: 4840–4853.

Smith NG, Malyshev SL, Shevliakova E, Kattge J, Dukes JS. **2016**. Foliar temperature acclimation reduces simulated carbon sensitivity to climate. *Nature Climate Change* **6**: 407–411.

Tan ZH, Zeng J, Zhang YJ, *et al.* 2017. Optimum air temperature for tropical forest photosynthesis: Mechanisms involved and implications for climate warming. *Environmental Research Letters* **12**.

Vargas G G, Cordero S RA. **2013**. Photosynthetic responses to temperature of two tropical rainforest tree species from Costa Rica. *Trees* **27**: 1261–1270.

Vårhammar A, Wallin G, Mclean CM, *et al.* 2015. Photosynthetic temperature responses of tree species in Rwanda: Evidence of pronounced negative effects of high temperature in montane rainforest climax species. *New Phytologist* **206**: 1000–1012.

Wang YP, Leuning R. **1998**. A two-leaf model for canopy conductance, photosynthesis and partitioning of available energy I: Model description and comparison with a multi-layered model. *Agricultural and Forest Meteorology* **91**: 89–111.

Way DA, Oren R. **2010**. Differential responses to changes in growth temperature between trees from different functional groups and biomes: a review and synthesis of data. *Tree Physiology* **30**: 669–688.

Williams JW, Jackson ST, Kutzbach JE. **2007**. Projected distributions of novel and

disappearing climates by 2100 AD. *Proceedings of the National Academy of Sciences* **104**: 5738–5742.

Wise RR, Olson AJ, Schrader SM, Sharkey TD. **2004**. Electron transport is the functional limitation of photosynthesis in field-grown Pima cotton plants at high temperature. *Plant, Cell and Environment* **27**: 717–724.

Wright IJ, Westoby M, Reich PB, *et al.* 2004. The worldwide leaf economics spectrum. *Nature* **428**: 821–827.

Wu J, Guan K, Hayek M, *et al.* 2017. Partitioning controls on Amazon forest photosynthesis between environmental and biotic factors at hourly to interannual timescales. *Global Change Biology* **23**: 1240–1257.

Yamaguchi DP, Nakaji T, Hiura T, Hikosaka K. **2016**. Effects of seasonal change and experimental warming on the temperature dependence of photosynthesis in the canopy leaves of Quercus serrata. *Tree Physiology* **36**: 1283–1295.

Yamori W, Hikosaka K, Way DA. **2014**. Temperature response of photosynthesis in C3, C4, and CAM plants: Temperature acclimation and temperature adaptation. *Photosynthesis Research* **119**: 101–117.

Yamori W, Masumoto C, Fukayama H, Makino A. **2012**. Rubisco activase is a key regulator of non-steady-state photosynthesis at any leaf temperature and, to a lesser extent, of steady-state photosynthesis at high temperature. *Plant Journal* **71**: 871–880.

Zuur A, Ieno EN, Walker N, Saveliev AA, M. SG. **2009**. *Mixed effects models and extensions in ecology with R*. New York, NY: Springer.

2.8 Tables and Figures

Table 2.1 Abbreviations and descriptions

Variable	Description	Units
ACi	Refers to the net photosynthetic assimilation at a range of leaf internal CO_2 concentrations	unitless
A_{max}	Light saturated photosynthesis, estimated from light response curves	μmol m^{-2} s^{-1}
A_{net}	Net photosynthesis measured at saturating irradiance	μmol m^{-2} s^{-1}
A_{opt}	The value of A_{net} at the optimum temperature	μmol m^{-2} s^{-1}
A_{25}	Rate of net photosynthesis at 25 ºC	μmol m^{-2} s^{-1}
E_{aV}	The activation energy of the V_{cmax} temperature response curve	kJ mol^{-1}
E_{aJ}	The activation energy of the J_{max} temperature response curve	kJ mol^{-1}
g_s	Stomatal conductance	mol m^{-2} s^{-1}
J_{max}	The maximum rate of photosynthetic electron transport	μmol m^{-2} s^{-1}
J_{25}	The rate of J_{max} at 25 ºC	μmol m^{-2} s^{-1}
J:V	The ratio between J_{25} and V_{25}	unitless
k_{opt}	The value of J_{max} or V_{cmax} at the optimum temperature	μmol m^{-2} s^{-1}
MAP	Mean annual precipitation	mm
MAT	Mean annual temperature	ºC
T_{leaf}	Leaf temperature	ºC
T_{opt}	The optimum temperature for net photosynthesis	ºC
T_{optJ}	Optimum temperature of maximum photosynthetic electron transport	ºC

T_{optV}	Optimum temperature for maximum Rubisco carboxylation	ºC
T_{range}	Mean annual temperature range	ºC
V_{cmax}	Maximum rate of Rubisco carboxylation	μmol m^{-2} s^{-1}
VPD	Vapor pressure deficit	kPa
V_{25}	The rate of V_{cmax} at 25 ºC	μmol m^{-2} s^{-1}
Ω	The difference between T_{opt} and the temperature where the rate of photosynthesis that is 37% of A_{opt} (photosynthetic thermal niche)	ºC

Table 2.2 List of A_{net} and J_{max}/V_{cmax} data sources. Analysis shows if the data sources were either used in A_{net} or A_{net} response to a range of internal CO_2 concentrations (A_{ci}) temperature response curves. MAT is the mean annual temperature; MAP is the mean annual precipitation. Data type show whether data are originally from A_{net} or A_{ci} curves. Data combination method describes how data were combined to form an individual sample. The number in parentheses lists the number of samples in each dataset after data were combined.

Analysis	Forest classification	Seed source/ Study Location (latitude, longitude)	Altitude	Species	MAT (°C)	MAP (mm)	*in situ*/ *ex situ*	Successional type	Light conditions	Evergreen/ deciduous	Reference	Data type	Data combination method
A_{net}	Upland tropical forest	Trocha Union, Peru (-13.11,-71.61)	3297	16[1]	11.6	515	*in situ*	NA	Sun	NA	Bahar *et al.* (2017)	A_{ci}	Study site (Latitude) (4)
		Esperanza, Peru (-13.18, -71.60)	2580	17[1]	15.5	545			Sun				
		San Pedro (01), Peru (-13.05, -71.54)	1740	21[1]	19.5	2005			Sun				
		San Pedro (02), Peru (-13.05, 71.54)	1499	19[1]	20.6	2371			Sun				
	Tall Forest (sub canopy)	Queensland, Australia (-17.76, 145.54)	768	*Alangium villosum* *Neisosperma poweri*	20.6	1750	*in situ*	NA	Shade	NA	Bloomfield *et al.* (2014)	A_{ci}	Study site/ Light environment (3)
	Tall savanna woodland	(-17.85, 145.53) (-17.03, 145.60)	860	*Corymbia intermedia*	20.1	1433			Sun				
			683	*Corymbia intermedia* *Lophostemon suaveolens* *Planchonia careya*	21.2	2050			Sun				
	Tropical wet forest (canopy)	Luquillo, Puerto Rico, USA (18.33, -65.73)	96	*Guarea guidonia*	25.1	2115	*in situ*	Mid	Sun	Evergreen	Cavaleri and Carter (unpublished)	A_{net} / A_{ci}	Species (4)
	Tropical wet forest (understory)			*Piper glabrescens* *Prestoea montana* *Psychotria brachiata*				NA Early Early	Shade Shade Shade				
	Tropical forest (sapling)	Panama (9.12, -79.70)	35	*Inga goldmani*	26.6	2260	*ex situ*	Mid	Sun	NA	Cheesman and Winter (2013)	A_{net}	Species (1)
	Lowland tropical forest	Queensland, Australia (-16.17, 145.29)	159	*Syzygium graveolens*	24.9	1973	*in situ*	NA	Sun	Evergreen	Crous (unpublished)	A_{net}	Species (1)
	Tropical forest	Para, Brazil (-3.02, -54.97)	135	*Sextonia rubra*	25.5	1968	*in situ*	NA	Sun	Evergreen	Doughty and Goulden 2008	A_{net}	Species (1)
	Tropical forest	Southwestern Rwanda (-2.17, 29.03) (-2.36, 29.44)[2]	1687	*Carapa grandiflora* *Entandrophragma excelsum* *Polyscias fulva*	17.8	1492	*in situ*	Late Late NA	Sun/Shade Sun/Shade Sun/Shade	NA	Dusenge *et al.* 2015	A_{ci}	Species/Light environment (6)

	Subtropical moist forest	Arecibo, Puerto Rico, USA (18.24, -66.43)	121	*Coria alliodora* *Ocotea leucoxylon*	24.8	1704	*in situ*	Late Late	Sun Sun	NA	Fonseca da Silva *et al.* 2017	*LRC*	Species (2)
	Subtropical moist forest Subtropical wet forest	Arecibo, Puerto Rico, USA (18.24, -66.43) Luquillo, Puerto Rico, USA (18.33, -65.73)	121	*Castilla elastica* *Guarea guidonia* *Ocotea leucoxylon* *Dacryodes excelsa*	24.8	1704	*in situ*	Early Mid Late Late	Sun Sun/Shade Sun Shade	Evergreen	Mau et al. 2018 and Mau and Cavaleri (unpublished)	A_{net}/A_{c_i}	Species/ Light environment (5)
	Tropical forest	Queensland, Australia (-17.00, 145.34)	503	*Argyrodendron peralatum*	22.3	1702	*in situ*	NA	Sun/Shade	Evergreen	Pearcy 1987	A_{ci}	Species/ Light environment (2)
	Semi-deciduous moist forest	Panama City, Panama (8.99, -79.54)	75	*Amphilophium paniculatum* *Aristolochia tonduzii* *Astronium graveolens* *Bignonia corymbosa* *Bonamia trichantha* *Castilla elastica* *Cecropia peltata* *Chrysophyllum cainito* *Doliocarpus major* *Ficus insipida* *Luehea seemannii* *Macrocnemum roseum* *Nectandra cuspidata* *Passiflora vitifolia* *Pittoniotis trichantha* *Schefflera morototoni* *Securidaca diversifolia* *Serjania mexicana* *Spondias mombin* *Stigmaphyllon lindenianum* *Zuelania guidonia*	26.6	1902	*in situ*	NA	Sun	Semi-deciduous	Slot and Winter 2017a	A_{net}	Species (42)
	Moist evergreen	Colon, Panama (9.28, -79.97)	115	*Adelphia platyrachis* *Anacardium excelsum* *Apeiba membranacea* *Brosimum utile* *Carapa guianensis* *Cordia bicolor* *Garcinia madruno* *Guatteria dumetorum* *Heisteria scandens* *Manilkara bidentata* *Miconia minutiflora* *Protium panamense* *Simarouba amara* *Tachigali versicolor* *Tapirira guianensis* *Terminalia amazonia* *Tocoyena pittieri* *Tontelea ovalifolia* *Vantanea depleta* *Virola multiflora* *Vochysia ferruginea*	26.2	3188	*in situ*	NA	Sun	Evergreen	Slot and Winter 2017a	A_{net}	
		Gamboa, Panama	35	*Lagerstroemia speciosa*	26.6	2260	*in situ*		Sun			A_{ci}	

	Lowland tropical	(9.12, -79.70)						Early successional		NA	Slot and Winter 2017a		
	Vargus	Costa Rica	32	*Dipteryx oleifera* *Zygia longifolia*	26.1	1197	*in situ*	Late successional Early successional	Sun	NA	Vargas and Cordero 2013	A_{net}	Species (2)
A_{Ci}	Tropical wet forest (understory)	Luquillo, Puerto Rico, USA (18.33, -65.73)	96	*Piper glabrescens* *Prestoea montana* *Psychotria brachiata*	25.1	2115	*in situ*	NA Early Early	Shade Shade Shade	Evergreen	Cavaleri and Carter (unpublished)	A_{ci}	Species (3)
	Lowland tropical forest	Queensland, Australia (-16.17, 145.29)	159	*Cardwellia sublimis* *Endiandra microneura*	24.9	1973	*in situ*	NA	Sun	Evergreen	Crous (unpublished)	A_{ci}	Species (2)
	Tropical forest	Southwestern Rwanda (-2.36, 29.44)[2]	2093	*Entandrophragma excelsum*	16.4	1436	*in situ*	NA	Sun	NA	Dusenge *et al.* 2015	A_{ci}	Species/Light environment (6)
	Subtropical moist forest	Arecibo, Puerto Rico, USA (18.24, -66.43)	121	*Castilla elastica*	24.8	1704	*in situ*	Early	Sun	Evergreen	Mau and Cavaleri (unpublished)	A_{ci}	Species/ Light environment (5)
	Tropical rainforest	Queensland, Australia (-16.17, 145.29)	159	*Acmena graveolens* *Argyrodendron peralatum*	24.9	1973	*in situ*	NA	Sun	Evergreen	Kelly (2014)	A_{ci}	Species (2)
	Lowland tropical	Gamboa, Panama (9.12, -79.70)	35	*Calophyllum longifolium* *Ficus insipida* *Garcinia madruno* *Lagerstroemia speciosa*	26.6	2260	*in situ*	Late Early Late Early	Sun	NA	Slot and Winter 2017a	A_{ci}	Species (4)
	Rainforest	Manaus, Brazil (-2.63, -60.12)	86	*Abuta panurensis* *Brosimum parinarioides* *Eschweilera coriacea* *Ipomoea carnea* *Licania oblongifolia* *Licaria guianensis* *Macherium sp.* *Miconia ruficalyx* *Micropholis guyanensis* *Micropholis guyanensis subsp. duckeana* *Parinari excelsa* *Peltogine excelsa* *Pouteria anomola* *Pouteria caimito* *Tachi sp.* *Tetracera amazonica* *Vochysiacea sp.*	27.1	2201	*in situ*	NA	Sun	NA	Tribuzy 2005	A_{ci}	Species (19)
	Tropical forest	Southwestern, Rwanda (-2.36, 29.44)	2093	*Carapa grandiflora* *Cedrela serrata* *Entandrophragma exelsum* *Eucalyptus maidenii* *Eucalyptus microcorys* *Hagenia abyssinica*	16.4	1436	*in situ*	Late Early Late Early Early Early	Sun	Evergreen	Varharmmar *et al.* 2015	A_{ci}	Species (6)

[1]Species were grouped by study site and analyzed as a one sample per study site. Species and site information can be found in Bahar *et al.* (2017) and Asner *et al.* (2014). [2]Data were collected from two sites; however, species were combined across both locations. Climate data were used for Lat,Long (-2.17, 29.03) all measurements. Site information can be found in Dusenge *et al.* 2015. Altitude, MAT, and MAP was extracted from the WorldClim database.

Table 2.3 Regression equations for each photosynthetic parameter response to individual climate variables. Photosynthetic parameters are: the optimum temperatures of net photosynthesis (T_{opt}; °C), the rate of net photosynthesis at 25 °C (A_{25}; µmol m^{-2} s^{-1}) at 25 °C, photosynthetic thermal niche or width of the temperature response curve (Ω; °C), the optimum temperatures of the maximum rate of Rubisco carboxylation (V_{cmax}) and photosynthetic electron transport (J_{max}) (T_{optV}, T_{optJ} respectively; °C), the rate of V_{cmax} (V_{25}; µmol m^{-2} s^{-1}) and J_{max} (J_{25}; µmol m^{-2} s^{-1}) at 25 °C, and the activation energy term for V_{cmax} (E_{aV}; kJ mol^{-1})and J_{max} (E_{aJ}; kJ mol^{-1}).

	Coefficients					
	Intercept	MAT	MAP	Yearly range	p-value	Adj R^2
T_{opt}	14.85 ± 2.26	0.60 ± 0.09			**<0.001**	0.36
	23.66 ± 4.84		-0.06(0.03)x^2 + 1.21(0.77)x		**0.007**	0.10
	32.74 ± 1.34			-0.28 ± 0.11	**0.013**	0.07
A_{25}	9.25 ± 3.76	-3.45 × 10^{-2} ± 15.12 × 10^{-2}			0.820	-0.01
	8.15 ± 1.65		1.07 × 10^{-4} ± 6.90 × 10^{-4}		0.876	-0.01
	7.99 ± 1.72			3.55 × 10^{-2} ± 14.55 × 10^{-2}	0.808	-0.01
Ω	-3.62 ± 4.83	0.55 ± 0.20			**0.007**	0.09
	8.04 ± 2.20		7.73 × 10^{-4} ± 9.32 × 10^{-4}		0.409	0.00
	10.65 ± 2.43			-0.07 ± 0.20	0.712	-0.01
T_{optV}	33.17 ± 3.17	0.27 ± 0.13			**0.047**	0.12
	32.88 ± 3.64		3.42 × 10^{-3} ± 1.80 × 10^{-3}		0.070	0.10
	38.72 ± 4.22			0.09 ± 0.37	0.813	-0.04
V_{25}	95.90 ± 17.96	-2.15 ± 0.73			**0.007**	0.24
	103.67 ± 20.28		-3.02 × 10^{-2} ± 1.00 × 10^{-2}		**0.006**	0.24

	18.16 ± 25.26			2.19 ± 2.18	0.326	0.00
E_{aV}	37.75 ± 32.63	1.96 ± 1.32			0.150	0.05
	26.31 ± 36.65		36.65 ± 0.02		0.115	0.06
	125.07 ± 41.03			-3.45 ± 3.55	0.340	0.00
T_{optJ}	25.41 ± 3.89	0.45 ± 0.16			**0.008**	0.19
	24.69 ± 4.27		$5.85 \times 10^{-3} \pm 2.11 \times 10^{-3}$		**0.010**	0.18
	41.15 ± 5.07			-0.42 ± 0.44	0.350	0.00
J_{25}	210.15 ± 29.55	-5.70 ± 1.20			**<0.001**	0.42
	211.91 ± 33.96		$-7.04 \times 10^{-2} \pm 1.68 \times 10^{-2}$		**<0.001**	0.36
	28.75 ± 45.42			3.70 ± 3.91	0.352	0.00
E_{aJ}	-7.93 ± 26.49	3.00 ± 1.07			**0.009**	0.19
	-12.41 ± 29.11		$3.88 \times 10^{-2} \pm 1.44 \times 10^{-2}$		**0.012**	0.17
	124.28 ± 33.06			-5.15 ± 2.85	0.081	0.07
J:V	2.83 ± 0.32	$-4.59 \times 10^{-2} \pm 1.33 \times 10^{-2}$			**0.003**	0.34
	2.90 ± 0.38		$5.94 \times 10^{-4} \pm 1.92 \times 10^{-4}$		**0.006**	0.29
	-14.04 ± 3.38			$-0.10(0.02)x^2 + 2.57(0.56)x$	**<0.001**	0.50

Each biochemical temperature response variable was linearly fit to a climate model, which included mean annual temperature (MAT; °C), mean annual precipitation (MAP; mm), mean yearly temperature range (T_{range}; °C). T_{opt} response to MAT and *J:V* response to T_{range} were fit with a polynomial transformation. Values given are coefficient mean ± se.

Table 2.4 Selected terms for the best fit model using stepwise model selection. Terms that are included in the best fit model are denoted with an "X". β_0 is the dependent variable, MAT is mean annual temperature (°C), MAP is mean annual precipitation (mm), T_{range} is annual temperature range, Alt is altitude group included as a categorical variable (< 500m, 500-1000 m, 1000-2000 m, >2000m), Lt is light (either sun or shade).

β_0	*MAT*	*MAP*	T_{range}	*Alt*	*Lt*	*MAT* × *Alt*	*MAP* × *Alt*	T_{range} × *Alt*	*MAT* × *Lt*	*MAP* × *Lt*	T_{range} × *Lt*	*Alt* × *Lt*
T_{opt}	X	X	X							X		
A_{25}			*		X							
Ω	X				X						X	
T_{optV}	X											
V_{25}		X										
E_{aV}		X										
T_{optJ}	X											
J_{25}	X											

E_{aJ}	X		
J:V	X		

* A_{25} best fit model only includes light, which has two categorical terms (sun and shade). Because categorical terms alone cannot be used to build a predictive model, the term "Light" was removed from the full model. The 2nd A_{25} model selected "T_{range}" alone as the best predictor of A_{25}, denoted with *. The 2nd best model was used in the best predictive equations in Table 3. Shading indicates that light environment is not included in V_{cmax} and J_{max} full models due to insufficient data.

Table 2.5 Summary of best predictive models for net photosynthetic temperature response parameters: the optimum temperatures of net photosynthesis (T_{opt}; °C), the rate of net photosynthesis at 25 °C (A_{25}; µmol m^{-2} s^{-1}) at 25 °C, photosynthetic thermal niche or width of the temperature response curve (**Ω**; °C), the optimum temperatures of the maximum rate of Rubisco carboxylation (V_{cmax}) and photosynthetic electron transport (J_{max}) (T_{optV}, T_{optJ} respectively; °C), the rate of V_{cmax} (V_{25}; µmol m^{-2} s^{-1}) and J_{max} (J_{25}; µmol m^{-2} s^{-1}) at 25 °C, and the activation energy term for V_{cmax} (E_{aV}; kJ mol^{-1}) and J_{max} (E_{aJ}; kJ mol^{-1}). Equations are given for coefficients selected in Table 2.2.

Equation	p-value	F-statistic	Adj R^2	df
$T_{opt} = 39.30(9.00)\beta_0\text{MAP:SH} + 7.35 \times 10^{-4}(4.23 \times 10^{-4})\beta_0\text{MAP:SUN} - 8.80 \times 10^{-2}(0.31)\text{MAT} - 2.13 \times 10^{-3}(6.47 \times 10^{-4}) - 2.97(1.07)T_{range}$	<0.001	19.02	0.49	4,71
$A_{25} = 8.46(1.89) - 2.80 \times 10^{-2}(0.15)T_{range}$	0.859	0.032	-0.01	1,74
$\Omega = 2.00(9.36)\beta_{0SH} - 34.19(8.96)\beta_{0SUN} + 1.28(0.23)\text{MAT} - 1.26(0.59)\beta_0 T_{range}\text{:SH} + 0.88(0.25)\beta_0 T_{range}\text{:SUN}$	<0.001	9.02	0.31	4,68
$T_{optV} = 33.17(3.17)\beta_0 + 0.27(0.13)\text{MAT}$	0.047	4.40	0.12	1,24

$V_{25} = 103.67(20.28)\beta_0 - 3.02 \times 10^{-2}(1.00 \times 10^{-2})MAP$	0.006	9.07	0.24	1,24
$E_{aV} = 26.31(36.65)\beta_0 + - (1.81 \times 10^{-2})MAP$	0.063	2.67	0.06	1,24
$T_{optJ} = 25.41(3.89)\beta_0 - 0.45(0.16)MAT$	0.008	8.19	0.19	1,29
$J_{25} = 210.15(29.55)\beta_0 - 5.70(1.20)MAT$	<0.001	22.69	0.42	1,29
$E_{aJ} = -7.93(16.49)\beta_0 + 3.00\ (1.07)MAT$	0.009	7.80	0.19	1,29
$J:V = 2.83(0.32) - 4.59 \times 10^{-2}(1.33 \times 10^{-2})MAT$	0.003	11.86	0.34	1,20

Each biochemical temperature response variable was fit to a climate model, which included mean annual temperature (MAT; °C), mean annual precipitation (MAP; mm), mean yearly temperature range (T_{range}; °C). Anet parameters included categorical variables of light environment (sun or shade) and altitude group (< 500m, 500-1000 m, 1000-2000 m, >2000m) and the two-way interactions between each climate variable (MAT, MAP, T_{range}) and categorical variable. 'Best' predictive models where selected using stepwise selection. Values inside of parentheses represent ± standard error.

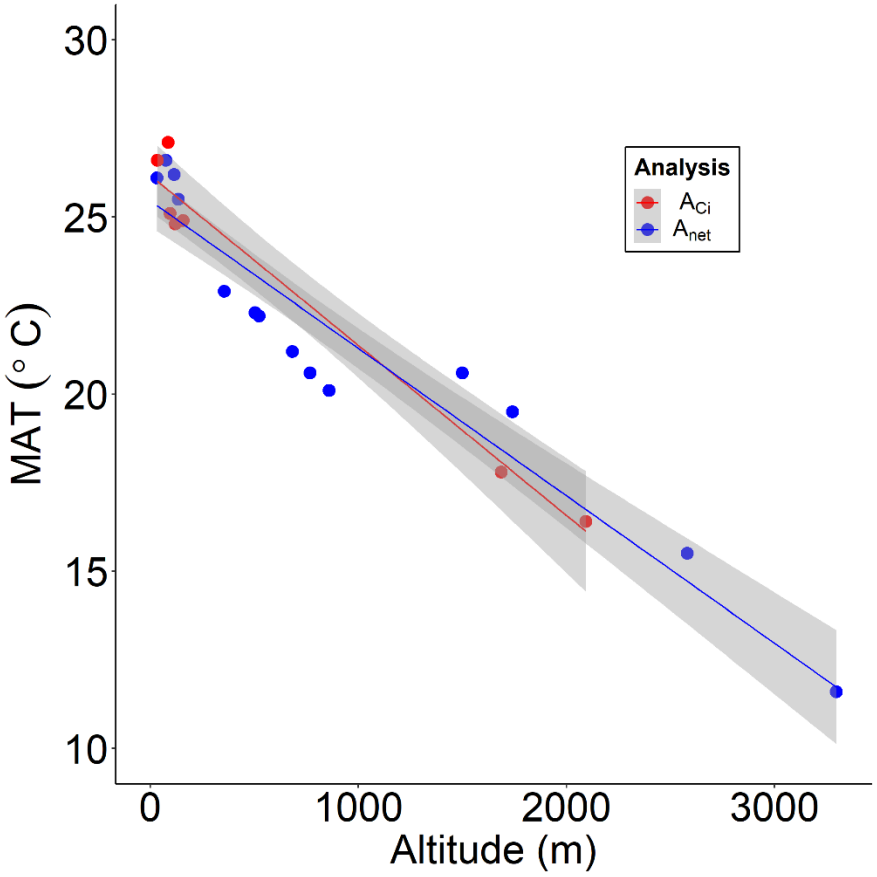

Figure 2.1 Scatterplots of the A_{net} and A_{Ci} dataset mean annual temperature (MAT) correlation with altitude. Color of datapoints and regression line represent locations of data used for A_{Ci} (V_{cmax} and J_{max} parameters; red) and A_{net} (blue) data analysis. Both datasets had strong correlations between MAT and altitude (A_{Ci} r^2 = 0.96; A_{net} r^2 = 0.92).

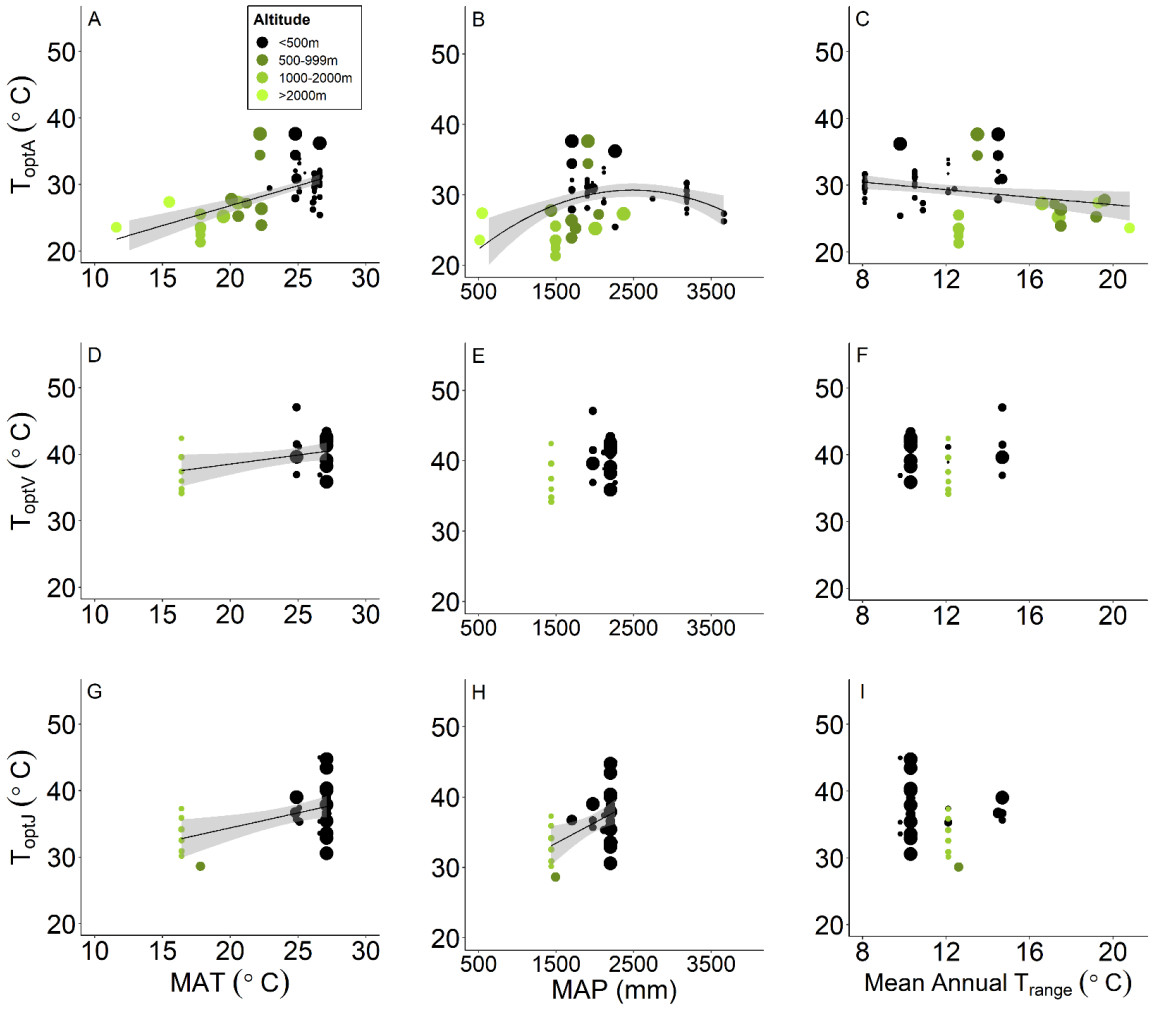

Figure 2.2 The optimum temperature of net photosynthesis and biochemical responses to three primary climate variables. The optimum temperature of net photosynthesis (T_{opt}) response to **A)** mean annual temperature (MAT), **B)** mean annual precipitation (MAP), and **C)** mean annual temperature range (T_{range}). The optimum temperature of net photosynthesis (T_{optV}) response to **D)** mean annual temperature (MAT), **E)** mean annual precipitation (MAP), and **F)** mean annual temperature range (T_{range}). The optimum temperature of net photosynthesis (T_{optJ}) response to **G)** mean annual temperature (MAT), **H)** mean annual precipitation (MAP), and **I)** mean annual temperature range

(T_{range}). Regression equations are weighted by number of observations that are used to calculate each temperature response mean. Size of data point depicts weight of each mean where larger data points carry a greater weight. Solid line represents significant linear regression fits. T_{opt} response to MAP (Fig. 2B) is fit with a polynomial transformation. Shaded area around line represents confident intervals. Color represents altitude groupings of < 500m (black), 500-999m (dark green), 1000-2000m (green), >2000m (light green).

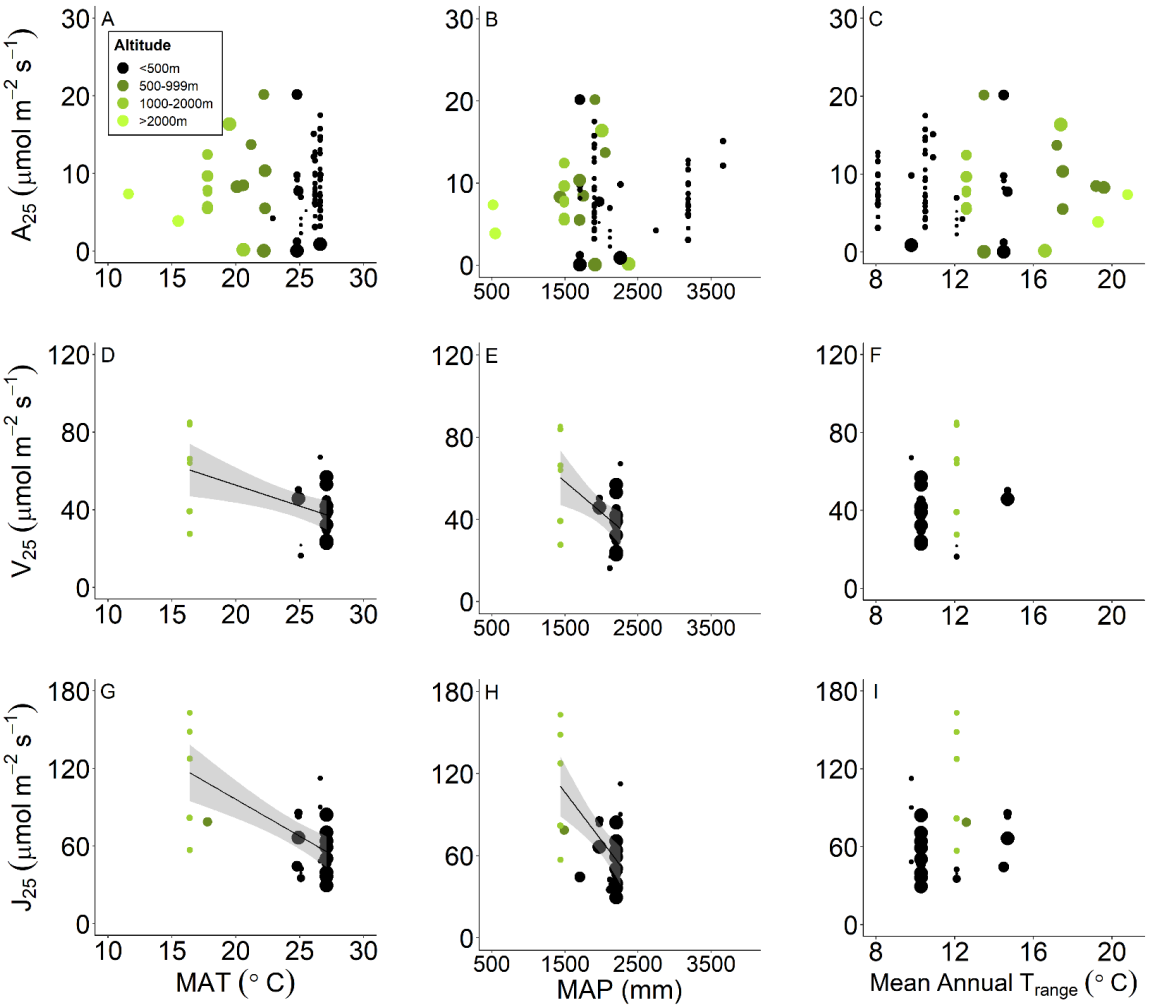

Figure 2.3 The rate of net and the biochemical components of photosynthesis at 25 °C responses to three primary climate variables. The rate of net photosynthesis at 25 °C (A_{25}) response to **A)** mean annual temperature (MAT), **B)** mean annual precipitation (MAP), and **C)** mean annual temperature range (T_{range}). The rate of V_{cmax} at 25 °C (V_{25}) response to **D)** mean annual temperature (MAT), **E)** mean annual precipitation (MAP), and **F)** mean annual temperature range (T_{range}). The rate of J_{max} at 25 °C (J_{25}) response to **G)** mean annual temperature (MAT), **H)** mean annual precipitation (MAP), and **I)** mean annual temperature range (T_{range}). Regression equations are weighted by number of

observations that are used to calculate each temperature response mean. Size of data point depicts weight of each mean where larger data points carry a greater weight. Solid line represents significant linear regression fits. Shaded area around line represents confident intervals. Color represents altitude groupings of < 500m (black), 500-999m (dark green), 1000-2000m (green), >2000m (light green).

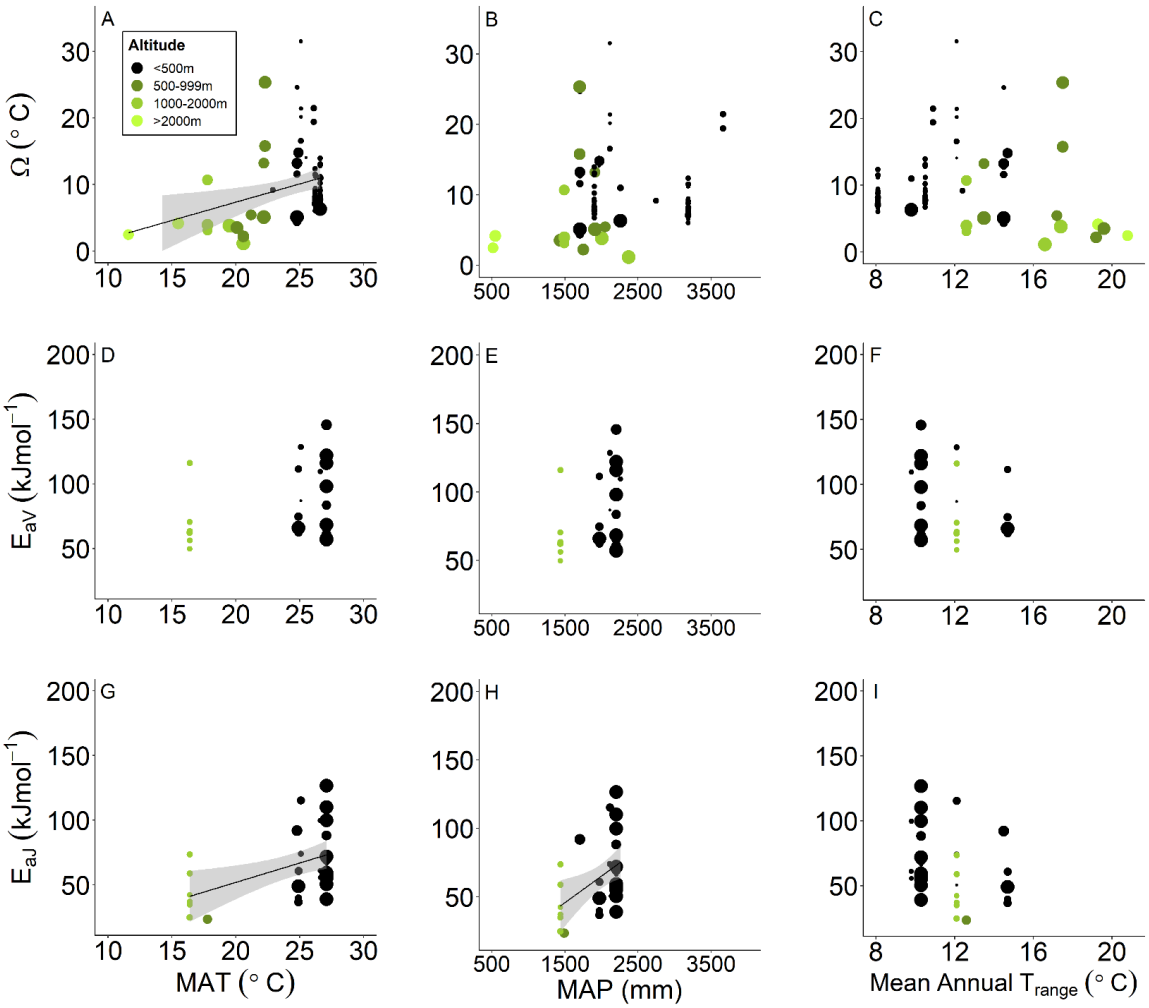

Figure 2.4 The net photosynthetic thermal nice and the activation energies of the biochemical components of photosynthesis responses to three primary climate variables. The net photosynthetic thermal niche (Ω) response to **A)** mean annual temperature (MAT), **B)** mean annual precipitation (MAP), and **C)** mean annual temperature range (T_{range}). The activation energy of V_{cmax} temperature response curve (E_{aV}) response to **D)** mean annual temperature (MAT), **E)** mean annual precipitation (MAP), and **F)** mean annual temperature range (T_{range}). The activation energy of J_{max} temperature response curve (E_{aJ}) response to **G)** mean annual temperature (MAT), **H)** mean annual

precipitation (MAP), and **I)** mean annual temperature range (T_{range}). Regression equations are weighted by number of observations that are used to calculate each temperature response mean. Size of data point depicts weight of each mean where larger data points carry a greater weight. Solid line represents significant linear regression fits. Shaded area around line represents confident intervals. Color represents altitude groupings of < 500m (black), 500-999m (dark green), 1000-2000m (green), >2000m (light green).

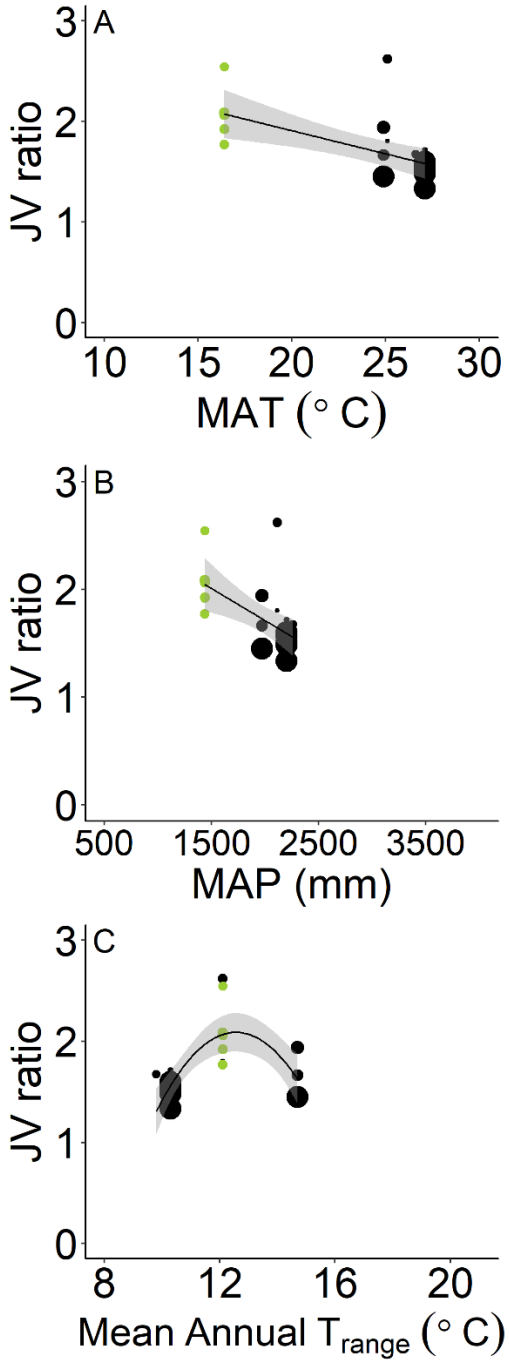

Figure 2.5 The ratio between rate of J_{max} and V_{cmax} responses to three primary climate variables. The ratio between the rate of J_{max} at 25 °C and V_{cmax} at 25 °C (*JV*) responses to **A)** mean annual temperature (MAT), **B)** mean annual precipitation (MAP), and **C)** mean

annual temperature range (T_{range}). Regression equations are weighted by number of observations that are used to calculate each temperature response mean. Size of data point depicts weight of each mean where larger data points carry a greater weight. Solid line represents significant linear regression fits. *J:V* response to T_{range} (Fig. 5C) is fit with a polynomial transformation. Shaded area around line represents confident intervals. Color represents altitude groupings of < 500m (black), 500-999m (dark green), 1000-2000m (green), >2000m (light green).

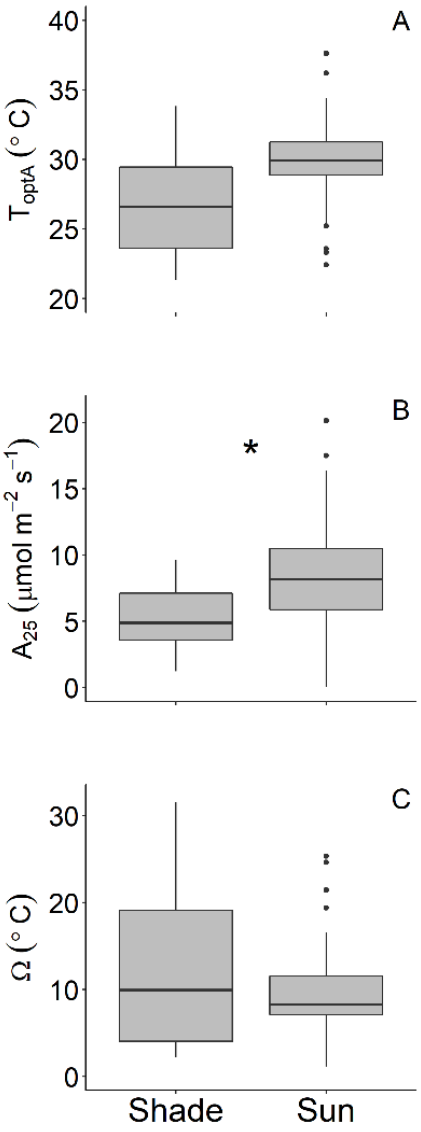

Figure 2.6 Boxplots displaying the net photosynthetic parameter differences with leaf light environment. The distribution of shade and sun growth leaves for **A)** net photosynthetic optimum temperature (T_{opt}), **B)** the rate of net photosynthesis at 25 °C (A_{25}), and **C)** photosynthetic thermal niche (Ω). The boxes display median and interquartile range. The whiskers represent 1.5 times the interquartile range. Data beyond

the whiskers are outside of 1.5 times the interquartile range. * denotes a significant difference between shade and sun leaves ($p < 0.05$).

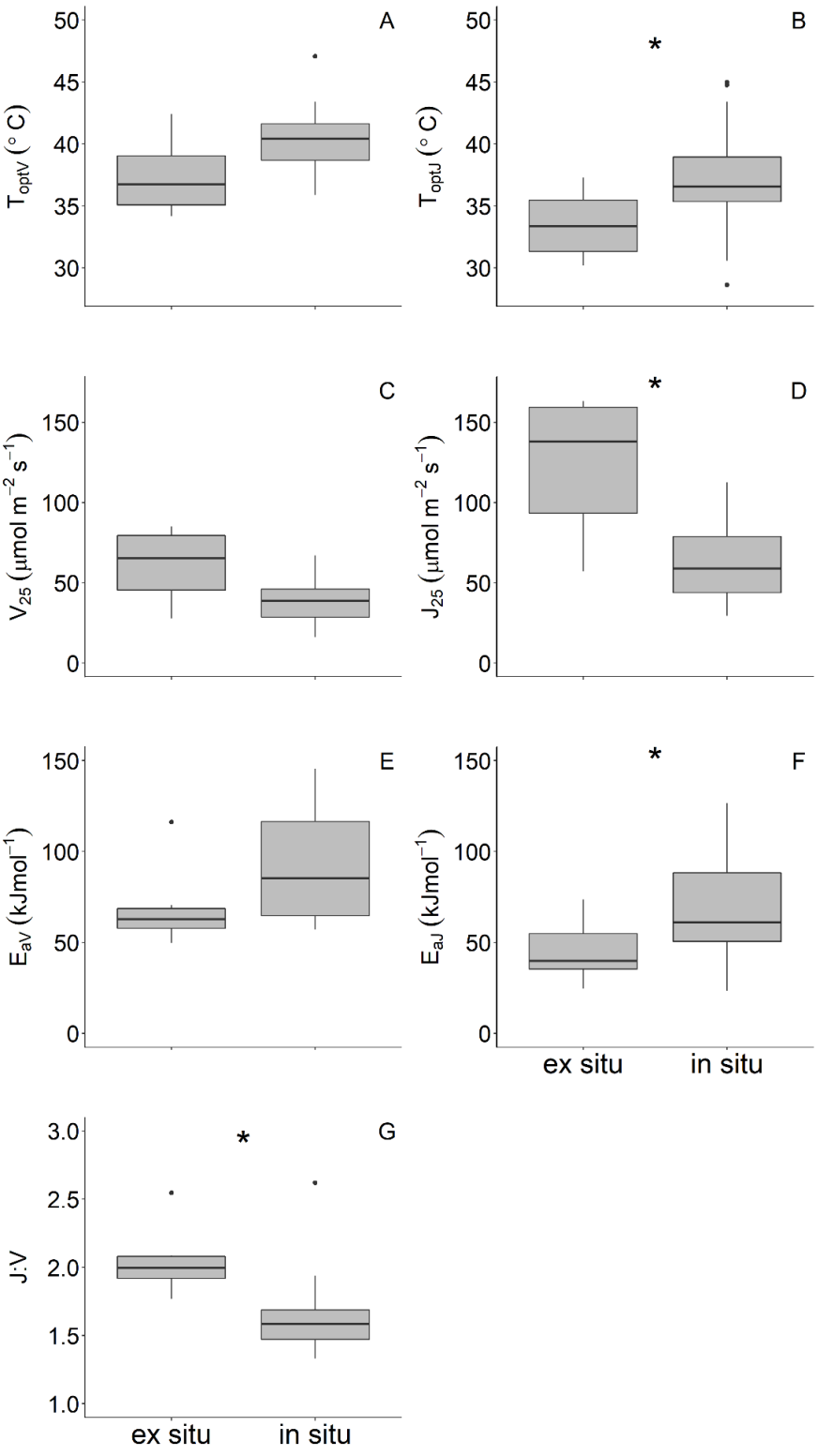
A
B
C
D
E
F
G
T_{optV} (° C)
T_{optJ} (° C)
V_{25} (µmol m^{-2} s^{-1})
J_{25} (µmol m^{-2} s^{-1})
E_{aV} (kJmol^{-1})
E_{aJ} (kJmol^{-1})
J:V
*
ex situ
in situ

Figure 2.7 Boxplots displaying the differences in biochemical parameters of photosynthesis between plants grown *in* or *ex situ*. The distribution of *ex situ* and *in situ* grown plants for **A)** optimum temperature of maximum Rubisco carboxylation (V_{cmax}) (T_{optV}), **B)** optimum temperature of maximum photosynthetic electron transport (J_{max}) (T_{optJ}), **C)** the rate of V_{cmax} at 25 °C (V_{25}), **D)** the rate of J_{max} at 25 °C (J_{25}), **E)** the activation energy of V_{cmax} temperature response (E_{aV}), **F)** the activation energy of J_{max} temperature response (E_{aJ}), and **G)** the ration between J_{25} and V_{25}. The boxes display median and interquartile range. The whiskers represent 1.5 times the interquartile range. Data beyond the whiskers are outside of 1.5 times the interquartile range. * denotes a significant difference between evergreen and semi-deciduous species ($p < 0.05$).

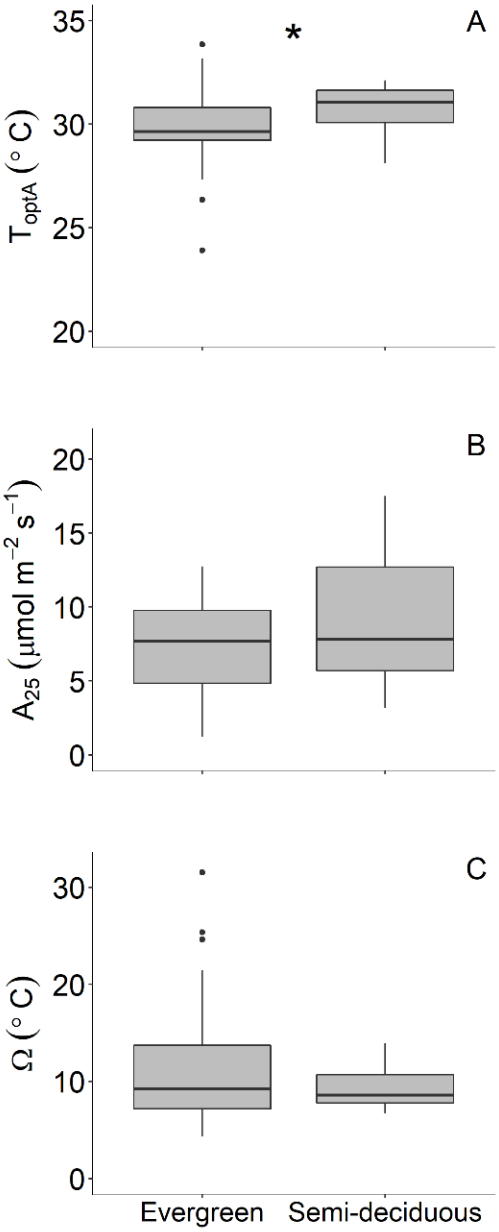

Figure 2.8 Boxplots displaying the net photosynthetic parameter differences between evergreen and semi-deciduous species. The distribution of evergreen and semi-deciduous species for **A)** net photosynthetic optimum temperature (T_{opt}), **B)** the rate of net photosynthesis at 25 °C (A_{25}), and **C)** photosynthetic thermal niche (Ω). The boxes

display median and interquartile range. The whiskers represent 1.5 times the interquartile range. Data beyond the whiskers are outside of 1.5 times the interquartile range. * denotes a significant difference between evergreen and semi-deciduous species ($p < 0.05$).

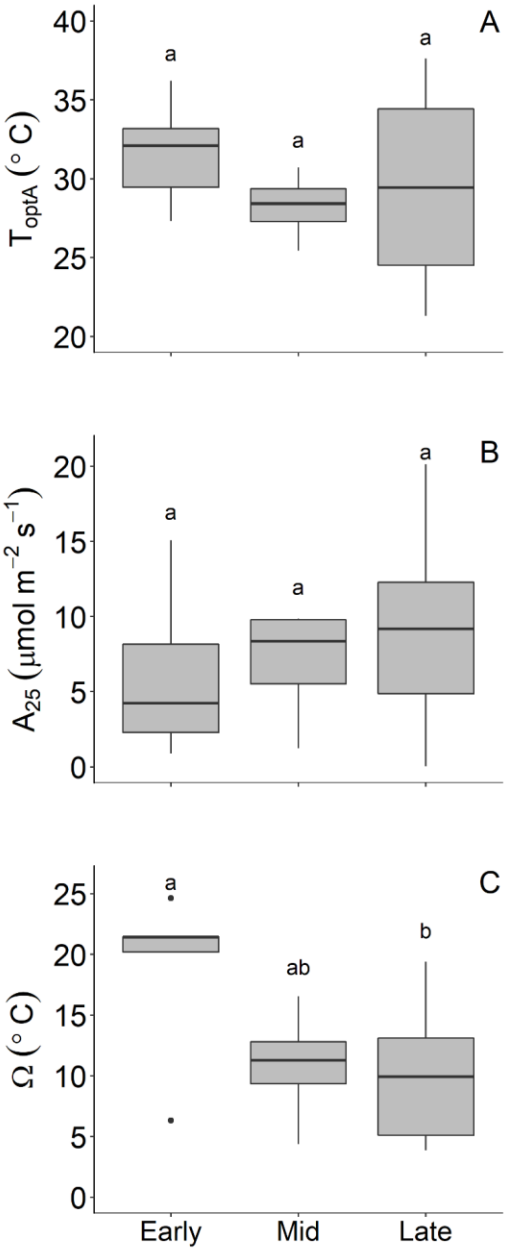

Figure 2.9 Boxplots displaying the net photosynthetic parameter differences between successional strategies. The distribution of early and late successional species for **A)** net photosynthetic optimum temperature (T_{opt}), **B)** the rate of net photosynthesis at 25 °C (A_{25}), and **C)** photosynthetic thermal niche (**Ω**). The boxes display median and

interquartile range. The whiskers represent 1.5 times the interquartile range. Data beyond the whiskers are outside of 1.5 times the interquartile range. Different letters are results of a *post hoc* Tukey HSD test and indicate a statistical difference between successional types ($p < 0.05$).

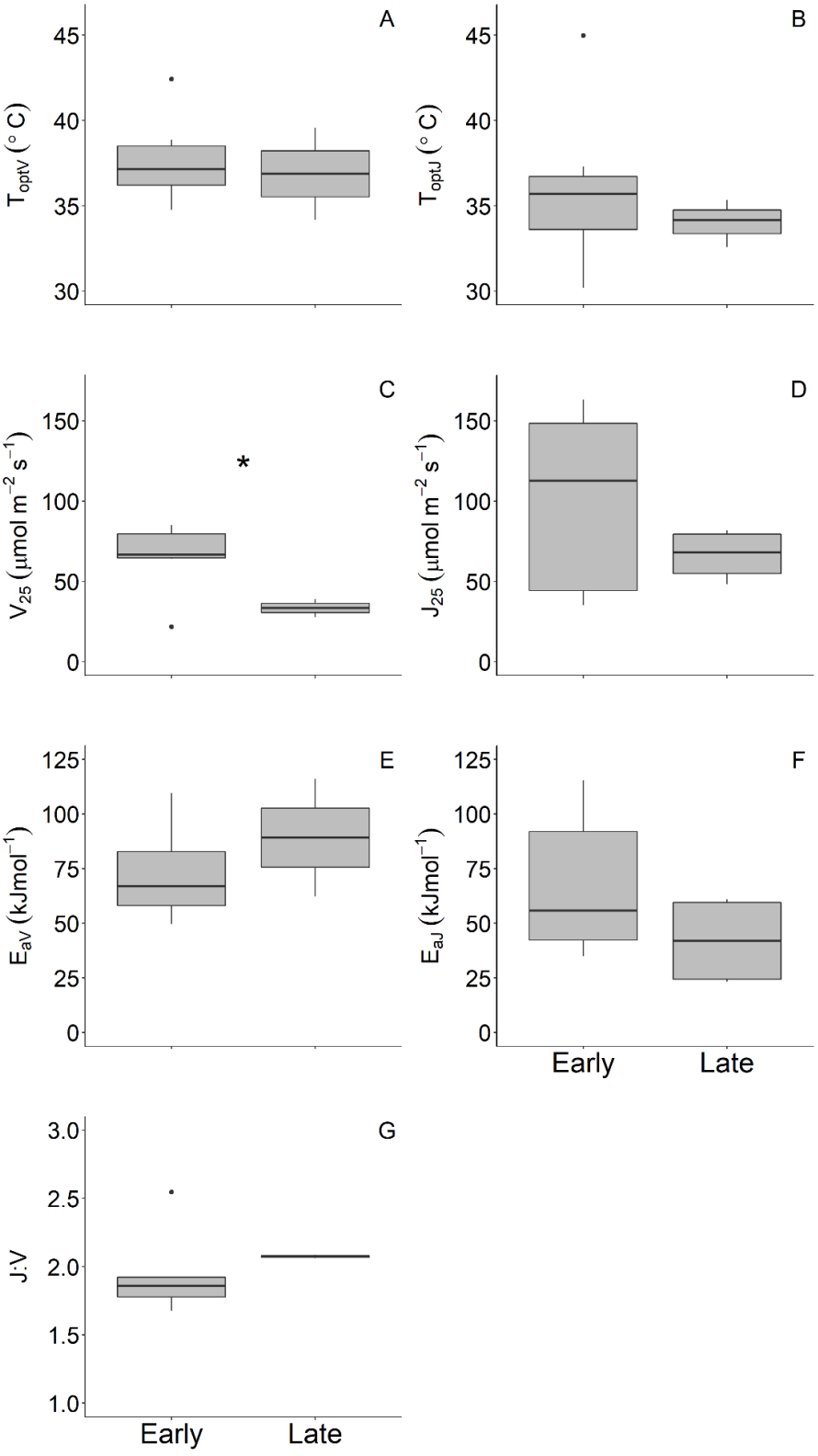
A
B
C
D
E
F
G
T_{optV} (° C)
T_{optJ} (° C)
V_{25} (µmol m^{-2} s^{-1})
J_{25} (µmol m^{-2} s^{-1})
E_{aV} (kJmol^{-1})
E_{aJ} (kJmol^{-1})
J:V
45
40
35
30
150
100
50
0
125
75
25
3.0
2.5
2.0
1.5
1.0
*
Early
Late

Figure 2.10 Boxplots displaying the differences in biochemical parameters of photosynthesis between successional strategies. The distribution of early and late successional species for **A)** optimum temperature of maximum Rubisco carboxylation (V_{cmax}) (T_{optV}), **B)** optimum temperature of maximum photosynthetic electron transport (J_{max}) (T_{optJ}), **C)** the rate of V_{cmax} at 25 °C (V_{25}), **D)** the rate of J_{max} at 25 °C (J_{25}), **E)** the activation energy of V_{cmax} temperature response (E_{aV}), **F)** the activation energy of J_{max} temperature response (E_{aJ}), and **G)** the ration between J_{25} and V_{25}. The boxes display median and interquartile range. The whiskers represent 1.5 times the interquartile range. Data beyond the whiskers are outside of 1.5 times the interquartile range. * denotes a significant difference between successional types ($p < 0.05$).

3 *In situ* experimental warming of the rainforest understory induces acclimation of photosynthesis but not respiration

3.1 Abstract

Despite the importance of tropical forests to global carbon balance, our understanding is quite limited of how tropical plant physiology will respond to climate warming. We implemented an *in situ* field-scale +4 °C infrared warming experiment in a Puerto Rican rain forest understory, the first of its kind in any tropical forest. We investigated responses of gas exchange and leaf traits of two common understory shrubs, *Psychotria brachiata* and *Piper glabrescens*. Both species showed photosynthetic acclimation through broadened thermal niches, and *P. brachiata* showed greater acclimation potential with smaller stomata and up-regulation of photosynthetic rates and optimum photosynthetic temperatures (T_{opt}). Contrary to expectation, neither species showed evidence of respiratory acclimation. Soil moisture, not temperature, was the strongest environmental driver. T_{opt} tended to increase as soil moisture decreased, while rates of photosynthesis, stomatal conductance, and basal respiration all declined as soils dried. Our study provides evidence that tropical understory species may have greater thermal acclimation potential than canopy foliage; however, the degree and mechanisms of acclimation vary by species. *P. brachiata* plasticity may allow quicker responses to heat waves or episodic disturbance, while the wider thermal niches of *P. glabrescens* could mitigate negative effects of chronic warming.

3.2 Introduction

Tropical biomes are expected to approach temperatures outside their historical climate boundaries within the 20 years (Diffenbaugh and Scherer 2011; Mora *et al.* 2013). Reduced surface evaporation due to deforestation could exacerbate this imminent warming (Zhang *et al.*, 2001). Tropical forests cycle a disproportionate amount of Earth's carbon relative to their total land area, and have the highest photosynthetic rates and carbon density of all terrestrial ecosystems on Earth (Beer *et al.*, 2010; Pan *et al.*, 2013; Schimel *et al.*, 2015). However, the magnitude and even direction of the effects of climate warming on tropical forest carbon balance are not well constrained (Korner 2004; Lloyd and Farquhar 2008; Booth *et al.*, 2012; Cavaleri *et al.*, 2015). Ecosystem carbon balance is determined by the uptake of carbon dioxide (CO_2) into the system through photosynthesis, and the release of CO_2 through respiration; however, these two processes respond differently to temperature. Photosynthesis increases with increasing temperatures until an optimum (T_{opt}; Table 3.1) is reached, after which photosynthesis declines (Berry & Bjorkman, 1980), whereas respiration rises exponentially with temperature and eventually declines at very high temperatures that cause membrane dysfunction (reviewed in Atkin *et al.*, 2005). With continued warming, CO_2 release could exceed uptake, possibly inducing a positive feedback to exacerbate climate warming (Cox *et al.*, 2000; Zhang *et al.*, 2014; Drake *et al.*, 2016). The negative effects of increasing temperatures could be mitigated if tropical plants thermally acclimate. Both

photosynthesis and respiration have the capability to thermally acclimate through various mechanisms.

Photosynthetic thermal acclimation can be measured as an *up-regulation* of either the optimum temperature of photosynthesis (T_{opt}) or the rate of photosynthesis at that optimum temperature (A_{opt}) (Way & Yamori, 2014). Respiratory acclimation to warming, on the other hand, manifests as a *down-regulation* of either the temperature sensitivity or the basal rate of respiration (Atkin & Tjoelker, 2003). Global meta-analyses (Way & Oren, 2010; Slot & Kitajima, 2015) and an *in situ* tropical canopy warming experiment (Slot *et al.*, 2014) have shown that tropical plant respiration will likely acclimate to climate warming; however, there is still large uncertainty and conflicting evidence surrounding photosynthetic acclimation (Cunningham & Read, 2003; Slot & Winter, 2017a; Smith & Dukes, 2017; Crous *et al.*, 2018). Importantly, there are currently no published studies investigating how tropical species respond to whole-plant *in situ* warming.

Photosynthesis responds negatively to supraoptimal temperatures through several different mechanisms, including higher rates of photorespiration (von Caemmerer & Quick, 2000), Rubisco activase dysfunction (Portis, 1995, Salvucci *et al.*, 2001; Sage *et al.*, 2008), excessive membrane fluidity (Havaux, 1996; Wise *et al.*, 2004), and greater rates of daytime respiration relative to gross photosynthesis (Way and Sage, 2008; reviewed in Way and Yamori, 2014). High temperatures can also inhibit photosynthesis indirectly due to higher vapor pressure deficit, which induces stomatal closure (Farquhar & Sharkey, 1982).

Photosynthetic thermal acclimation can occur through biochemical or morphological adjustments. Biochemical processes underlying photosynthetic acclimation include the stabilization of thylakoid membranes (Huner 1988, Havaux *et al.* 1996) and Rubisco activase (Portis 2003, Salvucci *et al.* 2001; Sage and Kubien, 2007). Morphological adjustments could include changes in stomatal size or density (Jin *et al.* 2011, Hill *et al.* 2014). Plants acclimate to maximize carbon gain; therefore, functional type and growth environment will likely affect which mode of acclimation occurs (Yamori *et al.*, 2014; Smith and Dukes, 2017). For example, leaves developing in the humid understory are often more limited by light than stomatal conductance (Pearcy, 1987; Kenzo *et al.*, 2012); therefore, understory species may more readily acclimate through biochemical instead of stomatal adjustments.

We can investigate mechanisms controlling photosynthetic acclimation by measuring the components of net photosynthesis, including temperature responses of the maximum rates of electron transport (J_{max}) and Rubisco carboxylation (V_{cmax}) (Medlyn *et al.*, 2002*a*). J_{max} and V_{cmax} can also acclimate through positive shifts in their optimum temperatures, or by increasing their basal reaction rates (rate at 25 °C) (Way & Yamori, 2014). J_{max} and V_{cmax} are also strong controls in many numerical models of plant function, and thus an improved understanding of how they respond to warming would be of significant value.

Respiration response to temperature is generally characterized by the slope and basal respiratory responses to temperature. The parameter Q_{10} describes the exponential slope of the instantaneous respiratory response to temperature, and is defined as the factor

by which the respiration rate increases with every 10 °C increase in temperature. The basal rate of respiration is often quantified as the rate of respiration at 25 °C (R_{25}) (e.g. Atkin *et al.*, 2015). Respiration increases exponentially with increasing temperature due to the exponential response of enzymatic activity (reviewed in Atkin *et al.*, 2005).

Respiratory acclimation (*i.e.*, "down-regulation) can occur either due to decreased Q_{10} or through a declined basal rate of respiration (Atkin & Tjoelker, 2003). The mechanisms underlying respiratory acclimation include: declined rates of enzymatic reactions, lowered abundance of mitochondria and proteins, adenylate control, and substrate limitation (Dewar *et al.*, 1999; Atkin & Tjoelker, 2003). The capacity for respiratory acclimation is relatively consistent across biomes, plant growth forms, and functional types (Campbell *et al.*, 2007; Slot and Kitajima, 2015); however, evergreen trees may have an advantage over deciduous trees due to temperature fluctuations experienced over the lifetime of longer-lived leaves (Tjoelker *et al.*, 1999; Slot and Kitajima, 2015).

A scarcity of data in tropical forests, particularly for *in situ* studies, causes uncertainty in modeling tropical ecosystem carbon exchange (Cavaleri *et al.*, 2015; Lombardozzi *et al.* 2015, Mercado *et al.*, 2018). In particular, data that inform models on how vegetation will respond to climate warming is severely lacking for tropical systems (Arneth *et al.*, 2012; Booth *et al.*, 2012; Cernusak *et al.*, 2013; Huntingford *et al.*, 2013). Tropical forests experience more narrow variations in temperature than other latitudinal zones, which may cause them to be less able to acclimate to climate warming than ecosystems that experience wider diurnal, seasonal, and inter-annual temperature ranges

(Janzen 1967, Cunningham and Read 2003, Drake *et al.*, 2015). Many models suggest that carbon gain will be stimulated; however, the degree of stimulation varies (Lombardozzi *et al.*, 2015; Smith *et al.*, 2016; Mercado *et al.*, 2018), with some suggesting that warmer temperatures will upregulate rates of tropical Rubisco carboxylation but less so for photosynthetic electron transport and respiration (e.g. Smith *et al.*, 2016). Recently, Mercado *et al.*, (2018) predicted that both photosynthetic processes will be upregulated, positively stimulating carbon storage in tropical regions. To more accurately model future carbon cycling of these key ecosystems, we need to understand if these systems are able to thermally acclimate and examine the underlying mechanisms of acclimation (Huntingford *et al.*, 2013).

There are limited examples of how tropical species will respond to experimental warming *in situ* (Doughty, 2011; Slot *et al.*, 2014), and to date, no studies have investigated how tropical plants respond to larger-scale, *in situ* whole-plant warming. We tested the following hypotheses in the first ever field-scale warming experiment in a tropical rain forest (Kimball *et al.*, 2018). We hypothesized that 1) net photosynthesis will not acclimate to experimental warming, 2) reductions in photosynthesis after T_{opt} in the shaded, humid understory environment will be driven primarily by reductions in biochemical reactions rather than stomatal closure, and 3) respiration will acclimate to experimental warming, primarily due to substrate limitations imposed by reduced photosynthesis.

3.3 Materials and Methods

3.3.1 Study site and meteorological variables

This experiment was conducted at the Tropical Responses to Altered Climate Experiment (TRACE) site located at the USDA Forest Service Sabana Field Research Station, within the Luquillo Experimental Forest (18º18'N, 65º50'W). This forest is located at 100 m elevation and is classified as a subtropical wet forest (Holdridge, 1967), with Utisol soil classification (Scatena, 1989). Mean annual precipitation during the years 2014-2016 was 2271 mm, and mean annual temperature is 24 °C (Harris *et al.*, 2012). The wet season is May through November, and January through April is drier on average. In 2016, the basal area of trees > 1 cm was 38.76 m^2 ha^{-1} and stand density was 3100 trees ha^{-1}. The forest had secondary growth regenerated from abandoned agricultural land for 70 years. During the time of the study, the understory was dominated by two woody shrub species, *Psychotria brachiata* and *Piper glabrescens* and a palm species, *Prestoea montana*. The most abundant canopy species were *Presotea montana*, *Syzgium jambos*, *Ocotea leucoxylon*, and *Casearia arborea*.

The TRACE experiment is comprised of three heated and three control 4 m diameter plots located in the forest understory. The heated plots (initiated Sept 2016) were warmed +4 °C using six infrared (IR) heating panels positioned in a hexagonal ring and raised 2.6 m above the ground (Fig. 3.1). Control plots received identical treatment and infrastructure, but with no electrical power cabling and non-heated black metal panels instead of IR panels, see Kimball *et al.*, (2018) for more detail of experimental design and infrastructure.

Daily rainfall used in this study was collected from an above-canopy tower weather station located approximately 2 km from the TRACE site. Daily rainfall (mm) was collected using a 10 cm plastic funnel draining into a 180 ml plastic bottle. Surface vegetation temperature of each plot was monitored using infrared thermometers (SI-121, Apogee Instruments, Logan, UT). Below canopy air temperature (CS215, Campbell Scientific, Logan, UT) and surface vegetation temperatures were recorded using a multiplexor and datalogger (AM16/32, CR1000, Campbell Scientific). Soil moisture and temperature were measured at the edge, center, and midway between center and edge of each plot at 0-10 cm depth, and additional probes were installed at 20-30 cm depth at the plot center (CS655, Campbell Scientific).

3.3.2 Sampling Design

We measured net photosynthesis, leaf respiration, and leaf traits during four measurement campaigns: two before warming and two after the initiation of warming. Pre-warming measurements were taken in January (winter) and August 2016 (summer). Warming was initiated on September 28, 2016, and post-warming measurements were taken in January (winter), after four months of warming, and May-June 2017 (summer), after eight months of warming (Fig. 3.2).

Measurements were conducted on the first fully expanded leaf of two species: *Psychotria brachiata*, an early successional shrub that can be prevalent in the shaded understory but performs well in an open canopy environment (Devoe, 1989; Valladares *et al.*, 2000; Pearcy *et al.*, 2004), and *Piper glabrescens*, a mid-successional shrub species (Myster and Walker, 1997). 2-4 leaves per species per plot were sampled during each

measurement campaign, each from separate individual plants whenever possible. In the cases where three leaves for a species was not available, extra leaves from that species were measured from a separate plot. There were some instances, particularly for *P. glabrescens*, where there were not enough individual plants throughout the plots to get an adequate samples size. In these cases, two leaves for an individual plant were measured.

3.3.3 Net photosynthesis and stomatal conductance response to temperature

We measured photosynthetic temperature response at eight temperatures (20, 25, 27, 30, 33, 35, 37, 40 °C) on attached leaves using an LI6400XT infrared gas analyzer fitted with the 2 x 3 cm leaf chamber (6400-02B, Li-COR Inc., Lincoln, NE, USA). Temperature was controlled by cycling hot or cold water through the Expanded Temperature Control Kit (6400-88, Li-COR Inc.) using gravity (Mau *et al.*, 2018). Photosynthetic photon flux density was controlled at 800 µmol m^{-2} s^{-1} based on previously measured light response curves (*data not shown*), CO_2 concentration at 400 ppm, and flow rate between 150 to 500 µmol m^{-2} s^{-1} to keep vapor pressure deficit (VPD) between 1 and 2 kPa; although, it was difficult to keep VPD below 2 kPa at temperatures above 35 °C. Each leaf was allowed at least approximately five minutes to equilibrate to new chamber conditions, with stability taking longer for lower measurement temperatures. Measurement duration for a single temperature response curve ranged between 40-75 minutes and were conducted between the hours of 8am-4pm. The duration of each measurement campaign lasted 21 - 35 days.

Net photosynthetic temperature response parameters were extracted using June *et al.*, (2004):

$$A_{net} = A_{opt} \times e^{-\left(\frac{T_{leaf} - T_{opt}}{\Omega}\right)} \qquad \text{Equation (1)}$$

where A_{net} is net assimilation at the instantaneous leaf temperature (T_{leaf}), and Ω is the difference in T_{opt} and the temperature where photosynthesis is reduced to 37% of A_{opt}. Ω is a measure of the width of the temperature response curve, where a relatively larger value of Ω indicates a wider curve, or broader photosynthetic thermal niche. In eight out of the 124 curves, A_{net} peaked outside the range of measured temperatures, and in these instances, T_{opt} and A_{opt} were determined as the temperature at the maximum rate of photosynthesis and Ω was not extracted. Therefore, Ω statistical analyses were based on 116 of the 124 temperature response curves. For each temperature response curve, we also extracted the rate of stomatal conductance at the photosynthetic optimum temperature (g_{s_Opt}). Finally, we estimated the apparent maximum rate of Rubisco carboxylation ($\hat{V}_{cmax}$) using the 'one-point method' for each photosynthetic temperature response curve (De Kauwe *et al.*, 2016*a*,*b*). We extracted two parameters associated with the maximum apparent rate of Rubisco carboxylation ($\hat{V}_{cmax}$): the optimum temperature of $\hat{V}_{cmax}$ ($T_{\hat{V}opt}$) and the optimum carboxylation rate at that temperature ($\hat{V}_{opt}$) (See Appendix A **Methods A1** for methods of parameter extraction).

3.3.4 A-C_i curves and chlorophyll fluorescence

To further investigate mechanisms underlying photosynthetic acclimation, we performed CO_2 response curves (*A*-C_i curves), at multiple temperatures in order to measure temperature responses of the maximum rates of Rubisco carboxylation (V_{cmax}) and the maximum rates of electron transport (J_{max}). Due to the time intensive nature of *A*-C_i curves, only the most common species, *P. brachiata*, was used for V_{cmax} and J_{max} measurements. Pretreatment measurements were collected July 2015 and post-treatment measurements were taken July – August 2017, after approximately nine months of warming (Fig. 3.2). V_{cmax} and J_{max} were extracted from *A*-C_i curves constructed from twelve CO_2 concentrations from 0 – 1200 ppm, experiencing saturating irradiance (800 µmol m^{-2} s^{-1}) at five temperatures (20, 25, 30, 35, 40 ºC) using a LI6400XT (Li-COR Inc). Flow was adjusted to control VPD from 1-2 kPa; however, VPD often exceeded 3 kPa high temperature (See Appendix A **Methods A2** for methods of extraction of the parameters: optimum temperatures of J_{max} (T_{Jopt}) and V_{cmax} (T_{Vopt}) and the rates of J_{max} at T_{Jopt} and V_{cmax} at T_{Vopt}).

Maximum photochemical performance of photosystem II (*Fv/Fm*) was evaluated on *P. brachiata*, *P. glabrescens*, and the most common tree seedling found within the plots, *Guarea guidonia* on 18 July 2017, after nine months of experimental warming. Predawn, dark adapted *Fv/Fm* measurements were measured on attached foliage using a handheld portable fluorometer (FluorPen FP Max, Photo Systems Instruments, Drasov, Czech Republic). *Fv/Fm* was measured on the first fully expanded leaf from six individuals per species, using separate plants when possible. Chlorophyll concentration

was measured subsequent to the fluorescence measurement using a chlorophyll content meter (CCM-200+, OPTI-SCIENCES, Hudson, NH, USA).

3.3.5 Leaf dark respiration

When possible, we measured foliar dark respiration (R_d) on the same leaves that we used to measure net photosynthesis. R_d measurements were conducted using a LI6400XT fitted with the 6400-05 conifer chamber head wrapped in aluminum foil and a water jacket (Expanded Temperature Control Kit 6400-088 Li-COR Inc., Lincoln, NE, USA). We used this chamber because it allows for larger leaf areas within the chamber, providing more accurate detection of the low rates of R_d. For each measurement, a single leaf was rolled or folded loosely to fit in the chamber and to allow adequate air mixing. Whether or not entire leaves fit inside of the chamber, respiration rates were corrected by the actual leaf area inside the chamber. We measured respiration – temperature response curves at five temperatures (25, 30, 35, 37, 40 °C) and began measurements at least one hour after sunset. Chamber CO_2 was controlled at 400 ppm. Each curve took approximately 25 – 35 minutes to complete.

Each respiratory response curve was fitted to the nonlinear equation:

$$R_d = \beta_0 \times exp(T_{leaf} \times \beta_1) \qquad \text{Equation 2}$$

where R_d is the respiration rate (µmol m^{-2} s^{-1}) at T_{leaf} and β_0 and β_1 are model parameters. The change in respiration rate with every 10 °C (Q_{10}) is calculated as:

$$Q_{10} = exp(10 \times \beta_1) \qquad \text{Equation 3}$$

R_{25} was calculated using:

$$R_{25} = \frac{R_{Tleaf}}{Q_{10}^{(T_{leaf}-25)/10}} \qquad \text{Equation 4}$$

where R_{Tleaf} is the respiration rate at T_{leaf}. R_{25} was calculated for each measurement temperature and then averaged to obtain one value for each leaf.

3.3.6 R:A ratio

The ratio of leaf respiration to photosynthesis (*R:A*) was calculated by dividing R_{25} by the photosynthetic rate at 25 °C (A_{25}). A_{25} was extracted from Equation 1 by setting T_{leaf} equal to 25. For the eight curves that would not fit Equation 1, the actual photosynthetic rate measured at 25 °C was used for the values of A_{25}. When respiration and photosynthesis were measured on separate leaves, measurements were matched from the same individual plant.

3.3.7 Leaf Traits

Directly after leaf collection, leaves were either immediately measured for fresh mass (g) and leaf area or refrigerated for fewer than 36 hours. Entire leaves were scanned, and leaf area was analyzed using ImageJ v.1.50. Leaves were then dried in a 60 ºC oven and weighed for dry mass (g). Leaf mass per area (*LMA*) was calculated as the dry mass (g) divided by the leaf area (cm^2). Leaf water content (LWC) was calculated as:

$$\left(\frac{Fresh\ mass\ (g) - Dry\ mass\ (g)}{Fresh\ mass\ (g)}\right) \times 100 \qquad \text{Equation 5}$$

Dried leaves were ground to a fine powder using a ball mill (SPEX™ SamplePrep 8000M Mixer/Mill, Metuchen, NJ) and then analyzed for leaf nitrogen and carbon content using an elemental analyzer (Elemental Americas, Mt Laurel, NJ). Leaf N per area (N_{area}) was calculated by multiplying N (g g^{-1}) by *LMA* (g cm^{-2}).

We measured stomatal morphology during August 2016 (pre-warming), January 2017 (post-warming, 4 months), May-early June 2017 (8 months post-warming, hereafter 8m-old) for both *P. glabrescens* and *P. brachiata*. We also measured a new *P. brachiata* leaf cohort late June 2017 (8 months post-warming, hereafter 8m-new). Stomatal impressions were collected by applying clear nail varnish to the abaxial side of the leaf. Clear cellophane tape was used to remove the dried varnish, and mounted to glass microscope slides. Photos of the slides were taken under 20x magnification using a

compound light microscope (Eclipse 400, Nikon Instruments Inc., Melville, New York, USA) and camera (DFC295, Leica Microsystems Inc., Buffalo Grove, Illinois, USA) fitted with a .55X coupler. Stomatal density was calculated as the number of stomata within the 20x magnified area and divided by total visible area using ImageJ v.1.50. Stomatal size was calculated by multiplying the length and width, including guard cells, of each stoma visible within the magnified area.

3.3.8 Statistical analysis

Temperature response parameters (A_{opt}, T_{opt}, Ω, g_{s_Opt}, $T_{\hat{V}opt}$, $\hat{V}_{opt}$, Q_{10}, R_{25}, *R:A*) and leaf traits (*LMA*, *LWC*, leaf area, carbon to nitrogen ratio (*C:N*), N_{mass}, N_{area}) values were compared individually for each species using a gain score analysis, which is calculated as the difference between post treatment and pretreatment plot averages, calculated for each season individually. Gain scores were analyzed using two-way ANOVAs by treatment, season, and their interaction. V_{cmax} and J_{max} parameter gain scores were analyzed for treatment differences using Student's t-tests. Stomatal morphology (size and density) was also analyzed using gain scores; however, there were no pretreatment data measured for the winter season (Fig. 3.2B,C). All stomatal morphology gain scores were calculated as the difference between post treatment and summer pretreatment plot averages using two-way ANOVAs by treatment and warming duration (4m, 8m-old, or 8m-new months); whereas, *P. glabrescens* ANOVAs only had two warming duration terms (4m and 8m-old). Gain scores were used to analyze how plot environmental variables: daily maximum (T_{vegMAX}), mean ($T_{vegMEAN}$), and minimum (T_{vegMIN}) surface vegetation and soil volumetric water content at 10 cm (VWC_{10}) differed

between treatment and season. Daily means of T_{vegMAX}, $T_{vegMEAN}$, T_{vegMIN}, and VWC_{10} were used from dates of measurement campaigns only. *Fv/Fm* did not meet the assumptions of normality; therefore, treatments were compared for each species using Mann-Whitney *U* rank sum tests. Chlorophyll content was analyzed for differences between treatments using Student's t-tests.

Because of the low statistical power inherent in these time-intensive physiological measurements, few treatment effects were detected (*i.e.*, using categorical data). Therefore, we also used regression analyses to investigate physiological responses to environmental variables (*i.e.*, using continuous data). ANCOVAs were used to investigate how photosynthetic temperature response parameters responded to T_{vegMAX}, $T_{vegMEAN}$, and soil volumetric water content at depths of 0-10 and 20-30 cm (VWC_{10}, and VWC_{20}, *respectively*) for each species. Respiratory temperature response parameters were analyzed in response to T_{vegMIN}, $T_{vegMEAN}$, VWC_{10}, and VWC_{20} because respiration was measured at night, when minimum temperatures occur. Two Q_{10} values higher than 3 standard deviations from the mean were removed. Environmental variables on the day prior to gas exchange sampling were used because the heaters were turned off for safety during sampling days. In addition, we used hierarchical partitioning to quantify which environmental variable had the highest explanatory power on parameter variance using the 'heir.part' package in R (Walsh & Mac Nally, 2013).

3.4 Results

3.4.1 Environmental variables

On average, the summer sampling campaigns were both hotter and rainier than the winter campaigns. Average daily precipitation was 3-6 times higher, and average daily below-canopy air temperature (T_{air}) was ~3.5 ºC warmer in summer than winter (Appendix A Table A1; Fig. 3.2A). Daily average minimum T_{air} showed slightly less variability between seasons (~1-4 ºC), while maximum T_{air} showed a greater difference between summer and winter campaigns (~3-7 ºC; Table A1). Similarly, control plot mean daily vegetation temperature ($T_{vegMEAN}$) ranged from 23.5-25.3ºC during summer and 20.7-21.9 ºC during winter campaigns (Fig. 3.2B, Table A1).

The infrared warming treatment resulted in hotter vegetation and drier soils compared to the control plots during both seasons. Daily mean, maximum, and minimum vegetation temperature gain scores (*i.e.,* the difference between post- and pre- treatment) showed a treatment effect (Table A2), where heated leaf T_{vegMAX} was ~ 4 ºC greater, heated leaf $T_{vegMEAN}$ was ~ 3 ºC greater, and heated leaf T_{vegMIN} was ~ 2 ºC greater compared to the control plots for both seasons (Fig. A1A-C). We did find a "seasonal" effect for $T_{vegMEAN}$, T_{vegMIN}, and VWC_{10} (Table A2; Fig. A1B-D); however, this does not indicate actual seasonal differences in these environmental parameters. Gain scores measure the change from pre- to post-treatment; therefore, a "seasonal" effect in the gain score indicates that there is more inter-annual variation during one of the seasons. Additionally, soil volumetric water content at 10 cm (VWC_{10}) gain score was ~34% lower in the heated plots than the control (Table A2; Fig. A1D), showing that the warming

treatment did significantly alter the heated plants' growth environment through both higher vegetation temperatures and lower soil moisture (Fig. 3.2B,C), and this treatment effect was consistent across seasons.

3.4.2 Treatment effects on net photosynthesis and foliar respiration

While *Piper glabrescens* did not show treatment effects for any photosynthetic parameters, *Psychotria brachiata* did shift to a broader photosynthetic thermal niche under the warming treatment. Gain score analysis showed the optimum temperatures of photosynthesis (T_{opt}) and the rates of both photosynthesis and stomatal conductance at that optimum temperature (A_{opt} and g_{s_opt}) were not detectably different between warming and control plots for either study species (Table 3.2; Fig A2A-D,G,H). However, the photosynthetic thermal niche (Ω) of *P. brachiata* was ~ 6 °C wider in the heated plots compared to the control plots ($p = 0.044$, Table 3.2, Fig. A2E), while *P. glabrescens* Ω did not differ between the heated and control plots (Fig. A2F).

For both species, photosynthetic optimum temperatures (i.e., T_{opt}) exceeded maximum daily vegetation temperatures in both heated and control plots during all measurement campaigns. T_{opt} values ranged from 30-32 °C in control plots and 32-34 °C in heated plots for both species (Table A3). Control plot T_{opt} was ~7 °C higher than maximum vegetation temperature for *P. brachiata* and ~6-9 °C higher for *P. glabrescens*, with greater differences during the winter (Table A3; Fig. 3.3).

We found no evidence of a warming treatment effect on foliar respiration temperature response or the ratio between respiration and photosynthesis at 25 °C (*R:A*)

for either species. Neither *P. brachiata* nor *P. glabrescens* showed significant treatment, season, or interaction effects on the gain scores of Q_{10}, R_{25}, *or R:A* (Table 3.2, Fig. 3.4, Fig A3A-F).

3.4.3 Treatment effects on component processes of net photosynthesis

We investigated underlying mechanisms of photosynthetic thermal acclimation by exploring the shifts in temperature responses of component processes of net photosynthesis, including apparent maximum rates of Rubisco carboxylation ($\hat{V}_{cmax}$), maximum rates of Rubisco carboxylation (V_{cmax}), and maximum rates of electron transport (J_{max}) (Table A4). Consistent with our analyses of net photosynthesis, we detected no warming treatment effects for the temperature responses of maximum electron transport rate or maximum rubisco carboxylation or evidence of stress on Photosystem II. There were no treatment or interaction effects for the optimum temperature of $\hat{V}_{cmax}$ ($T_{\hat{V}opt}$) or the rate of $\hat{V}_{cmax}$ at the optimum temperature ($\hat{V}_{opt}$) (Table 3.2; Fig. A4). Similarly, neither the optimum temperature of V_{cmax} (T_{Vopt}; Student's t-test p = 0.226), rate of V_{cmax} at T_{Vopt} (Student's t-test p = 0.791), the optimum temperature of J_{max} (T_{Jopt}; Student's t-test p = 0.509), nor the rate of J_{max} at T_{Jopt} (Student's t-test p = 0.764) gain scores differed between treatments (Fig. A5). Whitney Mann tests showed no difference in dark adapted chlorophyll fluorescence (Fv/Fm) values (i.e., PSII stress response) after 9 months of warming for *P. brachiata* (Fv/Fm = 0.775, p = 0.255), *P. glabrescens* (Fv/Fm = 0.727, p = 0.399), or *Guarea guidonia* (Fv/Fm = 0.784, p = 0.117, Fig. A6).

3.4.4 Gas exchange parameter responses to environmental variables

While categorical gain score analysis of treatment and season did not reveal many statistically significant treatment effects, we did find evidence of acclimation when looking at the responses to continuous environmental variables across plots and seasons. Optimum photosynthetic temperatures and thermal niches increased for both species as vegetation became warmer, though responses were stronger for *P. brachiata*. For both species, T_{opt} increased significantly with both daily mean and maximum vegetation temperatures (Table A5; Figs. 3.5A,B). T_{opt} of *P. brachiata* increased more steeply with mean and maximum T_{veg} than *P. glabrescens*, showing a nearly significant interaction term for $T_{vegMEAN}$ (p=0.079; Table A5; Figs. 3.5A,B). While A_{opt} did not show significant responses to either temperature variable, the plots revealed patterns of a slight increase with temperature for *P. brachiata*, and as in T_{opt}, the interaction with $T_{vegMEAN}$ was nearly significant (p = 0.085; Table A5; Figs. 3.5E,F). Contrary to results of the gain score analysis, thermal niche broadened for both species as vegetation temperatures rose, where Ω was strongly correlated with both increasing maximum and mean daily temperatures (Table A5; Figs. 3.5I,J). As shown by the significant species effect in all Ω ANCOVAs, *P. glabrescens* had a higher Ω compared to *P. brachiata*, indicating a broader photosynthetic thermal niche (Table A5; Figs 3.5I-J). Neither species revealed relationships between g_{s_Opt} and T_{veg} (Table A5; Figs. 3.5M,N).

Optimum temperatures and thermal niches increased with decreasing deeper (10-20 cm) soil moisture, and photosynthesis and stomatal conductance at the optimum temperature decreased as deeper soil moisture dried. Overall, none of the photosynthetic

parameters showed response to shallow soil moisture (VWC_{10}; Table A5; Figs. 3.5C, G, K, O). T_{opt} responded more strongly and increased with decreasing soil moisture from 20-30 cm (VWC_{20}; Table A5; Fig. 3.5D). A_{opt} slightly declined with decreasing VWC_{20} for both species (Table A5; Fig. 3.5H). Similar to T_{opt}, Ω increased with decreasing VWC_{20} (Table A5; Fig. 3.5L). g_{s_Opt} decreased with decreasing VWC_{20} (Table A5; Fig. 3.5P).

Foliar respiration showed no evidence of thermal acclimation for either species and Q_{10} *increased* slightly with increasing nighttime temperatures, which is the opposite direction of our expectation of a down-regulation. Respiratory temperature sensitivity (Q_{10}) did not respond to $T_{vegMEAN}$, but Q_{10} increased slightly with increasing T_{vegMIN} ($p = 0.063$; Table A5; Figs. 3.6A,B) for both species. Basal respiration rates (R_{25}), however, were not correlated with either mean or minimum daily temperatures (Table 3.3, Figs. 3.6E,F).

Both Q_{10} and R_{25} appeared to down-regulate as deeper soils dried, while patterns with shallow soil moisture were more inconclusive. Both species' Q_{10} and R_{25} decreased with decreasing VWC_{20} (Table A5; Figs. 3.6D,H). A nearly significant interaction ($p = 0.051$; Table A5; Fig 3.6C) showed that *P. brachiata* Q_{10} decreased with decreasing VWC_{10}, while *P. glabrescens* Q_{10} showed the opposite pattern. On the other hand, *P. glabrescens* R_{25} decreased with decreasing VWC_{10} while *P. brachiata* showed no response ($p = 0.015$; Table A5; Fig. 3.6G).

Hierarchical partitioning revealed that most variation in photosynthesis and respiratory parameters was controlled, unexpectedly, by deeper soil moisture (20-30 cm),

rather than temperature. Variance in T_{opt}, A_{opt}, and g_{s_Opt} were all strongly controlled by VWC_{20} for both study species (Fig. 3.7). Variance of thermal niche (Ω) for *P. brachiata* was strongly driven by VWC_{20} (Fig. 3.7A); however, *P. glabrescens* Ω variance was better explained by vegetation temperature (Fig. 3.7B). Q_{10} variance was relatively evenly explained by vegetation temperature and soil moisture (Fig. 3.7), particularly for *P. glabrescens,* while VWC_{20} explained most of the variance in R_{25} (Fig. 3.7).

3.4.5 Adjustments in leaf morphological and chemical traits

Stomatal morphology of *P. brachiata* only was altered with prolonged experimental warming. Stomatal density was not altered for either species (Table 3.3, Fig A7A,B). *P. brachiata* leaves had smaller stomata in the heated compared to the control plots after eight months of warming, but *P. glabrescens* showed no change (Table 3.3; Fig. A7C,D).

Neither species showed evidence of treatment effects for leaf morphology or leaf chemistry, with the exception of *P. glabrescens* shifting to a lower leaf mass per area (*LMA*) with prolonged warming. *P. brachiata LMA* gain scores had no significant treatment or interaction effects (Table 3.4; Fig. A8A). A significant interaction between treatment and season showed that *P. glabrescens* heated leaf *LMA* was higher than the control in the winter (4 months post warming), but the opposite response occurred during the summer after 8 months of warming (Table 3.4; Fig. A8B). There were no treatment or season effects for any other measured leaf trait (Table 3.4; Fig. 3.8C-L). In addition, leaf chlorophyll content did not shift after nine months warming for *P. brachiata* (SPAD =

44.02 ± 1.91, p = 0.104), *P. glabrescens* (SPAD = 16.11 ± 0.58, p = 0.508), or *G. guidonia* (SPAD = 23.40 ± 1.51, p = 0.565).

3.5 Discussion

3.5.1 Evidence of photosynthetic acclimation

Contrary to our hypothesis, we did find evidence of photosynthetic thermal acclimation through increased thermal niche breadth in both species and an up-regulation of both T_{opt} and A_{opt} for *P. brachiata*. A wider thermal niche shows evidence of acclimation because these plants can maintain carbon gain under a wider range of temperatures. Other studies have found that tropical species have some ability to photosynthetically acclimate to warmer temperatures (Cheesman & Winter, 2013; Slot & Winter, 2017a, but not always Fauset *et al.*, 2019) or stimulate photosynthesis (Krause *et al.*, 2013); however, acclimation was limited and has only been found in greenhouses or growth chambers (Cheesman & Winter, 2013; Slot & Winter, 2017a; Smith & Dukes, 2017). This emphasizes the importance of *in situ* studies that may provide a more comprehensive representation of how plants will respond to climate warming. Despite indications of A_{net} acclimation (Fig. 3.5A,E,I; Fig. A2E), we did not detect evidence of thermal acclimation of the biochemical components of net photosynthesis. While both J_{max} and V_{cmax} have been found to acclimate within days (Smith & Dukes, 2017), it is possible that longer-term warming was required to detect a shift of these processes. Overall, there are limited examples of how tropical plant photosynthesis changes with prolonged warming, and evidence is even more limited for the biochemical components of photosynthesis.

Our results are contrary to the findings of Slot and Winter (2017*a*), where higher growth temperature *decreased* photosynthetic thermal niche width in tropical seedlings, while they did find some evidence of increased T_{opt}. Doughty (2011) did not find any evidence of photosynthetic acclimation in a tropical forest canopy warming experiment. There may be differences between canopy and understory foliage in how thermal niches respond to elevated growth temperature. Within tropical forests, leaf temperatures and vapor pressure deficits increase dramatically from the understory to the canopy top (Rey-Sánchez *et al.*, 2016); therefore, canopy leaves may have narrow thermal niches to conserve water status. Due to high heat stress, leaves in the canopy are *already* operating at or above thermal thresholds for photosynthesis (Doughty & Goulden, 2008; Mau *et al.*, 2018). Thus, canopy foliage may not have the plasticity to up-regulate physiology to the same degree as understory plants.

3.5.2 No evidence of respiratory acclimation

Contrary to our initial hypotheses on tropical plant photosynthesis, there is a greater consensus suggesting that tropical plants will be able to acclimate their rates of respiration (Slot & Kitajima, 2015); however, we found no evidence of respiratory acclimation for either species. Additionally, we found surprising evidence for a slight up-regulation of Q_{10} with increasing nighttime temperatures (Fig. 3.6B). While there are few studies to corroborate respiratory acclimation through *in situ* tropical warming studies, Slot *et al.* (2014) found that canopy leaves exposed to seven days of nighttime warming were able to acclimate through a down-regulation of the basal rate of respiration (R_{25}). Studies on juvenile tropical species have found evidence of both decreased slope

(Cheesman & Winter, 2013; Krause *et al.*, 2013) or both decreased basal rate and slope (Cheesman & Winter, 2013; Drake *et al.*, 2015) of respiratory acclimation. Our hypothesis that respiration would acclimate was primarily based on our assumption that photosynthesis would not acclimate, leading to substrate limitation (Dewar *et al.*, 1999; Atkin and Tjoelker, 2003; Aspinwall *et al.*, 2016). We did find evidence for photosynthetic acclimation, however, which could mean that substrate was not limited. Further, there were no treatment differences in the ratio of respiration to photosynthesis (*R:A*) (Table 3.2; Fig. A3E,F) and, because these species were operating well below their optimum temperatures, warming would likely not negatively affect leaf carbon balance for these two species.

3.5.3 Soil moisture: a stronger driver than temperature

Our study aimed to investigate how plants specifically respond to elevated temperature; however, along with heating plant tissues, our warming treatment caused soil drying (Fig. A1D). Changing precipitation patterns and soil drying is predicted to have large impacts on ecosystem carbon balance (Ciais *et al.*, 2005; Phillips *et al.*, 2009; Kao & Ganguly, 2011; Sherwood & Fu, 2014). Importantly, hierarchical partitioning revealed that deeper soil moisture, even more so than vegetation temperature or shallow soil moisture, was the most influential climate variable determining variation in many gas exchange parameters (Fig. 3.7), with the exception of parameters that describe both photosynthetic (Ω) and respiratory (Q_{10}) temperature sensitivity. Deeper soil moisture may have been a stronger driver than shallow soil moisture because it was less variable in general (Kimball *et al.*, 2018). T_{opt} increased as soil moisture decreased (Fig. 3.5D),

providing evidence that neither species T_{opt} is likely to be negatively affected by a drying climate. Similar to our results, a study in an Oak-grassland-savanna ecosystem also found that soil drying had a positive effect on T_{opt} (Ma *et al.*, 2017). On the other hand, photosynthetic rate and stomatal conductance at T_{opt} both decreased as soils dried (Fig. 3.5H,P), suggesting that drying soil could potentially have a negative effect on carbon gain. Similarly, a long-term study found that photosynthesis declined as soil moisture decreased in 11 boreal and temperate species, likely due to stomatal conductance restrictions (Reich *et al.*, 2018). R_{25} also decreased as soil moisture decreased, perhaps following the trend of A_{opt}, where decreased substrate may have limited the rate of respiration in drier soils. The role soil moisture played in our species` physiological responses reinforces the importance of investigating how both temperature and moisture affect plant gas exchange responses to climate change.

3.5.4 Warming induced shifts in leaf and stomatal traits

Many model simulations of tropical forests have predicted that temperature will negatively affect carbon gain through lowered stomatal conductance (Doughty and Goulden, 2008; Lloyd and Farquhar, 2008; Galbraith *et al.*, 2010), rather than more direct effects to photosynthetic machinery. Although relatively rare, studies at both the leaf or canopy level (Doughty and Goulden, 2008; Lloyd and Farquhar, 2008; Slot and Winter, 2017*c*) and ecosystem scale (Doughty and Goulden, 2008; Tan *et al.*, 2017) in tropical forests have also found that photosynthesis at supra-optimum temperatures is determined by plant water status (but see Galbraith *et al.*, 2010). While we did not find evidence that experimental warming affected stomatal conductance in either of our study species, *P.*

brachiata did shift toward lower stomatal size in the heated leaves (Fig. A7C). Smaller stomata suggest that *P. brachiata* might be acclimating to maintain plant water status. Other studies have found that warming can either increase (Hill *et al.*, 2014; Becker *et al.*, 2017; Jumrani *et al.*, 2017; Shen *et al.*, 2017) or decrease (Shen *et al.*, 2017; Rodrigues *et al.*, 2018) stomatal density or size. For example, Wu *et al.*, (2018) found that subtropical tree species with smaller stomata are better able to maintain rates of stomatal conductance and photosynthesis under high temperature-induced water deficits. Smaller stomata size allows stomata to close more quickly (Aasamaa *et al.*, 2001), allowing plants to have more dynamic responses to environmental conditions (Hetherington & Woodward, 2003). Stomatal morphological plasticity may give *P. brachiata* an advantage in the balance between carbon gain and water loss.

The only clear leaf trait response we found was a decline in leaf mass per area (*LMA*) with prolonged warming for *P. glabrescens*. Other tropical warming studies have found *LMA* to decline with experimental warming (Scafaro *et al.*, 2017; Slot & Winter, 2017a, 2018; but see Cheesman and Winter 2013). This pattern may be the result of a reduction of nonstructural carbohydrates or a reduced investment in Rubisco (Poorter *et al.*, 2009; Scafaro *et al.*, 2017); however, few studies have specifically investigated mechanisms inducing changes in *LMA* with experimental warming.

3.5.5 Implications for a warmer future

Our two study species showed contrasting mechanisms that could prevent a negative shift in carbon gain under elevated temperatures. *P. brachiata* had higher plasticity to respond to elevated temperatures than *P. glabrescens* (Figs. 3.5A,B,E, Fig.

A2E, Fig. A7C); however, *P. glabrescens* had an overall broader thermal niche (Fig. 3.3). Our study site is located in an area with frequent hurricanes, which can rapidly increase the light and temperature environment experienced by understory species. The higher plasticity in *P. brachiata* may allow this species to respond more quickly to new environmental conditions. Early successional species such as *P. brachiata* are often associated with higher plasticity (Valladares *et al.*, 2000, 2002); while, more shade tolerant species, such as *P. glabrescens*, are generally adapted to thrive in relatively stable environmental conditions (Valladares *et al.*, 2002; Niinemets & Valladares, 2004). Opposite to our findings, faster growing, early successional species are often associated with wider thermal niches (Michaletz *et al.*, 2016); however, this might not be true for tropical species (Slot and Winter 2017*a*). As a result, these two species may respond differently to the greater hurricane intensity and frequency predicted to occur in response to climate change (Knutson *et al.*, 2015; Bacmeister *et al.*, 2018). While higher *P. brachiata* plasticity may allow quicker responses to both warming and disturbance, the wider thermal niches found in *P. glabrescens* could potentially mitigate negative effects of climate warming.

3.5.6 Conclusions

Our study presents results from the first whole-plant *in situ* experimental warming study in a tropical forest and found results that are dissimilar to common hypotheses surrounding tropical plant physiological acclimation to elevated temperatures. We did not find evidence for respiratory acclimation; however, photosynthesis showed a capacity to acclimate for both *P. brachiata* and *P. glabrescens*. Of our two study species, *P.*

brachiata may be more resilient to climate warming due to higher plasticity in traits that conserve water and promote carbon gain; however, *P. glabrescens* was, overall, less sensitive to changes in temperature. Both species were operating well below T_{opt}, suggesting that increasing temperatures that fall within +4 °C of current conditions will likely not negatively influence carbon gain. Lastly, soil moisture played an important role in determining the variation of many gas exchange variables, where T_{opt} tended to increase in drier soils and the rate of photosynthesis and stomatal conductance at T_{opt} and basal respiration rates all declined as soils dried. The role that soil moisture plays in influencing plant carbon gain should be considered in *in situ* warming studies.

3.6 Acknowledgements

This research was funded by U.S. Department of Energy award numbers DE-SC-0011806, 89243018S-SC-000014, and DE-SC-0018942 awarded to MAC, TEW, and SCR. SCR was also supported by the U.S. Geological Survey. The USDA Forest Service's International Institute of Tropical Forestry (IITF) and University of Puerto Rico-Río Piedras provided additional support. All research at IITF is done in collaboration with the University of Puerto Rico. ECS was also funded by Michigan Technological University Ecosystem Science Center and a Summer Undergraduate Research Fellowship. KRC was also funded by Michigan Technological Finishing Fellowship and Michigan Tech Ecosystem Science Center. We are very grateful to TRACE project manager Aura M. Alonso-Rodríguez for logistical support. We are also grateful to Kaylie Butts, Benjamin Miller, Talia Anderson, Jamarys Torres-Díaz, Grace Anna Schilz, Jack Zwart, and Brian Peacock for their excellent field and lab assistance.

3.7 Reference List

Aasamaa K, Sõber A, Rahi M. **2001**. Leaf anatomical characteristics associated with shoot hydraulic conductance, stomatal conductance and stomatal sensitivity to change in leaf water status in temperate deciduous trees. *Australian Journal of Plant Physiology* **28**: 765–774.

Arneth A, Mercado L, Kattge J, Booth BBB. **2012**. Future challenges of representing land-processes in studies on land-atmosphere interactions. *Biogeosciences* **9**: 3587–3599.

Aspinwall MJ, Drake JE, Campany C, Värhammar A, Ghannoum O, Tissue DT, Reich PB, Tjoelker MG. **2016**. Convergent acclimation of leaf photosynthesis and respiration to prevailing ambient temperatures under current and warmer climates in *Eucalyptus tereticornis*. *New Phytologist* **212**: 354–367.

Atkin OK, Bloomfield KJ, Reich PB, Tjoelker MG, Asner GP, Bonal D, Bönisch G, Bradford MG, Cernusak LA, Cosio EG, *et al.* 2015. Global variability in leaf respiration in relation to climate, plant functional types and leaf traits. *New Phytologist* **206**: 614–636.

Atkin OK, Bruhn D, Hurry VM, Tjoelker MG. **2005**. The hot and the cold : unravelling the variable response of plant respiration to temperature. *Functional Plant Biology* **32**: 87–105.

Atkin OK, Tjoelker MG. **2003**. Thermal acclimation and the dynamic response of plant respiration to temperature. *Trends in Plant Science* **8**: 343–351.

Bacmeister JT, Reed KA, Hannay C, Lawrence P, Bates S, Truesdale JE, Rosenbloom N, Levy M. **2018**. Projected changes in tropical cyclone activity under future warming scenarios using a high-resolution climate model. *Climatic Change* **146**: 547–560.

Becker VI, Goessling JW, Duarte B, Cacador I, Liu F, Rosenqvist E, Jacobsen S-E. **2017**. Combined effects of soil salinity and high temperature on photosynthesis and growth of quinoa plants (*Chenopodium quinoa*). *Functional Plant Biology* **44**: 665–678.

Beer C, Reichstein M, Tomelleri E, Ciais P, Jung M, Carvalhais N, Rodenbeck C, Arain MA, Baldocchi D, Bonan GB, *et al.* 2010. Terrestrial gross carbon dioxide uptake: global distribution and covariation with climate. *Science* **329**: 834–839.

Berry J, Bjorkman O. **1980**. Photosynthetic response and adaptation to temperature in higher plants. *Annual Review of Plant Physiology* **31**: 491–543.

Booth BBB, Jones CD, Collins M, Totterdell IJ, Cox PM, Sitch S, Huntingford C, Betts RA, Harris GR, Lloyd J. **2012**. High sensitivity of future global warming to land carbon cycle processes. *Environmental Research Letters* **7**: 024002.

von Caemmerer S, Quick WP. **2000**. Rubisco: physiology *in vivo*. In: Leegood RC, Sharkey TD, von Caemmerer S, eds. *Photosynthesis: Physiology and Metabolism*. Dordrecht: Springer Netherlands, 85–113.

Campbell C, Atkinson L, Zaragoza-Castells J, Lundmark M, Atkin O, Hurry V. **2007**. Acclimation of photosynthesis and respiration is asynchronous in response to

changes in temperature regardless of plant functional group. *New Phytologist* **176**: 375–389.

Cavaleri MA, Reed SC, Smith WK, Wood TE. **2015**. Urgent need for warming experiments in tropical forests. *Global Change Biology* **21**: 2111–2121.

Cernusak LA, Winter K, Dalling JW, Holtum JAM, Jaramillo C, Körner C, Leakey ADB, Norby RJ, Poulter B, Turner BL, *et al.* 2013. Tropical forest responses to increasing atmospheric CO_2: Current knowledge and opportunities for future research. *Functional Plant Biology* **40**: 531–551.

Cheesman AW, Winter K. **2013**. Elevated night-time temperatures increase growth in seedlings of two tropical pioneer tree species. *New Phytologist* **197**: 1185–1192.

Ciais P, Reichstein M, Viovy N, Granier A, Ogée J, Allard V, Aubinet M, Buchmann N, Bernhofer C, Carrara A, *et al.* 2005. Europe-wide reduction in primary productivity caused by the heat and drought in 2003. *Nature* **437**: 529–533.

Cox PM, Betts RA, Jones CD, Spall SA, Totterdell IJ. **2000**. Acceleration of global warming due to carbon-cycle feedbacks in a coupled climate model. *Nature* **408**: 184–187.

Crous KY, Sharwood E, Drake JE, Tjoelker MG, Aspinwall MJ, Ghannoum O. **2018**. Photosynthetic capacity and leaf nitrogen decline along a controlled climate gradient in provenances of two widely distributed *Eucalyptus* species. *Global Change Biology* **24**: 4626–4644.

Cunningham SC, Read J. **2003**. Do temperate rainforest trees have a greater ability to acclimate to changing temperatures than tropical rainforest trees? *New Phytologist* **157**: 55–64.

Devoe NN. **1989**. *Differential seedling and regerneration in openings and beneath closed canopy in sub-tropical wet forest*. PhD dissertation, Yale University, New Haven, CT, USA.

Dewar RC, Medlyn BE, Mcmurtrie RE. **1999**. Acclimation of the respiration/photosynthesis ratio to temperature: insights from a model. *Global Change Biology* **5**: 615–622.

Diffenbaugh NS, Scherer M. **2011**. Observational and model evidence of global emergence of permanent, unprecedented heat in the 20th and 21st centuries. *Climatic Change* **107**: 615–624.

Doughty CE. **2011**. An in situ leaf and branch warming experiment in the Amazon. *Biotropica* **43**: 658–665.

Doughty CE, Goulden ML. **2008**. Are tropical forests near a high temperature threshold? *Journal of Geophysical Research* **113**: G00B07.

Drake JE, Aspinwall MJ, Pfautsch S, Rymer PD, Reich PB, Smith RA, Crous KY, Tissue DT, Ghannoum O, Tjoelker MG. **2015**. The capacity to cope with climate warming declines from temperate to tropical latitudes in two widely distributed *Eucalyptus* species. *Global Change Biology* **21**: 459–472.

Drake JE, Tjoelker MG, Aspinwall MJ, Reich PB, Barton CVM, Belinda E, Duursma RA. 2016. Does physiological acclimation to climate warming stabilize the ratio of canopy respiration to photosynthesis? *New Phytologist* **211**: 850–863.

Farquhar GD, Sharkey TD. **1982**. Stomatal conductance and photosynthesis. *Annual Review of Plant Physiology* **33**: 317–345.

Fauset S, Oliveira L, Buckeridge MS, Foyer CH, Galbraith D, Tiwari R, Gloor M. 2019. Contrasting responses of stomatal conductance and photosynthetic capacity to warming and elevated CO_2 in the tropical tree species *Alchornea glandulosa* under heatwave conditions. *Environmental and Experimental Botany* **158**:28–39.

Galbraith D, Levy PE, Sitch S, Huntingford C, Cox P, Williams M, Meir P. **2010**. Multiple mechanisms of Amazonian forest biomass losses in three dynamic global vegetation models under climate change. *New Phytologist* **187**: 647–665.

Harris NL, Lugo AE, Brown S, Heartsill Scalley T. (Eds.) **2012**. *Luquillo Experimental Forest: Research History and Opportunities*. EFR-1. Washington, DC: U.S. Department of Agriculture. 152 p.

Havaux M. **1996**. Short-tern response of Photosystem I to heat stress. *Photosynthesis Research* **47**: 85–97.

Havaux M, Tardy F, Ravenel J, Chanu D, Parot P. **1996**. Thylakoid membrane stability of heat stress studied by flash spectroscopic measurements of the electrochromic shift in intact potato leaves: influence of the xanthophyll content. *Plant, Cell and*

Environment **19**: 1359–1368.

Hetherington AM, Woodward FI. **2003**. The role of stomata in sensing and driving environmental change. *Nature* **424**: 901–908.

Hill KE, Guerin GR, Hill RS, Watling JR. **2014**. Temperature influences stomatal density and maximum potential water loss through stomata of Dodonaea viscosa subsp . angustissima along a latitude gradient in southern Australia. *Australian Journal of Botany* **62**: 657–665.

Huner NPA. **1988**. Low-temperature induced alterations in photosynthetic membranes. *Critical Reviews in Plant Sciences* **7**: 257–278.

Huntingford C, Zelazowski P, Galbraith D, Mercado LM, Sitch S, Fisher R, Lomas M, Walker AP, Jones CD, Booth BBB, *et al.* 2013. Simulated resilience of tropical rainforests to CO_2 -induced climate change. *Nature Geoscience* **6**: 268–273.

Janzen DH. **1967**. Why Mountain Passes are Higher in the Tropics. *The American Naturalist* **101**: 233–249.

Jin B, Wang L, Wang J, Jiang K, Wang Y, Jiang X, Ni C, Wang Y, Teng N. **2011**. The effect of experimental warming on leaf functional traits, leaf structure and leaf biochemistry in *Arabidopsis thaliana*. *BCM Plant Biology* **11**.

Jumrani K, Bhatia VS, Pandey GP. **2017**. Impact of elevated temperatures on specific leaf weight, stomatal density, photosynthesis and chlorophyll fluorescence in soybean. *Photosynthesis Research* **131**: 333–350.

June T, Evans JR, Farquhar GD. **2004**. A simple new equation for the reversible temperature dependence of photosynthetic electron transport: a study on soybean leaf. *Functional Plant Biology* **31**: 275–283.

Kao SC, Ganguly AR. **2011**. Intensity, duration, and frequency of precipitation extremes under 21st-century warming scenarios. *Journal of Geophysical Research Atmospheres* **116**: 1–14.

De Kauwe MG, Lin YS, Wright IJ, Medlyn BE, Crous KY, Ellsworth DS, Maire V, Prentice IC, Atkin OK, Rogers A, *et al.* 2016a. A test of the 'one-point method' for estimating maximum carboxylation capacity from field-measured, light-saturated photosynthesis. *New Phytologist* **210**:1130-1144.

De Kauwe MG, Lin YS, Wright IJ, Medlyn BE, Crous KY, Ellsworth DS, Maire V, Prentice IC, Atkin OK, Rogers A, *et al.* 2016b. Corrigendum. *New Phytologist* **210**: 1130–1144.

Kenzo T, Yoneda R, Sano M, Araki M, Shimizu A, Tanaka-Oda A, Chann S. **2012**. Variations in leaf photosynthetic and morphological traits with tree height in various tree species in a cambodian tropical dry evergreen forest. *Japan Agricultural Research Quarterly* **46**: 167–180.

Kimball BA, Alonso-Rodríguez AM, Cavaleri MA, Reed SC, González G, Wood TE. **2018**. Infrared heater system for warming tropical forest understory plants and soils. *Ecology and Evolution **8***: 1932-1944.

Knutson TR, Sirutis JJ, Zhao M, Tuleya RE, Bender M, Vecchi GA, Villarini G, Chavas D. **2015**. Global projections of intense tropical cyclone activity for the late twenty-first century from dynamical downscaling of CMIP5/RCP4.5 scenarios. *Journal of Climate* **28**: 7203–7224.

Korner C. **2004**. Through enhanced tree dynamics carbon dioxide enrichment may cause tropical forests to lose carbon. *Philosophical Transactions of the Royal Society B: Biological Sciences* **359**: 493–498.

Krause GH, Cheesman AW, Winter K, Krause B, Virgo A. **2013**. Thermal tolerance, net CO_2 exchange and growth of a tropical tree species, *Ficus insipida*, cultivated at elevated daytime and nighttime temperatures. *Journal of Plant Physiology* **170**: 822–827.

Lloyd J, Farquhar GD. **2008**. Effects of rising temperatures and [CO_2] on the physiology of tropical forest trees. *Philosophical transactions of the Royal Society of London. Series B, Biological sciences* **363**: 1811–7.

Lombardozzi DL, Bonan GB, Smith NG, Dukes JS, Fisher RA. **2015**. Temperature acclimation of photosynthesis and respiration: A key uncertainty in the carbon cycle-climate feedback. *Geophysical Research Letters* **42**: 8624–8631.

Ma S, Osuna JL, Verfaillie J, Baldocchi DD. **2017**. Photosynthetic responses to temperature across leaf–canopy–ecosystem scales: a 15-year study in a Californian oak-grass savanna. *Photosynthesis Research* **132**: 277–291.

Mau A, Reed S, Wood T, Cavaleri M. **2018**. Temperate and tropical forest canopies are

already functioning beyond their thermal thresholds for photosynthesis. *Forests* **9**: 47.

Medlyn BE, Dreyer E, Ellsworth D, Forstreuter M, Harley PC, Kirschbaum MUF, Le Roux X, Montpied P, Strassemeyer J, Walcroft A., *et al.* 2002. Temperature response of parameters of a biochemically based model of photosynthesis. II. A review of experimental data. *Plant, Cell and Environment* **25**: 1167–1179.

Mercado LM, Medlyn BE, Huntingford C, Oliver RJ, Clark DB, Sitch S, Zelazowski P, Kattge J, Harper AB, Cox PM. **2018**. Large sensitivity in land carbon storage due to geographical and temporal variation in the thermal response of photosynthetic capacity. *New Phytologist* **218**: 1462–1477.

Michaletz ST, Weiser MD, McDowell NG, Zhou J, Kaspari M, Helliker BR, Enquist BJ. **2016**. The energetic and carbon economic origins of leaf thermoregulation. *Nature Plants* **2**: 1–8.

Mora C, Frazier AG, Longman RJ, Dacks RS, Walton MM, Tong EJ, Sanchez JJ, Kaiser LR, Stender YO, Anderson JM, *et al.* 2013. The projected timing of climate departure from recent variability. *Nature* **502**: 183–7.

Myster RW, Walker LR. **1997**. Plant Successional Pathways on Puerto Rican Landslides. *Journal of Tropical Ecology* **13**: 165–173.

Niinemets Ü, Valladares F. **2004**. Photosynthetic acclimation to simultaneous and interacting environmental stresses along natural light gradients: Optimality and constraints. *Plant Biology* **6**: 254–268.

Pan Y, Birdsey RA., Phillips OL, Jackson RB. **2013**. The structure, distribution, and biomass of the world's forests. *Annual Review of Ecology, Evolution, and Systematics* **44**: 593–622.

Pearcy R. **1987**. Photosynthetic gas exchange responses of Australian tropical forest trees in canopy, gap and understorey micro-environments. *Functional Ecology* **1**: 169–178.

Pearcy RW, Valladares F, Wright SJ, De Paulis EL. **2004**. A functional analysis of the crown architecture of tropical forest *Psychotria* species: Do species vary in light capture efficiency and consequently in carbon gain and growth? *Oecologia* **139**: 163–177.

Phillips OL, Lewis SL, Lloyd J, López-González G, Peacock J, Quesada CA, Van Der Heijden G, Baker TR, Feldpausch TR, Gloor E, *et al.* 2009. Drought sensitivity of the Amazon rainforest. *Science* **323**: 1344–1347.

Poorter H, Niinemets Ü, Poorter L, Wright IJ, Villar R. **2009**. Causes and consequences of variation in leaf mass per area (LMA): A meta-analysis. *New Phytologist* **182**: 565–588.

Portis AR. **1995**. The regulation of Rubisco by Rubisco activase. *Journal of Experimental Botany* **46**: 1285–1291.

Portis AR. **2003**. Rubisco activase - Rubisco's catalytic chaperone. *Photosynthesis Research* **75**: 11–27.

Reich PB, Sendall KM, Stefanski A, Rich RL, Hobbie SE, Montgomery RA. **2018**.

Effects of climate warming on photosynthesis in boreal tree species depend on soil moisture. *Nature* **562**: 263-267

Rey-Sánchez A, Slot M, Posada J, Kitajima K. **2016**. Spatial and seasonal variation in leaf temperature within the canopy of a tropical forest. *Climate Research* **71**: 75–89.

Rodrigues WP, Martins MQ, Fortunato AS, Rodrigues AP, Semedo JN, Simões-Costa MC, Pais IP, Leitão AE, Colwell F, Goulao L, *et al.* 2016. Long-term elevated air [CO_2] strengthens photosynthetic functioning and mitigates the impact of supra-optimal temperatures in tropical *Coffea arabica* and *C. canephora* species. *Global Change Biology* **22**: 415–431.

Sage RF, Kubien DS. **2007**. The temperature response of C3 and C4 photosynthesis. *Plant, Cell and Environment* **30**: 1086–1106.

Sage RF, Way DA, Kubien DS. **2008**. Rubisco, Rubisco activase, and global climate change. *Journal of Experimental Botany* **59**: 1581–1595.

Salvucci ME, Osteryoung KW, Crafts-Brandner SJ, Vierling E. **2001**. Exceptional sensitivity of Rubisco activase to thermal denaturation in vitro and in vivo. *Plant physiology* **127**: 1053–1064.

Scafaro AP, Xiang S, Long BM, Bahar NHA, Weerasinghe LK, Creek D, Evans JR, Reich PB, Atkin OK. **2017**. Strong thermal acclimation of photosynthesis in tropical and temperate wet-forest tree species: The importance of altered Rubisco content. *Global Change Biology* **23**: 2783–2800.

Scatena F. **1989**. *An Introduction to the Physiography and History of the Bisley Experimental Watersheds in the Luquillo Mountains of Puerto Rico*. General Technical Report SO-72. New Orleans, LA, USA: United States Department of Agriculture Sourthern Forest Experiment Station. 22p

Schimel D, Pavlick R, Fisher JB, Asner GP, Saatchi S, Townsend P, Miller C, Frankenberg C, Hibbard K, Cox P. **2015**. Observing terrestrial ecosystems and the carbon cycle from space. *Global Change Biology* **21**: 1762–1776.

Shen HF, Zhao B, Xu JJ, Liang W, Huang WM, Li HH. **2017**. Effects of heat stress on changes in physiology and anatomy in two cultivars of Rhododendron. *South African Journal of Botany* **112**: 338–345.

Sherwood S, Fu Q. **2014**. A drier future? *Science* **343**: 737–739.

Slot M, Kitajima K. **2015**. General patterns of acclimation of leaf respiration to elevated temperatures across biomes and plant types. *Oecologia* **177**: 885–900.

Slot M, Rey-Sánchez C, Gerber S, Lichstein JW, Winter K, Kitajima K. **2014**. Thermal acclimation of leaf respiration of tropical trees and lianas: Response to experimental canopy warming, and consequences for tropical forest carbon balance. *Global Change Biology* **20**: 2915–2926.

Slot M, Winter K. **2017a**. Photosynthetic acclimation to warming in tropical forest tree seedlings. *Journal of Experimental Botany* **68**: 2275–2284.

Slot M, Winter K. **2017b**. In situ temperature relationships of biochemical and stomatal

controls of photosynthesis in four lowland tropical tree species. *Plant Cell and Environment* **40**: 3055–3068.

Slot M, Winter K. **2018**. High tolerance of tropical sapling growth and gas exchange to moderate warming. *Functional Ecology* **32**: 599–611.

Smith NG, Dukes JS. **2017**. Short-term acclimation to warmer temperatures accelerates leaf carbon exchange processes across plant types. *Global Change Biology*: 4840–4853.

Smith NG, Malyshev SL, Shevliakova E, Kattge J, Dukes JS. **2016**. Foliar temperature acclimation reduces simulated carbon sensitivity to climate. *Nature Climate Change* **6**: 407–411.

Tan ZH, Zeng J, Zhang YJ, Slot M, Gamo M, Hirano T, Kosugi Y, Da Rocha HR, Saleska SR, Goulden ML, *et al.* 2017. Optimum air temperature for tropical forest photosynthesis: Mechanisms involved and implications for climate warming. *Environmental Research Letters* **12:** 0054022.

Tjoelker MG, Reich PB, Oleksyn J. **1999**. Changes in leaf nitrogen and carbohydrates underlie temperature and CO 2 acclimation of dark respiration in five boreal tree species. *Plant, Cell and Environment* **22**: 767–778.

Valladares F, Chico JM, Aranda I, Balaguer L, Dizengremel P, Manrique E, Dreyer E. **2002**. The greater seedling high-light tolerance of *Quercus robur* over *Fagus sylvatica* is linked to a greater physiological plasticity. *Trends in Ecology & Evolution* **16**: 395–403.

Valladares F, Wright SJ, Lasso E, Kitajima K, Pearcy RW. **2000**. Plastic Phenotypic Response to Light of 16 Congeneric Shrubs from a Panamanian Rainforest. *Ecology* **81**: 1925–1936.

Walsh C, Mac Nally R. **2013**. hier.part: Hierarchical Partitioning. R package version 1.0-4.

Way DA, Oren R. **2010**. Differential responses to changes in growth temperature between trees from different functional groups and biomes: a review and synthesis of data. *Tree Physiology* **30**: 669–688.

Way DA, Sage RF. **2008**. Thermal acclimation of photosynthesis in black spruce [*Picea mariana* (Mill.) B.S.P.]. *Plant, Cell and Environment* **31**: 1250–1262.

Way DA, Yamori W. **2014**. Thermal acclimation of photosynthesis: On the importance of adjusting our definitions and accounting for thermal acclimation of respiration. *Photosynthesis Research* **119**: 89–100.

Wise RR, Olson AJ, Schrader SM, Sharkey TD. **2004**. Electron transport is the functional limitation of photosynthesis in field-grown *Pima* cotton plants at high temperature. *Plant, Cell and Environment* **27**: 717–724.

Wu G, Liu H, Hua L, Luo Q, Lin Y, He P, Feng S, Liu J, Ye Q. **2018**. Differential responses of stomata and photosynthesis to elevated temperature in two co-occurring subtropical forest tree species. *Frontiers in Plant Science* **9**: 1–8.

Yamori W, Hikosaka K, Way DA. **2014**. Temperature response of photosynthesis in

C3, C4, and CAM plants: Temperature acclimation and temperature adaptation. *Photosynthesis Research* **119**: 101–117.

Zhang H, Henderson-Sellers A, Mcguffie K. **2001**. The compounding effects of tropical deforestation and greenhouse warming on climate. *Climatic Change* **49**: 309–338.

Zhang Y, Yu G, Yang J, Wimberly MC, Zhang X, Tao J, Jiang Y, Zhu J. **2014**. Climate-driven global changes in carbon use efficiency. *Global Ecology and Biogeography* **23**: 144–155.

3.8 Tables and Figures

Table 3.1 Abbreviations and descriptions.

Variable	Description	Units
A_{net}	Net photosynthesis	µmol m^{-2} s^{-1}
A_{opt}	Rate of photosynthesis at T_{opt}	µmol m^{-2} s^{-1}
A_{25}	Rate of photosynthesis at 25 ºC	µmol m^{-2} s^{-1}
C:N	Ratio of carbon to nitrogen	unitless
Fv/Fm	Maximum photochemical performance of photosystem II	unitless
g_{s_opt}	Rate of stomatal conductance at T_{opt}	mol m^{-2} s^{-1}
J_{max}	The maximum rate of photosynthetic electron transport	µmol m^{-2} s^{-1}
LMA	Leaf mass per area	g cm^{-2}
LWC	Percent leaf water content	%
Q_{10}	Factor that describes the rate respiration increases for every 10 ºC increase in temperature	unitless
N_{area}	Nitrogen per unit area	g cm^{-2}
N_{mass}	Nitrogen per unit mass	mg g^{-1}
R:A	Ratio of respiration at 25 ºC to photosynthesis at 25 ºC	unitless
R_d	Dark respiration	µmol m^{-2} s^{-1}
R_{25}	Rate of respiration at 25 ºC	µmol m^{-2} s^{-1}
T_{Jopt}	Optimum temperature of photosynthetic electron transport	(ºC)
T_{leaf}	Leaf temperature	(ºC)
T_{opt}	The optimum temperature for net photosynthesis	(ºC)
T_{vegMAX}	Mean maximum daily surface vegetation temperature	(ºC)
$T_{vegMEAN}$	Mean daily surface vegetation temperature	(ºC)
T_{vegMIN}	Mean minimum daily surface vegetation temperature	(ºC)
T_{Vopt}	Optimum temperature for Rubisco carboxylation	(ºC)
$T_{\hat{V}opt}$	Optimum temperature of apparent Rubisco carboxylation	(ºC)

$\hat{V}_{opt}$	The rate of carboxylation at $T_{\hat{V}opt}$	μmol m^{-2} s^{-1}
V_{cmax}	Maximum rate of Rubisco carboxylation	μmol m^{-2} s^{-1}
$\hat{V}_{cmax}$	Apparent maximum rate of Rubisco carboxylation	μmol m^{-2} s^{-1}
VPD	Vapor pressure deficit	kPa
VWC_{10}	Soil volumetric water content from 10-20 cm depth	m^3 m^{-3}
VWC_{20}	Soil volumetric water content from 20-30 cm depth	m^3 m^{-3}
Ω	The difference in T_{opt} and the rate of photosynthesis that is 37% of T_{opt}	unitless

Table 3.2 P-values and degrees of freedom from ANOVA results of gain score of leaf gas exchange variables.

Species		*df*	T_{opt}	A_{opt}	Ω	g_{s_Opt}	*df*	$T_{\hat{V}opt}$	$\hat{V}_{opt}$	*df*	Q_{10}	R_{25}	*df*	*A:R*
Psychotria brachiata	Treatment	1,8	0.898	0.617	**0.044**	0.382	1,7	0.936	0.424	1,8	0.380	0.422	1,8	0.700
	Season	1,8	0.711	0.776	0.598	0.359	1,7	**0.090**	**0.050**	1,8	0.915	0.707	1,8	0.980
	Treatment × Season	1,8	0.555	0.650	0.542	0.258	1,7	0.887	0.270	1,8	0.612	0.400	1,8	0.200
Piper glabrescens	Treatment	1,5	0.828	0.700	0.678	0.239	1,2	0.732	0.330	1,6	0.396	0.930	1,4	0.678
	Season	1,5	0.761	0.553	0.707	**0.015**	1,2	0.741	0.421	1,6	0.750	0.293	1,4	0.256
	Treatment × Season	1,5	0.240	0.401	0.153	0.887	1,2	0.127	0.168	1,6	0.357	0.743	1,4	0.906

Variables were pooled by individual plots within each measurement campaign and gain scores were calculated as post treatment – pretreatment. Variables listed are the optimum temperature of photosynthesis (T_{opt}) (ºC), the photosynthetic rate at T_{opt} (A_{opt}) (μmol m^{-2} s^{-1}), the width of the photosynthetic – temperature response curve (Ω), the rate of stomatal conductance at T_{opt} (g_{s_Opt}) (mol m^{-2} s^{-1}), the apparent optimum temperature of Rubisco carboxylation ($T_{\hat{V}opt}$) (ºC), the rate of Rubisco carboxylation at ($\hat{V}_{opt}$) (μmol m^{-2} s^{-1}), respiration increase with every 10 ºC (Q_{10}), the rate of leaf dark respiration at 25 ºC (R_{25}) (μmol m^{-2} s^{-1}), and the ratio between R_{25} and

photosynthesis at 25 ºC (*R:A*). Bolded p-values denote a significance ($p < 0.1$). df shows the degrees of freedom for the effect and residuals of the ANOVA.

Table 3.3 P-value results and degrees of freedom of stomatal traits gain score (i.e., post-treatment – pretreatment) two-way ANOVA.

Species		*df*	*Stomatal density*	*Stomatal size*
Psychotria brachiata	Treatment	1,12	0.819	**0.017**
	Warming duration	2,12	0.120	0.991
	Treatment × Warming duration	2,12	0.369	0.145
Piper glabrescens	Treatment	1,4	0.198	0.325
	Warming duration	1,4	0.845	**0.001**
	Treatment × Warming duration	1,4	0.661	0.323

Bolded p-values denote a significance ($p < 0.1$). df shows the degrees of freedom for the effect and residuals of the ANOVA. Stomatal traits listed are stomatal density ($m\ m^{-2}$) and stomatal size (μm^2).

Table 3.4 P-values and degrees of freedom from ANOVA results of gain scores (i.e., post-treatment – pretreatment) of leaf trait variables.

Species		*df*	*LMA*	N_{area}	N_{mass}	*C:N*	*LWC*	*df*	L_{area}
Psychotria	Treatment	1,8	0.697	0.139	0.176	0.260	0.961	1,8	0.494
brachiata	Season	1,8	0.669	0.440	0.241	**0.087**	**0.015**	1,8	0.201
	Treatment × Season	1,8	0.539	0.654	0.920	0.754	0.716	1,8	0.594
Piper	Treatment	1,6	0.689	0.551	0.637	0.598	0.458	1,5	0.547
glabrescens	Season	1,6	**0.027**	0.853	0.288	0.218	0.131	1,5	0.766
	Treatment × Season	1,6	**0.068**	0.477	0.840	0.899	0.474	1,5	0.448

Variables were pooled by individual plots and response ratios were calculated as individual variable post treatment – pretreatment. Variables listed are leaf mass per area (*LMA*; g cm^{-2}), nitrogen on an area basis (N_{area}; g cm^{-2}), nitrogen on a mass basis (N_{mass}; mg g^{-1}), carbon to nitrogen ratio (C:N), leaf water content (*LWC*; *%*), and leaf area (L_{area}; cm^2). Bolded p-values denote a significance ($p < 0.1$). df shows the degrees of freedom for the effect and residuals of the ANOVA.

Fig. 3.1 Photograph of one of the of experimental warming plots. Photo credit: Aura M. Alonso-Rodríguez.

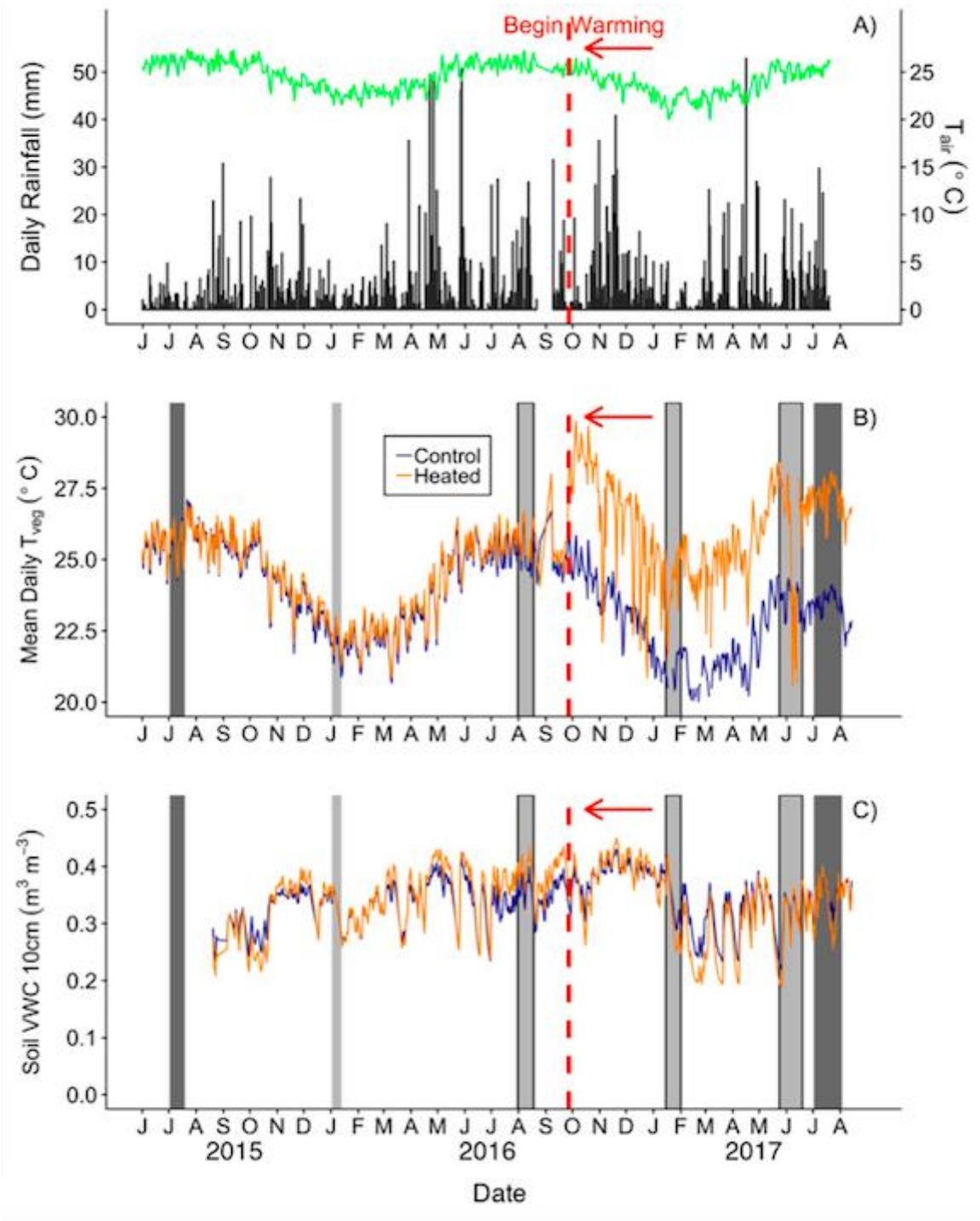

Fig. 3. 2 Environmental summaries throughout the duration of the pretreatment and posttreatment campaigns. **A)** Daily rainfall (black bars) and average daily air temperature

(T_{air}; green line). **B)** Mean daily surface vegetation temperature of the heated (orange) and control (dark blue) plots. **C)** Mean daily soil moisture for the heated and control plots. The dates shown range from July 1st 2015 – August 15th 2017. The vertical red dashed line depicts the beginning of the warming treatment in the heated plots. The light gray bars depict A_{net}, R_{dark}, and leaf trait sampling campaigns. The sampling campaigns that are light gray bars outlined in black (August 2016, January 2017, and June 2017) depict campaigns where stomatal morphology was measured. The dark gray bars depict the V_{cmax} and J_{max} sampling campaigns. Dark adapted chlorophyll fluorescence and chlorophyll content were measured on July 18th, 2017. Rainfall and air temperature were collected from an above canopy weather station. Air temperature (ºC) (HMP50-L, Campbell Scientific) was logged using a datalogger (CR1000, Campbell Scientific).

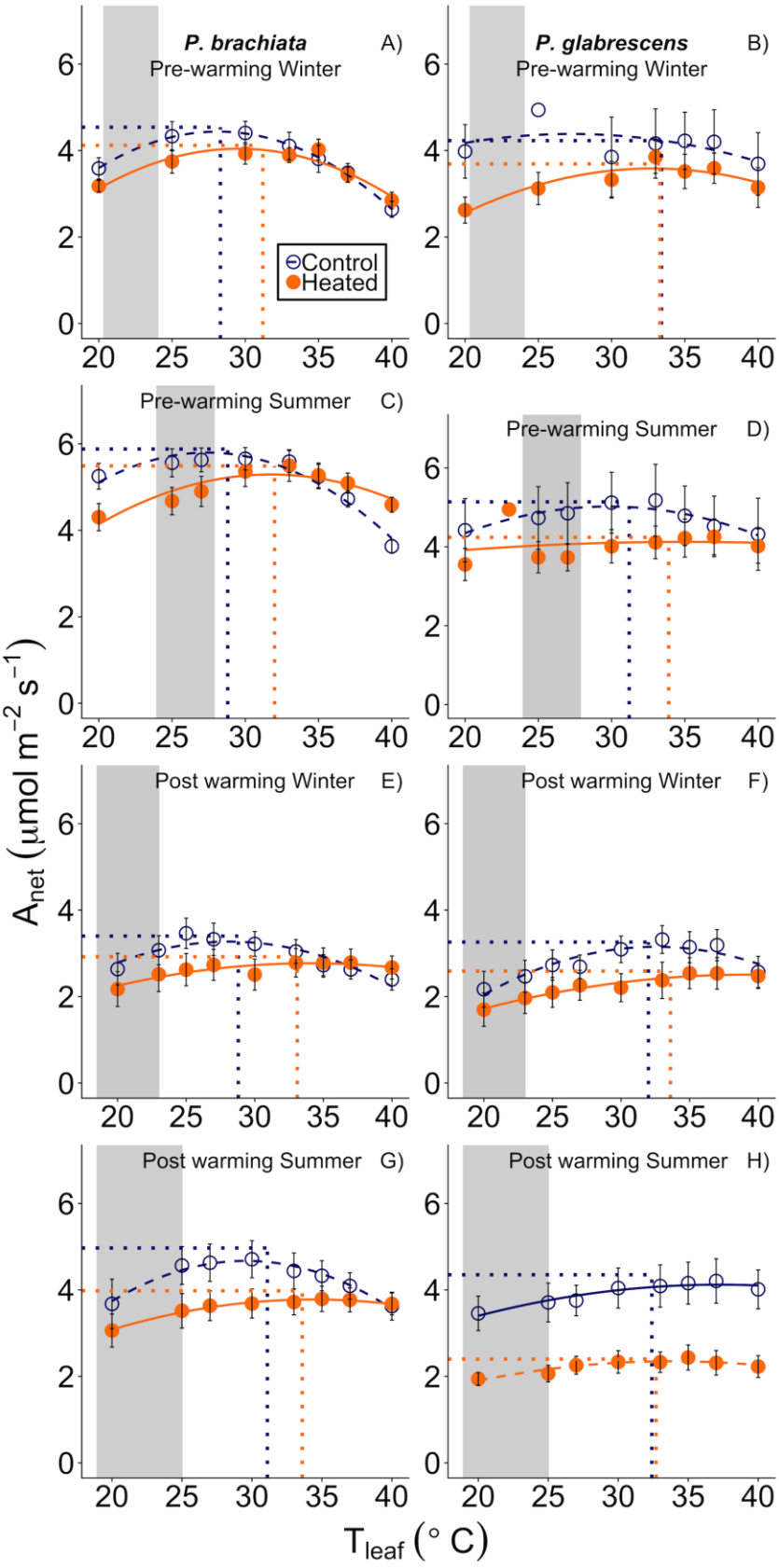
P. brachiata
A)
Pre-warming Winter
P. glabrescens
B)
Pre-warming Winter
Control
Heated
Pre-warming Summer
C)
Pre-warming Summer
D)
Post warming Winter
E)
Post warming Winter
F)
Post warming Summer
G)
Post warming Summer
H)
A_{net} (μmol m^{-2} s^{-1})
T_{leaf} (° C)

Fig. 3.3 Net photosynthetic (A_{net}) response to instantaneous leaf temperatures (T_{leaf}). The relationship between net photosynthesis and temperature was plotted separately for each measurement campaign and species: **A)** *Psychotria brachiata* pre-warming winter season, **B)** *Piper glabrescens* pre-warming winter season, **C)** *P. brachiata* pre-warming summer season, **D)** *P. glabrescens* pre-warming summer season, **E)** *P. brachiata* 4 months post-warming winter season, **F)** *P. glabrescens* 4 months post-warming winter season, **G)** *P. brachiata* 8 months post-warming summer season, **H)** *P. glabrescens* 8 months post-warming summer season. Control plot (dark blue open circles) and heated plot (orange closed circles) are means ± se at each leaf temperature. Lines are fit to each temperature response using the June *et al.* (2004) method (Equation 1) for control (dark blue; dashed) and heated (orange; solid) plots separately. Dotted vertical lines represent the optimum temperature for photosynthesis. Dotted horizontal lines represent the rate of photosynthesis at the optimum temperature for plants in control (dark blue blue) and heated (orange) plots separately. Gray boxes represent the range of the average minimum and maximum daily vegetation temperature observed for the control plots. Average minimum and maximum temperatures are calculated for each measurement campaign separately.

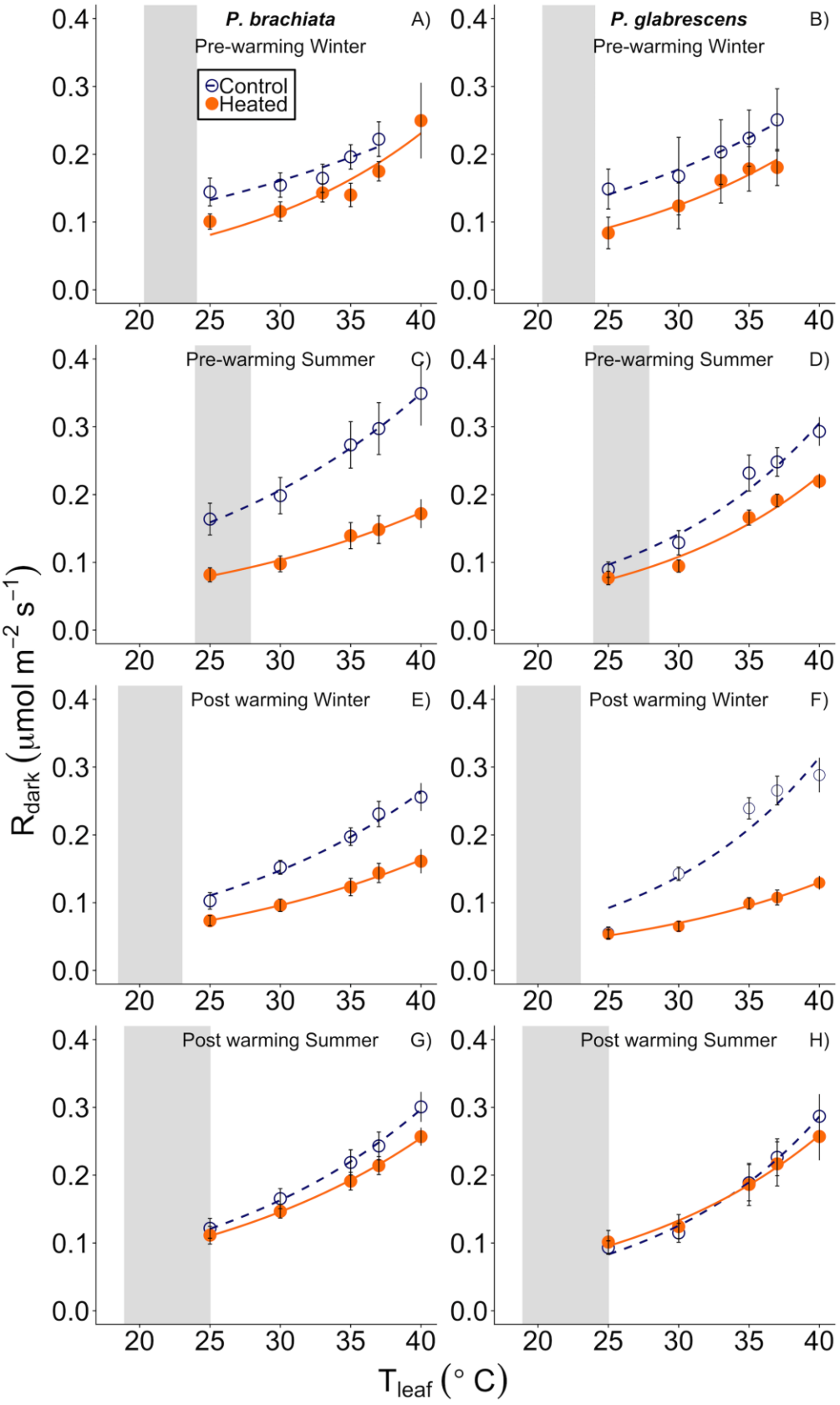
P. brachiata
A)
Pre-warming Winter
Control
Heated
P. glabrescens
B)
Pre-warming Winter
Pre-warming Summer
C)
Pre-warming Summer
D)
Post warming Winter
E)
Post warming Winter
F)
Post warming Summer
G)
Post warming Summer
H)
R_{dark} (µmol m^{-2} s^{-1})
T_{leaf} (° C)
0.0
0.1
0.2
0.3
0.4
20
25
30
35
40

Fig. 3.4 Leaf respiratory (R_{dark}) response to instantaneous leaf temperatures (T_{leaf}). The respiratory response to temperature was plotted separately for each measurement campaign and species separately: A) *Psychotria brachiata* pre-warming winter season, B) *Piper glabrescens* pre-warming winter season, C) *P. brachiata* pre-warming summer season, D) *P. glabrescens* pre-warming summer season, E) *P. brachiata* 4 months post-warming winter season, F) *P. glabrescens* 4 months post-warming winter season, G) *P. brachiata* 8 months post-warming summer season, H) *P. glabrescens* 8 months post-warming summer season. Control plot (dark blue open circles) points and heated plot (orange; closed) points are means ± se at each leaf temperature. Exponential fit lines were fit to control (dark blue; dashed) and heated (orange; solid) plots separately. Gray boxes represent the range of the average minimum and maximum daily vegetation temperature for the control plots. Average minimum and maximum temperatures are calculated for each measurement campaign separately.

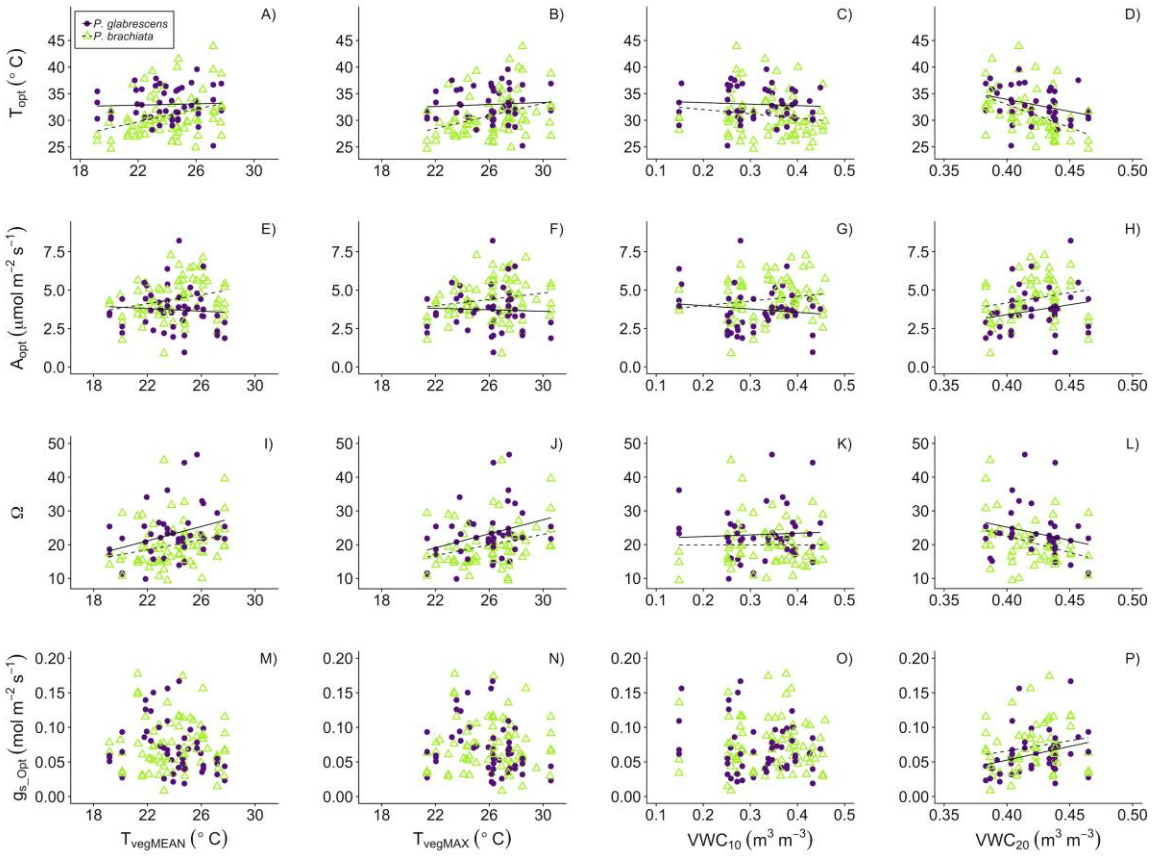

Fig. 3.5. Photosynthetic parameter responses to maximum (T_{vegMAX}), mean ($T_{vegMEAN}$) daily vegetation temperature, soil moisture at 10 cm (VWC_{10}), and 20 cm depth (VWC_{20}). **A)** The optimum temperature of photosynthesis (T_{opt}) response to $T_{vegMEAN}$ of *P. brachiata* (green triangles) and *P. glabrescens* (purple circles), **B)** T_{opt} response to T_{vegMAX}, **C)** T_{opt} response to VWC_{10}, **D)** T_{opt} response to VWC_{20}, **E)** the rate of photosynthesis at T_{opt} (A_{opt}) response to $T_{vegMEAN}$, **F)** A_{opt} response to T_{vegMAX}, **G)** A_{opt} response to VWC_{10}, **H)** A_{opt} response to VWC_{20}, **I)** the rate of stomatal conductance at T_{opt} (g_{s_Opt}) response to $T_{vegMEAN}$, **J)** g_{s_Opt} response to T_{vegMAX}, K) g_{s_Opt} response to VWC_{10}, **L)** g_{s_Opt} response to VWC_{20}, **M)** photosynthetic thermal niche (Ω) response to $T_{vegMEAN}$, **N)** Ω response to T_{vegMAX}, **O)** Ω response to VWC_{10}, and **P)** Ω response to VWC_{20}. Fit

lines (solid - *P. glabrescens*; dashed – *P. brachiata*) indicated individual species fit when there is an overall significant environmental response, species difference, or an interaction between the environmental variable and species (Table B4).

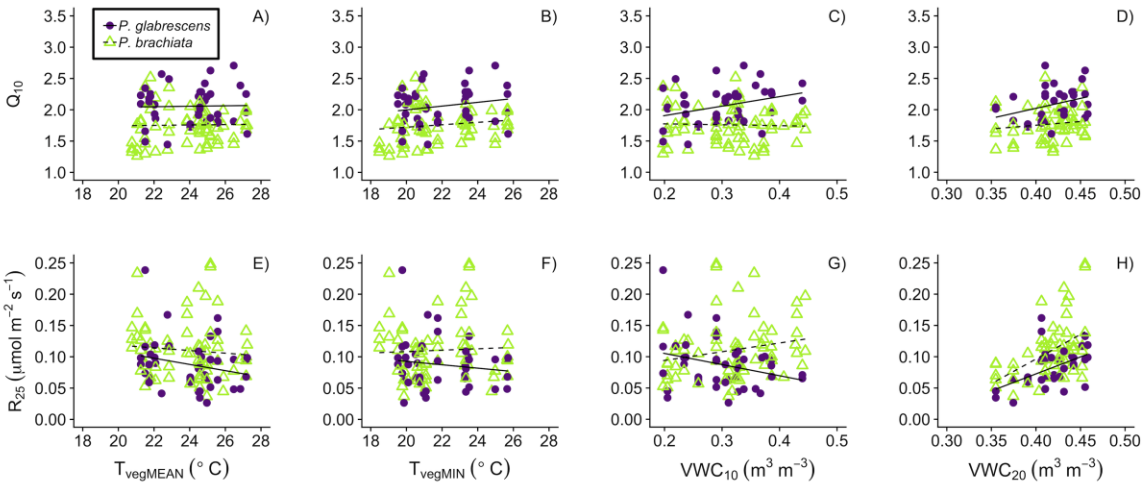

Fig. 3.6 Respiratory parameter responses to mean ($T_{vegMEAN}$), min (T_{vegMIN}) daily vegetation temperature, soil moisture at 10-20 cm (VWC_{10}), and 20-30 cm depth (VWC_{20}). **A)** The increase in respiration for every 10 ºC (Q_{10}) response to $T_{vegMEAN}$ of *P. brachiata* (green triangles) and *P. glabrescens* (purple circles), **B)** Q_{10} response to T_{vegMIN} **C)** Q_{10} response to VWC_{10}, **D)** Q_{10} response to VWC_{20}, **E)** the rate of respiration at 25 ºC (R_{25}) response to $T_{vegMEAN}$, **F)** R_{25} response to T_{vegMIN}, **G)** R_{25} response to VWC_{10}, and **H)** R_{25} response to VWC_{20}. Fit lines (solid - *P. glabrescens*; dashed – *P. brachiata*) indicated individual species fit when there is an overall significant environmental response, species difference, or an interaction between the environmental variable and species (Table B4).

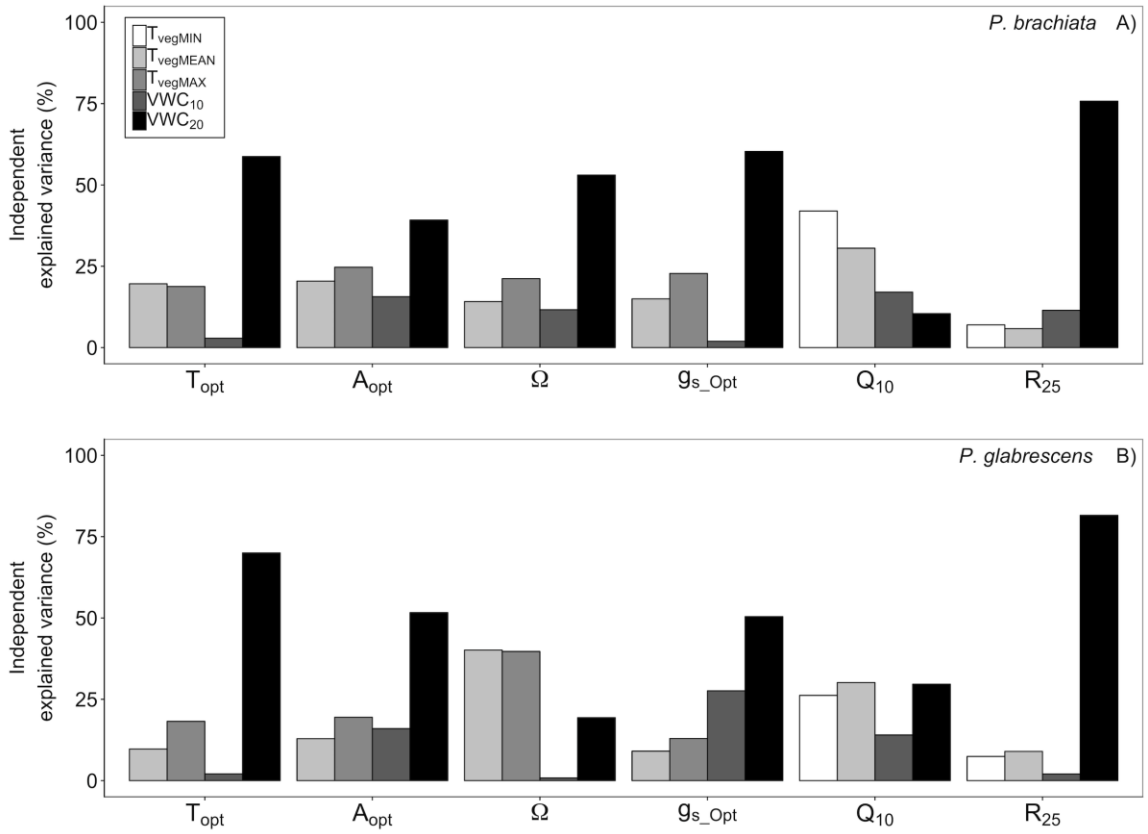

Fig. 3.7 Hierarchical partitioning results of gas exchange parameter variances explained by environmental variables. Percentage of optimum temperature for photosynthesis (T_{opt}), the rate of photosynthesis at T_{opt} (A_{opt}), photosynthetic thermal niche (Ω), the rate of stomatal conductance at T_{opt} (g_{s_Opt}), increase in respiration for every 10 ºC (Q_{10}), and the rate of dark respiration at 25 ºC (R_{25}) variance explained independently by environmental variables for **A)** *Psychotria brachiata* and **B)** *Piper glabrescens*. T_{opt}, A_{opt}, Ω, and g_{s_Opt} hierarchical partitioning was analyzed for mean daily vegetation temperature ($T_{vegMEAN}$) (light gray), mean daily maximum vegetation temperature (T_{vegMAX}) (medium gray), soil

volumetric water content at 0-10 cm depth (VWC_{10}) (dark gray), and soil volumetric water content at 20-30 cm depth (VWC_{20}) (black). Q_{10} and R_{25} hierarchical partitioning was analyzed for mean daily minimum vegetation temperature (T_{vegMIN}) (white), $T_{vegMEAN}$ (light gray), VWC_{10} (dark gray), and VWC_{20} (black).

4 Tropical trees partially acclimate to *in situ* leaf-level warming but upper canopy photosynthesis limited by stomatal conductance

4.1 Abstract

Tropical forest canopies cycle large amounts of carbon, yet we still have a limited understanding of how these critical ecosystem components will respond to climate warming. To investigate tropical forest physiological thermal acclimation, we implemented *in situ* leaf-level + 3 °C warming on leaves across the canopy height from the understory to the upper canopy. We assessed acclimation by measuring temperature responses of photosynthesis, stomatal conductance, and leaf respiration of two Puerto Rican tropical tree species, *Guarea guidonia* and *Ocotea sintensii*, after approximately one month of daytime and nighttime warming. We additionally measured shifts in leaf functional traits on the same leaves. Neither study species showed evidence of net photosynthetic acclimation; however, *O. sintensii* acclimated by shifting the optimum temperature of photosynthetic electron transport to a higher temperature in the understory leaves. The only evidence for respiratory acclimation was in *G. guidonia*, where respiratory temperature sensitivity (Q_{10}) was down regulated in the heated leaves. We found no shifts in stomatal conductance with warming; however, the upper and mid canopy leaves were much more sensitive to increasing temperatures when compared to the lower canopy and understory of both treatment and control leaves. Surprisingly, the optimum temperatures for net photosynthesis (T_{opt}) decreased with increasing canopy height, perhaps limited by stomatal conductance in the upper canopy. Additionally, we

found that the canopy leaves were often operating above T_{opt}, and *O. sintensii* upper canopy T_{opt} was similar to the mean daytime upper temperatures. Overall, we found no evidence of photosynthetic acclimation in the upper canopy, where leaves are particularly sensitive to shifts in temperature. Further warming may put these species' upper canopy leaves at risk of reduced CO_2 uptake.

4.2 Introduction

The balance between plant photosynthesis and respiration plays a critical role in controlling Earth's atmospheric carbon fluxes (Liu *et al.* 2015); therefore, understanding how these processes respond to increasing temperature is necessary to accurately predict the future climate (Luo 2007; Smith and Dukes 2013; Dusenge *et al.* 2019). Photosynthesis, or carbon dioxide (CO_2) uptake, has a peaked response to temperature, where net photosynthesis declines after the optimum temperature (T_{opt}) is reached (Berry and Bjorkman 1980). Respiration, or CO_2 release, increases nonlinearly with temperature due to quickening enzymatic rates (reviewed in Atkin *et al.* 2005). The rate of respiration will eventually decline with extremely high temperatures due to disruption of membrane integrity or protein denaturation; however, respiratory function drops at temperatures much higher than those of net photosynthesis (e.g. O'Sullivan *et al.* 2017). Because respiration continues to increase with moderately high temperatures, whereas photosynthesis declines, if these two processes are not able to acclimate to warmer temperatures, we could see systems shift towards a greater loss of greenhouse gases to the atmosphere.

Tropical forests are major components of Earth's carbon cycle, while only making up a fraction of Earth's surface area (Pan *et al.* 2013); however, rising temperatures, due to climate warming, may reduce tropical forest CO_2 uptake (Malhi *et al.* 2009; Brienen *et al.* 2015). Tropical forests are predicted to reach temperatures outside of their historical climate norms more quickly than other biomes (Diffenbaugh and Scherer 2011; Mora *et*

al. 2013), and the narrow diurnal, seasonal, and interannual temperature ranges that tropical forests experience suggests that, compared to more temperate forests, tropical plants have lower thermal plasticity and a lower capability to acclimate to climate warming (Janzen 1967; Cunningham and Read 2002, 2003). Thermal acclimation of photosynthesis occurs when overall CO_2 uptake is enhanced, or up-regulated, with higher growth temperatures. Photosynthetic acclimation manifests as a positive shift in the optimum temperature and/or a higher rate of peak photosynthesis (Berry and Bjorkman 1980; Way and Yamori 2014). Thermal acclimation of respiration occurs through overall declined CO_2 release at higher growth temperatures (i.e. down-regulation), either due to reduced respiratory basal rates or reduced sensitivity to temperature (Atkin and Tjoelker 2003). Despite the important role that tropical forests play in global carbon uptake, there are few studies that investigate thermal acclimation of tropical plant physiology (Cavaleri *et al.* 2015; Dusenge and Way 2017). In addition, there is only one study investigating *in situ* respiratory acclimation of tropical canopy leaves after nighttime leaf-level warming (Slot *et al.* 2014), and only one study investigating photosynthetic responses to warming in a forest canopy. The latter study only inspected shifts in rates of net photosynthesis but not shifts in the photosynthetic temperature responses (Doughty 2011). The limited number of warming experiments leaves a gap in our understanding of thermal acclimation potential of the upper canopy, where the majority of carbon is cycled in forest ecosystems (Ellsworth and Reich 1993; Kumagai *et al.* 2006).

Tropical forest canopies have been shown to often exceed their photosynthetic thermal thresholds (Doughty and Goulden 2008; Mau *et al.* 2018), potentially risking

declined CO_2 uptake. Experiments in growth chambers and glass houses suggest that tropical photosynthesis can partially acclimate to warmer temperatures (Slot and Winter 2017a; Smith and Dukes 2017), however, it is yet to be determined if their results will scale to mature, canopy trees. The first-ever tropical canopy leaf warming study found that warming individual leaves an average of + 2 °C above ambient temperature can cause damage to the photosynthetic apparatus, leading to reduced rates of photosynthesis (Doughty 2011). While the thermal acclimation potential of T_{opt} within a canopy vertical gradient has rarely been investigated (but see Carter and Cavaleri 2018), upper canopy leaves may have a higher acclimation potential than lower canopy and understory leaves. Studies that investigated acclimation of the photosynthetic electron transport optimum temperature found evidence of acclimation to higher irradiance (Niinemets *et al.* 1999; Niinemets and Valladares 2004) and leaves exposed to light can have higher heat tolerances than darkened leaves (Krause *et al.* 2015). This evidence suggests that upper canopy leaves may have a higher capability for thermal acclimation than their shaded counterparts. Upper canopies are exposed to much more variable environmental conditions on a daily basis, including high heat, light, wind, and vapor pressure deficit (VPD).

Higher temperatures cause accompanying increases in VPD, which can induce stomatal closure and thus lowered CO_2 uptake at higher temperatures (Lin *et al.* 2012). Unless reductions in stomatal conductance are ameliorated through elevated atmospheric CO_2, reduced stomatal conductance may be the physiological process most likely to moderate photosynthesis (Lloyd and Farquhar 2008; Slot and Winter 2017b) or tropical

forest productivity as a whole (Galbraith *et al.* 2010) as the climate continues to warm. Because the rate of stomatal conductance is correlated with photosynthetic capacity, and photosynthetic capacity increases with canopy height, so too does stomatal conductance (Buckley 2005; Kenzo *et al.* 2015). Leaves in the upper canopy have a higher capacity for stomatal conductance in order to support the higher photosynthetic capacity experienced by the upper canopy leaves, but high stomatal thermal sensitivity may make these upper canopy leaves more vulnerable to stomatal limitations to CO_2 availability.

Much of the evidence for respiratory acclimation suggests that tropical forest autotrophic respiration will acclimate to climate warming (Way and Oren 2010; Slot and Kitajima 2015; Aspinwall *et al.* 2016). However, it is less understood how respiratory acclimation can vary with height. Foliar respiration on an area basis increases with increasing canopy height in tropical forests (Meir *et al.* 2001; Cavaleri *et al.* 2008; Weerasinghe *et al.* 2014; Asao *et al.* 2015); however, the relationship between respiratory dependence on temperature (Q_{10}; which is the increase in respiration for every 10 °C increase in temperature) and height is less understood. Neither Cavaleri *et al.* (2008) nor Weerasinghe *et al.* (2014) found differences in Q_{10} with canopy height in tropical rainforests in Costa Rica or Australia (respectively). Another study in a temperate forest found that Q_{10} can increase with canopy height, but the pattern is not conserved across species (Turnbull *et al.* 2003). Han *et al.* (2017) found increasing stem Q_{10} with canopy height and attributed the increase to tissue temperature differences along the vertical gradient, which suggests an increase in Q_{10} with increasing tissue temperature instead of the reduction that we would expect to see with acclimation. The only evidence of

respiratory acclimation along a canopy vertical gradient investigated seasonal temperature acclimation in a Japanese temperate forest and found no variation in respiratory acclimation throughout the canopy (Araki *et al.* 2017). Considered together, these studies suggest that tropical forest respiration is capable of acclimation, but acclimation may be consistent across the height gradient.

Understanding the plant physiological response to whole-ecosystem level warming is important to provide an understanding of how ecosystems will respond to the warming climate (Wood *et al.* 2012); however, whole ecosystem-level warming is logistically difficult in a forested ecosystem. This is particularly true for tropical forests, where canopy heights can reach more than 50 meters (Feldpausch *et al.* 2010, Pan *et al.* 2013). When ecosystem-level warming cannot be implemented, leaf-level warming can give us valuable insight on the mechanistic responses of warming response (Cavaleri *et al.* 2015). Even with the important role that canopies play in forested systems, *in situ* canopy-level warming has rarely been implemented in mature forests. Studies have implemented canopy warming in temperate forests using open top chambers (Yamaguchi *et al.* 2016), heated cables (Nakamura *et al.* 2010), large infrared heaters (Nakamura *et al.* 2016), or heating pads (Carter and Cavaleri 2018). A whole ecosystem warming experiment has been established in a boreal system (Hanson *et al.* 2017), and two studies have implemented leaf-level warming in tropical ecosystems (Doughty 2011; Slot *et al.* 2014). This work represents the first 24-hour mature canopy warming experiment in a tropical forest where both photosynthetic and respiratory acclimation have been investigated. We tested the following hypotheses using a novel leaf-level warming device

implemented throughout the vertical gradient of a tropical forest canopy: 1) photosynthesis will acclimate to leaf-level warming, and the positive acclimation response will be stronger higher in the canopy, where more extreme climate variations already occur; 2) respiration will acclimate to experimental leaf warming; however, acclimation response will be uniform throughout the canopy gradient; 3) both photosynthesis and respiration will increase with canopy height; however, the ratio between photosynthesis and respiration will decrease with canopy height in the heated leaves due to a greater photosynthetic acclimation response higher in the canopy.

4.3 Methods

4.3.1 Study site

This experiment was conducted on a 20.1 m canopy access tower (UpRight Inc., Dublin, Ireland) built at the USDA Forest Service Sabana Field Research Station, within the Luquillo Experimental Forest (18º18'N, 65º50'W). Mean annual precipitation during the two years prior to experimental warming was 2271 mm, mean annual temperature is 24 °C (Harris *et al.* 2012). The forest is classified as a subtropical wet forest with a wet season that runs May through November and, while there is no true dry season, January through April receives less rainfall. The site is located on Utilsol soils (Scatena 1989) at 100 m elevation. In 2016, the secondary growth forest had a basal area of 39 m^2 ha^{-1} and a stand density of 3100 trees ha^{-1}. The most abundant canopy trees at the time of the study were *Presotea montana*, *Syzgium jambos*, *Ocotea leucoxylon*, and *Casearia arborea.*

4.3.2 Leaf-level warming

Within-canopy physiological acclimation was assessed by implementing a leaf-level warming device within the canopy gradient. We heated leaves of two species accessible from the canopy access tower, *Guarea guidonia* and *Ocotea sintensii*. *G. guidonia* is a shade tolerant species and *Ocotea* spp. have been classified as partially shade tolerant (Rozendaal *et al.* 2006). 2-4 leaves per species were successfully heated at each canopy height for a total of 29 heated /control pairs (Table B1). Most leaves were heated for 23-29 days but one leaf was heated for 16 days, one was heated 18 days, and one leaf was heated for 33 days (Table B1). To avoid the interactive effects of carbon importation that occurs in developing leaves (Turgeon, 2006), all of the leaves selected for warming were fully developed at the time of warming initiation. Leaf level warming was implemented using a leaf warming device, which heated an individual leaf +3 °C higher than a paired control leaf. Individual leaves were heated as outlined in Carter and Cavaleri (2018). Briefly, heated leaf temperatures were controlled by turning a relay module (SSR-25 DA, Fotek Controls Co., Taiwan), and thus a heating pad (100 watt 120VAC, 24100k Kat's Five Star Manufacturing Group Inc., Springfield, TN), off when the heated leaf temperature was more than 3 °C higher than the control leaf temperature. Leaf thermocouples (TT-T-30 SLE(ROHS), OMEGA Engineering Inc., Norwalk, CT, USA) were adhered to the abaxial side of each heated and control leaf using breathable medical tape (Slot *et al.* 2016). Heating pads were attached to a metal frame that was positioned underneath the leaf. The metal frame was attached to a sturdy branch, which allowed the heating pad to experience the same movement as the leaf (Figure 4.1). Heated leaves were selected to ensure that they received a similar light environment to

their associated control leaf. Leaves were heated throughout the daytime and nighttime hours.

For each heated and control leaf, we measured net photosynthesis, stomatal conductance, photosynthetic electron transport, and respiratory responses to temperature. We additionally measured leaf traits: nitrogen per unit leaf area (N_{area}), nitrogen per unit leaf mass (N_{mass}), leaf chlorophyll, leaf mass per area (*LMA*), leaf area, and percent leaf water content. Four heated leaves were removed from the photosynthetic and photosynthetic electron transport data analysis because they had negative values, values close to zero, or unstable net assimilation and stomatal conductance rates, likely due to heating damage to the leaf or petiole. Two of the leaves were *O. sintensii* at 18 meters height, one was *O. sintensii* at 20.1 meters, and one was *G. guidonia* in the understory (1.8 meters). Except for the *O. sintensii* leaf at 20.1 m, which was not included in any data analysis, these leaves were included in the respiration and leaf trait analysis because they were not outliers for either of these datasets. Leaf heaters were turned off in the morning prior to measuring net photosynthesis. In order to ensure that any leaf acclimation was captured in our measurements, photosynthesis and respiration were measured as close to within 24 hours of turning off the heaters as possible. Due to weather interference, there were several cases where heaters were off for approximately 48 hours before photosynthesis and respiration were measured.

4.3.3 Photosynthesis and stomatal conductance

Photosynthetic-temperature curves were constructed at (25, 27, 30, 33, 35, 37, 40 °C) using an LI6400XT infrared gas analyzer that was fitted with the fluorometer attachment, which measures gas exchange and chlorophyll fluorescence, to estimate photosynthetic electron transport (ETR), in a 2 cm^2 area (6400-044, Li-COR Inc., Lincoln, NE, USA). Measurements were conducted between the hours of 8:00am-3:30pm. Prior to measuring net photosynthesis and ETR, each leaf was light-acclimated to saturating light for at least twenty minutes; after which, temperature response curves were measured. This ensured that fluorescence was measured on light-adapted leaves for the entirety of the temperature response curve. Temperature was controlled using a water jacket (Expanded Temperature Control Kit 6400-88, Li-COR Inc.) which used gravity to cycle hot or cold water from thermoses using plastic tubes (Mau *et al.* 2018).

The optimum temperature of net photosynthesis (T_{opt}) was determined by fitting A_{net} response to temperature to the curve derived from June *et al.* (2004):

$$A(T) = A_{opt} \times e^{-(\frac{T_{leaf} - T_{opt}}{\Omega})^2} \qquad \text{Equation 1}$$

where A_{opt} is the net photosynthetic rate at the optimum temperature for net photosynthesis (T_{opt}) and Ω is the photosynthetic thermal niche or the difference in temperature between T_{opt} and the temperature where A_{net} declines to 37% of its rate at T_{opt}

or, more specifically, the width of the curve's peak. Photosynthetic electron transport (ETR) was measured at the same time as A_{net}. We were unable to fit Equation 1 to three of the 59 response curves because we did not measure enough points above or below the optimum temperature for the model to converge. For these measurements, two *O. sintinsii* in the upper canopy and one *G. guidonia* in the understory, we estimated T_{opt} as the temperature where photosynthesis was at its highest point and A_{opt} was the rate of photosynthesis at this point. One *O. sintensii* control leaf in the understory had T_{opt} that was overestimated at 73 °C. These data were removed for ETR data analysis only.

Unlike the response of net photosynthesis, which is peaked, stomatal conductance (g_s) declined linearly with temperature. We therefore extracted the intercepts ($\beta_{0\_gs\text{-}T}$) and slopes ($\beta_{1\_gs\text{-}T}$) and of the linear gs-T_{leaf} relationship for each measured photosynthetic-temperature curve.

The optimum temperature of photosynthetic electron transport (T_{optETR}) was extracted by fitting ETR to the Equation 1 and replacing ETR for A_{net}, where ETR_{opt} is the electron transport rate at T_{optETR}. ETR for each leaf was corrected for absorption using the chlorophyll- absorption relationship described in Bauerle *et al.* (2004):

$$\text{Absorptance} = 89.2 - 56.8\, e^{-0.0723 * Chl} \qquad \text{Equation 2}$$

where Chl is chlorophyll content. Chlorophyll content was measured subsequent to the assimilation/ fluorescence measurement using a chlorophyll content meter (CCM-200+, OPTI-SCIENCES, Hudson, NH, USA).

4.3.4 Respiration

Dark respiration (R_d) was measured on the same leaves as photosynthesis and was assessed predawn (1:30am-5:30am), the night after photosynthesis measurements were collected. There were six instances where *O. sintensii* leaves broke in between the photosynthesis and respiration measurements: two control leaves from 18.0 m, one control from 19.8 m, one control from 16.2 m, and two heated from 18.0 m. When this occurred, we measured either the leaf on the same stem in a similar cohort or, especially for a heated leaf, a leaf that was positioned very close to the heater and received residual heat from the leaf heater.

R_d measurements were conducted using a LI6400 fitted with the 6400-05 conifer chamber head and 6400-088 expanded temperature kit (Li-COR Inc., Lincoln, NE, USA). The conifer chamber was wrapped in aluminum foil to make sure that dark adaptation was not disrupted during the respiration measurements. Individual heated and control leaves were placed in the conifer chamber where the leaf was allowed to acclimate and stabilize to the chamber conditions before measurements began. Respiratory response to temperature curves were constructed by measuring the rate of respiration at 25, 30, 35, 37, 40 °C. Flow was controlled at 400 µmol m^{-2} s^{-1}. After all measurements were

completed, leaves were collected and scanned for leaf area using a desktop scanner (EPSON Stylus NX420). Leaf scans were analyzed for leaf area using ImageJ v.1.50 image analysis software. Each R_d measurement was corrected for calculated leaf area.

Each respiratory response curve was fitted to the nonlinear equation:

$$R_d = \beta_0 \times \exp(T_{leaf} \times \beta_1) \qquad \text{Equation 3}$$

where R_d is the respiration rate ($\mu mol\ m^{-2}\ s^{-1}$) at T_{leaf} and β_0 and β_1 are model parameters. The change in respiration rate with every 10 °C is calculated as:

$$Q_{10} = \exp(10 \times \beta_1) \qquad \text{Equation 4}$$

Respiration at 25 °C (R_{25}) is estimated by substituting 25 for T_{leaf} in Equation 3.

4.3.5 R:A Ratio

The ratio between R_{25} and photosynthesis at 25 °C (R:A) was calculated by dividing R_{25} by A_{25}. A_{25} was calculated by plugging in T_{leaf} = 25 and the already calculated A_{opt}, T_{opt}, and Ω terms into Equation 1 and solving for A_{net}. For the three curves that did not fit Equation 1, A_{net} at the measured 25 °C was used as A_{25}.

4.3.6 Leaf Traits

Leaf traits were collected directly after respiration measurements were completed. Samples were taken back to the laboratory and stored in the refrigerator no more than 36 hours between collection and analysis. Refrigerated samples were then weighed for fresh mass and scanned for leaf area using a desktop scanner. Samples were then dried in a 60 °C degree oven for at least 48 hours before collecting dry mass. Dried leaf samples were ground to a powder using a ball mill (SPEX™ SamplePrep 8000M Mixer/Mill, Metuchen, NJ) and analyzed for nitrogen and carbon content with an elemental analyzer (Elemental Americas, Mt Laurel, NJ). Scanned leaf area images were analyzed using ImageJ analysis software v.1.50. Leaf mass per area (*LMA*) was calculated by taking the dry mass (g) and dividing by leaf area (cm^2). Percent leaf water content (*%LWC*) was calculated by taking the fresh mass (g) minus the dry mass (g), dividing by the dry mass (g) and multiplying by 100. N per leaf area (N_{area}) was calculated by multiplying N ($g\ g^{-1}$) by *LMA*.

4.3.7 Data analysis

Warming device efficacy was evaluated by investigating the instances of temperature spiking in the heated leaves across canopy height. Temperature spiking was assessed through the heated leaf maximum temperature ($T_{leafMAX}$) and the frequency of data logger datapoints where the heated leaves reached temperatures greater than 10 °C above the control leaves ($\Delta T > 10$ °C). Effects of height, species, and the interaction between height and species on temperature spiking were assessed using an ANCOVA.

Throughout the experiment, notes were taken daily on the functioning of the warming device for each leaf. Prior to warming efficacy data analysis and control leaf environmental summaries, datalogger data were removed if a heater malfunctioned or we had to begin warming a different leaf due to temperature spiking-induced leaf damage. We also removed datapoints $T_{leaf} < 0$ °C, as these temperatures were well outside of the temperature range experienced in this forest.

We investigated the height response of daytime mean temperatures ($T_{leafMEAN}$) and daily maximum temperatures ($T_{leafMAX}$) of control leaves using linear regressions. We then extracted the 'upper' portion of *O. sintensis* control $T_{leafMEAN}$ and $T_{leafMAX}$ and compared them to *O. sintensis* 'upper' canopy T_{opt} and T_{optETR} using Student's t-test to see if the leaf temperatures and photosynthetic optimum temperatures were significantly different from one other. The same analyses were conducted with *G. guidonia* mid canopy as this was the highest portion of the canopy that *G. guidonia* was accessible from the canopy tower.

Photosynthetic parameters (T_{opt}, A_{opt}, Ω, T_{optETR}, and ETR_{opt}), respiratory parameters (R_{25} Q_{10}, and *R:A*), stomatal conductance parameters ($\beta_{0\_gs\text{-}T}$ and $\beta_{1\_gs\text{-}T}$) and leaf traits (leaf area, *LMA*, *%LWC*, N_{mass}, N_{area}, and Chlorophyll content) were all analyzed for effects of treatment, canopy height, and the interaction between treatment and canopy height using ANCOVA analyses. Separate ANCOVAs were run for each species. To further investigate stomatal sensitivity across the canopy gradient, the canopy was split into four categories: understory (0-1.5 meters), lower canopy (9-12.6 m), mid canopy (14.4-16.2 m), and upper canopy (18-19.8 m). Further ANCOVAs were run for

each species investigating stomatal conductance response to temperature, canopy class, and the interaction between temperature and canopy class. Pairwise comparison of canopy class slopes and intercepts were conducted using 'emmeans' package (Lenth, 2019) in R statistical software (R Core Team 2018). All data analyses were conducted using R statistical software version 3.5.0.

4.4 Results

4.4.1 Warming device and environmental conditions

Overall, our warming apparatus effectively heated leaves + 3 °C above control leaves (Fig. 4.2). Instances of temperature spikes where the differences between heated and control leaf temperature were greater than 10 °C ($\Delta T > 10$ °C) occurred less than 1% of the time (Appendix B Table B2; Fig. B2A). There were differences between species (Table B1), where *O. sintensii* had a higher frequency of temperature spikes than *G. guidonia*. In addition, all heated *O. sintensii* leaves had four or more instances of temperature spiking; whereas, temperature spiking above 10 °C occurred in 10 of the 17 heated *G. guidonia* leaves. Shown by the significant species effect, *O. sintensii* also had higher heated leaf maximum temperature compared to *G. guidonia* (Table B2, Fig. B1B). Notably, *O. sintensii* average max daily heated T_{leaf} ranged from 38-46 °C in the mid and upper canopies, while *G. guidonia* mid canopy averaged 37.6 °C at 14.4 m and 39.3°C at 16.2 m (Fig. B1B).

Control leaf daily daytime mean temperatures ($T_{leafMEAN}$) varied across the canopy vertical gradient by only 1-3 °C, while maximum ($T_{leafMAX}$) temperatures spanned 6-8 °C.

G. guidonia daytime $T_{leafMEAN}$ ranged from 26.8 to 28.2 °C from the understory to the mid canopy (the tallest canopy layer for *G. guidonia*) ($p < 0.001$; $R^2 = 0.20$; Fig. 4.3A). Similarly, there was minimal within-canopy variation of *O. sintensii*, where $T_{leafMEAN}$ increased from 26.2 to 29.0 °C from the understory to the upper canopy ($p = 0.001$; $R^2 = 0.04$; Fig. 4.3B). *G. guidonia* $T_{leafMAX}$ ranged from 30.5 to 36.7 °C ($p < 0.001$; $R^2 = 0.20$; Fig. 4.3A), and *O. sintensii* $T_{leafMAX}$ ranged from 31.3 to 39.1 °C ($p < 0.001$; $R^2 = 0.16$; Fig. 4.3B). In addition, likely due to selection of leaves that were commonly exposed to sun flecks, there was a temperature spike in *O. sintensii* mid canopy where $T_{leafMAX}$ daily mean was 40.9 °C at 14.4 m (Fig. 4.3B).

4.4.2 Gas exchange responses to experimental warming

Neither of our study species showed evidence of acclimation of net photosynthesis after four weeks of leaf-level warming. Neither *G. guidonia* nor *O. sintensii* showed significant treatment or treatment × height interaction effects for optimum temperature of net photosynthesis (T_{opt}), photosynthesis at that optimum temperature (A_{opt}), or photosynthetic thermal niche (Ω) (Table 4.1; Fig. 4.4). These results suggest that these species did not acclimate through upregulation of temperature response parameters, nor did they show stress responses of warming through declined rates of net photosynthesis in response to leaf-level warming. In addition, we found no treatment or treatment × height interaction effects for the slope ($\beta_{1\_gs\text{-}T}$) or intercept ($\beta_{0\_gs\text{-}T}$) of stomatal conductance response to temperature for either species (Table 4.1; Fig. B2).

Unlike the results for net photosynthesis, we did find evidence of electron transport rate acclimation for *O. sintensii*; however, acclimation was only in the understory. The ANCOVA models for both *G. guidonia* and *O. sintensii* showed no significant treatment effects for optimum temperature of electron transport rate (T_{optETR}) (Table 4.1; Fig. 4.5A,B). *G. guidonia* also showed neither significant treatment nor treatment × height interaction effects suggesting that warming did not affect T_{optETR} (Fig. 4.5A). There was a significant treatment × height interaction for *O. sintensii* that was largely driven by the understory leaves (Fig. 4.5B). The heated leaves had a steeper T_{optETR} slope with height, where understory T_{optETR} was ~5 °C greater for heated leaves than control, but the treatment effect disappeared in the canopy. There were no significant treatment or treatment × height interactions for either species' ETR_{opt} (Table 4.1, Fig. 4.5C,D).

We found evidence of respiratory thermal acclimation in only *G. guidonia*. Heated *G. guidonia* leaves showed treatment effect indicating a down-regulation of Q_{10} compared to the control leaves (Table 4.1; Fig. 4.6A). The lack of treatment × height interaction suggests that the treatment effect was consistent across canopy height. *O. sintensii* had no significant treatment or treatment × height interaction effects for Q_{10} (Table 4.1; Fig. 4.6B). Neither species had significant treatment or interaction effects for either R_{25} or the ratio between respiration and photosynthesis at 25 °C (*R:A;* Table 4.1; Fig. 4.6C-F).

4.4.3 Gas exchange responses to height

Net photosynthesis increased with canopy height for both of our study species and, surprisingly, the optimum temperature for net photosynthesis declined as canopy height increased. ANCOVA results showed that both of our study species had significant T_{opt} height effects (Table 4.1). *G. guidonia* T_{opt} ranged from 33.1 °C in the understory to 28.0 °C in the mid canopy (Fig. 4.4A), while *O. sintensii* T_{opt} ranged from 35.5 °C in the understory to 32.7 °C in the upper canopy leaves (Fig. 4.4B). Almost doubling from the understory to the upper canopy, *O. sintensii* A_{opt} increased with increasing canopy height (Fig. 4.4D). Although the slope was not as steep as *O. sintensii*, *G. guidonia* A_{opt} also increased with increasing canopy height (Table 4.1; Fig. 4.4C).

Showing a similar pattern as net photosynthesis, the optimum temperature of photosynthetic electron transport also declined and the rate of electron transport at the optimum temperature increased with increasing canopy height for both of our study species. Both *G. guidonia* and *O. sintensii* had a significant height effects for T_{optETR} (Table 4.1, Fig. 4.5A,B). *G. guidonia* T_{optETR} decreased from 42.1 to 36.5 °C from understory to mid canopy. As described previously, *O. sintensii* heated and control leaves had differing responses to canopy height (Fig.4.5B). *G. guidonia* and *O. sintensii* ETR_{opt} increased with rising canopy height (Table 4.1; Fig 4.5C,D).

When investigating whether actual leaf temperatures exceeded photosynthetic optimum temperatures, we found that temperature optima of net photosynthesis was still lower than maximum leaf temperatures, while temperature optima of electron transport approached maximum leaf temperatures in both species in the top portions of *G. guidonia* and *O. sintensii* canopies. *G. guidonia* mid canopy T_{opt} (Student's t-test $p = 0.001$) and

T_{optETR} ($p = 0.001$) were higher than their associated daily daytime mean leaf temperature ($T_{leafMEAN}$; Fig. 4.3). *G. guidonia* T_{opt} values were lower than $T_{leafMAX}$ in the middle canopy ($p = 0.003$; Fig. 4.3A). T_{optETR} was similar to $T_{leafMAX}$ in the *G. guidonia* mid canopy ($p = 0.352$; Fig. 4.3A). Similar to *G. guidonia*, *O. sintensii* T_{opt} values were lower than $T_{leafMAX}$ in their highest canopy ranges ($p < 0.001$; $p = 0.003$; Fig. 4.3B) but *O. sintensii* T_{opt} did not differ from $T_{leafMEAN}$ in the upper canopy ($p = 0.682$; Fig. 4.3B). T_{optETR} was similar to $T_{leafMAX}$ in *O. sintensii* upper canopy ($p = 0.140$) and higher than $T_{leafMEAN}$ ($p < 0.001$; Fig. 4.3B).

Temperature sensitivity of stomatal conductance increased with height for both species, suggesting that stomatal conductance was more limited at higher temperatures in the upper canopy. g_s - T_{leaf} response slope ($\beta_{1\_gs\text{-}T}$) decreased with increasing canopy height (Table 4.1; Fig. B1A,B), while the opposite response occurred for the intercept ($\beta_{0\_gs\text{-}T}$, Table 4.1; Fig. B1C,D). To further quantify temperature responses of stomatal conductance within the canopy, we separated the canopy into four distinct positions. ANCOVA results showed significant T_{leaf} × height class interactions (*G. guidonia* $p < 0.001$; *O. sintensii* $p = 0.002$; Fig. 4.6). Post hoc pairwise comparisons showed that *G. guidonia* mid canopy had a steeper, more negative slope than both the lower canopy ($p < 0.001$) and understory ($p = 0.005$; Fig. 4.7A). There were no g_s - T_{leaf} slope differences between the lower canopy and the understory ($p = 0.979$). *G. guidonia* g_s - T_{leaf} intercepts were higher in the mid canopy compared to the lower canopy ($p = 0.001$) and there were no intercept differences between *G. guidonia* g_s - T_{leaf} mid canopy and understory ($p = 0.092$) or understory and lower canopy ($p = 0.860$; Fig. 4.7A). *O sintensii* upper canopy g_s - T_{leaf} slope was more negative than in the understory ($p = 0.001$) but not than the mid

canopy ($p = 0.148$; Fig. 4.7B). There was also no g_s - T_{leaf} slope difference between *O. sintensii* mid canopy and understory ($p = 0.110$; Fig. 4.7B). The understory, however, had a lower g_s - T_{leaf} intercept than both the upper ($p < 0.001$) and mid ($p < 0.001$) canopies). There was no intercept difference between *O. sintensii* upper and mid canopy ($p = 0.396$; Fig. 4.7B). These results suggest that, for each species, stomatal sensitivity to temperature tends to increase with increasing canopy height.

The slope of the leaf respiration-temperature response was constant across the vertical canopy gradient for both species; however, respiration rates at a constant temperature and the ratio of respiration to photosynthesis both increased with increasing heights in both species. The height effects on Q_{10} were not significant for either species (Table 4.1, Fig. 4.6A,B). Both R_{25} and R:A had a positive relationships with canopy height for both species (Table 4.1, Fig. 4.6C-F).

4.4.4 Leaf traits

Warming did not affect either leaf area or leaf mass per area (*LMA*); however, the two species differed in how canopy height affected these leaf morphological traits. Leaf area of *O. sintensii* did change with height; however, *G. guidonia* leaf area declined with height (Table B3; Fig. B3A,B). *LMA* increased from 32.87 to 87.83 g^{-1} cm^2 for *G. guidonia* and 60.00 to 142.33 g^{-1} cm^2 for *O. sintensii* throughout the height gradient (Table B3; Fig. B3C,D). Neither species showed significant treatment or height × treatment interactions for leaf area or *LMA* (Table B3).

Percent leaf water content *(%LWC*) declined with height for both study species; however, the two species responded differently to the warming treatment. While *O. sintensii* showed no effect of warming on %LWC, *G. guidonia* revealed a nearly significant treatment × height interaction (Table B3). *G. guidonia %LWC* was reduced in the heated leaves compared to control, but only in the understory. *O. sintensii* did not have a significant interaction effect; however, *%LWC* declined with height (Table B3; Fig. B3F).

Leaf nitrogen was not affected by warming; however, nitrogen per unit leaf area (N_{area}) increased with canopy height for both species and nitrogen per unit mass (N_{mass}) decreased with increasing canopy height for *O. sintensii*. *G. guidonia* N_{area} ranged from 1.09 g m^{-2} in the understory to 2.96 g m^{-2} in the mid canopy (Table B3; Fig. B3G) and from 1.32 to 2.78 g m^{-2} in *O. sintensii* upper canopy (Table B3; Fig. B3H). *G. guidonia* N_{mass} showed no response to the warming treatment or canopy height (Table B3; Fig. B3I), while *O. sintensii* N_{mass} slightly declined from 21.80 mg g^{-1} in the understory to 18.78 mg g^{-1} in the upper canopy (Table B3; Fig. B3J).

Leaf warming did not affect chlorophyll content; however, the chlorophyll content response to height differed between the two study species. *G. guidonia* chlorophyll content had a positive relationship with height, ranging from 30.51 in the understory to 132.73 in the mid canopy (Fig. B3K). Chlorophyll content of *O. sintensii*, however, did not change with height, and averaged 50.4 ± 2.0 across all canopy heights (Fig. B3L).

4.5 Discussion

4.5.1 Evidence for respiratory but not net photosynthetic acclimation

With partial support for our hypotheses, we found evidence for respiratory acclimation; however, net photosynthesis did not acclimate at any canopy position. We expected that photosynthetic acclimation would occur higher in the canopy but not in the lower canopy levels. Instead we found that photosynthetic electron transport rates acclimated to a higher T_{opt} in the lower canopy and only for *O. sintensii* (Fig. 4.5B). Even with acclimation of lower canopy *O. sentensii* T_{optETR}, neither species showed evidence of net photosynthetic acclimation (Fig. 4.4). *In situ* tropical canopy warming studies are rare, but one study in Brazil's Amazon rainforest that heated individual canopy leaves found that photosynthesis declined with leaf-level warming (Doughty 2011). Unlike Doughty (2011), we did not find evidence of photosynthetic decline, but a decline in photosynthesis does suggest that photosynthesis did not fully acclimate in the Brazilian canopy leaves. Recent studies investigating tropical seedling acclimation have found that seedlings can photosynthetically acclimate to higher growth temperatures (Scafaro *et al.* 2017; Slot and Winter 2017a; Smith and Dukes 2017). In addition, Smith and Dukes (2017) found that tropical seedling acclimation was more likely to occur in processes associated with the light reactions of photosynthesis (e.g., photosynthetic electron transport), as opposed to processes associated with the carbon reactions of photosynthesis (e.g. Rubisco carboxylation). Electron transport acclimation often occurs through stabilization of the thylakoid membrane (Havaux 1996; Neta-Sharir *et al.* 2005) or

implementation of cyclic electron transport (Havaux 1996; Schrader *et al.* 2004), which allows for maintained adenosine triphosphate (ATP) phosphorylation even when photosystem II function has declined (Schrader *et al.* 2004). Tropical forests often have dense canopies; therefore, acclimation of the photosynthetic processes associated with light capture may provide an advantage for the plant. Our results of electron transport acclimation in the understory supports this hypothesis for one of our study species; however, we did not investigate potential acclimation of Rubisco carboxylation. We cannot rule out the possibility that Rubisco carboxylation acclimated in one or both of our study species, as tropical species have been shown to acclimate through higher upregulated levels of Rubisco (Scarfaro *et al.* 2017).

Similar to photosynthesis we found partial support for our respiratory hypothesis in that respiration acclimated for *G. guidonia*, but not *O. sintensii*. Meta-analyses conducted globally (Slot and Kitajima 2015) and experimental studies across the tropics (Cheesman and Winter 2013; Slot *et al.* 2014; Drake *et al.* 2015; Aspinwall *et al.* 2016; Smith and Dukes 2017; Slot and Winter 2018) suggest that plant respiration will acclimate to warmer temperatures. The only other leaf-level warming study in a tropical forest canopy found tropical leaves can acclimate within seven days of experimental warming (Slot *et al.* 2014). Even when photosynthesis does not systematically acclimate, tropical leaf respiration often does (Cheesman and Winter 2013; Slot and Winter 2018). We only found acclimation in one of our study species (Fig. 4.6), suggesting that there may be different respiratory acclimation potential between species. *G. guidonia* had a lower Q_{10} in the heated leaves. Q_{10} acclimation is more likely to occur with fully mature

leaves (Atkin and Tjoelker 2003; Atkin *et al.* 2005), which was the case with our study. Q_{10} acclimation is often associated with either lower substrate availability (due to decreased sugar production from photosynthesis) or adenylate supply for ATP production (Atkin and Tjoelker 2003). While respiratory acclimation has been found to occur globally, leaves that were fully developed during the implementation of a new growth temperature can have a lesser ability to acclimate (Turnbull *et al.* 1993; Loveys *et al.* 2003). This could have potentially limited the acclimation potential of both of our study species and may explain why we did not detect *O. sintensii* respiratory acclimation. Even with the lack of net photosynthetic and respiratory acclimation in *O. sintensii* and lack of net photosynthetic acclimation in *G. guidonia*, we did not see any warming effect on *R:A* (Fig. 4.6E,F), which suggests that the balance between these two processes were not disrupted for these two species' leaves.

4.5.2 Photosynthesis and respiration response to canopy height

Because photosynthetic capacity is higher in leaves grown in sun compared to shaded environments (Niinemets 2007; Urban *et al.* 2007; Scartazza *et al.* 2016), we expected that photosynthesis and respiration would increase as canopy height increased. We found support for this hypothesis, where both A_{opt} and R_{25} rose with canopy height (Figs. 4.3C,D; 4.5C,D). Our A_{opt} results do, however, contradict recent findings of a study conducted in close proximity to our experiment. Mau *et al.* (2018) found that A_{opt} increased with increasing canopy height across temperate and tropical moist forests, but not in a tropical wet forest. Our study consisted of a greater height gradient than Mau *et al.* (2018), which could have contributed to our contrasting results. Our results support

other studies that find that the rate of photosynthesis increases with increasing canopy height within tropical systems (Thomas and Bazzaz 1999; Meir and Grace 2002; Weerasinghe *et al.* 2014; Kenzo *et al.* 2016; but see Kenzo *et al.* 2012) and across biomes (Meir and Grace 2002; Scartazza *et al.* 2016). Respiration is also higher in the upper canopy (Cavaleri *et al.* 2008; Weerasinghe *et al.* 2014; Asao *et al.* 2015; Kenzo *et al.* 2016; but see Kenzo *et al.* 2015) due to higher respiratory needs to maintain high rates of photosynthesis.

Few studies have investigated how R:A response to canopy vertical gradients; however, Weerasinghe *et al.* (2014) found that *R:A* are consistent across the canopy gradient after accounting for respiration inhibition in the light. We found that *R:A* increased with increasing canopy height (Fig. 4.6E,F), supporting a study conducted in a Costa Rican tropical forest (Cavaleri *et al.* 2008). This seems to show opposition to Weerasinghe *et al.* (2014); however, we measured leaf respiration in the dark. Leaf respiration is inhibited in the light (Hurry *et al.* 2005; Crous *et al.* 2012); therefore, if we had accounted for a depressed rate of photosynthesis under the higher light in the upper canopy, we might have found a relatively consistent *R:A* throughout the canopy.

4.5.3 Stomatal conductance temperature sensitivity limits upper canopy photosynthesis

Stomatal conductance is one of the primary processes that limits photosynthesis above T_{opt} (Lin *et al.* 2012) and may be the most important photosynthetic thermal limitation in tropical trees (Slot and Winter 2017b). Studies that have investigated shifts in stomatal conductance with warming have found inconsistent results. A recent study by

Fauset *et al.* (2019) found that plants grown in warming chambers switched from a positive, in ambient conditions, to a negative stomatal conductance relationship to increasing VPD. In contrast, Slot and Winter (2017a) found no difference in stomatal conductance between seedlings grown at different temperatures; however, they did find that stomatal conductance increased at temperatures higher than 40 °C. We did not find any treatment effects on either the slope or the intercept of the stomatal conductance response to temperature for either study species (Table 4.1); however, we did find greater stomatal sensitivity to temperature in the upper canopy compared to the lower canopy leaves (Fig. 4.7). Tropical forest upper canopy stomatal conductance has been classified as particularly sensitive to rising VPD (Siddiq *et al.* 2017), and upper canopy stomatal conductance can limit photosynthesis (Kenzo *et al.* 2012). Instead of a direct reduction of the rate of photosynthesis, we found a decline in T_{opt} as canopy height increased (Figs. 4.4A,B), perhaps limited by the high temperature sensitivity of the upper canopy stomatal conductance.

4.5.4 Leaf temperature and proximity to T_{opt}

Few studies have specifically investigated how T_{opt} varies throughout a forest canopy (Carter and Cavaleri 2018; Mau *et al.* 2018) and the one study that has studied this in a tropical forest did not find a T_{opt} vertical gradient trend in a tropical wet forest (Mau *et al.* 2018). We found that T_{opt} decreased with increasing canopy height (Fig. 4.3A,B) and, importantly, the upper canopy leaves experienced maximum temperatures well above T_{opt} (Fig. 4.3). Additionally, *O. sintensii* T_{opt} approached control $T_{leafMEAN}$ in the upper canopy (Fig. 4.3B), suggesting that these leaves were often operating above

their thermal thresholds. These results support other studies that found that tropical species (Vårhammar *et al.* 2015) and, in particularly, tropical forest upper canopies (Doughty and Goulden 2008; Mau *et al.* 2018) are operating above their photosynthetic thermal optimums. We found that $T_{leafMAX}$ exceeded T_{opt} in the upper canopy of both of our study species. This is particularly important as the light-exposed upper canopies of tropical forests cycle more carbon than the shaded lower canopy and understory leaves (Ellsworth and Reich 1993). If this portion of the canopy is often exceeding the optimum temperature for photosynthesis and T_{opt} is not acclimating to warmer temperatures, the upper canopy leaves could have a lower capability for carbon uptake (Pau *et al.* 2018).

4.5.5 Conclusion

We hypothesized that respiration would acclimate, and photosynthetic acclimation would more likely occur in the upper canopy, high light environment. We found partial support for these hypotheses, where respiration acclimated to +3 ° C experimental leaf-level canopy warming in one of our study species, *G. guidonia*. Our other study species, *O. sintensii*, acclimated the optimum temperature for photosynthetic electron transport; however, acclimation only occurred in the understory. Acclimation of T_{optETR} did not result in net photosynthetic acclimation, suggesting that ETR is not limiting to photosynthesis for *O. sintensii*. Upper canopy stomatal conductance was particularly sensitive to increasing temperature and the decreasing T_{opt} with canopy height suggests that photosynthesis was limited by stomatal conductance in the upper canopy. Photosynthesis was operating beyond the maximum mid canopy temperatures for *G. guidonia* and beyond mean daytime temperatures for *O. sintensis*. The lack of

acclimation in these two species mid and upper canopies suggest that climate warming may push these two species even further beyond their operating temperatures.

4.6 Acknowledgements

This research was funded by U.S. Department of Energy award numbers DE-SC-0011806, 89243018S-SC-000014, and DE-SC-0018942. The USDA Forest Service's International Institute of Tropical Forestry (IITF) and University of Puerto Rico-Río Piedras provided additional support. All research at IITF is done in collaboration with the University of Puerto Rico. Additional funding was provided by Michigan Technological Finishing Fellowship and Michigan Tech Ecosystem Science Center. We are very grateful to TRACE project manager Aura M. Alonso-Rodríguez for logistical support. We are also grateful to Benjamin Miller, Elsa Schwartz, Michael Schmid, and Jack Zwart for their excellent field and lab assistance.

4.7 References

Araki MG, Gyokusen K, Kajimoto T. **2017**. Vertical and seasonal variations in temperature responses of leaf respiration in a Chamaecyparis obtusa canopy. *Tree Physiology* **37**: 1269–1284.

Asao S, Bedoya-Arrieta R, Ryan MG. **2015**. Variation in foliar respiration and wood

CO_2 efflux rates among species and canopy layers in a wet tropical forest. *Tree Physiology* **35**: 148–159.

Aspinwall MJ, Drake JE, Campany C, *et al.* 2016. Convergent acclimation of leaf photosynthesis and respiration to prevailing ambient temperatures under current and warmer climates in Eucalyptus tereticornis. *New Phytologist* **212**: 354–367.

Atkin OK, Bruhn D, Hurry VM, Tjoelker MG. **2005**. The hot and the cold : unravelling the variable response of plant respiration to temperature. *Functional Plant Biology* **32**: 87–105.

Atkin OK, Tjoelker MG. **2003**. Thermal acclimation and the dynamic response of plant respiration to temperature. *Trends in Plant Science* **8**: 343–351.

Bauerle WL, Weston DJ, Bowden JD, Dudley JB, Toler JE. **2004**. Leaf absorptance of photosynthetically active radiation in relation to chlorophyll meter estimates among woody plant species. *Scientia Horticulturae* **101**: 169–178.

Berry J, Bjorkman O. **1980**. Photosynthetic response and adaptation to temperature in higher plants. *Annual Review of Plant Physiology* **31**: 491–543.

Brienen RJW, Phillips OL, Feldpausch TR, *et al.* 2015. Long-term decline of the Amazon carbon sink. *Nature* **519**: 344–348.

Buckley TN. **2005**. The control of stomata by water balance. *New Phytologist* **168**: 275–292.

Carter KR, Cavaleri MA. **2018**. Within-Canopy Experimental Leaf Warming Induces Photosynthetic Decline Instead of Acclimation in Two Northern Hardwood Species. *Frontiers in Forests and Global Change* **1**:11. doi: 10.3389/ffgc.2018.00011

Cavaleri MA, Oberbauer SF, Ryan MG. **2008**. Foliar and ecosystem respiration in an old-growth tropical rain forest. *Plant, Cell and Environment* **31**: 473–483.

Cavaleri MA, Reed SC, Smith WK, Wood TE. **2015**. Urgent need for warming experiments in tropical forests. *Global Change Biology* **21**: 2111–2121.

Cheesman AW, Winter K. **2013**. Growth response and acclimation of CO2 exchange characteristics to elevated temperatures in tropical tree seedlings. *Journal of Experimental Botany* **64**: 3817–3828.

Crous KY, Zaragoza-Castells J, Ellsworth DS, *et al.* 2012. Light inhibition of leaf respiration in field-grown Eucalyptus saligna in whole-tree chambers under elevated atmospheric CO2 and summer drought. *Plant, Cell and Environment* **35**: 966–981.

Cunningham S, Read J. **2002**. Comparison of temperate and tropical rainforest tree species: photosynthetic responses to growth temperature. *Oecologia* **133**: 112–119.

Cunningham SC, Read J. **2003**. Do temperate rainforest trees have a greater ability to acclimate to changing temperatures than tropical rainforest trees? *New Phytologist* **157**: 55–64.

Diffenbaugh NS, Scherer M. **2011**. Observational and model evidence of global emergence of permanent, unprecedented heat in the 20th and 21st centuries. *Climatic*

Change **107**: 615–624.

Doughty CE. **2011**. An in situ leaf and branch warming experiment in the Amazon. *Biotropica* **43**: 658–665.

Doughty CE, Goulden ML. **2008**. Are tropical forests near a high temperature threshold? *Journal of Geophysical Research: Biogeosciences* **114**: 1–12.

Drake JE, Aspinwall MJ, Pfautsch S, *et al.* 2015. The capacity to cope with climate warming declines from temperate to tropical latitudes in two widely distributed Eucalyptus species. *Global Change Biology* **21**: 459–472.

Dusenge ME, Duarte AG, Way DA. **2019**. Plant carbon metabolism and climate change: elevated CO2 and temperature impacts on photosynthesis, photorespiration and respiration. *New Phytologist* **221**: 32–49.

Dusenge ME, Way DA. **2017**. Warming puts the squeeze on photosynthesis - Lessons from tropical trees. *Journal of Experimental Botany* **68**: 2073–2077.

Ellsworth DS, Reich PB. **1993**. Canopy structure and vertical patterns of photosynthesis and related leaf traits in a deciduous forest. *Oecologia* **96**: 169–178.

Fauset S, Oliveira L, Buckeridge MS, *et al.* 2019. Contrasting responses of stomatal conductance and photosynthetic capacity to warming and elevated CO2 in the tropical tree species Alchornea glandulosa under heatwave conditions. *Environmental and Experimental Botany* **158**: 28–39.

Feldpausch TR, Banin L, Phillips OL, *et al.* 2010. Height-diameter allometry of tropical forest trees. *Biogeosciences Discussions* **7**: 7727–7793.

Galbraith D, Levy PE, Sitch S, *et al.* 2010. Multiple mechanisms of Amazonian forest biomass losses in three dynamic global vegetation models under climate change. *New Phytologist* **187**: 647–665.

Han F, Wang X, Zhou H, Li Y, Hu D. **2017**. Temporal dynamics and vertical variations in stem CO2 efflux of Styphnolobium japonicum. *Journal of Plant Research* **130**: 845–858.

Hanson PJ, Riggs JS, Robert Nettles W, *et al.* 2017. Attaining whole-ecosystem warming using air and deep-soil heating methods with an elevated CO2 atmosphere. *Biogeosciences* **14**: 861–883.

Harris N, Lugo A, Brown S, Heartsill Scalley T. **2012**. *Luquillo Experimental Forest: Research History and Opportunities*. EFR-1. Washington, DC: U.S. Department of Agriculture. 152 p.

Havaux M. **1996**. Short-tern response of Photosystem I to heat stress. *Photosynthesis Research* **47**: 85–97.

Hurry V, Igamberdiev A, Keergerg O, Parnik T, Atkin O, Zaragoza-Castells J. **2005**. Respiration in photosynthetic cells: gas exchange components, interactions with photorespiration and the oper- ation of mitochondria in the light In: Lambers H, Ribas-Carbo M, eds. *Plant respiration*. Dordrecht, The Netherlands, 43–61.

Janzen DH. **1967**. Why Mountain Passes are Higher in the Tropics. *The American Naturalist* **101**: 233–249.

Kenzo T, Iida S, Shimizu T, *et al.* 2016. Seasonal and height-related changes in leaf morphological and photosynthetic traits of two dipterocarp species in a dry deciduous forest in Cambodia. *Plant Ecology and Diversity* **9**: 505–520.

Kenzo T, Inoue Y, Yoshimura M, Yamashita M, Tanaka-Oda A, Ichie T. **2015**. Height-related changes in leaf photosynthetic traits in diverse Bornean tropical rain forest trees. *Oecologia* **177**: 191–202.

Kenzo T, Yoneda R, Sano M, *et al.* 2012. Variations in leaf photosynthetic and morphological traits with tree height in various tree species in a cambodian tropical dry evergreen forest. *Japan Agricultural Research Quarterly* **46**: 167–180.

Krause GH, Winter K, Krause B, Virgo A. **2015**. Light-stimulated heat tolerance in leaves of two neotropical tree species, Ficus insipida and Calophyllum longifolium. *Functional Plant Biology* **42**: 42–51.

Kumagai T, Ichie T, Yoshimura M, *et al.* 2006. Modelling CO_2 exchange over a Bornean tropical rain forest using measured vertical and horizontal variations in leaf-level physiological parameters and leaf area densities. *Journal of Geophysical Research Atmospheres* **111**: 1–16.

Lin YS, Medlyn BE, Ellsworth DS. **2012**. Temperature responses of leaf net photosynthesis: The role of component processes. *Tree Physiology* **32**: 219–231.

Liu YY, Van Dijk AIJM, De Jeu RAM, *et al.* 2015. Recent reversal in loss of global terrestrial biomass. *Nature Climate Change* **5**: 470–474.

Lloyd J, Farquhar GD. **2008**. Effects of rising temperatures and [CO2] on the physiology of tropical forest trees. *Philosophical transactions of the Royal Society of London. Series B, Biological sciences* **363**: 1811–7.

Loveys B, Atkinson L, Sherlock D, Roberts R, Fitter A, Atkin O. **2003**. Thermal acclimation of leaf and root respiration : an investigation comparing inherently fast- and slow- growing plant species. *Global Change Biology* **9**: 895–910.

Luo Y. **2007**. Terrestrial Carbon–Cycle Feedback to Climate Warming. *Annual Review of Ecology, Evolution, and Systematics* **38**: 683–712.

Malhi Y, Aragão LEOC, Galbraith D, *et al.* 2009. Exploring the likelihood and mechanism of a climate-change-induced dieback of the Amazon rainforest. *Proceedings of the National Academy of Sciences of the United States of America* **106**: 20610–20615.

Mau A, Reed S, Wood T, Cavaleri M. **2018**. Temperate and tropical forest canopies are already functioning beyond their thermal thresholds for photosynthesis. *Forests* **9**: 47.

Meir P, Grace J. **2002**. Scaling relationships for woody tissue respiration in two tropical rain forests. *Plant, Cell and Environment* **25**: 963–973.

Meir P, Grace J, Miranda AC. **2001**. Leaf respiration in two tropical rainforests: Constraints on physiology by phosphorus, nitrogen and temperature. *Functional Ecology* **15**: 378–387.

Mora C, Frazier AG, Longman RJ, *et al.* 2013. The projected timing of climate departure from recent variability. *Nature* **502**: 183–7.

Motzer T, Munz N, Küppers M, Schmitt D, Anhuf D. **2005**. Stomatal conductance, transpiration and sap flow of tropical montane rain forest trees in the southern Ecuadorian Andes. *Tree Physiology* **25**: 1283–1293.

Nakamura M, Makoto K, Tanaka M, Inoue T, Son Y, Hiura T. **2016**. Leaf flushing and shedding, bud and flower production, and stem elongation in tall birch trees subjected to increases in aboveground temperature. *Trees - Structure and Function* **30**: 1535–1541.

Nakamura M, Muller O, Tayanagi S, Nakaji T, Hiura T. **2010**. Experimental branch warming alters tall tree leaf phenology and acorn production. *Agricultural and Forest Meteorology* **150**: 1026–1029.

Neta-Sharir I, Isaacson T, Lurie S, Weiss D. **2005**. Dual role for tomato heat shock protein 21: Protecting photosystem II from oxidative stress and promoting color changes during fruit maturation. *Plant Cell* **17**: 1829–1838.

Niinemets Ü. **2007**. Photosynthesis and resource distribution through plant canopies. *Plant, Cell and Environment* **30**: 1052–1071.

Niinemets Ü, Oja V, Kull O. **1999**. Shape of leaf photosynthetic electron transport versus temperature response curve is not constant along canopy light gradients in temperate deciduous trees. *Plant, Cell & Environment* **22**: 1497–1513.

Niinemets Ü, Valladares F. **2004**. Photosynthetic acclimation to simultaneous and interacting environmental stresses along natural light gradients: Optimality and constraints. *Plant Biology* **6**: 254–268.

O'Sullivan OS, Heskel MA, Reich PB, *et al.* 2017. Thermal limits of leaf metabolism across biomes. *Global Change Biology* **23**: 209–223.

Pan Y, Birdsey RA, Phillips OL, Jackson RB. **2013**. The Structure, Distribution, and Biomass of the World's Forests. *Annual Review of Ecology, Evolution, and Systematics* **44**: 593–622.

Pan Y, Birdsey R a., Phillips OL, Jackson RB. **2013**. The Structure, Distribution, and Biomass of the World's Forests. *Annual Review of Ecology, Evolution, and Systematics* **44**: 593–622.

Pau S, Detto M, Kim Y, Still CJ. **2018**. Tropical forest temperature thresholds for gross primary productivity. *Ecosphere* **9**: 1–12.

Rozendaal DMA, Hurtado VH, Poorter L. **2006**. Plasticity in leaf traits of 38 tropical tree species in response to light; relationships with light demand and adult stature. *Functional Ecology* **20**: 207–216.

Scafaro AP, Xiang S, Long BM, *et al.* 2017. Strong thermal acclimation of photosynthesis in tropical and temperate wet-forest tree species: The importance of altered Rubisco content. *Global Change Biology* **23**: 2783–2800.

Scartazza A, Di Baccio D, Bertolotto P, Gavrichkova O, Matteucci G. **2016**.

Investigating the European beech (Fagus sylvatica L.) leaf characteristics along the vertical canopy profile: leaf structure, photosynthetic capacity, light energy dissipation and photoprotection mechanisms. *Tree Physiology* **31**: 1–17.

Scatena F. **1989**. *An Introduction to the Physiography and History of the Bisley Experimental Watersheds in the Luquillo Mountains of Puerto Rico*.

Schrader SM, Wise RR, Wacholtz WF, Ort DR, Sharkey TD. **2004**. Thylakoid membrane responses to moderately high leaf temperature in Pima cotton. *Plant, Cell and Environment* **27**: 725–735.

Siddiq Z, Chen YJ, Zhang YJ, Zhang JL, Cao KF. **2017**. More sensitive response of crown conductance to VPD and larger water consumption in tropical evergreen than in deciduous broadleaf timber trees. *Agricultural and Forest Meteorology* **247**: 399–407.

Slot M, Garcia MA, Winter K. **2016**. Temperature response of CO 2 exchange in three tropical tree species. *Functional Plant Biology* **43**: 468–478.

Slot M, Kitajima K. **2015**. General patterns of acclimation of leaf respiration to elevated temperatures across biomes and plant types. *Oecologia* **177**: 885–900.

Slot M, Rey-Sánchez C, Gerber S, Lichstein JW, Winter K, Kitajima K. **2014**. Thermal acclimation of leaf respiration of tropical trees and lianas: Response to experimental canopy warming, and consequences for tropical forest carbon balance. *Global Change Biology* **20**: 2915–2926.

Slot M, Winter K. **2017a**. Photosynthetic acclimation to warming in tropical forest tree

seedlings. *Journal of Experimental Botany* **68**: 2275–2284.

Slot M, Winter K. **2017b**. In situ temperature relationships of biochemical and stomatal controls of photosynthesis in four lowland tropical tree species. *Plant Cell and Environment* **40**: 3055–3068.

Slot M, Winter K. **2018**. High tolerance of tropical sapling growth and gas exchange to moderate warming. *Functional Ecology* **32**: 599–611.

Smith NG, Dukes JS. **2013**. Plant respiration and photosynthesis in global-scale models: Incorporating acclimation to temperature and CO2. *Global Change Biology* **19**: 45–63.

Smith NG, Dukes JS. **2017**. Short-term acclimation to warmer temperatures accelerates leaf carbon exchange processes across plant types. *Global Change Biology*: 4840–4853.

Thomas SC, Bazzaz FA. **1999**. Asymptotic Height as a Predictor of Photosynthetic Characteristics in Malaysian Rain Forest Trees. *Ecology* **80**: 1607–1622.

Turnbull MH, Doley D, Yates DJ. **1993**. The dynamics of photosynthetic acclimation to changes in light quantity and quality in three Australian rainforest tree species. *Oecologia* **94**: 218–228.

Turnbull MH, Whitehead D, Tissue DT, Schuster WSF, Brown KJ, Griffin KL. **2003**. Scaling foliar respiration in two contrasting forest canopies. *Functional Ecology* **17**: 101–114.

Urban O, Košvancová M, Marek M V., Lichtenthaler HK. **2007**. Induction of

photosynthesis and importance of limitations during the induction phase in sun and shade leaves of five ecologically contrasting tree species from the temperate zone. *Tree Physiology* **27**: 1207–1215.

Vårhammar A, Wallin G, Mclean CM, *et al.* 2015. Photosynthetic temperature responses of tree species in Rwanda: Evidence of pronounced negative effects of high temperature in montane rainforest climax species. *New Phytologist* **206**: 1000–1012.

Way DA, Oren R. **2010**. Differential responses to changes in growth temperature between trees from different functional groups and biomes: a review and synthesis of data. *Tree Physiology* **30**: 669–688.

Way DA, Yamori W. **2014**. Thermal acclimation of photosynthesis: On the importance of adjusting our definitions and accounting for thermal acclimation of respiration. *Photosynthesis Research* **119**: 89–100.

Weerasinghe LK, Creek D, Crous KY, *et al.* 2014. Canopy position affects the relationships between leaf respiration and associated traits in a tropical rainforest in Far North Queensland. *Tree Physiology* **34**: 564–584.

Wood TE, Cavaleri MA, Reed SC. **2012**. Tropical forest carbon balance in a warmer world: A critical review spanning microbial- to ecosystem-scale processes. *Biological Reviews* **87**: 912–927.

Yamaguchi DP, Nakaji T, Hiura T, Hikosaka K. **2016**. Effects of seasonal change and experimental warming on the temperature dependence of photosynthesis in the canopy leaves of Quercus serrata. *Tree Physiology* **36**: 1283–1295.

4.8 Tables and Figures

Table 4.1 ANCOVA results and model coefficients for leaf gas exchange response to treatment, height, and the interaction between treatment and height. Bold p-values indicate significance at $\alpha<0.05$ level.

		ANCOVA					Model coefficients			
Species	**Gas exchange parameter**	**df**	**Treatment**	**Height**	**Tmt × Ht**	**Adj R^2**	**Control y-intercept**	**Control slope**	**Heated y-intercept**	**Heated slope**
G. guidonia	T_{opt}	3,28	0.726	**0.001**	0.272	0.267	35.62 ± 1.11	-0.19 ± 0.10	2.12 ± 1.68	-0.17 ± 0.15
	A_{opt}	3,28	0.288	**0.030**	0.226	0.138	6.82 ± 1.04	0.08 ± 0.09	-2.60 ± 1.58	0.17 ± 0.14
	Ω	3,26	0.427	0.218	0.077	0.084	12.31 ± 1.64	0.33 ± 0.52	3.50 ± 2.75	-0.44 ± 0.24
	T_{optETR}	3,23	0.702	**0.008**	0.568	0.183	41.18 ± 1.40	-0.25 ± 0.12	1.43 ± 2.54	-0.12 ± 0.21
	ETR_{opt}	3,23	0.314	**0.005**	0.442	0.245	54.50 ± 10.92	2.01 ± 0.96	-25.08 ± 19.87	1.30 ± 1.65
	$\beta_{1\_gs\text{-}T}$	3,25	0.963	**0.007**	0.885	0.169	$2.32 \times 10^{-3} \pm 2.21 \times 10^{-3}$	$-4.84 \times 10^{-4} \pm 1.95 \times 10^{-4}$	$1.75 \times 10^{-4} \pm 41.35 \times 10^{-4}$	$0.49 \times 10^{-4} \pm 3.36 \times 10^{-4}$
	$\beta_{0\_gs\text{-}T}$	3,25	0.853	**0.010**	0.934	0.149	$-8.17 \times 10^{-5} \pm 8.58 \times 10^{-2}$	$1.71 \times 10^{-2} \pm 0.74 \times 10^{-2}$	$-2.24 \times 10^{-2} \pm 15.25 \times 10^{-2}$	$-9.81 \times 10^{-4} \pm 1.27 \times 10^{-2}$

	R:A	3,28	0.142	**0.003**	0.643	0.254	$1.84 \times 10^{-2} \pm 1.55 \times 10^{-2}$	$0.30 \times 10^{-2} \pm 0.14 \times 10^{-2}$	$0.34 \times 10^{-2} \pm 2.35 \times 10^{-2}$	$0.09 \times 10^{-2} \pm 0.21 \times 10^{-2}$
	Q_{10}	1,29	**0.049**	0.940	0.465	0.053	2.16 ± 0.13	$5.57 \times 10^{-3} \pm 11.86 \times 10^{-3}$	-0.30 ± 0.18	$1.24 \times 10^{-2} \pm 1.68 \times 10^{-2}$
	R_{25}	1,29	0.568	**<0.001**	0.756	0.493	$1.46 \times 10^{-2} \pm 6.95 \times 10^{-2}$	$2.45 \times 10^{-2} \pm 0.63 \times 10^{-2}$	$-0.30 \times 10^{-2} \pm 9.88 \times 10^{-2}$	$0.28 \times 10^{-2} \pm 0.89 \times 10^{-2}$
O. sintensii	T_{opt}	3,23	0.449	**0.021**	0.634	0.132	34.15 ± 2.81	-0.39 ± 0.18	-0.75 ± 3.99	0.13 ± 0.26
	A_{opt}	3,23	0.461	**0.007**	0.885	0.194	4.86 ± 1.91	0.28 ± 0.12	-0.24 ± 2.71	-0.03 ± 0.18
	Ω	3,21	0.178	0.956	0.794	-0.04	22.66 ± 4.28	-2.44 ± 6.12	0.06 ± 0.275	-0.11 ± 0.42
	T_{optETR}	3,23	0.144	**<0.001**	**0.009**	0.638	42.44 ± 1.78	-0.35 ± 0.11	6.34 ± 2.32	-0.43 ± 015
	ETR_{opt}	3,23	0.124	**<0.001**	0.980	0.317	50.04 ± 16.43	3.27 ± 1.02	-6.77 ± 21.42	-0.03 ± 1.39
	$\beta_{1\_gs\text{-}T}$	3,23	0.226	**0.003**	0.704	0.283	$-1.48 \times 10^{-3} \pm 1.73 \times 10^{-3}$	$-3.20 \times 10^{-4} \pm 1.11 \times 10^{-4}$	$-0.89 \times 10^{-4} \pm 24.55 \times 10^{-4}$	$0.79 \times 10^{-4} \pm 1.63 \times 10^{-4}$
	$\beta_{0\_gs\text{-}T}$	3.23	0.454	0.001	0.959	0.295	$1.06 \times 10^{-1} \pm 0.72 \times 10^{-1}$	$1.27 \times 10^{-2} \pm 0.46 \times 10^{-2}$	$-0.75 \times 10^{-1} \pm 10.24 \times 10^{-1}$	$-2.61 \times 10^{-3} \pm 6.73 \times 10^{-3}$
	R:A	3,23	0.610	**0.012**	0.965	0.154	$1.14 \times 10^{-2} \pm 1.59 \times 10^{-2}$	$0.82 \times 10^{-2} \pm 2.25 \times 10^{-2}$	$0.21 \times 10^{-2} \pm 0.10 \times 10^{-2}$	$6.65 \times 10^{-5} \pm 149.14 \times 10^{-5}$

	Q_{10}	3,25	0.382	0.571	0.773	-0.068	2.00 ± 0.13	$-1.70 \times 10^{-3} \pm 8.15 \times 10^{-3}$	0.11 ± 0.18	$-3.41 \times 10^{-3} \pm 11.69 \times 10^{-3}$
	R_{25}	3,25	0.797	**<0.001**	0.829	0.410	$-0.12 \times 10^{-2} \pm 10.89 \times 10^{-2}$	$2.48 \times 10^{-2} \pm 0.70 \times 10^{-2}$	$2.32 \times 10^{-2} \pm 15.44 \times 10^{-2}$	$-0.22 \times 10^{-2} \pm 01.00 \times 10^{-2}$

Fig. 4.1 Examples of leaf heaters in the upper canopy of *Ocotea sintensii*.

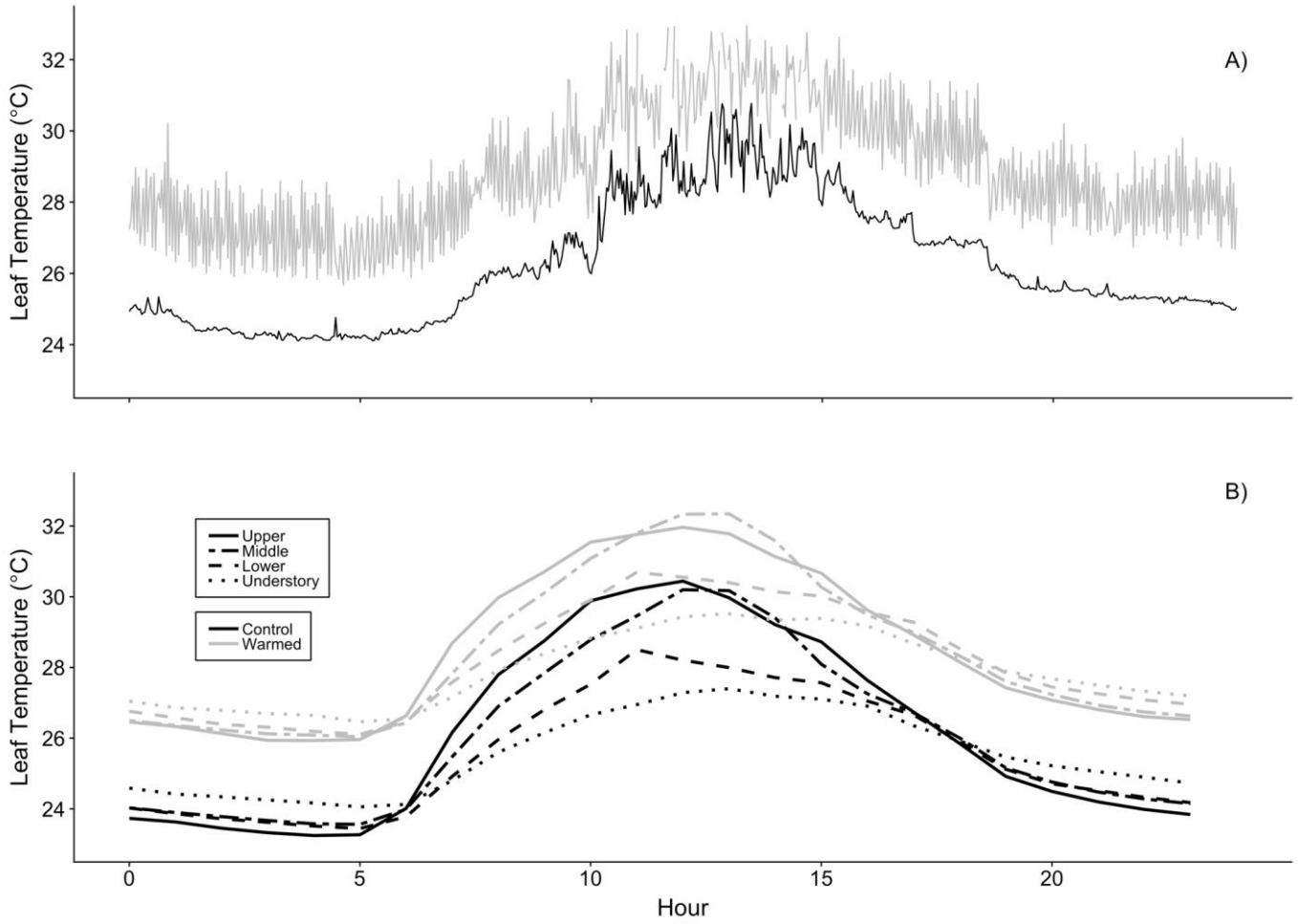
A)
Leaf Temperature (°C)
32
30
28
26
24
B)
Upper
Middle
Lower
Understory
Control
Warmed
Leaf Temperature (°C)
32
30
28
26
24
0
5
10
15
20
Hour

Fig. 4.2 Performance of leaf-level warming. A) 24 hours of heating for one control and associated heated leaf. Example leaf was *Guarea guidonia* 14.4 m height on July 22, 2017 and B) mean heated and control leaf temperature at the four canopy positions for *G. guidonia* and *Ocotea sintensii* combined. Control leaves are represented by black lines and heated lines are represented by grey lines. Upper canopy is depicted by solid lines, mid canopy is depicted by dot-dash lines, lower canopy is depicted by dashed lines, and understory is depicted by dotted lines.

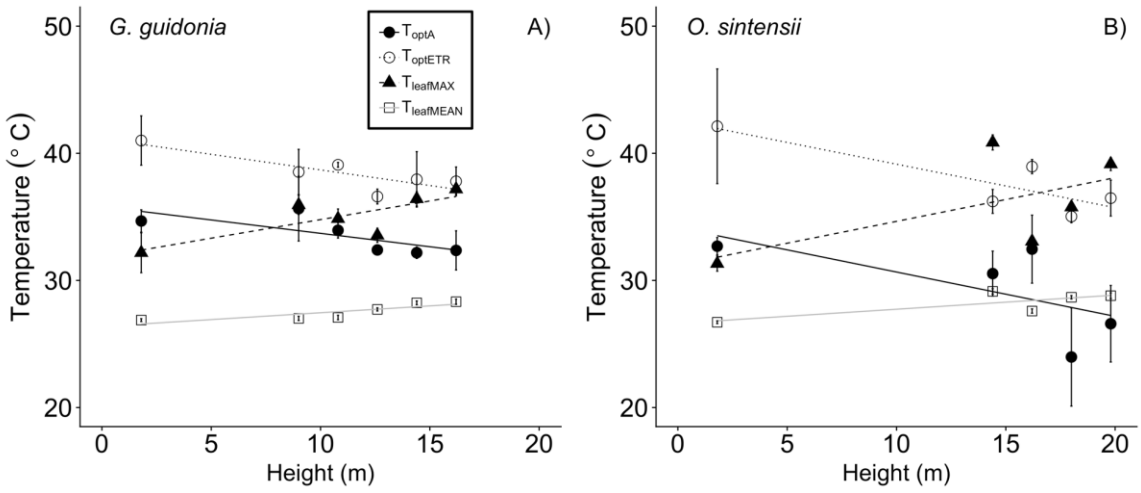

Fig. 4.3 Optimum temperatures and leaf temperature throughout the canopy. Control leaf optimum temperatures of net photosynthesis (T_{opt}, filled circle, solid black line) and photosynthetic electron transport (T_{optETR}, empty circle, dotted black line) compared to the mean daily maximum leaf temperature ($T_{leafMAX}$, filled triangle, dashed black line) and mean daily daytime leaf temperature ($T_{leafMEAN}$, empty square, solid gray line) for A) *G. guidonia* and B) *O. sintensii*. $T_{leafMAX}$ $T_{leafMEAN}$ were calculated as a daily mean for each species at each canopy position. Data are shown for control leaves only. Error bars represent SEM. Equations for T_{opt} and T_{optETR} are given in Table 4.1). *G. guidonia* $T_{leafMEAN}$ equation is $T_{leafMEAN} = 25.39(0.14) + 0.03(0.01)Height$, *G. guidonia* $T_{leafMAX}$ equation is $T_{leafMAX} = 30.96(0.69) + 0.36(0.06)Height$, *O. sintensii* $T_{leafMEAN}$ equation is $T_{leafMEAN} = 25.55(0.15) + 0.03(0.01)Height$, and *O. sintensii* $T_{leafMAX}$ equation is $T_{leafMAX} = 31.43(0.76) + 0.31(0.05)Height$. Equation values given in parentheses represent SEM.

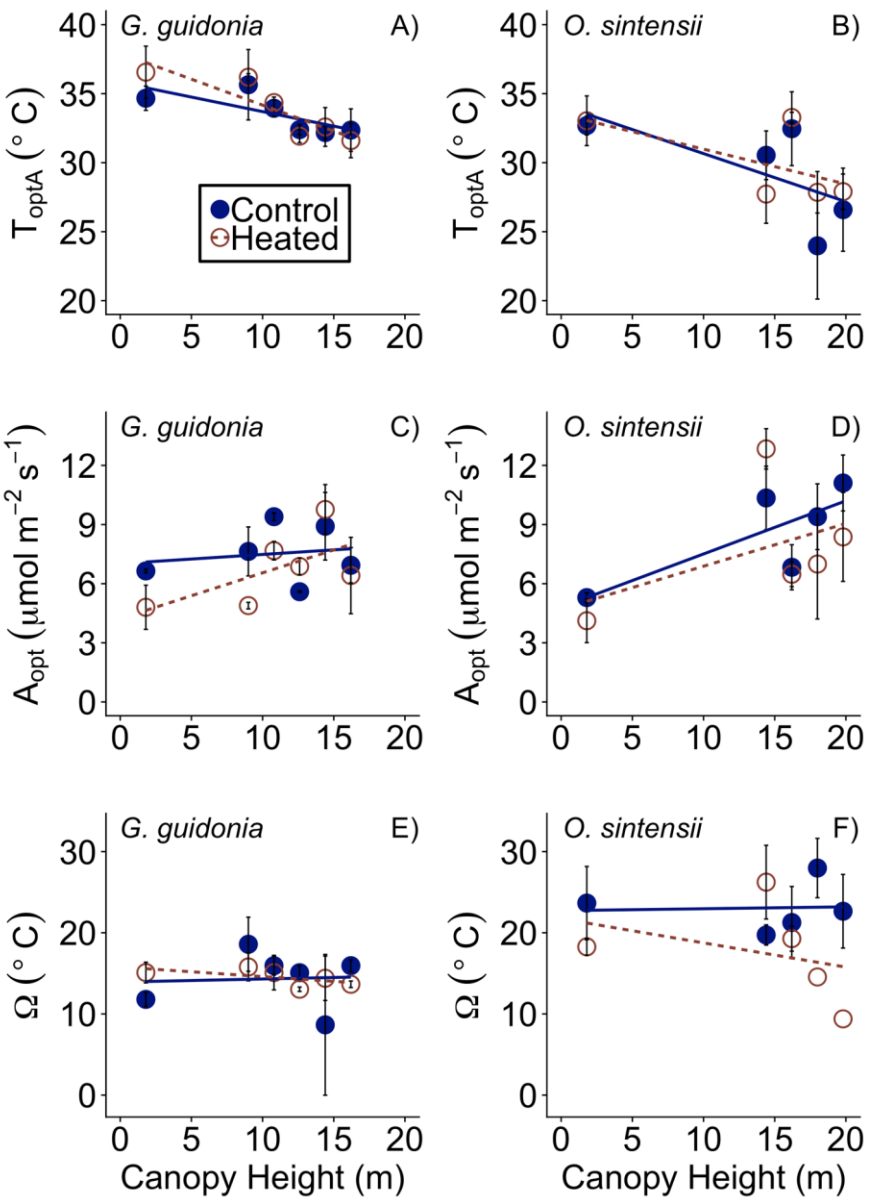

Fig. 4.4 Net Photosynthetic temperature response parameter responses to canopy height. **A)** *Guarea guidonia* optimum temperature for net photosynthesis (T_{opt}), **B)** *Ocotea sintensii* T_{opt}, **C)** *G. guidonia* rate of net photosynthesis at T_{opt} (A_{opt}), **D)** *O. sintensii* A_{opt} **E)** *G. guidonia* photosynthetic thermal niche (Ω), and **F)** *O. sintensii* Ω response to canopy height for heated (red open circles) and control (blue closed circles) leaves.

Linear regressions were fit individually for heated (red dashed) and control (blue solid) leaves.

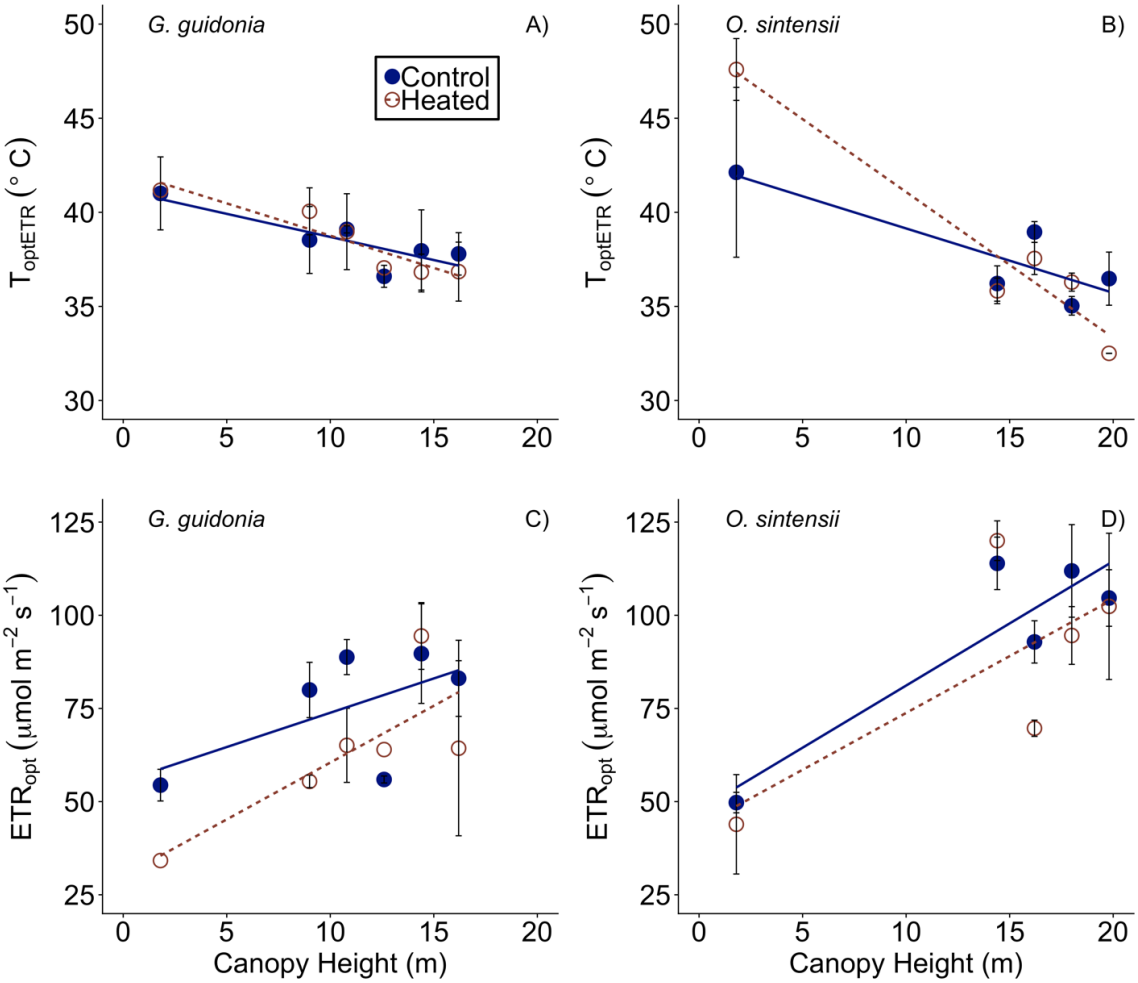

Fig. 4.5 Photosynthetic electron transport temperature response parameter responses to canopy height. **A)** *Guarea guidonia* optimum temperature for photosynthetic electron transport (T_{optETR}), **B)** *Ocotea sintensii* T_{optETR}, **C)** *G. guidonia* rate of net photosynthesis at T_{optETR} (ETR_{opt}), **D)** *O. sintensii* ETR_{opt} response to canopy height for heated (red open circles) and control (blue closed circles) leaves. Linear regressions were fit individually for heated (red dashed) and control (blue solid) leaves.

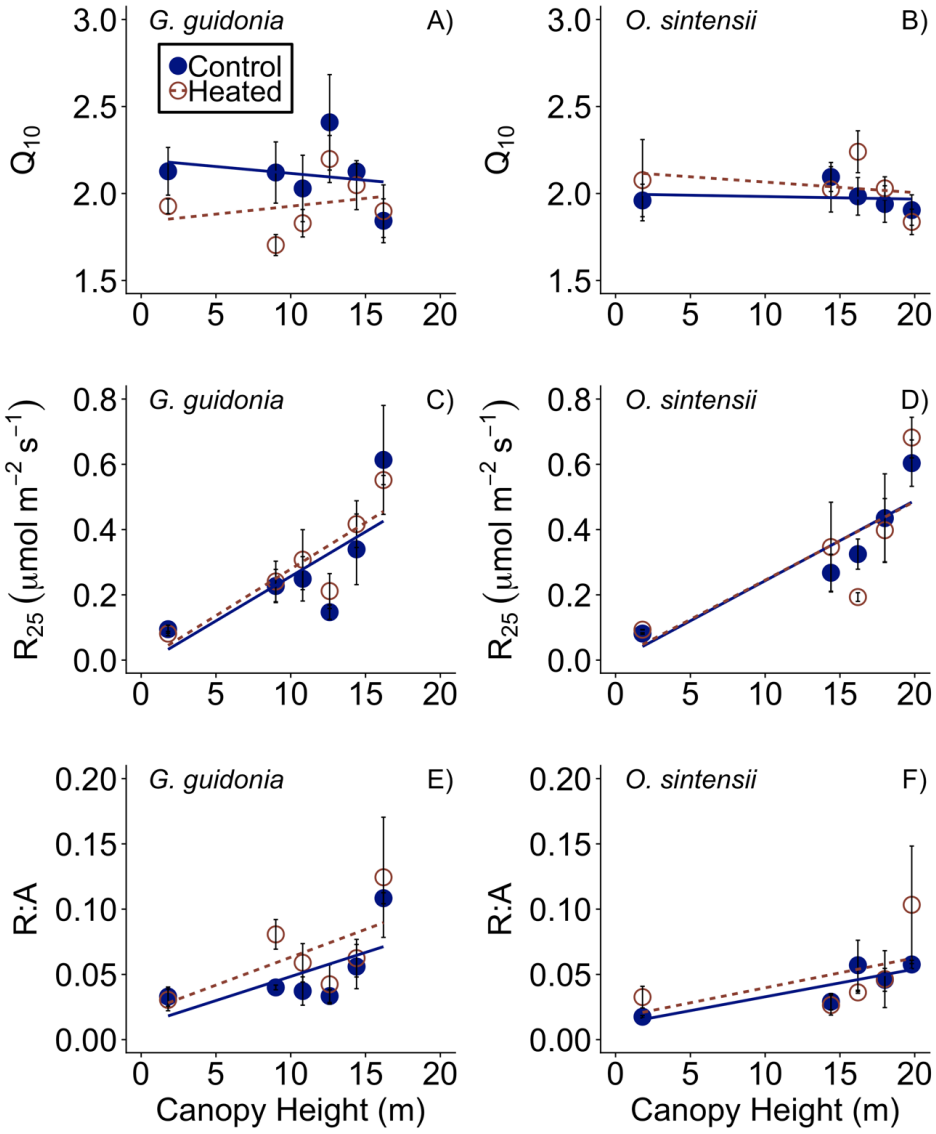

Fig. 4.6 Leaf respiration temperature response parameter responses to canopy height. **A)** *Guarea guidonia* respiratory increase with every 10 °C increase in leaf temperature (Q_{10}), **B)** *Ocotea sintensii* Q_{10}, **C)** *G. guidonia* rate of leaf respiration at 25 °C (R_{25}), **D)** *O. sintensii* R_{25} **E)** *G. guidonia* ratio between R_{25} and photosynthesis at 25 °C (*R:A*), and **F)** *O. sintensii R:A* response to canopy height for heated (red open circles) and control (blue

closed circles) leaves. Linear regressions were fit individually for heated (red dashed) and control (blue solid) leaves.

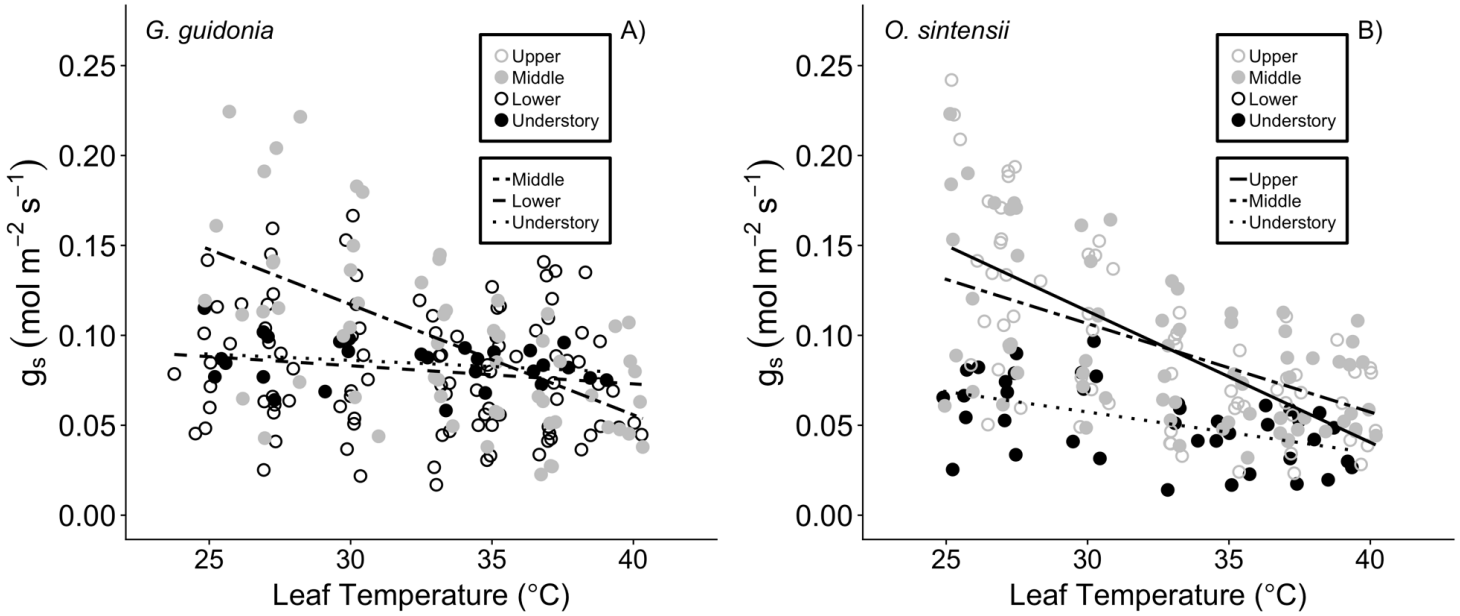

Fig. 4.7 Stomatal conductance response to leaf temperature at different canopy positions. Stomatal conductance response to leaf temperature for A) *G. guidonia* and B) *O. sintensii*. Canopy positions shown for *G. guidonia* are understory (0-1.5 meters; black filled circle), lower canopy (9-12.6 m; black open circle), mid canopy (14.4-16.2 m; gray open circle). Canopy positions shown for *O.*

sintensii are the understory, mid, and upper canopy (18-19.8 m; gray open circle). Lines depict regression lines for the understory (dotted), lower canopy (dashed), mid (dot-dashed), and upper (solid) canopies.

5 Dissertation Conclusion

Tropical forests play a disproportionate role in global carbon uptake (Dixon *et al.* 1994; Pan *et al.* 2013); yet; these systems have been identified as one of the regions with the highest levels of carbon modeling uncertainty (Booth *et al.* 2012; Cavaleri *et al.* 2015; Lombardozzi *et al.* 2015; Mercado *et al.* 2018). Additionally, Earth system models as a whole need better mechanistic representations of vegetation responses to temperature (Friedlingstein *et al.* 2006; Booth *et al.* 2012; Rogers 2016); particularly, there is need for quantifications at the regional scale (Mercado *et al.* 2018). The goal of this dissertation was to help close this critical gap in our understanding of tropical forest physiological responses to temperature using both a meta-analytic and experimental approach.

Global algorithms have been developed to quantify photosynthetic responses to temperature (Medlyn *et al.* 2002; Kattge and Knorr 2007; Kumarathunge *et al.* 2019); however, investigations of these responses for specific geographic regions are needed ensure accurate representation of carbon fluxes (Mercado *et al.* 2018). Our tropical photosynthesis meta-analysis showed that, that for most temperature response parameters, mean annual temperature was the single best explanatory factor describing photosynthetic temperature responses to climate. Additionally, the optimum temperature of net photosynthesis (T_{opt}) response to mean annual temperature was similar to global trends (Kumarathunge *et al.* 2019), suggesting that carbon models that use single global algorithms are likely to represent tropical net photosynthetic thermal responses with some degree of accuracy. Compared to global trends (Kumarathunge *et al.* 2019), the optimum temperatures of the biochemical components of photosynthesis, particularly for

maximum Rubisco carboxylase (V_{cmax}), did not rise as rapidly in response to increasing growth temperature. This has important implications for modeling, as global vegetation models often use the biochemical optimum temperatures instead of net photosynthesis. Global models that assume similar temperature response trends across biomes could be misrepresenting global carbon fluxes. This study also revealed that data describing tropical photosynthesis for different light environments, growth environments (*in*/*ex situ*), functional types, and successional strategies is severely lacking. There is a strong need to measure temperature responses in a range of different environments and functional types to more accurately model tropical photosynthetic responses to temperature.

Tropical forests experience a very narrow range in temperature, which may cause them to be less able to acclimate to climate warming than ecosystems that experience a wider diurnal, seasonal, and inter-annual range (Janzen 1967; Cunningham and Read 2003). Tropical species' respiration has been shown to acclimate to experimental warming conducted in growth chambers (Smith and Dukes 2017), large outdoor chambers (Slot and Winter 2018) and within a mature forest canopy (Slot *et al.* 2014). More recent studies on seedlings have shown that tropical species can acclimate photosynthetically to warming temperatures (Slot and Winter 2017; Smith and Dukes 2017), providing contrasting evidence to more traditional theory on tropical species thermal acclimation. Contrary to what most studies have found regarding respiratory acclimation, we only found respiratory acclimation in one of the four species that were experimentally warmed. In our understory warming experiment, only one species had a positive correlation between T_{opt} of net photosynthesis and vegetation temperature.

Furthermore, neither of our canopy species showed evidence of net photosynthetic acclimation. Our results suggest that growth chamber studies on tropical seedlings may not accurately represent how mature plants respond to warming.

Another main finding of this dissertation was that soil moisture, more so than temperature, played a large role in controlling both photosynthesis and respiration response to temperature in our understory warming experiment. Both T_{opt} and the photosynthetic thermal niche increased as soils dried; however, both the rate of photosynthesis and stomatal conductance at the optimum temperature declined with drying soils. These results reinforce the idea that climate induced changes in soil moisture could have large effects on ecosystem carbon balance (Ciais *et al.* 2005; Phillips *et al.* 2009; Sherwood and Fu 2014). Our results are similar to another recent study on temperate and boreal species, which found that plant responses to experimental warming was dependent on soil moisture (Reich *et al.* 2018). Taken together, these studies provide evidence that soil moisture should be considered alongside temperature effects in large-scale warming experiments.

Finally, our canopy study revealed that, for our two study species, upper canopy leaves are approaching or have already surpassed their physiological thermal thresholds. Both of our study species' experienced maximum temperatures above their photosynthetic optimum and *Ocotea sintensii*'s mean temperatures were similar to their optimum temperatures. Other studies at the leaf (Mau *et al.* 2018), canopy (Doughty and Goulden 2008), and ecosystem level (Huang *et al.* 2019) have shown similar results. The proximity to leaf thermal thresholds combined with the lack of photosynthetic

acclimation in our canopy leaves further support for accumulating evidence that tropical forest upper canopies are particularly vulnerable to adverse effects due to climate warming.

5.1 References

Booth BBB, Jones CD, Collins M, *et al.* 2012. High sensitivity of future global warming to land carbon cycle processes. *Environmental Research Letters* **7**: 024002.

Cavaleri MA, Reed SC, Smith WK, Wood TE. **2015**. Urgent need for warming experiments in tropical forests. *Global Change Biology* **21**: 2111–2121.

Ciais P, Reichstein M, Viovy N, *et al.* 2005. Europe-wide reduction in primary productivity caused by the heat and drought in 2003. *Nature* **437**: 529–533.

Cunningham SC, Read J. **2003**. Do temperate rainforest trees have a greater ability to acclimate to changing temperatures than tropical rainforest trees? *New Phytologist* **157**: 55–64.

Dixon RK, Brown S, Houghton RA, Solomon AM, Trexler MC, Wisniewski J. **1994**. Carbon pools and flux of global forest ecosystems. *Science* **263**: 185–190.

Doughty CE, Goulden ML. **2008**. Are tropical forests near a high temperature threshold? *Journal of Geophysical Research: Biogeosciences* **114**: 1–12.

Friedlingstein P, Cox P, Betts R, *et al.* 2006. Climate-carbon cycle feedback analysis: Results from the C4MIP model intercomparison. *Journal of Climate* **19**: 3337–3353.

Huang M, Piao S, Ciais P, *et al.* 2019. Air temperature optima of vegetation

productivity across global biomes. *Nature Ecology and Evolution* **3**: 772–779.

Janzen DH. **1967**. Why Mountain Passes are Higher in the Tropics. *The American Naturalist* **101**: 233–249.

Kattge J, Knorr W. **2007**. Temperature acclimation in a biochemical model of photosynthesis: A reanalysis of data from 36 species. *Plant, Cell and Environment* **30**: 1176–1190.

Kumarathunge DP, Medlyn BE, Drake JE, *et al.* 2019. Acclimation and adaptation components of the temperature dependence of plant photosynthesis at the global scale. *New Phytologist* **222**: 768–784.

Lombardozzi DL, Bonan GB, Smith NG, Dukes JS, Fisher RA. **2015**. Temperature acclimation of photosynthesis and respiration: A key uncertainty in the carbon cycle-climate feedback. *Geophysical Research Letters* **42**: 8624–8631.

Mau A, Reed S, Wood T, Cavaleri M. **2018**. Temperate and tropical forest canopies are already functioning beyond their thermal thresholds for photosynthesis. *Forests* **9**: 47.

Medlyn BE, Dreyer E, Ellsworth D, *et al.* 2002. Temperature response of parameters of a biochemically based model of photosynthesis. II. A review of experimental data. *Plant, Cell and Environment* **25**: 1167–1179.

Mercado LM, Medlyn BE, Huntingford C, *et al.* 2018. Large sensitivity in land carbon storage due to geographical and temporal variation in the thermal response of photosynthetic capacity. *New Phytologist* **218**: 1462–1477.

Pan Y, Birdsey RA, Phillips OL, Jackson RB. **2013**. The Structure, Distribution, and Biomass of the World's Forests. *Annual Review of Ecology, Evolution, and Systematics* **44**: 593–622.

Phillips OL, Lewis SL, Lloyd J, *et al.* 2009. Drought sensitivity of the amazon rainforest. *Science* **323**: 1344–1347.

Reich PB, Sendall KM, Stefanski A, Rich RL, Hobbie SE, Montgomery RA. **2018**. Effects of climate warming on photosynthesis in boreal tree species depend on soil moisture. *Nature* **562**: 263–267.

Rogers A. **2016**. Viewpoints A roadmap for improving the representation of photosynthesis in Earth system models. *New Phytologist*: 22–42.

Sherwood S, Fu Q. **2014**. A drier future? *Science* **343**: 737–739.

Slot M, Rey-Sánchez C, Gerber S, Lichstein JW, Winter K, Kitajima K. **2014**. Thermal acclimation of leaf respiration of tropical trees and lianas: Response to experimental canopy warming, and consequences for tropical forest carbon balance. *Global Change Biology* **20**: 2915–2926.

Slot M, Winter K. **2017**. Photosynthetic acclimation to warming in tropical forest tree seedlings. *Journal of Experimental Botany* **68**: 2275–2284.

Slot M, Winter K. **2018**. High tolerance of tropical sapling growth and gas exchange to moderate warming. *Functional Ecology* **32**: 599–611.

Smith NG, Dukes JS. **2017**. Short-term acclimation to warmer temperatures accelerates leaf carbon exchange processes across plant types. *Global Change Biology*: 4840–4853.

A Appendix A - Chapter 3 Supplementary material

Ch. 3 Supplemental methods

Supplemental Methods A1 Extraction of parameters from net photosynthetic and stomatal conductance responses to temperature.

Extraction of parameters from net photosynthetic and stomatal conductance responses to temperature. g_{s_Opt} was extracted by fitting linear regressions to each g_s - temperature responses and extracting the rate of g_s at the photosynthetic optimum temperatures. Before g_{s_Opt} was extracted, g_s > 3 standard deviations away from the mean were determined to be outliers outside the range of instrumental error and were removed. Stomatal conductance parameters were extracted from the same curves as net photosynthesis, using the LI6400XT (Li-COR Inc.).

For each net photosynthesis measurement, we also estimated the apparent maximum rate of Rubisco carboxylation ($\hat{V}_{cmax}$) using the 'one-point method' (De Kauwe *et al.*, 2016*a*,*b*). We used constants from Bernacchi *et al.* (2001) estimation of Michalis constants for CO_2 and O_2 temperature dependencies and the CO_2 compensation point (Γ*) to calculate $\hat{V}_{cmax}$. We assumed a respiration rate of 1.5% of $\hat{V}_{cmax}$. $T_{\hat{V}opt}$ was extracted by fitting the $\hat{V}_{cmax}$ vs. temperature response curves to a peaked Arrhenius function (Medlyn *et al.*, 2002):

$$(T_k) = \left(k_{opt}\right) \frac{H_d \exp\left(\frac{H_a\left(T_k - T_{opt}\right)}{\left(T_k \mathrm{R} T_{opt}\right)}\right)}{H_d - H_a\left|1 - \exp\left(\frac{H_d\left(T_k - T_{opt}\right)}{\left(T_k \mathrm{R} T_{opt}\right)}\right)\right|} \qquad \text{Equation (A1)}$$

where T_k is the measured leaf temperature in Kelvin, (k_{opt}) is the value of $\hat{V}_{cmax}$ at the optimum temperature (μmol m^{-2} s^{-1}), H_a is the activation energy, or exponential increase,

in an Arrhenius function (kJ mol^{-1}), H_d is the decrease in $\hat{V}_{cmax}$ after $T_{\hat{V}opt}$ (kJ mol^{-1}), and R is the universal gas constant (8.314 $JK^{-1}mol^{-1}$). The 'one-point method' uses internal CO_2 concentration to calculate $\hat{V}_{cmax}$; therefore, we removed all data points that had internal CO_2 concentration less than 100 ppm and greater than 500 ppm, which resulted in the removal of 12 out of 1025 data points.

Supplemental Methods A2 Extraction of V_{cmax} and J_{max} temperature response parameters.

V_{cmax} and J_{max} were extracted from the net assimilation rate (A_{net}) response to internal CO_2 concentration (C_i) using the 'Ecophys' package (Duursma, 2015) in R version 3.5.0 (R Core Team, 2018), which implements the Farquhar, von Caemmerer, and Berry model (Farquhar *et al.*, 1980; von Caemmerer and Farquhar, 1981). Optimum temperatures of J_{max} (T_{Jopt}) and V_{cmax} (T_{Vopt}) were extracted by fitting the J_{max} and V_{cmax} vs. temperature response curves to Equation (A1) and replacing k_{opt} with J_{max} and V_{cmax}. Equation (A1) was fit to all measurements made within a single plot in each measurement campaign individually. V_{cmax} and J_{max} parameters were successfully extracted for two control and three heated plots; therefore, control plot gain scores were analyzed only with Student's t-tests using two of the three control plots.

References

Bernacchi CJ, Singsaas EL, Pimentel C, Portis AR, Long SP. **2001**. Improved temperature response functions for models of Rubisco-limited photosynthesis. *Plant, Cell and Environment* **24**: 253–259.

von Caemmerer S, Farquhar GD. **1981**. Some relationships between the biochemistry of photosynthesis and the gas exchange of leaves. *Planta* **153**: 376–387.

Duursma RA. **2015**. Plantecophys - An R Package for Analysing and Modelling Leaf Gas Exchange Data. *PLoS ONE* **10**: e0143346.

Farquhar GD, Caemmerer S Von, Berry JA. 1980. A biochemical model of photosynthesis CO2 fixation in leaves of C3 species. *Planta* **149**: 78–90.

De Kauwe MG, Lin YS, Wright IJ, Medlyn BE, Crous KY, Ellsworth DS, Maire V, Prentice IC, Atkin OK, Rogers A, *et al.* 2016a. A test of the 'one-point method' for estimating maximum carboxylation capacity from field-measured, light-saturated photosynthesis. *New Phytologist* **210**:1130-1144.

De Kauwe MG, Lin YS, Wright IJ, Medlyn BE, Crous KY, Ellsworth DS, Maire V, Prentice IC, Atkin OK, Rogers A, *et al.* 2016b. Corrigendum. *New Phytologist* **210**: 1130–1144.

Medlyn BE, Dreyer E, Ellsworth D, Forstreuter M, Harley PC, Kirschbaum MUF, Le Roux X, Montpied P, Strassemeyer J, Walcroft A, *et al.* 2002. Temperature response of parameters of a biochemically based model of photosynthesis. II. A review of experimental data. *Plant, Cell and Environment* **25**: 1167–1179.

Chapter 3 Supplemental Figures

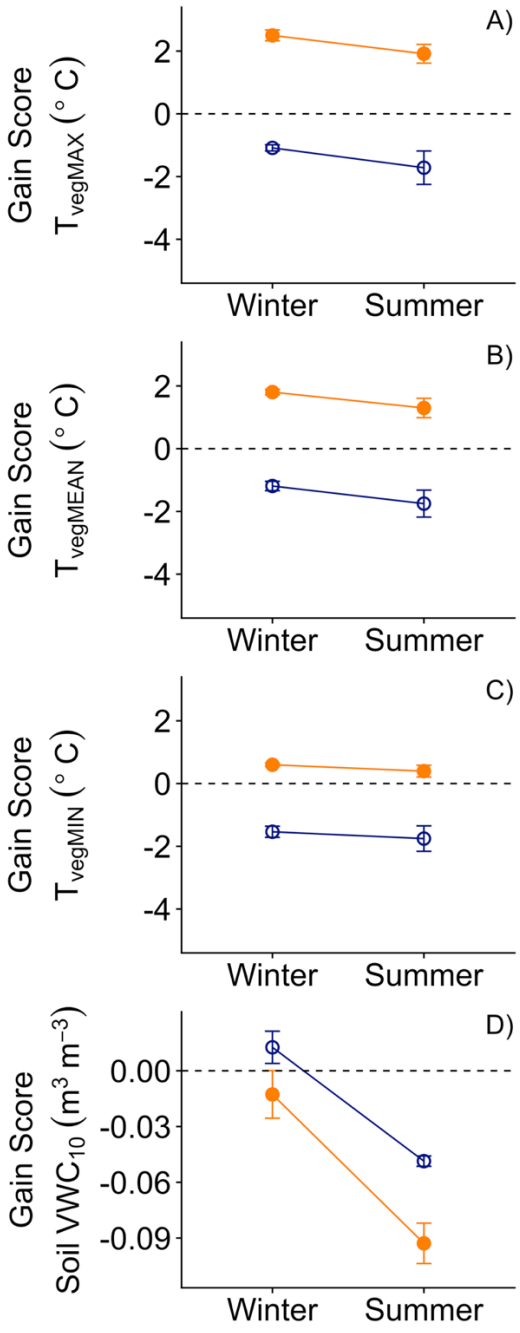

Fig. A1 Gain score analysis for heated and control plot vegetation temperature and soil moisture. **A)** Mean daily maximum (T_{vegMAX}), **B)** mean daily ($T_{vegMEAN}$), and **C)** mean daily minimum (T_{vegMIN}) vegetation temperature (°C) gain scores for of the heated

(orange filled) and control (dark blue open) plots during the winter and summer seasons. **D)** Mean soil moisture ($m^3\ m^{-3}$) gain scores at 10 cm depth (VWC_{10}) for the heated and control plots during both seasons. All vegetation temperature and soil moisture analyses showed a significant treatment effect between heated and control plots (Table A2.2).

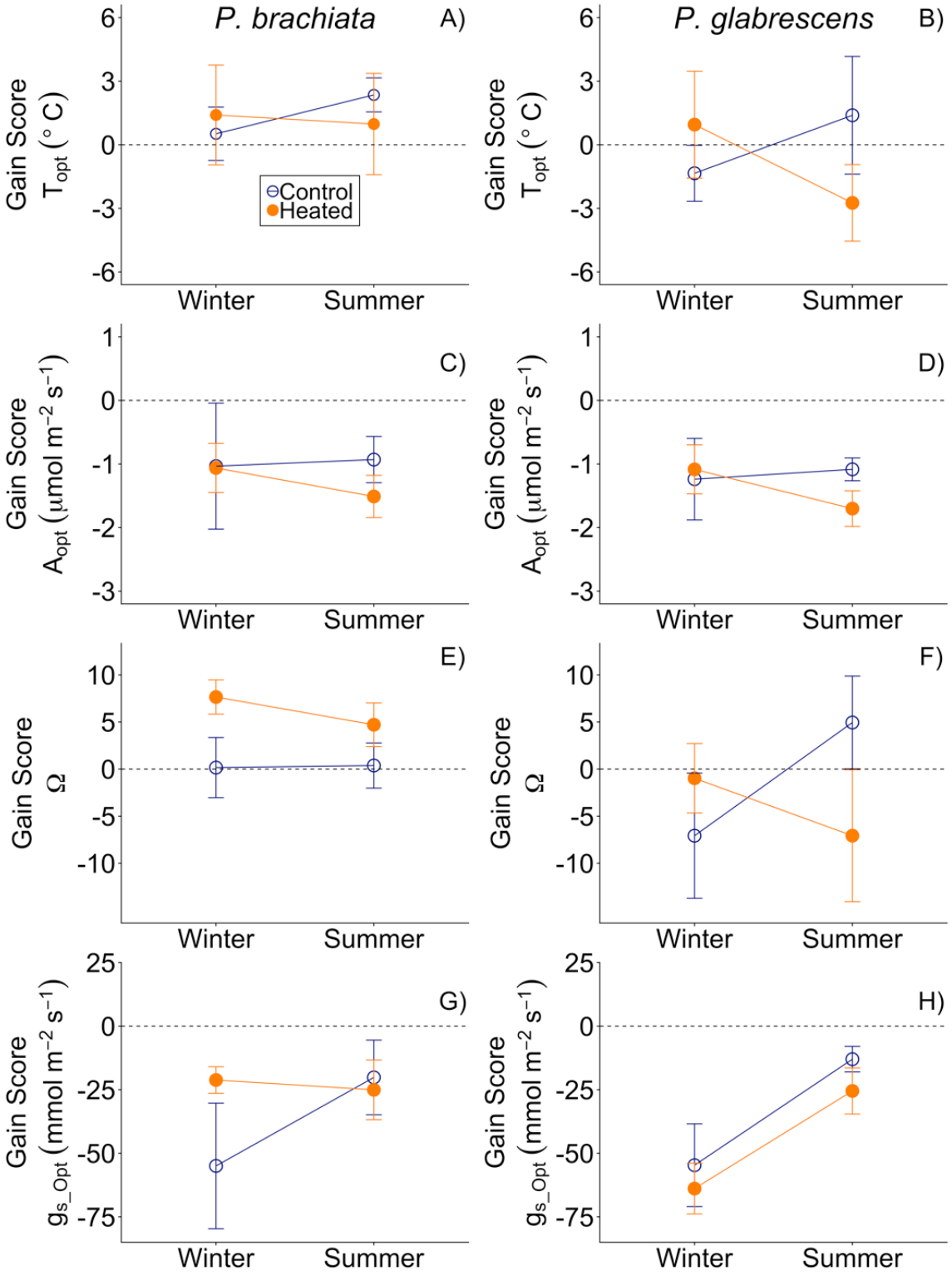
P. brachiata
A)
P. glabrescens
B)
Gain Score
T_{opt} (° C)
Control
Heated
Winter
Summer
C)
D)
Gain Score
A_{opt} (µmol m^{-2} s^{-1})
E)
F)
Gain Score
Ω
G)
H)
Gain Score
g_{s_Opt} (mmol m^{-2} s^{-1})

Fig. A2 Photosynthetic parameter gain scores between pretreatment and post- treatment measurements. Gain scores are shown for **A)** *Psychotria brachiata* optimum temperature for photosynthesis (T_{opt}) for the control (dark blue open) and heated (orange closed) plots, **B)** *Piper glabrescens* T_{opt}, **C)** *P. brachiata* photosynthetic rate at T_{opt} (A_{opt}), **D)** *P. glabrescens* A_{opt}, **E)** *P. brachiata* photosynthetic thermal niche (Ω), **F)** *P. glabrescens* Ω, **G)** *P. brachiata* rate of stomatal conductance at T_{opt} (g_{s_Opt}), and **H)** *P. glabrescens* g_{s_Opt}. Gain scores were calculated as post treatment – pretreatment for each plot per campaign individually. The only significant treatment effect was for *P. brachiata* Ω ($p = 0.044$; Table 2.2).

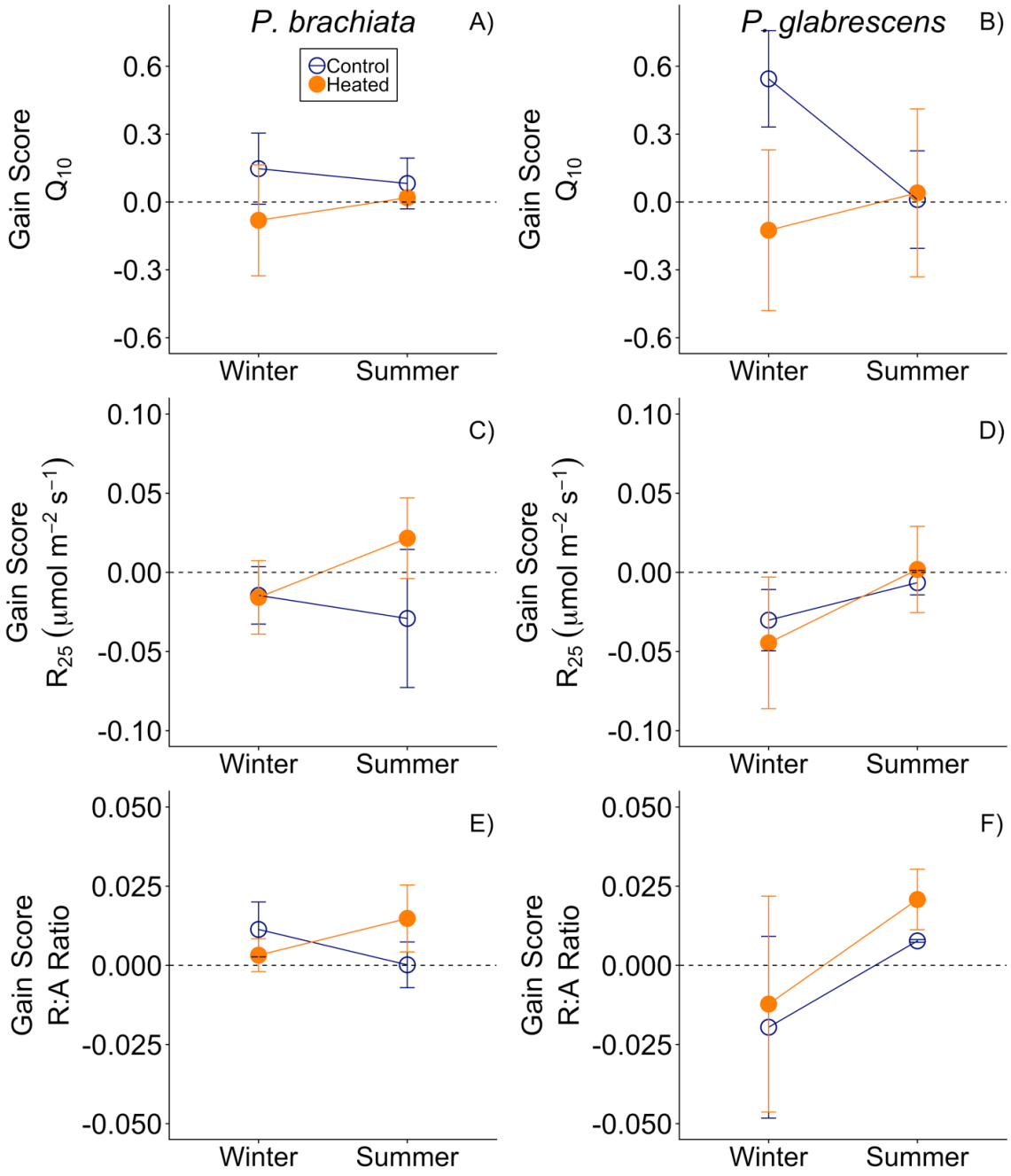

Fig. A3 Dark respiration parameter gain scores between pretreatment and post- treatment measurements. Gain scores are shown for **A)** *Psychotria brachiata* increase in respiration for every 10 ºC (Q_{10}) for the control (dark blue open) and heated (orange closed) plots, **B)** *Piper glabrescens* Q_{10}, **C)** *P. brachiata* rate of leaf dark respiration at 25 ºC (R_{25}), **D)** *P. glabrescens* R_{25}, **E)** *P. brachiata* ratio between respiration and photosynthesis (*R:A* ratio),

F) *P. glabrescens R:A* ratio. Gain scores were calculated as post treatment – pretreatment for each plot per campaign individually. There were no significant treatment or treatment interactions for any respiration parameters (Table 2).

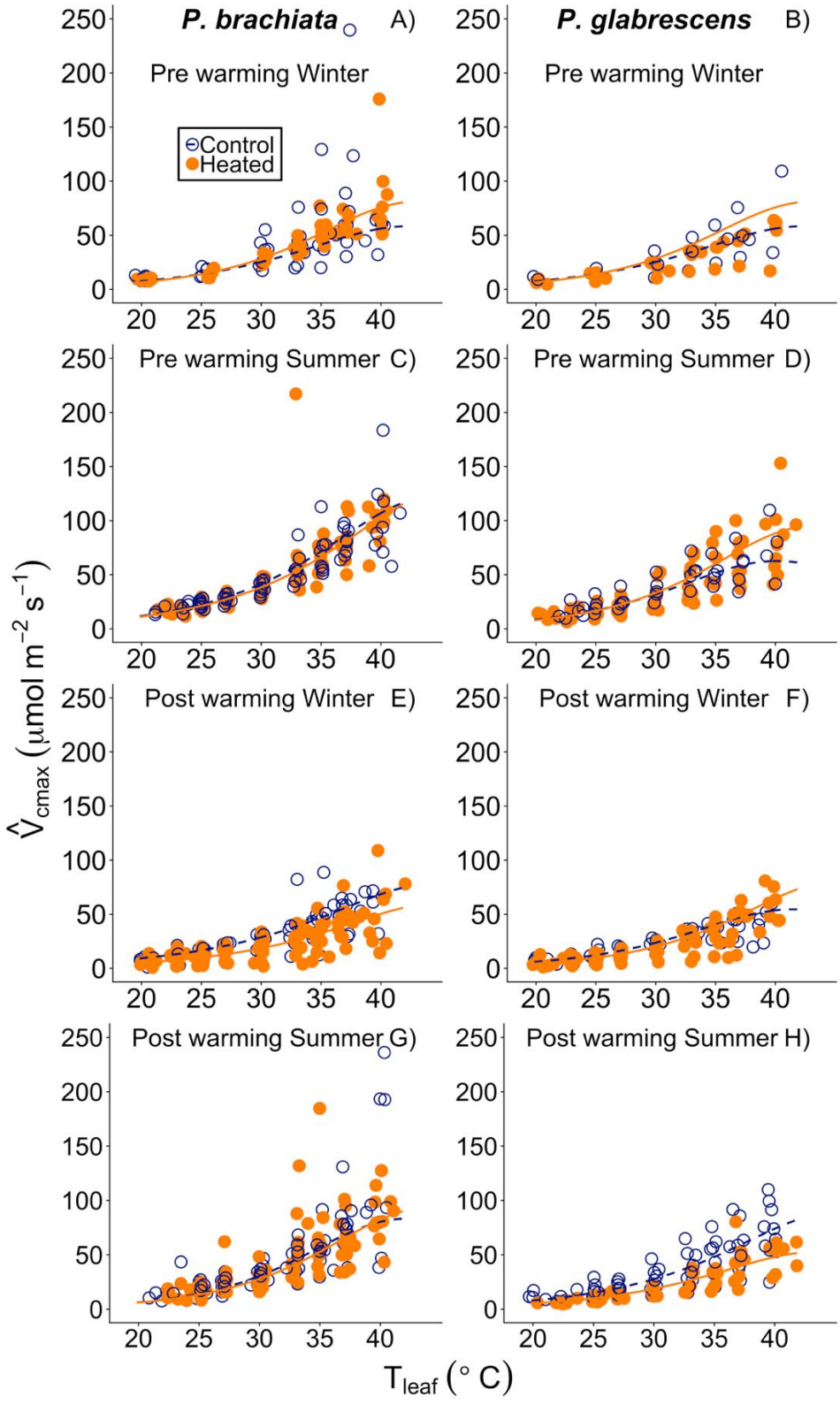
P. brachiata
A)
P. glabrescens
B)
Pre warming Winter
Control
Heated
Pre warming Summer C)
Pre warming Summer D)
Post warming Winter E)
Post warming Winter F)
Post warming Summer G)
Post warming Summer H)
$\hat{V}_{cmax}$ (μmol m^{-2} s^{-1})
T_{leaf} (° C)

Figure A4 Apparent maximum rate of Rubisco carboxylation ($\hat{V}_{cmax}$) response to leaf temperature (T_{leaf}). $\hat{V}_{cmax}$ response to temperature was plotted separately for each measurement campaign and species separately: **A)** *Psychotria brachiata* pre-warming winter season for control (dark blue open) points and heated (orange closed) leaf measurements,, **B)** *Piper glabrescens* pre-warming winter season, **C)** *P. brachiata* pre-warming summer season, **D)** *P. glabrescens* pre-warming summer season, **E)** *P. brachiata* 4 months post-warming winter season, **F)** *P. glabrescens* 4 months post-warming winter season, **G)** *P. brachiata* 8 months post-warming summer season, **H)** *P. glabrescens* 8 months post-warming summer season. Lines are fit to each temperature response using the Medlyn *et al.* (2002) method (Equation A1) for control (dark blue; dashed) and heated (orange; solid) separately.

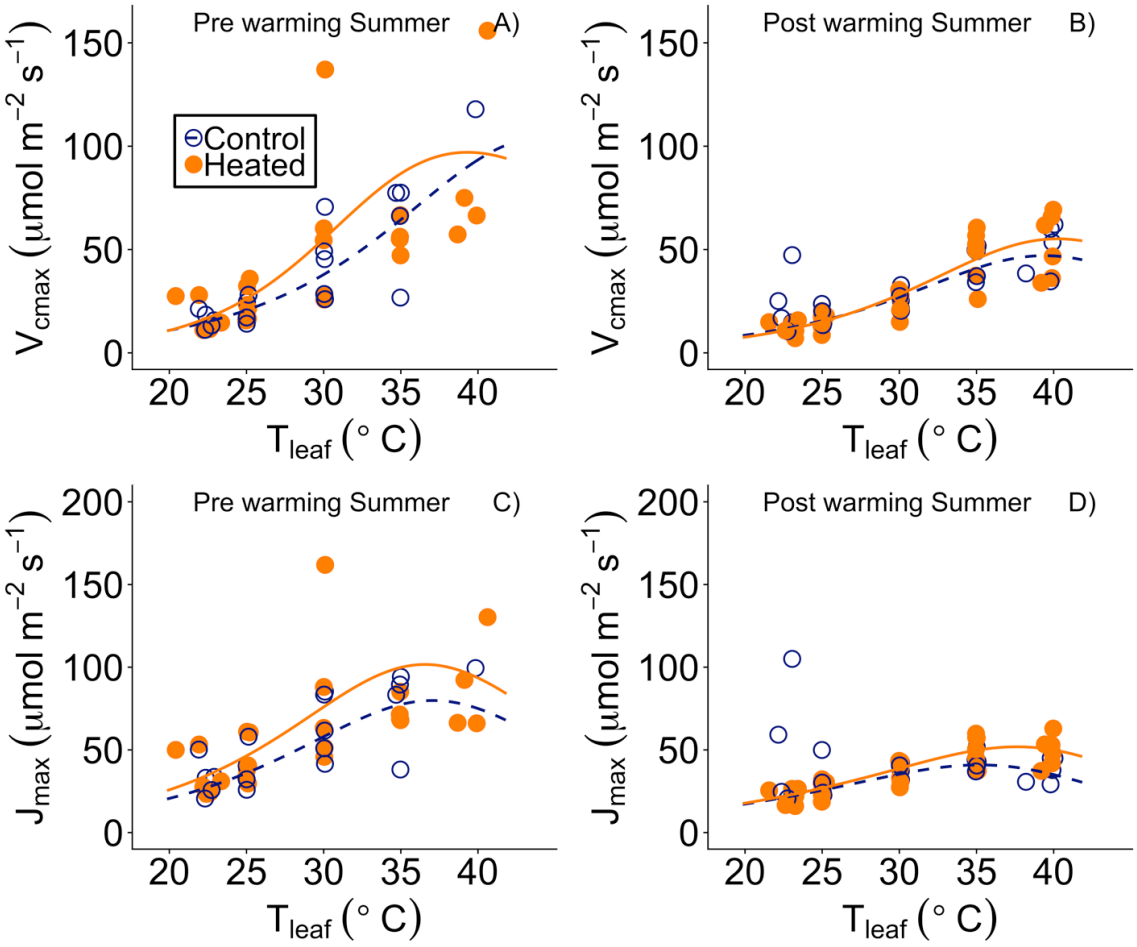

Figure A5 Biochemical parameter responses to leaf temperature (T_{leaf}). Parameter response to temperature was plotted separately for each measurement campaign separately for *Psychotria brachiata* summer season only: **A)** V_{cmax} pre-warming summer season for control (dark blue open) points and heated (orange closed) leaf measurements, **B)** V_{cmax} 9 months post-warming summer season, **C)** J_{max} pre-warming summer season, **D)** J_{max} 9 months post-warming summer season. Lines are fit to each temperature response using the Medlyn *et al.* (2002) method (Equation S1) for control (dark blue; dashed) and heated (orange; solid) separately.

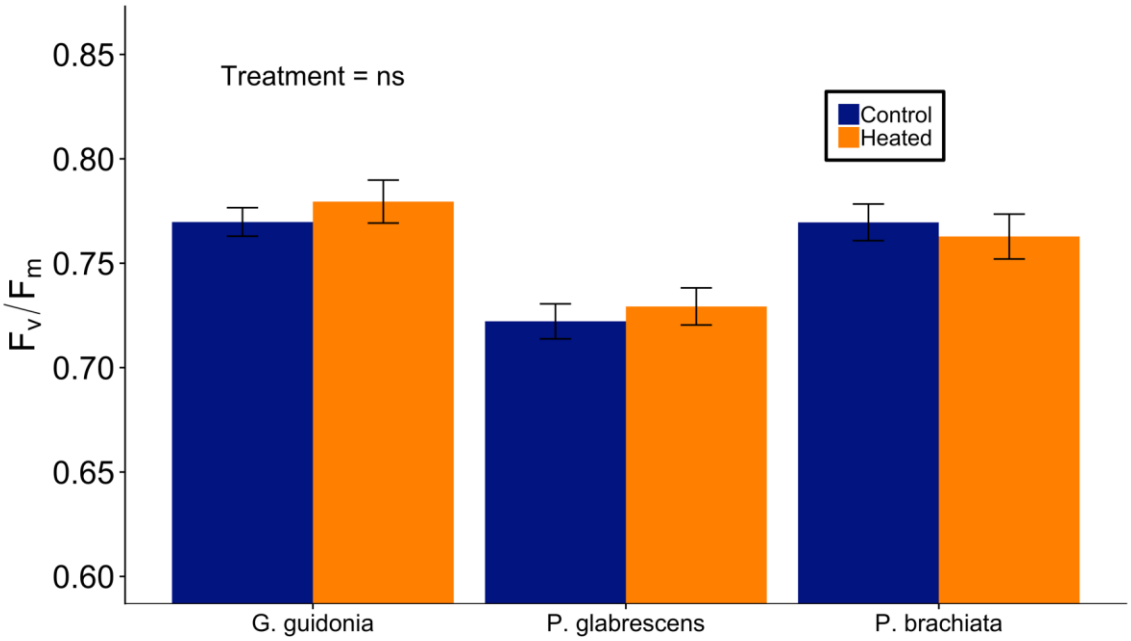

Fig. A6 Dark-adapted maximum chlorophyll fluorescence yield (*Fv/Fm*) for the three most common shrub/tree species found within the experimental plots. There were no significant treatment differences between control (dark blue) and heated (orange) *Fv/Fm* for *Guarea guidonia*, *Piper glabrescens*, and *Psychotria brachiata*. Error bars represent ± SEM.

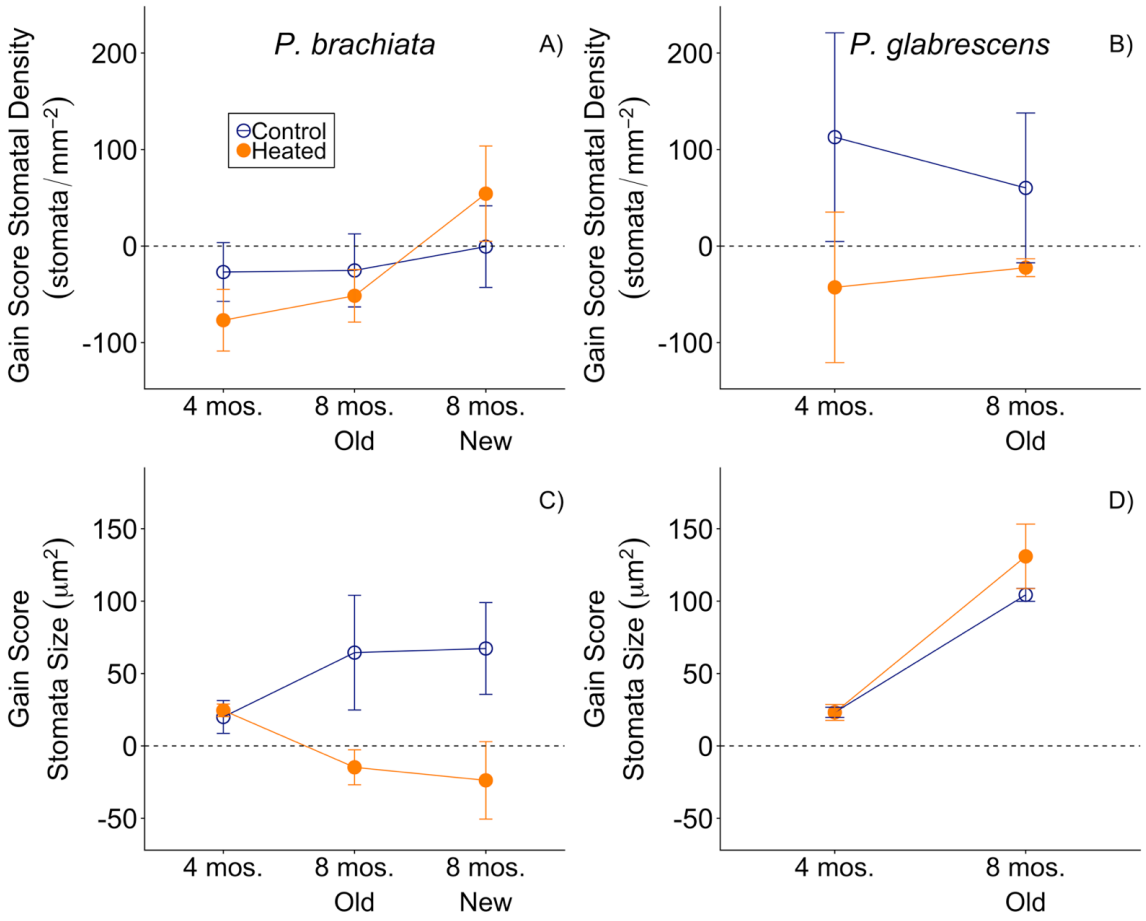

Fig. A7. Stomatal morphology trait gain scores between pretreatment and post- treatment measurements. Gain scores are shown for **A)** *Psychotria brachiata* stomatal density for the control (dark blue open) and heated (orange closed) plots, **B)** *Piper glabrescens* stomatal density, **C)** *P. brachiata* stomatal size, and **D)** *P. glabrescens* stomatal size. P. brachiata stomatal morphology measurements were made after four and eight months of warming, where eight-month measurements were made on "Old" fully developed leaves and "New" fully expanded but not fully developed leaves. P. glabrescens stomatal morphology was measured after four and eight (Old) months of warming. The mean of each plot of each stomatal morphology measurement campaign (Fig. 2.2) was determined and the gain score was calculated as post treatment – pretreatment for each plot per post warming campaign individually. Data collected during August 2016 were used as the pretreatment mean. The ANOVA showed a significant treatment effect for *P. brachiata* stomatal size ($p = 0.017$; Table 2.4).

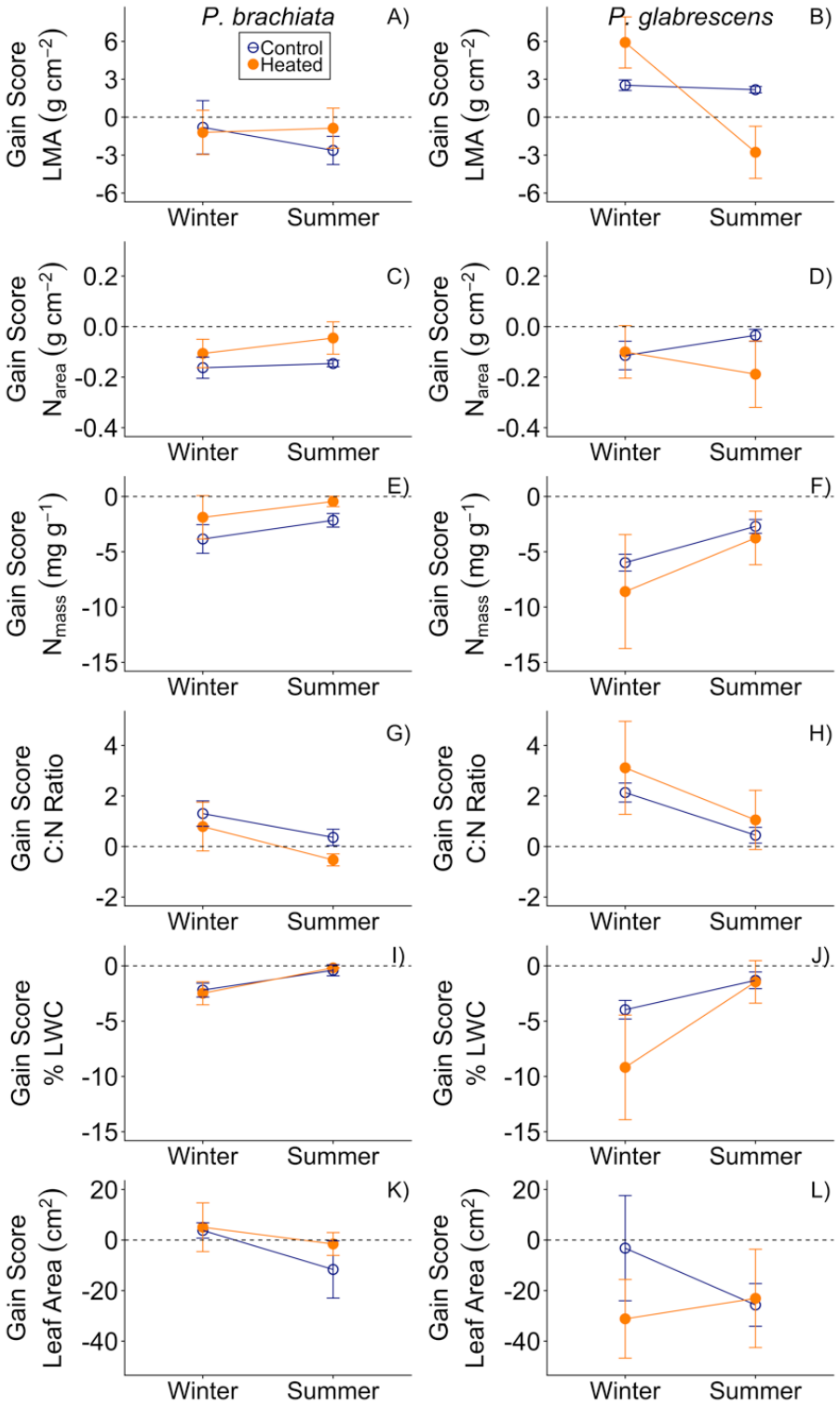

Fig. A8 Leaf trait gain scores between pretreatment and post- treatment measurements. Gain scores are shown for **A)** *Psychotria brachiata* leaf mass per area (*LMA*) for the

control (dark blue open) and heated (orange closed) plots, **B)** *Piper glabrescens LMA*, **C)** *P. brachiata* nitrogen on an area basis (N_{area}), **D)** *P. glabrescens* N_{area}, **E)** *P. brachiata* nitrogen on a mass basis (N_{mass}), **F)** *P. glabrescens* N_{mass}, **G)** *P. brachiata* carbon to nitrogen ratio (C:N), and **H)** *P. glabrescens* C:N ratio, **I)** *P. brachiata* percent leaf water content (% LWC), and **J)** *P. glabrescens* % LWC, **K)** *P. brachiata* leaf area, and **L)** *P. glabrescens* leaf area. The mean of each plot in each measurement campaign was determined and the gain score was calculated as post treatment – pretreatment for each plot per campaign individually. The ANOVA analysis showed a significant treatment × season interaction for *P. glabrescens* LMA ($p = 0.068$; Table 2.4).

Ch. 3 Supplemental Tables

Table A1 Mean daily vegetation temperature ($T_{vegMEAN}$) of the control plots, mean, minimum, and maximum daily air temperature (T_{air}) and rainfall during each measurement campaign.

Pre/Post Warming	Season	n	Control $T_{vegMEAN}$ (ºC)	n	Mean daily T_{air} (ºC)	Min daily T_{air} (ºC)	Max daily T_{air} (ºC)	Mean daily rainfall (mm)
Pre-warming	Winter	12	21.93 ± 0.16	12	22.42 ± 0.17	20.45 ± 0.25	25.30 ± 0.17	1.10 ± 0.48
	Summer	19	25.27 ± 0.14	19	25.98 ± 0.19	23.98 ± 0.19	28.64 ± 0.27	7.04 ± 1.94
Post-warming	Winter	18	20.73 ± 0.21	17	21.54 ± 0.26	21.54 ± 0.26	21.54 ± 0.26	1.83 ± 0.80
	Summer	27	23.51 ± 0.10	25	24.98 ± 0.14	22.71 ± 0.17	28.03 ± 0.26	5.95 ± 1.43

Averages (mean ± SE) are averaged only of the days during the measurement campaigns, except for post warming T_{air}, where values were not available post-warming for one day during the winter season and two days during the summer season (Fig. 2.2A,B).

Table A2 P-values and degrees of freedom from ANOVA results of gain score of vegetation temperature and soil moisture.

	df	T_{vegMAX}	$T_{vegMEAN}$	T_{vegMIN}	VWC_{10}
Treatment	1,8	**<0.001**	**<0.001**	**<0.001**	**0.007**
Season	1,8	0.410	**0.092**	**0.092**	**<0.001**
Treatment × Season	1,8	0.978	0.922	0.944	0.351

Variables were pooled by individual plots and gain scores were calculated as individual variable post treatment - pretreatment. Variables listed are the mean daily maximum vegetation temperature (°C) (T_{vegMAX}), mean daily vegetation temperature (°C) ($T_{vegMEAN}$), mean minimum daily vegetation temperature (°C) (T_{vegMIN}), and soil volumetric water content (m^3 m^{-3}) at 10 cm depth (VWC_{10}). Bolded p-values denote a significance ($p < 0.1$). df shows the degree of freedom for the effect and residuals of the ANOVA. In instances where the heaters in a particular plot were malfunctioning, data were removed.

Table A3 Mean daily maximum vegetation temperature (T_{vegMAX}) and the optimum temperature for photosynthesis (T_{opt}) of the heated and control plots for each species.

Pre/Post Warming	Season	Treatment	n	T_{vegMAX} (ºC)	n	*Psychotria brachiata* T_{opt} (ºC)	n	*Piper glabrescens* T_{opt} (ºC)
Pre-warming	Winter	Control	12	24.07 ± 0.14	8	28.2 ± 0.5	3	33.4 ± 1.2
		Heated	12	24.64 ± 0.14	8	31.2 ± 1.2	5	33.3 ± 1.3
	Summer	Control	19	27.97 ± 0.24	9	28.8 ± 0.8	5	31.2 ± 0.8
		Heated	19	27.91 ± 0.17	10	32.0 ± 1.2	9	33.6 ± 1.6
Post warming	Winter	Control	18	23.04 ± 0.18	9	28.8 ± 1.2	6	32.0 ± 0.9
		Heated	18	26.84 ± 0.17	9	33.1 ± 1.6	8	33.6 ± 1.1
	Summer	Control	27	25.04 ± 0.18	10	31.1 ± 1.5	9	32.4 ± 1.3
		Heated	27	29.34 ± 0.22	11	33.6 ± 1.6	6	32.7 ± 1.8

Averages (mean ± SE) are averaged only of the days during the measurement campaigns for T_{vegMAX}.

Table A4 Temperature response parameters estimated for the apparent maximum rate of Rubisco carboxylation ($\hat{V}_{cmax}$), maximum rate of Rubisco carboxylation (V_{cmax}), and the maximum rate of electron transport (J_{max}).

Species	Biochemical Parameter	*Season*	n	T_{opt} (ºC)	K_{opt} (μmol m^{-2} s^{-1})	H_a (kJ mol^{-1})	H_d (kJ mol^{-1})
Piper glabrescens	$\hat{V}_{cmax}$	Winter	7	43.03 ± 1.09	60.26 ± 7.04	112.92 ± 5.19	200
	$\hat{V}_{cmax}$	Summer	9	42.68 ± 1.08	74.94 ± 8.53	103.91 ± 6.19	200
Psychotria brachiata	$\hat{V}_{cmax}$	Winter	11	43.70 ± 0.66	69.34 ± 4.90	94.28 ± 3.33	200
	$\hat{V}_{cmax}$	Summer	12	44.19 ± 0.80	108.26 ± 9.06	105.56 ± 6.93	200
	V_{cmax}	Summer	10	40.53 ± 0.71	76.94 ± 12.89	106.31 ± 7.40	200
	J_{max}	Summer	10	36.80 ± 0.50	70.71 ± 11.12	74.02 ± 5.17	200

Parameter estimates (mean ± SE) are derived (Equation A1). Means of $\hat{V}_{cmax}$ parameters were estimated from individual A_{net} temperature response curves, averaged by plot separately by species for each measurement campaign, and then reported by season. Means were combined by season and not treatment because gain score analysis showed a significant seasonal effect and no treatment effect (Table 2.2). V_{cmax} and J_{max} were estimated by fitting Equation A1 to all curves from an individual plot together and then averaged, combining pre and post treatment plot averages. V_{cmax} and J_{max} was measured for the summer season only. T_{opt}, optimum temperature of the biochemical reaction; K_{opt}, rate of the biochemical reaction at the optimum temperature; H_a, activation energy of the biochemical-temperature response; H_d, deactivation energy of the biochemical-temperature response.

Table A5 Summary of ANCOVA results of gas exchange parameters responses to environmental variables. Gas exchange parameters are the optimum temperature of photosynthesis (T_{opt}; °C), the rate of photosynthesis at T_{opt} (A_{opt}; μmol m^{-2} s^{-1}), the rate of stomatal conductance at T_{opt} (g_{s_Opt}; mmol m^{-2} s^{-1}), the width of the photosynthetic – temperature response curve (Ω), the rate of respiration at 25 °C (R_{25}; μmol m^{-2} s^{-1}), and the change in respiration with every 10 °C (Q_{10}). Environmental variables are daily mean vegetation temperature ($T_{vegMEAN}$; °C), mean daily maximum vegetation temperature (T_{vegMAX}; °C), mean daily minimum vegetation temperature (T_{vegMIN}; °C), volumetric soil water content (VWC; m^3 m^{-3}) at 10-20 and 20-30 cm. Species is included as a categorical variable.

Environmental Variable		*df*	*Variable*	Species	*Variable* × Species	*adj* R^2	*P. glabrescens y-intercept*	*P. glabrescens slope*	*P. brachiata y-intercept*	*P. brachiata slope*
$T_{vegMEAN}$	T_{opt}	1,116	**0.014**	**0.002**	0.079	0.12	31.5 ± 5.62	0.06 ± 0.23	-14.95 ± 7.26	0.54 ± 0.30
	A_{opt}	1,116	0.163	**0.006**	0.085	0.07	4.73 ± 2.01	-0.04 ± 0.08	-3.81 ± 2.59	0.19 ± 0.11
	Ω	1,108	**0.004**	**0.015**	0.583	0.10	-2.20 ± 10.45	**1.06 ± 0.02**	4.43 ± 13.88	-0.32 ± 0.58
	g_{s_Opt}	1,116	0.271	0.436	0.150	0.01	0.17 ± 0.06	-0.004 ± 0.003	-0.10 ± 0.07	0.004 ± 0.003
	Q_{10}	1,106	0.610	**<0.001**	0.990	0.18	1.97 ± 0.59	0.004 ± 0.025	-0.29 ± 0.74	<0.000 ± 0.031
	R_{25}	1,106	0.124	**0.012**	0.546	0.05	0.21 ± 0.09	-0.01 ± 0.04	-0.45 ± 1.06	0.03 ± 0.42
T_{vegMAX}	T_{opt}	1,116	**0.008**	**0.002**	0.092	0.13	30.52 ± 5.99	0.10 ± 0.23	-15.04 ± 7.60	0.50 ± 0.29
	A_{opt}	1,116	0.231	**0.007**	0.230	0.06	4.36 ± 2.17	-0.02 ± 0.08	-2.64 ± 2.76	0.13 ± 0.11
	Ω	1,108	**0.002**	**0.013**	0.645	0.11	-3.76 ± 11.33	1.04 ± 0.44	3.34 ± 14.38	-0.26 ± 0.55
	g_{s_Opt}	1,116	0.203	0.419	0.156	0.01	0.19 ± 0.06	-0.005 ± 0.002	-0.10 ± 0.08	0.004 ± 0.002
T_{vegMIN}	Q_{10}	1,106	0.063	**<0.001**	0.700	0.21	1.40 ± 0.50	0.03 ± 0.02	-0.06 ± 0.62	-0.01 ± 0.02

	R_{25}	1,106	0.853	**0.010**	0.387	0.04	0.15 ± 0.08	-0.003 ± 0.004	-0.06 ± 0.10	0.004 ± 0.004
Soil *VWC*	T_{opt}	1,116	0.092	**0.006**	0.568	0.06	33.87 ± 2.31	-2.83 ± 7.03	-0.24 ± 3.10	-5.27 ± 9.19
10cm	A_{opt}	1,116	0.355	**0.007**	0.107	0.06	4.42 ± 0.81	-2.17 ± 2.45	-1.04 ± 1.08	5.21 ± 3.21
	Ω	1,108	0.979	**0.024**	0.793	0.02	21.40 ± 4.73	4.88 ± 14.17	-1.54 ± 6.16	-4.78 ± 18.18
	g_{s_Opt}	1,116	0.426	0.390	0.260	<0.01	0.10 ± 0.02	-0.10 ± 0.07	-0.03 ± 0.03	0.10 ± 0.09
	Q_{10}	1,106	0.733	**<0.001**	0.051	0.22	1.60 ± 0.21	**1.52 ± 0.69**	0.20 ± 0.26	-1.66 ± 0.84
	R_{25}	1,106	0.361	**0.011**	**0.015**	0.09	0.14 ± 0.03	0.18 ± 0.11	-0.07 ± 0.04	**0.32 ± 0.13**
Soil *VWC*	T_{opt}	1,92	**<0.001**	**0.016**	0.208	0.19	52.11 ± 10.37	-45.46 ± 24.49	15.59 ± 13.78	-41.36 ± 32.65
20cm	A_{opt}	1,92	0.053	**0.009**	0.985	0.08	-1.80 ± 4.01	13.00 ± 9.48	0.67 ± 5.34	0.24 ± 12.64
	Ω	1,84	**0.010**	**0.046**	0.767	0.09	56.63 ± 20.94	-78.61 ± 49.25	5.04 ± 27.39	-19.19 ± 64.69
	g_{s_Opt}	1,92	**0.030**	0.111	0.742	0.05	-0.11 ± 0.10	0.40 ± 0.23	0.05 ± 0.13	-0.10 ± 0.30
	Q_{10}	1,85	**0.030**	**<0.001**	0.309	0.28	0.75 ± 0.65	**3.18 ± 1.55**	0.53 ± 0.82	-2.00 ± 1.95
	R_{25}	1,85	**<0.001**	**<0.001**	0.389	0.29	-0.15 ± 0.09	**0.54 ± 0.22**	-0.07 ± 0.12	0.24 ± 0.28

ANCOVA degrees of freedom of the variable and residuals are listed in column three and p-values are listed in columns four through six. Bolded p-values indicates $p < 0.05$. Coefficients (± standard error) for each independent variable in the model are listed in the last four columns

Appendix B - Chapter 4 Supplementary Information

Ch. 4 Supplemental Figures

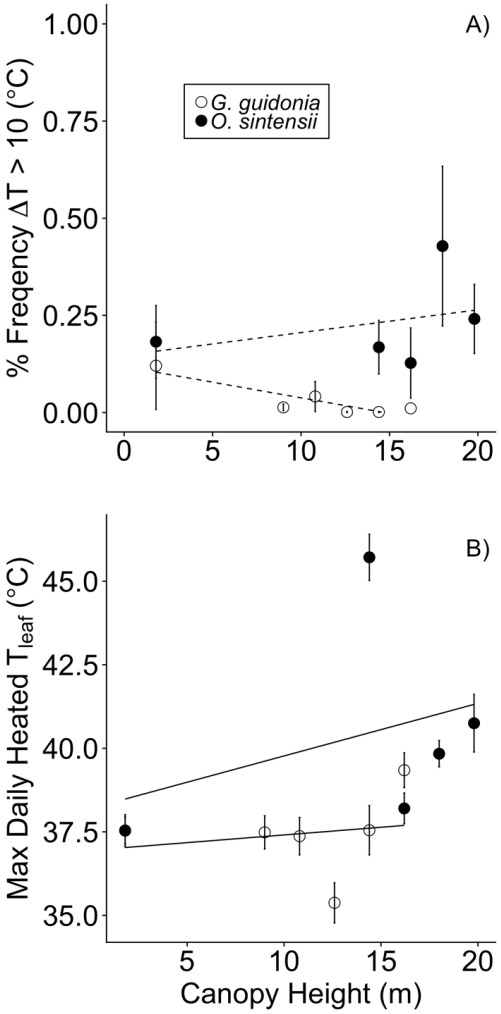

Fig. B1 Summary of heated leaf temperature spiking. **A)** The percent frequency of instances where the difference between the paired heated and control leaf was > 10 °C (ΔT > 10 °C) and **B)** maximum daily heated leaf temperature (T_{leaf}) for *Guarea guidonia* (open circles) and *Ocotea sintensii* (filled circles) throughout the canopy. Error bars denote SEM. Dashed lines represent a non-significant height effect. There were significant differences between species for both measures of temperature spiking (Table S1).

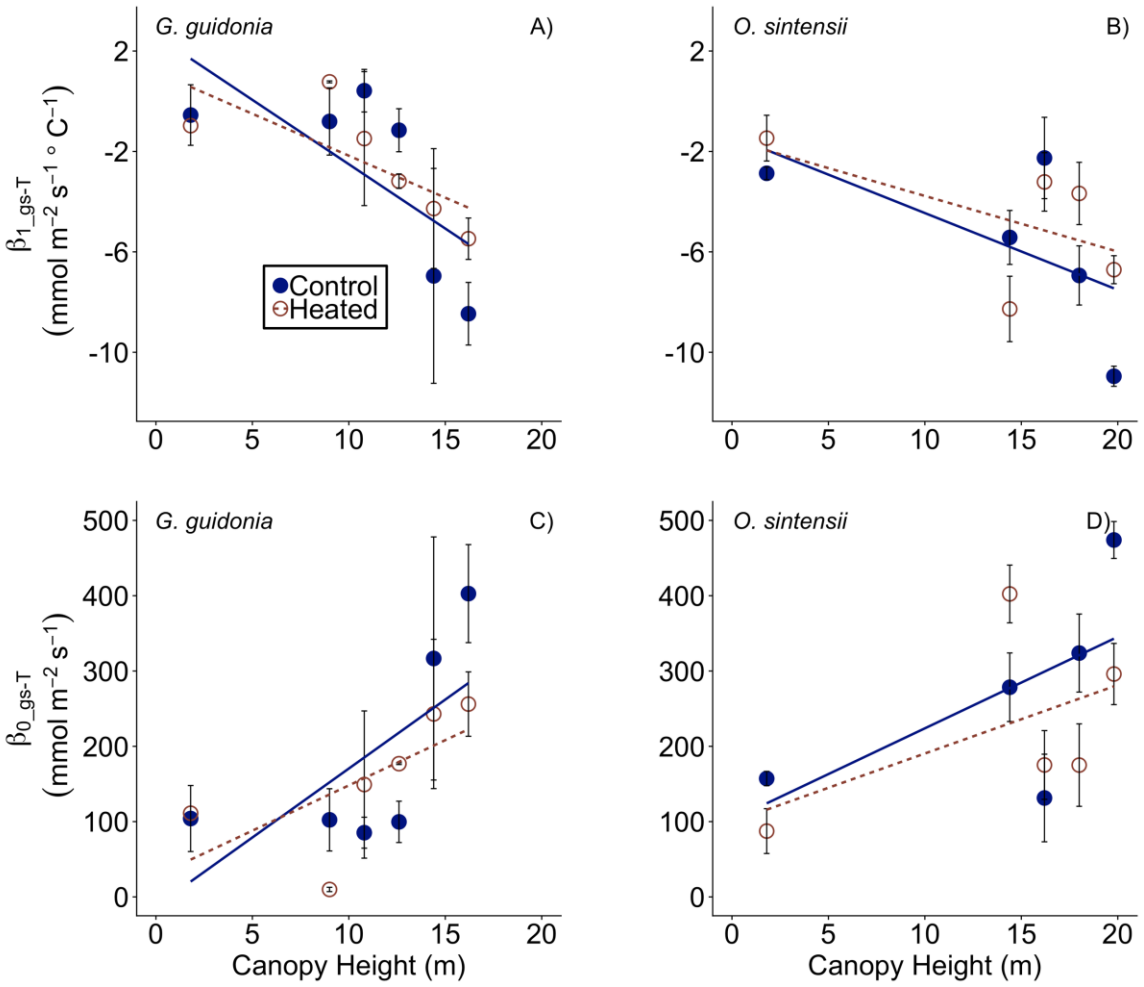

Fig. B2 Stomatal conductance (g_s) per leaf temperature (T_{leaf}) regression parameters response to canopy height. The slope of the g_s response to T_{leaf} ($\beta_{1\_gs\text{-}T}$) regression response to canopy height of heated (red filled) and control (blue empty) leaves for **A)** *Guarea guidonia* and **B)** *Ocotea sintensii*. The intercept of the g_s response to T_{leaf} ($\beta_{0\_gs\text{-}T}$) regression response to canopy height for **C)** *G. guidonia* and **D)** *O. sintensii*. Slopes and intercepts were extracted for each sample individually. There were no treatment effects; however, the slope of the g_s - T_{leaf} response decreased with increasing canopy height, while the intercept of the g_s - T_{leaf} response increased with rising canopy height (Table 1).

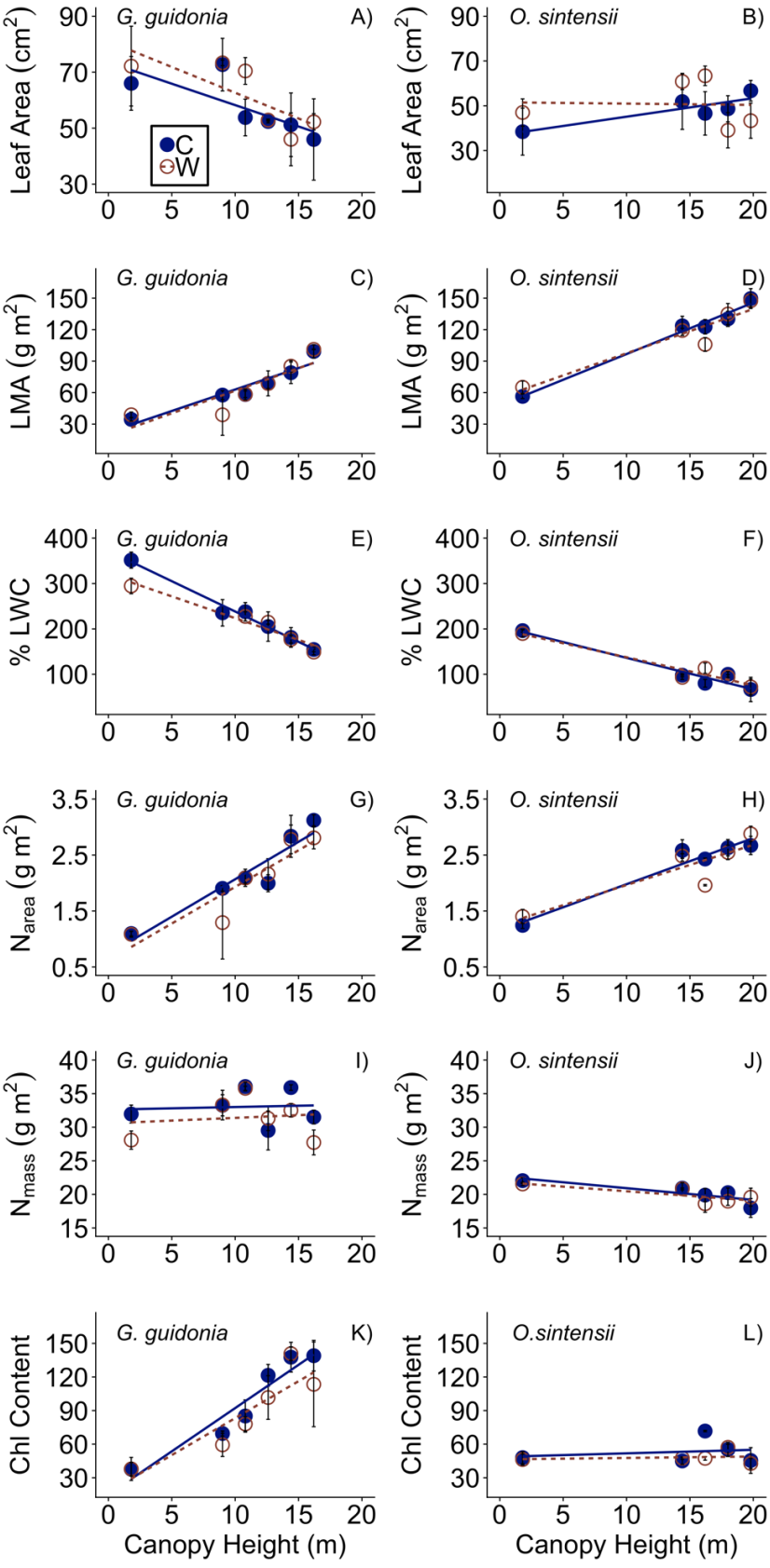
G. guidonia
A)
O. sintensii
B)
Leaf Area (cm2)
C
W
G. guidonia
C)
O. sintensii
D)
LMA (g m2)
G. guidonia
E)
O. sintensii
F)
% LWC
G. guidonia
G)
O. sintensii
H)
Narea (g m2)
G. guidonia
I)
O. sintensii
J)
Nmass (g m2)
G. guidonia
K)
O.sintensii
L)
Chl Content
Canopy Height (m)
Canopy Height (m)

Fig. B3 Leaf functional trait responses to canopy height. **A)** *Guarea guidonia* leaf area, **B)** *Ocotea sintensii* leaf area, **C)** *G. guidonia* leaf mass per area (*LMA*), **D)** *O. sintensii LMA* **E)** *G. guidonia* percent leaf water content (*%LWC*), **F)** *O. sintensii %LWC*, **G)** *G. guidonia* nitrogen per leaf area (N_{area}), **H)** *O. sintensii* N_{area} **I)** *G. guidonia* nitrogen per leaf mass (N_{mass}) **J)** *O. sintensii* N_{mass} **K)** *G. guidonia* chlorophyll (chl) content and **L)** *O. sintensii* chl content response to canopy height for heated (red open circles) and control (blue closed circles) leaves. Linear regressions were fit individually for heated (red dashed) and control (blue solid) leaves.

Ch. 4 Supplemental Tables

Table B1 Summary of heated leaves

Canopy Height	Species	Leaf number	Days warmed
1.8 m	*G. guidonia*	1	26
		2	26
		3	26
	O. sintensii	1	25
		2	25
		3	29
9 m	*G. guidonia*	1	27
		2	27
10.8 m	*G. guidonia*	1	28
		2	28
		3	28
12.6 m	*G. guidonia*	1	26
		2	26
14.4 m	*G. guidonia*	1	25
		2	25
		3	26
	O. sintensii	1	22
		2	27
		3	28
16.2 m	*G. guidonia*	1	26
		2	26
	O. sintensii	1	16
		2	33
18 m	*O. sintensii*	1	26
		2	18
		3	26
		4	27
19.8 m	*O. sintensii*	1	27
		2	27

Table B2 ANCOVA results for instances of temperature spiking.

	% Frequency Δ T > 10 °C	**Max daily heated T_{leaf}**
Species	0.007	< 0.001
Canopy height	0.717	0.015
Species × Canopy Height	0.206	0.231

Table B3 ANCOVA results of leaf trait response to treatment, height, and the interaction between treatment and height.

		ANCOVA					Equation			
Species	**Leaf Trait**	**df**	**Treatment**	**Height**	**Tmt × Ht**	**Adj R^2**	**Control y-intercept**	**Control slope**	**Heated y-intercept**	**Heated slope**
G. guidonia	Leaf Area	3, 30	0.438	**0.012**	0.777	0.13	69.44 ± 7.63	-1.17 ± 0.69	7.03 ± 10.79	-0.28 ± 0.98
	LMA	3, 30	0.865	< **0.001**	0.966	0.58	30.81 ± 7.33	3.34 ± 0.67	-0.53 ± 10.37	-0.04 ± 0.94
	%LWC	3, 29	0.257	< **0.001**	0.057	0.79	351.76 ± 14.32	-11.80 ± 1.30	-46.42 ± 20.36	3.65 ± 1.84
	N_{area}	3, 30	0.395	< **0.001**	0.860	0.64	1.00 ± 0.22	0.11 ± 0.02	-0.09 ± 0.31	$-5.05 \times 10^{-3} \pm 28.43 \times 10^{-3}$
	N_{mass}	3, 30	0.128	0.158	0.623	0.05	32.37 ± 1.56	0.10 ± 0.14	-2.73 ± 2.12	0.10 ± 0.20
	Chlorophyll	3,28	0.695	<**0.001**	0.615	0.71	17.05 ± 12.07	7.52 ± 1.09	1.00 ± 18.32	-0.82 ± 1.62
O. sintensii	Leaf Area	3, 28	0.904	0.421	0.264	-0.03	38.33 ± 8.15	0.72 ± 0.52	12.50 ± 11.53	-0.84 ± 0.74
	LMA	3, 28	0.739	< **0.001**	0.492	0.81	56.21 ± 7.88	4.37 ± 0.50	6.88 ± 11.15	-0.50 ± 0.71
	%LWC	3, 28	0.587	< **0.001**	0.639	0.79	193.78 ± 11.75	-6.10 ± 0.75	-5.27 ± 16.62	0.51 ± 1.06
	N_{area}	3, 28	0.570	< **0.001**	0.546	0.76	1.29 ± 0.15	$7.47 \times 10^{-2} \pm 0.98 \times 10^{-2}$	$9.07 \times 10^{-2} \pm 21.76 \times 10^{-2}$	$-0.85 \times 10^{-2} \pm 1.39 \times 10^{-2}$

N_{mass}	3, 28	0.599	**0.002**	0.750	0.23	22.33 ± 0.87	-0.15 ± 0.06	-0.70 ± 1.23	0.03 ± 0.08
Chlorophyll	3, 26	0.457	0.496	0.902	-0.07	48.25 ± 7.11	0.26 ± 0.46	-2.00 ± 10.05	-0.08 ± 0.65